CHAPTER ONE

INTRODUCTION

1.1 Background of study

Food, shelter and clothing constitute the three basic needs of man. The major challenge with the issue of food is that most of the food crops are seasonal. This means that they are only grown and cultivated at specific times of the year. Therefore, such food crops are abundant in some seasons and limited in other seasons of the year, creating scarcity and hunger. This hinders the realization of the sustainable development project which has one of its goals as "ending hunger in all its forms everywhere, achieving food security and improved nutrition and promote sustainable agriculture" (UN Report, 2013). This will help in providing for a secure and satisfying future for everyone in a society that is equitable, caring and attentive to basic human needs (Akintunde, 2007).

Another challenge is that some food crops are perishable food crops. This means that on their own they do not last long in terms of preservation. They spoil after a short time after harvest mainly due to their high moisture content. Some even spoil while transporting them to places where they are needed. These losses must be minimized by converting them from perishable to non-perishable forms through different methods of food preservation (Obot *et al.,* 2013). These challenges clearly show the importance of food preservation. Food preservation is the process of keeping the quality, texture etc of food crops fresh until when they will be used. Food preservation is also very important

because it will help to guide against unexpected high prices of agricultural products (Akinola *et al.,* 2006).

Food spoilage is caused mainly by the activities of the micro-organisms and enzymes in the food. The growth of the micro-organisms normally leads to faster rate of food spoilage. Hence to preserve food items is to limit the activities and growth of the micro-organisms in the food. The factors that affect the growth of the micro-organisms are intrinsic and extrinsic factors (Rajeev *et al.,* 2012).

The intrinsic factors include pH, moisture content, water activity, oxidation-reduction potentials, physical structure of the food, available nutrients, presence of anti-microbial agents etc. The extrinsic factors include temperature, relative humidity, carbon IV oxide or oxygen, types and numbers of micro-organisms in the food. The water activity and moisture content is considered the major factor among these factors because water is one of the most critical factors for life. Without water, food items become inhospitable for the growth and activities of micro-organisms (Rajeev *et al.,* 2012).

One of the ways of preserving food items is through drying. Drying is one of the major chemical engineering unit operations. It does not involve chemical reactions but the physical process of removing moisture through mass transfer. It is used in food preservation to remove water molecules from food particles. The agricultural product conservation through drying is based on the fact that the micro-organisms/enzymes require water for their metabolic activities. Therefore, reducing the available water level down to a safe storage level reduces the chemical reactions and the developments of the

micro-organisms (Paulo *et al.,* 2006). Drying is a moisture removal process due to simultaneous heat and mass transfer (Ravinder, 2014)**.** It is also a heat and mass transfer process resulting in the removal of water/moisture by evaporation from a solid, semi-solid or liquid (Wankhade *et al.,* 2012)**.** It is a thermo-physical and physio-chemical process whose dynamic principles are governed by heat and mass transfer law both inside and outside the products (Shahzad *et al.,* 2013)**.** In terms of food preservation, drying is the process of removal of excess moisture from food stuff in order to reduce the moisture content to the desired limit that hinders the growth and activities of micro-organisms (Sajith & Muraleedharan, 2014)**.**

Basically, drying involves the removal of water from the food product into the surrounding air. Drying preserves food by removing enough moisture from food to prevent decay and spoilage (Adu *et al.,* 2012). Not only that drying preserves food by inhibiting the growth and activity of micro-organisms, it also reduces the weight and bulk of food for cheaper transport, storage and packaging (Chenchaiah and Muthukmarappa, 2013; Khaled & Sayed, 2014; Kaptso *et al.,* 2013). Food is dried using hot air to remove the water. Drying reduces the water content of food and as such prolongs the shelf life. It also has the advantage of reducing the volume and weight of foods. When drying foods, the key is to remove moisture as quickly as possible at a temperature that does not seriously affect the flavor, texture and color of the food. For effective drying, the air should be hot, dry and moving. This means that for the food to be dried, hot dry air comes into contact with the food. The hot air absorbs water from

the food and is moved away from the food. New dry air takes its place and the process continues until the food has lost its water content. Hence, the basic objective in drying of food products is to preserve them through the removal of moisture (Chenchaiah and Muthukmarappa, 2013**).**

Food crops, like other biological materials do not behave like non-biological materials. The analysis of the drying process of biological materials for engineering design is usually more complicated because they are affected by temperature, moisture content, relative humidity, rate of air flow and overall variations in the physical properties of the materials (Mohsenin, 1986).

Agricultural and raw food materials are biological in nature and as such have certain unique characteristics which distinguish them from other non-biological materials. These biomaterials most often have irregular shape and size characterized by constant biochemical changes, diverse varieties, moisture variation, respiration and enzymatic activities (Wilhelm *et al.,* 2004). Ignoring these levels of variability, leads to frustration in designs of handling and processing equipment for these products (Mohsenin, 1986). Physical properties describe the unique characteristic ways food and agricultural materials respond to physical treatment. This includes thermal processes in which drying operations belong.

Cocoyam (colocasia taro) is an underexploited tuber crop although the literature is replete with its potential nutritional applications. Annual production of cocoyam in Nigeria is estimated at 26.587 million tonnes (FAO, 2006). Nigeria is the world's

largest producer of cocoyam, accounting for about 37% of total world output (FAO, 2006). Due to lack of efficient drying system, some of the cocoyam produced deteriorates and are therefore wasted. In the Eastern part of Nigeria, it serves as staple food and is used as a thickener in food preparations. This is because the starch grain of cocoyam is small and hence improves digestibility. This is an important factor when selecting a starchy food that will not be cumbersome on the digestive system (Ihekoronye and Ngoddy, 1985). The major drawback is that the shelf life of cocoyam is not long hence the need to increase its preservation through drying.

The sweet potato (*Ipomoea batatas*) is a dicotyledonous plant. Its large, starchy, sweet-tasting, tuberous roots are a root vegetable. The young leaves and shoots are sometimes eaten as greens. *Ipomoea batatas* is native to the tropical regions in America. Of the approximately 50 genera and more than 1,000 species of Convolvulaceae, *Ipomoea. batatas* is the only crop plant of major importance—some others are used locally, but many are poisonous. The sweet potato is only distantly related to the potato (*Solanum tuberosum*) and does not belong to the nightshade family. It is nutritious and contains many important elements such as calcium, iron, potassium etc which are necessary for proper maintenance of the human body. Hence the need to preserve it

1.2 Statement of the problem

One of the major reasons for food shortage is the unavailability of adequate preservation facilities. Some of the food crops are seasonal, being readily available during some periods of the year and scare during other periods due to inefficient preservation. Potato

5

and cocoyam, though very nutritious, easily deteriorates due to the high moisture content they contain which favors the growth and activities of micro-organisms. Drying is one of the ways of reducing the moisture content and hence increasing the shelf life. Despite the fact that Nigeria is one of the largest producers of these crops (the largest producer of cocoyam), there is insufficient data on the thermal and engineering properties of the drying of these crops.

Although heated air drying is usually adopted as a cost efficient method of food preservation, yet there is still insufficient understanding of the drying characteristics and behavior of much of Nigerian local staples, which has led to lack of interest in some of these crops due to poor processing and preservation practices. This has led to non-availability of technical information such as the drying rate constant, activation energy (E_a), Specific Energy consumption (SEC), moisture diffusivity (D_{eff}), thermal conductivity, specific heat capacity etc on some Nigerian crops in literature, even when they are good sources of dietary requirements. The implication of this is that they have remained unexploited and has limited information that otherwise would have been helpful in designing industrial dryers. Hence, this research work focuses on modeling the drying of potato and cocoyam using four drying methods so as to compare their effectiveness and the qualities of the dried products. It will also attempt to provide the necessary technical information on the drying of cocoyam and potato produced in Nigeria which will be useful in the optimal design of the dryers for effective and optimal storage of such Nigerian food crops. This is because in spite of their nutritional importance, cocoyam,

in particular, has not received any deliberate attention to address its research and development. It receives low research priority in all regional agricultural research centers and therefore, its contribution to food security and economy is underestimated.

1.3 Aim and objectives

The aim of this work was to study the kinetic modeling, drying characteristics and optimization of the drying of cocoyam and potato.

The specific objectives of this research work include:

1. To use sun drying, oven drying, conventional hot-air drying and solar drying to dry cocoyam and sweet potato slices.

2. To determine the engineering properties such as the specific heat capacity, the thermal conductivity etc of the dried and undried products

3. To model the kinetics of the drying process using standard drying kinetics models

4. To determine the activation energy and the effective moisture diffusivity

5. To evaluate the convective heat transfer coefficient of the process and optimize the drying process using RSM and ANN

1.4 Significance of the study

Food security has been defined by the FAO committee on World Food Security as the "economic and physical access to food, of all people, at all times". This implies that

food should be available throughout the year to sustain household energy and health, and to meet nutritional requirements. The availability of food must be coupled with the ability of every household to acquire it. It must be affordable, especially to the poor. A food security system should act as a food bank during periods of crop failure, natural disasters and external or internal hostilities.

Some food crops, fruits and vegetables are available in large quantities in particular seasons of the year while they become scarce in other seasons of the year. In their peak season, the selling prices are usually at the minimum and this may lead to lower profits or even losses for the farmer (Singh *et al.,* 2014)**.** Preservation of these fruits and vegetables can prevent the huge wastage, stabilize the prices and make them adequately available in the off-season at remunerative prices. Furthermore, food preservation has become an increasingly important component of the food industry as fewer people eat foods produced on their own land while others expect to be able to purchase and consume foods that are out of season. Hence, the need to preserve the food items. Drying is the best and convenient method for post-harvest management because it increases shelf life by reducing the moisture content of the product (Obot *et al.,* 2013)**.** The basic objective in drying of food products is to preserve them by limiting the microbial growth and their reactions (Chenchaiah and Muthukmarappa, 2013)**.**

Potato and cocoyam are some of the food crops produced in Nigeria in large quantities. Nigeria is the world's largest producer of cocoyam with an annual estimated production of 26.587 million tones (FAO, 2006) and the fourth biggest producer of potato in Sub-

Saharan Africa with production yield of about 843,000 tonnes per year (Ugonna *et al.,* 2013). They have high nutritional values being rich in carbohydrates, potassium, iron, calcium, digestive starch, essential amino acid, etc. The main draw back is that these crops are highly seasonal. Also, when stored as tubers, they do not stay a long time before spoiling. Hence, there is need to increase their preservation especially through drying. Equally, converting the dried products into flours will increase their preservation period. Furthermore, by comparing the drying with four different methods, the most effective drying method will be determined.

1.5 Scope

The scope of this work includes the kinetic modeling and evaluation of the drying characteristics of potato and cocoyam. It involves the use of four drying methods - sun drying, solar dryer, conventional hot-air dryer and oven dryer in drying cocoyam and potato. Optimization of the drying process involves the use of Response surface methodology and the Artificial neural network.

CHAPTER TWO

LITERATURE REVIEW

2.1 Introduction

2.1.1 Cocoyam (colocasia taro)

Cocoyam (*colocasia taro*) is one of the most important genera of the family *Araceae* (Ihekoronye & Ngoddy, 1985) and constitute one of the six most important root and tuber crops worldwide (Ekanem & Osuji, 2006). Although, some consider it less important than other tropical root crops such as yam, cassava and sweet potato, they are still a major staple in some parts of the tropics and sub-tropics (Opara, 2002). Cocoyam is an underexploited tuber crop although the literature is replete with its potential nutritional applications. Annual production of cocoyam in Nigeria is estimated at 26.587 million tonnes (FAO, 2006). Nigeria is the world's largest producer of cocoyam, accounting for about 37% of total world output (FAO, 2006). In the Eastern part of Nigeria, it serves as staple food and is used as a thickener in food preparations especially the varieties *Colocasia esculenta* and *Xanthosoma cultivar*. This is because the starch grain of cocoyam is small and has improved digestibility as this is an important factor when selecting a starchy food that will not be cumbersome on the digestive system (Ihekoronye & Ngoddy, 1985).

The cultivation of cocoyam requires minimal input, but the processing is laborious and time consuming (Lancester *et al*., 1982). To process into chips involves the following

unit operations: washing, boiling, peeling, chipping, drying and packaging. The quality of the dried chips produced is determined mainly in the drying stage. Undesirable biochemical changes and subsequent contamination and spoilage of the chips can only be prevented if the drying process is fast enough and the final product is dry enough (Maskan, 2000).

Cocoyam has nutritional advantages over root crops and other tuber crops (Lyonga & Nzietchueng, 1986). All these are lost to nutrition because of low production and utilization. They contribute significantly to the carbohydrate diet, even though ranked less important after yam, cassava and potato (Obomeghei. *et al*., 1998; FAO, 2006). Cocoyam is produced in abundance in eastern part of Nigeria, but less valued in this area as it is regarded as staple food for rural dwellers, the poor and the less privileged in society (IITA, 1992). Enwere (1998) reported that the corms and cormels are cooked and pounded with cassava or yam into fufu and eaten with soup, and that the cormels are exclusively used as a thickener in preparation of soup. The nutritional and chemical compositions as reported by FAO (2006) shows that cocoyam if fully exploited would enhance the food security of people living in the Tropics.

Despite the economic importance of cocoyam as a food material in some parts of the tropics and subtropics, there is limited information on their post harvest characteristics, which perhaps contributes to the very limited application of improved post harvest technologies to maintain quality and improve marketing potential. The tuber does not store well in the fresh form and is usually processed into cocoyam flour, pounded

cocoyam (Ede uli) and dry chips to enhance its storage potentials. When cocoyam chips is dried, it helps to reduce the volume –to-weight ratio which helps to lower shipping or transportation costs and also makes it available in season and out of season. Flours milled from other crops such as maize, millet, sorghum, cassava, potatoes and rice had been added to wheat flour to extend the use of the local crops and reduce the cost of wheat importation.

Plate 2.1 Cocoyam

2.1.2 Uses of cocoyam

Cocoyam has many uses which include:

i. Cocoyam improves digestibility because its starch grain is small

ii. It serves   as a staple food

iii. It can also be used as a food thickener

iv. It has more crude protein than root and other tubers and its starch is highly digestible because of the small size of the starch granules, its contents of calcium, phosphorus, vitamins A and B vitamins are reasonable.

v. Its roots are a major source of calories and one of the most efficient calories producers of all food crops, supplying up to 250 kilo calories/ha (Cock, 1985).

vi. The peels can be used as a source of feed to some class of animals especially when dried. It is also used to produce ethanol, glucose and meal for animals (IITA, 1996).

2.1.3 The nutritional value of cocoyam.

Cocoyam is very rich in vitamin B6 and magnesium, which help control high blood pressure and protect the heart. It is very rich in dietary fibre too, and good for proper glucose metabolism. Popular amongst diabetics in Africa, may be due to its content of loose carbohydrate in form of starch. Cocoyam flour, made from desiccated and grounded cocoyam is very rich in loose starch, thus making it easily digestible, yet it is rich in fibre and protein. In terms of its nutritional values, cocoyam is rich in digestive starch, good quality protein, vitamin C, thiamine, riboflavin, niacin and high scores of protein and essential amino acids (Amandikwa & Chinyere, 2012; Onayemi & Nwigwe, 1987; Lewu *et al.,* 2009).

2.1.4 Sweet Potato (*Ipomoea batatas*)

The origin and domestication of sweet potato is thought to be in either Central America or South America. In Central America, sweet potatoes were domesticated at least 5,000 years ago. In South America, Peruvian sweet potato remnants dating as far back as 8000 BC have been found. Sweet potatoes are cultivated throughout tropical and warm temperate regions wherever there is sufficient water to support their growth. Nigeria is the fourth biggest producer of potato in Sub-Saharan Africa with production yield of about 843,000 tonnes per year (Ugonna *et al.,* 2013).

The plant does not tolerate frost. It grows best at an average temperature of 24 °C (75 °F), abundant sunshine and warm nights. Annual rainfalls of 750–1,000 mm (30–39 in) are considered most suitable, with a minimum of 500 mm (20 in) in the growing season. The crop is sensitive to drought at the tuber initiation stage 50–60 days after planting, and it is not tolerant to water-logging, as it may cause tuber roots and reduce growth of storage roots if aeration is poor (Ahn Peter, 1993).

They grow well in many farming conditions and have few natural enemies; pesticides are rarely needed. Sweet potatoes are grown on a variety of soils, but well-drained, light- and medium-textured soils with a pH range of 4.5-7.0 are more favorable for the plant. They can be grown in poor soils with little fertilizer. However, sweet potatoes are very sensitive to aluminum toxicity and will die about six weeks after planting if lime is not applied at planting in this type of soil. Because they are sown by vine cuttings rather than seeds, sweet potatoes are relatively easy to plant. Because the rapidly growing vines shade out weeds, little weeding is needed. A commonly used herbicide to rid the soil of any unwelcome plants that may interfere with growth is DCPA, also known as Dacthal. In the tropics, the crop can be maintained in the ground and harvested as needed for market or home consumption. In temperate regions, sweet potatoes are most often grown on larger farms and are harvested before first frosts.

Plate 2.2 Sweet Potato

2.1.5 Uses of Sweet Potato.

i.   It is used as a source of starch

ii.   It is used as a staple food

iii. All parts of the plant are used for animal fodder.

iv.   Sweet potato vine is ideal for use in home aquariums, trailing out of the water with its roots submerged, as its rapid growth is fueled by toxic ammonia and nitrates, a waste product of aquatic life, which it removes from the water. This improves the living conditions for fish, which also find refuge in the vast root systems.

v.   Cuttings of sweet potato vine, either edible or ornamental varieties, will rapidly form roots in water and will grow in it, indefinitely, in good lighting with a steady supply of nutrients.

15

vi.   Young sweet potato leaves is used as baby food in East Africa

vii.   In South America, the juice of red sweet potatoes is combined with lime juice to make a dye for cloth. By varying the proportions of the juices, every shade from pink to black can be obtained.

viii.   Its flour is used to replace part of wheat flour in baked products. Example cakes, bread etc.

ix.   Its young leaves are used as vegetables in Guinea, Liberia, Sierra Leone as sources of Vitamins A, B_2 and C.

(Abidin, 2004; Xavier, 1999; FAO, 1990; Idelia and Glorioso, 2003)

2.1.6 Nutrient Content of potato

Besides simple starches, raw sweet potatoes are rich in complex carbohydrates, dietary fiber and beta-carotene (a provitamin A carotenoid), while having moderate contents of other micronutrients, including vitamin B5, vitamin B_6, manganese and potassium (right table). When cooked by baking, small variable changes in micronutrient content occur to include a higher content of vitamin C at 24% of the Daily Value per 100 g serving (right table), as well as an increase in polyphenol levels.

The nutrient content of sweet potato per 100g is approximately Energy (360KJ), Protein (1.6g), Fat (0.05g), Carbohydrates (20g), Fibre (3g), Sugar (4.18g) and small traces of elements such as Calcium, Iron, Magnesium, Potassium, Sodium, Zinc etc. It equally contains Vitamins A, C, and B_2. (Nutrient data lab, 2014).

2.2. Crop Storage

Crop drying and storage, are essential for all year round availability of food and raw materials for industries (Raghavan & Sosle, 2007). Safe storage time depends on the crop moisture and temperature. High moisture and temperature enhance growth of mold, hence, increasing crop spoilage. This relationship can be explained by the illustrations in Figure 2.1.
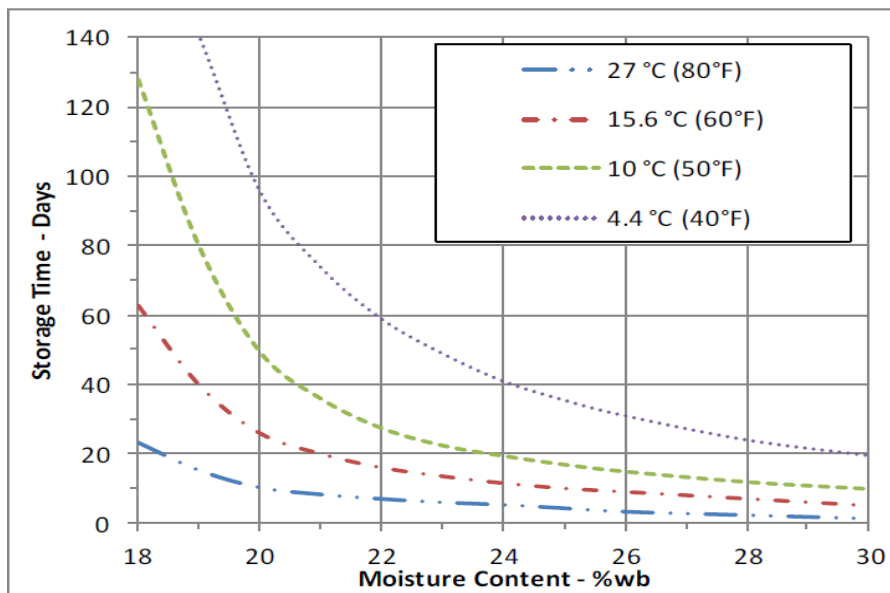
Figure 2.1: Allowable storage time for shelled corn. Adapted from Sauer (1992).

It is seen that at low temperature and moisture content, the time that corn can be safely stored will increase but the time will be shorter if the reverse is the case. Corn at 18% moisture content (wb) and temperature of 4.4 ^{o}C can be safely stored for more than 140 days; however, if its conditions are 30% (wb) and 27 ^{o}C, spoilage can occur in less than

one day. Keeping grain moisture and temperature at low levels is fundamental to increasing its lifespan.

2.3 Thermal Properties of Food Crops

Food crops often experience the movement of heat around and through them in various forms and degrees during growth harvest, handling, processing, transport, storage, and preparation for consumption. Only a few foods such as fresh fruit and some vegetables go from field to the table without any thermal processing. Most foods are thermally processed to extend their shelf life and maintain high quality. Foods are exposed to heat transfer numerous times during heating, cooling, freezing, frying, and/or baking. Thermal operations are also used to ensure safe food products for extended periods. A classic example is the pasteurization of milk, a heating process that eliminates bacteria. Pasteurization, followed by proper cooling, provides a safe milk product for weeks. Canned foods, which are good for years, are sterilized with heat processes. Juice, having been heated and aseptically packaged in boxes, is shelf stable without refrigeration for months.

Heat transfer occurs by conduction, convection, and radiation. These mechanisms can occur individually or simultaneously. In food processing, heat transfer is usually a combination of conduction and convection. Conduction is principally involved during heat transfer within solid-like materials, i.e. solids or static liquids. Convection is the transfer between solids (walls of pipes, vats, rooms) and fluids (food materials). In other cases, the food may be the solid and the fluid might be air or water. Radiant heat

transfer is less frequently used but is becoming more common in microwave and infrared heating. Having an understanding of the mechanisms of heat transfer allows the food engineer to better design equipment and processes.

The thermal properties are unique for each food. Each mechanism of heat transfer has an associated thermal property. The thermal properties include:

Specific Heat capacity (C_p): This is the heat required to increase the temperature of one unit mass by one degree

Thermal Conductivity (K): This is a measure of the ease with which heat flows through a material. For most food materials, it ranges between 0.2 and 0.5 W/mK.

Thermal diffusivity (α) : This is the relevant thermal property in transient heat transfer where temperature varies with time. Their value ranges from 1×10^{-7} to 2×10^{-7} m^2/s for most food crops.

2.4 Water Activity (a_w)

The amount of water in food and agricultural products affects the quality and perishability of these products. However, perishability is not directly with the same moisture content. In fact, perishability varies greatly among products with the same moisture content. A much better indicator of perishability is the availability of water in the product to support degradation activities such as microbial action.

Water in food which is not bound to food molecules can support the growth of bacteria, yeasts and molds (fungi). The term water activity (a_w) refers to this unbound water.

The water activity of a food is not the same thing as its moisture content. Although moist foods are likely to have greater water activity than are dry foods, this is not always so; in fact a variety of foods may have exactly the same moisture content and yet have quite different water activities

The term water activity is widely used in the food industry as an indicator of water available in a product. Water activity is defined as

$$a_w = \frac{P_w}{P_{ws}} \quad \text{or} \quad a_w = \Phi$$

$$\text{since} \qquad \Phi = \frac{P_w}{P_{ws}} \tag{2.1}$$

Where

Φ is the relative humidity, decimal

P_w is the partial pressure of water vapour at the specified conditions

P_{ws} is the partial pressure of water vapour at saturation and the temperature specified.

Thus, water activity is the equilibrium relative humidity (ERH) in decimal form for a product at a given temperature and moisture content.

Take a sample of a food product and place it in an enclosed container at a fixed temperature. The product will exchange moisture with the air surrounding it. After a period of time, as with the equilibrium moisture, an equilibrium condition will occur.

The product no longer has any net change in moisture. The water activity is equal to the decimal relative humidity at that condition.

Water activity a_w can also be calculated by the equation given by Olaoye *et al.,* (2012)

$$a_w = 1 - \exp[- \exp(0.914 + 0.5639 \ln M)] \tag{2.2}$$

Where

$$M = \frac{M_f}{100 - M_f} \tag{2.3}$$

and then

$$ERH = 100a_w \tag{2.4}$$

2.4.1 Factors that influence water activity

- **Drying:** Water activity is decreased by physically removing water

- **Solutes:** Water activity is decreased by adding solutes such as salt or sugar

- **Freezing:** Water activity is decreased by freezing

- **Combination:** One or more of the above can be combined for a greater influence on water activity. Example is salting and drying fish.

2.4.2 Uses of water activity

Water activity (a_w) has its most useful application in predicting the growth of bacteria, yeast, and mold. For a food to have a useful shelf-life without relying on refrigerated storage, it is necessary to control its level of water activity (a_w). This can effectively

increase the product's stability and make it possible to predict its shelf life under known ambient storage conditions.

Water activity is an important consideration for food product design and food safety.

Food designers use water activity to formulate shelf-stable food. If a product is kept below a certain water activity, then mold growth is inhibited. This results in a longer shelf life.

Water activity values can also help limit moisture migration within a food product made with different ingredients. If raisins of a higher water activity are packaged with bran flakes of a lower water activity, the water from the raisins migrates to the bran flakes over time, making the raisins hard and the bran flakes soggy. Food formulators use water activity to predict how much moisture migration affects their product.

Water activity is used in many cases as a critical control point for Hazard Analysis and Critical Control Points (HACCP) programs. Samples of the food product are periodically taken from the production area and tested to ensure water activity values are within a specified range for food quality and safety. Measurements can be made in as little as five minutes, and are made regularly in most major food production facilities.

2.4.3   Estimated Mold-free shelf life (MFSL)

Estimated mold-free shelf life (MFSL) is the estimated number of days that a dried food sample can stay before it can be attacked by molds and bacteria. It depends on the water

activity of the sample. The smaller the water activity, the higher the MFSL which means that the shelf life is increased and the food sample can stay for a longer number of days before yielding to the attacks of molds and bacteria. It is calculated by the formular given by Man and Jones (2000) as:

$$MFSL = 10^{7.91-8.1a_w}$$ (2.5)

Where

MFSL is mold-free shelf life (days),

a_w is the water activity

2.5 Drying

Drying is one of the unit operations involving mass transfer. It is a solid-liquid separation process aimed at reducing the moisture content of a solid (Oyoh & Menkiti, 2008). It is a separation process that involves the transfer of water molecules from a substance to another substance. In food processing, drying is used as one of the methods of preserving food items by reducing their moisture content to a low level where the growth of the micro-organism will be retarded (Junling *et al.,* 2008). It is an important operation in the food and pharmaceutical industries and is accomplished by air, vacuum, spray and freeze drying techniques (Singh *et al.,* 2014). Drying is a continuous process with changes in moisture content, air and crops drying and the humidity of air all occurring simultaneously and heat is transferred from the surrounding air from the sun to the surface of the crop in different models of heat transfer (Ici Turk, 2005). Because

of these considerations, drying has been a major part of food industry for many years, being a major way of preserving this dormancy.

Moisture control in postharvest processes involves reduction of moisture content to a level which becomes unfavourable for microorganisms and enzymes responsible for spoilage of foods and biomaterials. In a nutshell, freshly harvested crops have relatively high moisture content which has to be reduced to a desirable level, usually below 12% (wb) for most grains and slightly above that for fruits and vegetables before they can be safely stored.

Therefore, other reasons for crop drying include the following;

a) To enhance the mechanical properties of the crops, such as strength, hardness, and thermal insulation in order to stand mechanical impact of handling systems.

b) To reduce incidence of enzyme attacks, insect and fungal infestations, stain and decay

c) To reduce the weight and volume of the crops, thereby resulting in reduction of transportation cost and storage space.

Logically, therefore, drying of agricultural products is an important operation to get the desirable condition for their consumption, transportation, marketing and storage.

The major objective of drying is the reduction of the water level of the product for storage during a long time (Kaptso *et al.,* 2013)**.** This prevents or inhibits the growth

and the activities of micro-organisms and hence preserves the food. Drying reduces water content of food and as such prolongs the shell-life. Drying also has the advantage of reducing the volume and the weight of foods thereby minimizing the cost of packing, storage and transportation (Shahzad *et al.,* 2013; Chenchaiah and Muthukmarappa, 2013; Khaled & Sayed, 2014; Kaptso *et al.,* 2013)**.**

When drying food crops, the key is to remove moisture as quickly as possible at a temperature that does not seriously affect the flavor, texture and colour of the food. If the temperature is too low in the beginning, micro-organisms may grow before the food is adequately dried. If the temperature is too high and the humidity is too low, the food item may harden on the surface. This makes it more difficult for moisture to escape and the food will not dry properly (Adu *et al.,* 2012)**.**

For effective drying, the air should be hot, dry and moving. This means that

   i.   Air must be dry, so it can absorb the moisture from the product

  ii.   Air must be hot, so that the heat around the product will cause it to dry more quickly

 iii.   Air must be moving across the food so that it can get rid of the water vapor that it has collected.

These factors are inter-related and it is important that each factor is correct. Hence, successful drying depends on the availability of appropriate heat to draw out moisture without cooking the food, capability of dry air to absorb the released moisture and

adequate air circulation to carry off the moisture (Adu *et al.,* 2012)**.** Drying must be appropriate in all ramifications for it to be efficient in food preservation. This means, it must be neither under-drying nor over-drying. Under-drying leads to deterioration of product due to fungi or bacteria whereas over-drying may lead to case-hardening which results in the spoilage of the product (Akinola *et al.,* 2006)**.** The different types of drying include sun drying, solar drying, oven drying, thermal drying etc. The emphasis of this work is on sun drying, solar drying, conventional hot-air drying and oven drying.

2.5.1 Factors considered in drying

Two separate phenomena are involved in drying. First, moisture must move from the interior of a material to the surface of that material. Second, the surface water must be evaporated into the air. These two steps involve two very different phenomena. Movement of water from the interior to the surface must occur in one of two manners – capillary action or diffusion. Movement by capillary action would only occur during early stages of drying. As the drying process continues, internal moisture movement would occur by molecular diffusion of water vapor within the material. Removal of water from the surface involves evaporation of water from the surface into the surrounding air. The evaporation rate depends upon the condition of drying air and the concentration of water at the surface.

Air drying involves the passing of air over the object(s) to be dried. Typically, the air is heated prior to entering the drying region. Consider the drying process for a high moisture product such as an apple slice. The surface of the slice will be visibly covered with water immediately after slicing. As this water evaporates, the surface becomes slightly dry. Moisture cannot move from the interior of the slice as rapidly as it can

evaporate at the surface. Thus the governing factor in later stages of drying is the diffusion rate of moisture within the slice.

Factors affecting the drying rate will vary slightly depending upon the type of drying system used. However, in general, the following factors must be considered:

   i.   nature of the material: physical and chemical composition, moisture content, etc.;

   ii.   size, shape and arrangement of the pieces to be dried;

   iii.   wet-bulb depression ($t - t_{wb}$) , or relative humidity, or partial pressure of water vapor in the air (all are related and indicate the amount of moisture already in the air);

   iv.   air temperature; and

   v.   air velocity, u (drying rate is approximately proportion to $u^{0.8}$) is case hardening.

Another factor that must be considered in drying solid materials is case hardening. This problem can occur if the initially stage of drying occurs at low relative humidity this problem can occur if the initial stage of drying occurs at low relative humidity and high temperature. Under these conditions, moisture is removed from the surface of the material much faster than it can diffuse form within the material. The result is formation of a hardened relatively impervious layer on the surface of the material. Formation of such a layer causes subsequent drying to be much slower than it would otherwise be.

2.6 Crop drying models

Crop drying models are usually classified as deep-bed, thin-layer and single-kernel type. Deep-bed drying models are derived from the laws of heat and mass transfer with the assumption that there is no temperature and moisture content equilibrium between the drying air and the grain throughout the bed. In general, the model comprises mass and energy balances of grain and drying air and a thin-layer drying equation.

The term 'single-kernel drying model' is usually applied to any mathematical drying model, developed for hygroscopic porous materials, that is commonly used in the analysis of single-kernel drying. The models used were derived from either mechanistic approach or from non-equilibrium thermodynamics theories (Luikov, 1966; Whitaker, 1997). A model that incorporates both the above theories was developed by Fortes and Okos (1981) and was applied to grain drying analysis.

Thin-layer drying models are developed for layers of many grain thicknesses with the assumption that the drying air is in the same thermodynamic state as the grain in each layer, during each drying period, that is, there are no temperature and moisture gradients between the air and the grain. Thin-layer models can be derived from deep-bed models with the introduction of simplifying assumptions for the condition of low temperature and low air flow drying, when the near equilibrium condition is valid. (Ian & Arun, 1997).
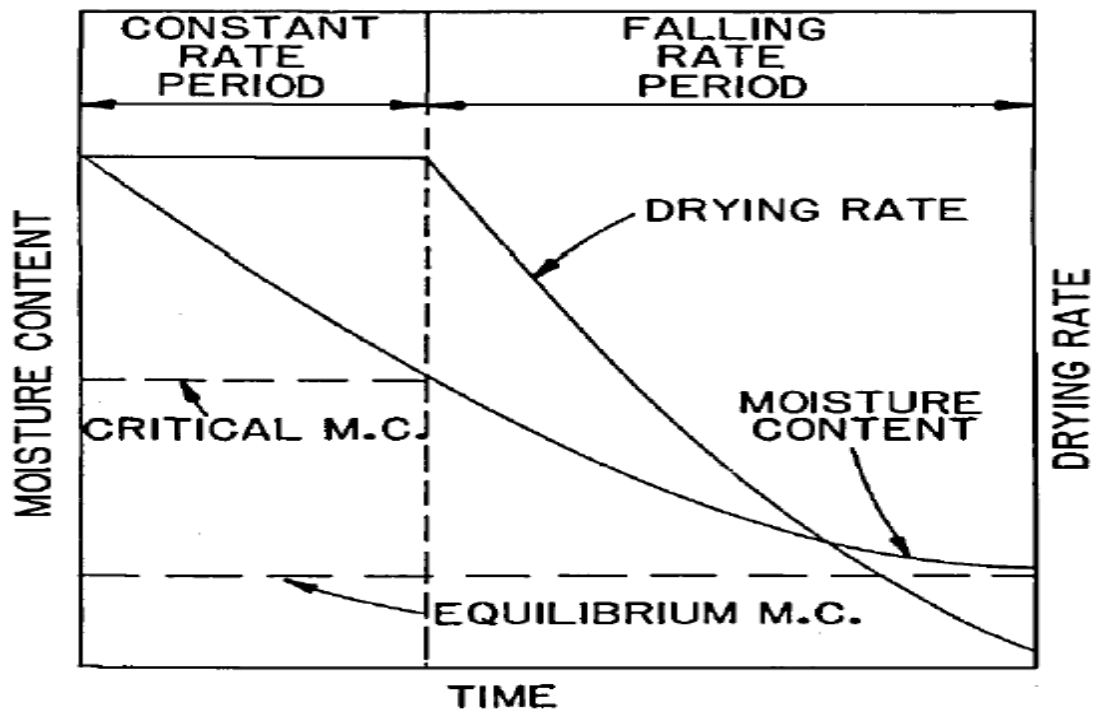
Figure 2.12a: Constant and falling rate periods in thin-layer drying of high moisture grain (Nwajinka et al, 2014)

2.7 Energy Requirements in Crop Drying

Crop drying is an energy intensive process compared with their production and other postharvest processes. For example, in the Midwest of United States, 60% of the energy required to produce corn is used to dry it as illustrated in figure 2.2 (Brooker et al., 1992). According to the above report, Crop drying requires a minimum of approximately 2.50 to 2.67 MJ/kg of energy, depending on the temperature at which water is evaporated. However, actual energy requirements for evaporating water from grain range from 3 to 8 MJ/kg (Gunasekaran & Thompson, 1986). Logically, since the cost of energy is increasing every day, reduction in the energy use for grain drying will be an important improvement for the agro industry.
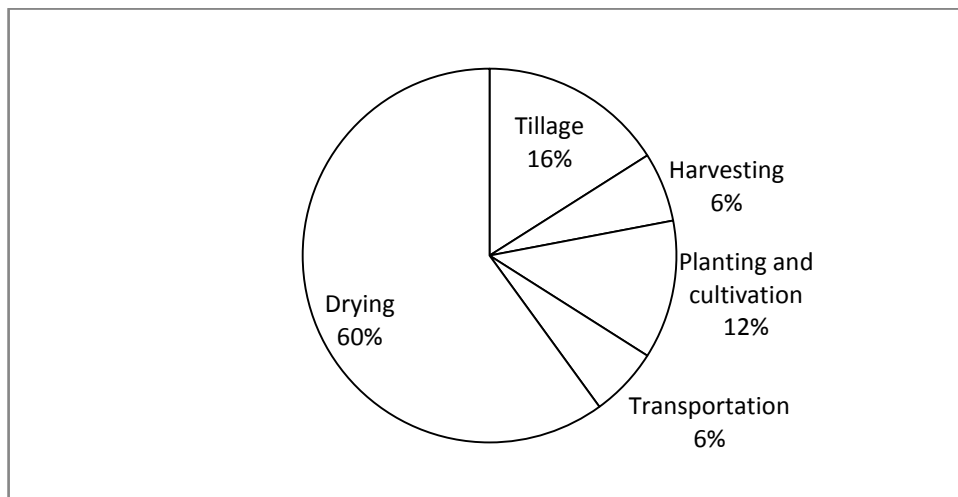
Figure 2.2b: Energy requirements for production of corn in the Midwestern United States as a percentage of the total (Brooker et al. 1992).

2.8   Drying Methods

Drying is a complex operation involving transfer of heat and mass along with several rate processes, such as physical or chemical transformations (Otto *et al.,* 1994).   It occurs by supplying heat to the wet materials and thus vaporizing the liquid content. Generally, heat may be supplied by convection (direct dryers), conduction (contact or indirect dryers), and radiation or volumetrically by placing the wet material in a microwave or radio frequency electromagnetic field. Most industrial dryers are of the convective type with hot air or direct combustion gases as the drying medium. Almost all drying applications involve removal of water. All modes except the dielectric (microwave and radio frequency) supply heat at the boundaries of the drying object so that the heat must diffuse into the solid primarily by conduction. The liquid must travel to the boundary of the material before it is transported away by the carrier medium which in most cases is a gas (or by application of vacuum for non-convective dryers). Transport of moisture within the solid may occur by any one or more of the following mechanisms of mass transfer (Earle, 1983):

• Vapor diffusion, if the liquid vaporizes within material

• Knudsen diffusion, if drying takes place at very low temperatures and pressures, e.g., in freeze drying

• Surface diffusion (possible although not proven)

• Hydrostatic pressure differences, when internal vaporization rates exceed the rate of
  vapor transport through the solid to the surroundings

• Liquid diffusion, if the wet solid is at a temperature below the boiling point of the liquid

• Combinations of the above mechanisms.

It is noteworthy that since the physical structure of the drying solid is subject to change during drying the mechanisms of moisture transfer may also change with elapsed time of drying.

2.9   Sun drying

Agricultural products can be dried using direct or indirect heat from the sun (solar radiation). When the heat of the sun is used directly, it is called open-sun drying but when the heat of the sun is not used directly on the crop surfaces, it is called solar drying or indirect sun drying.

2.9.1 Open sun drying

Sun drying is still the most common method used to preserve agricultural products. It involves exposing the food samples to direct heat from the sun where the heat rays from

the sun dries the food items (Fig 2.3). Traditional sun drying takes place by storing the product under direct sunlight (Singh *et al.,* 2014). Sun drying is only possible in areas where, in an average year, the weather allows foods to be dried immediately after harvest.
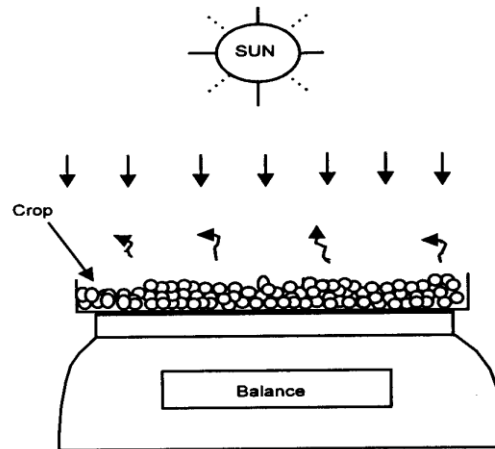
Fig 2.3: Experimental set up for Sun dry

The main advantages of sun drying are low capital and operating costs and the fact that little expertise is required. The main disadvantages of this method are as follows: contamination, theft or damage by birds, rats or insects; slow or intermittent drying and no protection from rain or dew that wets the product, encourages mould growth and may result in a relatively high final moisture content; low and variable quality of products due to over-drying or under-drying; large areas of land needed for the shallow layers of food; laborious since the crop must be turned, moved if it rains; direct exposure to sunlight reduces the quality (colour and vitamin content) of some fruits and vegetables. Moreover, since sun drying depends on uncontrolled factors, production of

uniform and standard products is not expected. The quality of sun dried foods can be improved by reducing the size of pieces to achieve faster drying and by drying on raised platforms, covered with cloth or netting to protect against insects and animals. In open sun drying, there is a considerable loss due to various reasons such as rodents, birds, insects and microorganisms. The unexpected rain or storm further worsens the situation. Further, over drying, insufficient drying, contamination by foreign material like dust dirt, insects, and micro-organism as well discoloring by UV radiation are characteristic for open sun drying (Singh *et al.,* 2014)**.**

In general, open sun drying does not fulfill the quality standards and therefore it cannot be sold in the international market. Drying is a critical step in the processing of dehydrated products because of the high energy requirement of the process (due to low thermal efficiency of dryers). Increased consumer awareness of food quality as well as the desire to produce a high quality has emphasized the necessity of optimization.

Some of the problems associated with open-air sun drying can be solved through the use of a solar dryer which comprises collector, a drying chamber and sometimes a chimney (Atul *et al.,* 2013). The conditions in tropical countries make the use of solar energy for drying food practically attractive and environmentally sound. Other methods of sun-drying are shown in Plate 2.4

(a)

(b)
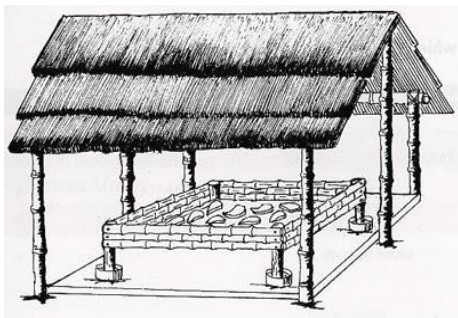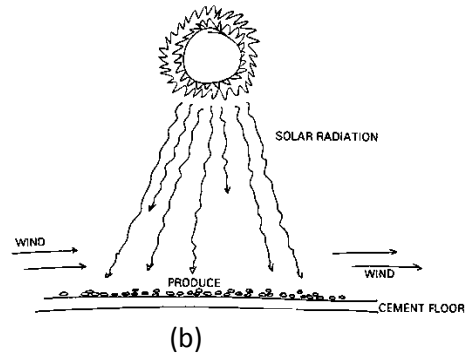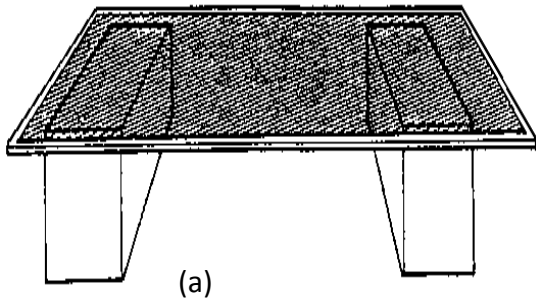
(c)

Plate 2.4: Different ways of sun drying (Fellows, 1997)

Improved sun drying was proposed by FAO (Fellows, 1997) in their "Expert consultation on planning the development of sun drying techniques in Africa". Clean smooth raised platforms, blackened surfaces that absorb solar radiation more efficiently or woven mats and mesh trays that facilitate the air movement around the product were recommended. Simple direct sun driers can also be made from trays of screening material propped upon wooden or concrete blocks to allow air to circulate under the produce (Plate 2.4). A layer of cheesecloth can be draped loosely over the produce,

protecting it from insects and birds while drying. A simple method for direct sun drying is to construct a raised platform from wood and cover the frame with loosely woven mats. Sliced fresh vegetable crops are dried in direct sunlight on straw mats. Air can pass over and below the produce, enhancing drying and reducing losses due to overheating.

2.9.2 Solar drying

Solar drying is often differentiated from 'sun drying' by the use of equipments to collect the sun's radiation in order to harness the radiative energy for drying applications (Singh *et al.,* 2014). This means that in solar drying, the sun's radiation is not directly applied to the food items whereas in sun drying, the sun's radiations are directly applied to the food products. The solar energy represents one of the sources of non-polluting and economic energy increasingly requested (Boubekri *et al.,* 2007).

Solar dryers use some means to collect solar radiation with the result that elevated temperatures and in turn, lower relative humidity is achieved for drying (Akinola *et al.,* 2006)**.** The dryers are less susceptible to variations in weather, although drying is obviously slower during inclement weather, but they provide shelter from the rain. The internal high temperatures also discourage the entry of pests into the dryer (Sajith & Muraleedharan, 2014).

Advantages of Solar drying:

The advantages of solar drying are numerous. The high temperature, movement of air, and low humidity increases the rate of drying. The solar collector helps to increase the temperature inside the drying chamber. Solar dryers are waterproof so the quality of the product is better in terms of nutrients, hygiene and colour. It permits early harvesting and reduces the field losses of the products. It permits better planning of harvesting season, and reduces spoilage in storage drastically. It permits the farmer to sell his product at better price during early period of harvesting season, Quality of the product gets enhanced significantly and hence farmer gets more money for his product, and transportation is easy with dried product.

Advantages of Solar drying:

The main disadvantage of the solar dryer is the limited time of solar insolation during the day, long drying times, and contamination of product, natural drying, and energy requirement, initial investment cost is very high.
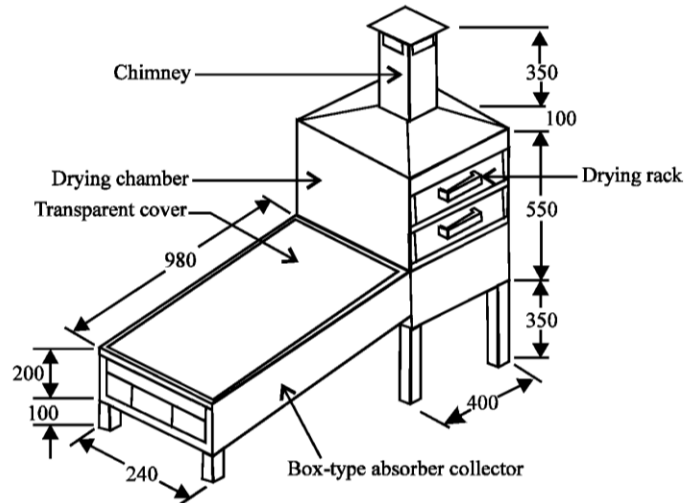
Plate 2.5 A solar dryer

2.10. Heated air dryers

Traditionally, a dryer is made up of five basic components: the air heater, the air mover, the air duct system, the chimney and the cabinet to hold the product. The drying chamber of a drier usually contains mesh trays on which the product is spread and is usually made of metal or sometimes wood. Hence, the heat loss to the side walls of the drying chamber causes loss of efficiency. As the hot air passes through the mesh drying takes place, and the air passes out of the dryer through the chimney. It is somehow difficult to predict what is going on in the closed cabinet as the drying progresses. This is achievable through modeling and simulation of the drying process if the parameters of the system are known. Since emphasis is more on the product, the knowledge of the changing properties that characterize drying is very critical in the process. The parameters of air, which are affected by thermal radiation, such as, pressure, velocity, relative humidity and temperature difference affect the efficiency of driers also. They

can be determined or calculated using basic knowledge of heat transfer, mass transfer and fluid mechanics with experimental back-up.

2.10.1 Hot-air conventional dryer

The conventional air-dryer was designed in such a way that it uses current to power the heater that supplies heat for the actual drying. The special feature in it is that the temperature, air velocity and humidity can be regulated. Because of the inconvenience in the use of hygrometer in the measurement of the relative humidity of the drying air, it was calculated using the experimental values of dry bulb and wet bulb temperatures respectively, (in ^{o}C). An example of hot air conventional dryer is shown in the Plate 2.5
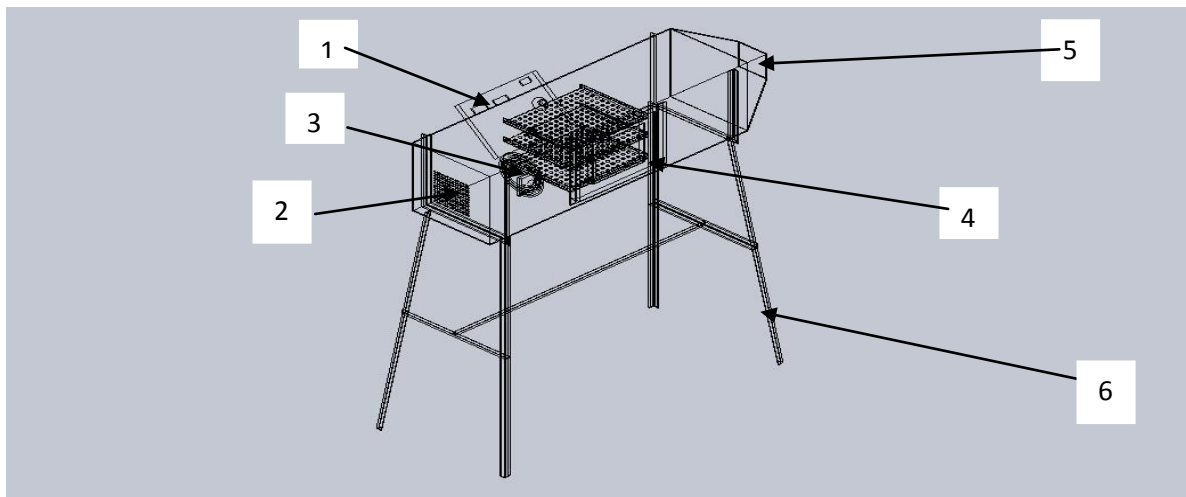
Plate 2.5: Cut-away view of a hot-air conventional drier

1=Control pannel, 2=Fan housing, 3=Electric heater, 4=Drying (crop) trays, 5=Exhust openning, 6= Frame support (Legs).

2.10.2 Oven dryer

This involves the use of high temperature to dry the food items in an oven. It has some of the advantages of solar drying because the product is protected against flies, rain and dust and even product can be left in the dryer overnight or during rain.

The major disadvantage is that the high temperature destroys the food quality.

2.11. Microwave dryers

Microwave energy has been widely used either as pretreatment prior to other drying process to enhance mass transfer rate, which could be attributed to the cell damage during microwave exposure (Wang *et al.,* 2012) or in combination with other drying process, as finishing drying method for osmotic dehydration, convective or vacuum drying. Microwave drying, however, results in adverse and unacceptable overall quality of product if the process is not controlled properly. Non-uniform temperature and moisture distribution are few major drawbacks in microwave drying as they lead to hot spot generation. Furthermore, microwave heating results in surface moisture build-up due to enhanced (pressure-driven) flow of moisture to the surface and the cold ambient air's inability to remove moisture at a high rate which ultimately lead to surface scorching (Wang *et al.,* 2008).

2.12. Moisture Content in Food and Agricultural Products

No agricultural product in its natural state is completely dry. Some water is always present. This moisture is usually indicated as a percent moisture content. These methods

are wet basis (m) and dry basis (M). In addition, the content may be expressed as a percent or as a decimal ratio. All the four will be used (Wet basis, dry basis, percent and decimal ratio) in analyzing moisture or food products.

The general governing equations for indicating moisture content are:

$$m = \frac{m_w}{m_w + m_d} = \frac{m_w}{m_t} \qquad (2.5)$$

$$M = \frac{m_w}{m_d} \qquad (2.6)$$

Where: m is decimal moisture content wet basis (wb),   M is decimal moisture content dry basis (db), m_d is mass of dry matter in the product, m_w is   mass   of water in the product, m_t is total mass of the product, water plus dry matter

The percent moisture content is found by multiplying the decimal moisture content by 100.

In addition, relationships between wet and dry moisture content on a decimal basis can be derived from the given.

$$M = \frac{m}{1-m} \qquad \text{or} \qquad m = \frac{M}{1+M} \qquad (2.7)$$

Use of the wet basis measurement is common in the grain industry where moisture content is typically expressed as percent wet basis. However, use of the wet basis has one clear disadvantage – the total mass changes as moisture is removed. Since the total mass is reference base for moisture content, the reference condition is changing as the moisture content changes. On the other hand, the amount of dry matter does not change.

Thus, the reference condition for dry basis measurements does not change as moisture is removed.

For given product, the moisture content dry basis is always higher than the wet basis moisture content. The difference between the two basis is small at low moisture levels, but it increases rapidly at higher moisture levels.

A final note regarding moisture content relates to high moisture materials such as fruits and vegetables. Many of these products have moisture contents near 0.90 (or 90%) (wb). On a dry basis this would be 900% if expressed as a percentage. For products of this type, moisture is often given as "mass of water per unit of dry product", the decimal basis we discussed earlier.

The moisture content of a wet solid in equilibrium with air of given humidity and temperature is termed the equilibrium moisture content (EMC) at that humidity and temperature. A plot of EMC at a given temperature versus the relative humidity is termed sorption isotherm. An isotherm obtained by exposing the solid to air of increasing humidity gives the adsorption isotherm, while that obtained by exposing the solid to air of decreasing humidity is known as the desorption isotherm. Clearly, the latter is of interest in drying as the moisture content of the solids progressively decreases. A phenomenon known as hysteresis occurs when the path describing the two isotherms are not identical.

2.13.   Equilibrium Moisture Content

Several equations have been developed to describe isotherms (Samapundo et al. 2007). These equations have different constants depending on the temperature range, which are often narrow, thereby not covering the simulation of wide range of temperatures.

There are three distinct zones, which are indicative of different water binding mechanisms at individual sites on the solid matrix. In the first region, water is tightly bound to the sites and is unavailable for reaction. In this region, there is essentially monolayer adsorption of water vapor and no distinction exists between the adsorption and desorption isotherms. In the second region the water is more loosely bound. The vapor pressure depression below the equilibrium vapor pressure of water at the same temperature is due to its confinement in smaller capillaries. Water in the third region is even more loosely held in larger capillaries. It is available for reactions and as a solvent (Okos, 1980). Desorption isotherms are also dependent on external pressure. However, in all practical cases of interest, this effect is often neglected. The total heat required to evaporate bound water is the sum of the latent heat of vaporization and the heat of wetting. The heat of vaporization is a function of the moisture content M. The heat of wetting is zero for unbound water and increases with decreasing M. it is the heat evolved when a given amount of water is adsorbed. Since ΔH_w is responsible for lowering the vapor pressure of bound water, at the same relative humidity, ΔH_w is almost the same for all materials.

2.14 Kinetics of drying process

Reduction of moisture from harvested crops has been found to deactivate enzymes or microorganisms that often cause undesired bio-chemical reactions and lead to quality deterioration in stored agricultural products (Jayaraman & Das Gupta, 2006). This process which is termed drying is greatly influenced by variations in composition and structure of food materials which often results in unique drying characteristic for different food product. Study of drying allows understanding of the controlling mechanisms involved and the prediction of the influence of the system parameters on dryer design and performance. Drying kinetics is important in the analysis of moisture transfer process in food materials undergoing drying. In studying the kinetics of drying, thermo-physical properties and transport properties are usually integrated in drying models. Moreover, movement of moisture within a food material during drying is a complex process with various mechanisms (kinetics).

The amount of moisture content in a product is predicted on the basis of the weight of water.

Moisture Content, MC, is given by

$$MC\ (\%) = \frac{M_i - M_d}{M_i}\ X\ 100 \qquad\qquad (2.7)$$

Where M_i is the mass of sample before drying and M_d is the mass of the sample after drying.

43

2.15 Moisture ratio

Thin-layer mathematical drying models describe the drying phenomenom in a unified way regardless of the controlling mechanisms (Agarry & Aworanti, 2012)**.** In thin layer drying model, the rate of change in material moisture content in the falling rate drying period is proportional to the instantaneous difference between material moisture content and the expected material moisture content when it comes into equilibrium with the drying air. It is assumed that the material layer is thin enough or the air velocity is high so that the conditions of the drying air (humidity and temperature) are kept constant throughout the material (Mohammed *et al.,* 2013).

Experimental evidence shows that a single drying constant almost invariably over-estimates the drying rate in the final stages of drying. During the convective drying, heat-transfer between the sample and the surroundings is controlled by the humidity-ratio of the air at the surface, the temperature of the plenum and temperature of the sample surface (Bablis *et al.,* 2004). Heated-air drying refers to the removal of free and bound moisture from a sample, by using heat energy in a specially designed dryer. During drying, there is simultaneous transfer of heat, to evaporate and transfer moisture to the surface and as vapor from the surface into the hot air stream, within an optimal period of time. Movement of moisture through the sample is in the form of water-vapor within the cell-cavities and bound water. Bound water is hydrogen-bonded to the hydroxyl groups of the polysaccharides. Therefore, the driving force responsible for moisture-transport is a combination of diffusion along the moisture concentration-

gradient and difference of vapor-pressure due to temperature gradient. The transfer of liquid within a drying sample may occur by the following mechanisms:

i. Diffusion in the continuous homogeneous solids,

ii. Capillary flow in the granular and porous solids,

iii. Flow caused by shrinkage and pressure gradients, and

iv. Flow caused by sequence of vaporization and condensation.

The attainment of critical moisture-content depends on the drying conditions (humidity and temperature) and the characteristics of the samples (shape, size, density, area and specific heat-capacity). Moisture in excess of free moisture-content, in equilibrium with the air, can only be removed upon prolonged contact of the sample with hot drying air.

The general theory of drying is based on the consideration of inert solid wetted with moisture and exposed to heated current of air. The air supplies the sensible heat, heat of vaporization and also acts as a carrier of the evaporated moisture. Thus drying is a process of simultaneous heat and mass transfer. For the purpose of analysis, drying is usually subdivided into two categories, namely;

i. Single kernel or thin layer drying: this is considered as the drying process involving material depth of not more than ten particles (depth$< 10 \ particles$) diameter.

ii. Deep bed drying: this consists of agglomeration of particles above ten particle diameter ($depth > 10 \ particle \ diameter$).

Since warming up period is often short and represents only 0.25% of the total drying period/time, it is often neglected in drying analysis.

2.16. Drying Rate Periods

The drying rate in crops is not constant throughout the whole period of drying. To understand this, the drying period is divided into short period of warming up, constant rate period, and falling rate period.

2.16.1. Warming-up period

The warming up period is the period when the usually lower temperature of the crops gets up to the temperature of the drying air. It is usually short and often neglected in drying analysis.

2.16.2. Constant rate period

During the constant drying-rate period, the surface of the sample behaves as free-water and drying continues as long as water is supplied to the surface as evaporation takes place. If moisture-movement within the solid is sufficiently rapid to maintain a saturated condition at the surface, and if heat is supplied by convection from warmer air only, the surface temperature is the wet bulb-temperature.

2.17 Drying kinetic models

In developing the thin-layer drying models, the required data consisted of the initial moisture content, moisture content of samples during the drying process, equilibrium

moisture content, drying air temperature and drying time. All of these required data were measured in the experiments, except for the equilibrium moisture content. Some researchers including Sacilik (2007), have suggested that when developing thin-layer drying models, the equilibrium moisture content of food can be assumed to be zero, since:

1) it is substantially less than the initial moisture content or

2) the relative humidity of the drying air fluctuates during drying. This assumption would always be correct if the drying temperature is not lower than 100°C.

However, if the drying temperature is below 100°C, this assumption will be valid solely at the beginning of drying process, because the moisture content of the sample is much higher than the equilibrium moisture content (Mt >> Me). However, when the sample is dried to a moisture content level that is close to its equilibrium moisture content, this assumption would lead to a significant deviation of the slope and linearity of the normalized drying curvez. The drying temperatures in the present study were in the range 60–80°C; thus, the equilibrium moisture contents were determined by drying a single layer of pumpkin seeds in a tray dryer at each temperature until the weights were constant.

Numerous studies have been conducted on the drying kinetics and product quality of foodstuffs that are undergoing isothermal convective drying, such as garlic, pumpkin, grapes, apple and orange skin (Madamba et al., 1996; Doymaz, 2007). Among the

theoretical, semi theoretical and empirical drying models reported in the literature, the most frequently used model for thin layer drying is the lumped parameter type such as the Newton equation. Kingsly et al., (2007) developed new simple but accurate analytical models for determining the mass transfer characteristics of different geometrically shaped products and presented a simple model of moisture transfer for multidimensional products. By considering the analogy between the heat diffusion and moisture transfer, drying time for infinite slab products was formulated. This analysis was extended to multidimensional products by introducing geometric shape factors.

The drying process depends on several parameters such as:

i.   the activity of water Aw of the product at the temperature Tp;
ii.   the drying air characteristics, such as the water partial pressure.

The study and modeling of the drying kinetics take into account the variation with time of heat and moisture transfers. As far as the moisture content M is concerned, its variation with time defines the drying rate:

$$-\frac{dM}{dt} = -\frac{1}{m_s}\frac{dm}{dt}$$ (2.8)

In the above relationship, m is the mass of the product sample at time t; $m_s = (m - m_w)$ is the dry mass; m is the mass of water in the sample. The drying rate is curve expressed as:

$$\frac{dM}{dt} = f(t)$$ (2.9)

It is often used to characterize the drying kinetics of a product. The first period in a drying process is a short transient phase, which is not always observed. It corresponds to a warming up stage. This transient period is followed by the constant rate drying phase. During this phase, the free water is evaporated, when it moves from inside the product to the surface. It is a period when the drying rate is constant. At the end of this phase, the moisture content M is equal to the critical moisture content M_{cr}. During this phase, it is assumed that the rate of the water removal from the surface of the product is equal to the one of heat transfer to the surface.

2.18. Psychometric of drying

Most dryers are of convective heated air type. In other words, hot air is used both to supply the heat for evaporation and to carry away the evaporated moisture from the product. Exceptions to this are freeze and vacuum dryers, which are used almost exclusively for drying heat-sensitive products though they tend to be significantly more expensive than dryers operated near to atmospheric pressure. Another exception is the emerging technology of superheated steam drying (Mujumdar, 2004). Drying with heated air implies humidification and cooling of the air in a well insulated (adiabatic) dryer. Thus, hygro-thermal properties of humid air are required for the design calculations of such dryers.

During the initial stage of drying, the rate of moisture loss can be considered as a function of some external parameters; namely, air-velocity in the chamber, drying air temperature, relative humidity and slice thickness(Majid *et al.,* 2011; Motevali *et al.,* 2012). Some of these factors may be difficult to vary and control.

2.19 Shrinkage ratio

Shrinkage is a common physical phenomenon of biomaterial drying, leading to change in organoleptical, textural and rehydration properties of the dried products, especially in fruits and vegetables. Many models have been developed to describe the shrinkage, including empirical and fundamental fitting of the experimental shrinkage data as a function of moisture content or moisture ratio. To describe the shrinkage of the food crops, volume ratio (V_R) and apparent density (g_t) were calculated as follows

$$V_R = V_t / V_o \qquad (2.20)$$

And $\qquad g_t = W_t / V_t \qquad (2.21)$

Where V_o is the initial volume,

$\qquad V_t$ *and* W_t are the volume and the weight of the material at a given time *t*.

Since the more the water removed the more contraction stresses are originated in the material, at a relative low drying rate, shrinkage of the material ideally equals the volume of removed water, therefore, it can be described by the linear empirical model as

$$V_R = aM_t + b \qquad (2.22)$$

Where *a* and *b* were the coefficient and the constant of the model, respectively.

Equally, the mass shrinkage ratio (S_R) is one of the most important structural variation appearing on crops due to weight loss and it is given by (Saeed *et al.,* 2008)**.**

$$S_R = W_t / W_o \qquad (2.23)$$

Where W_o is weight at initial time and W_t is weight at time t

2.20 Theoretical review

2.20.1 Effective moisture diffusivity

Wang and Brennan (1992) affirmed that drying of most food materials regularly took place in the falling rate period, which meant that the moisture transfer during drying was controlled by internal diffusion. The internal diffusion occurring during the falling rate period for most food materials is described by Fick's second law of diffusion (Crank, 1975).

$$\frac{\partial M}{\partial t} = D \, \nabla^2 M \qquad\qquad (2.24)$$

Where, D= diffusivity.

The analytical solution of Fick's second law of diffusion for slab-shaped material, with the assumptions of moisture transfer by diffusion, negligible shrinkage, and constant diffusion coefficients and temperature is provided by the Equation:

Therefore, on the assumption that the initial moisture-concentration (M_i) is uniform, the average moisture-content, M(t), of the product, after a drying time t, can be given by an analytical solution of the form (Jost, 1960),

$$\frac{\bar{M}(t)-M_e}{M_I-M_e} = \frac{8}{\pi^2}\left(\sum_{n=0}^{\infty} \frac{1}{(2n+1)^2} \exp\left[-\left(\frac{(2n+1)\pi}{2H}\right)^2 D_{eff} \, t\right]\right) \qquad (2.25)$$

where: D_{eff} is the effective moisture diffusion (m²/s), t is the drying time (s),

H is half-thickness of the slab (m).

But if $\frac{\bar{M}(t) - M_e}{M_i - M_e}$ is defined as moisture ratio (MR), then the equation can be written as:

$$MR = \frac{8}{\pi^2}\left(\sum_{n=0}^{\infty} \frac{1}{(2n+1)^2} \exp\left[-\left(\frac{(2n+1)\pi}{2H}\right)^2 D_{eff}\, t\right]\right) \tag{2.26}$$

Expansion of the first three terms (n = 0, 1 and 2) will produce Equation:

$$MR = \frac{8}{\pi^2}\left\{\exp\left[-\left(\frac{\pi}{2H}\right)^2 D_{eff}\, t\right] + \frac{1}{3^2}\exp\left[\left(\frac{3\pi}{2H}\right)^2 D_{eff}\, t\right] + \frac{1}{5^2}\exp\left[-\left(\frac{5\pi}{2H}\right)^2 D_{eff}\, t\right] + \right.$$

$$\left. \dots \right\} \tag{2.27}$$

This equation is derived on the assumption that D_{eff} and M_e are constants, but in reality D_{eff} varies with temperature and moisture-content, while M_e also varies with temperature. As supported by the observations of Sacilik (2007) and Saykova et al. (2009), it is noticeable that the first term of the series solution in Equation 5 will dominate the other terms.

Also, for long period of drying (t is sufficiently large), only the first-term in the series in the equation is significant (with $D_{eff}\, t/4H^2 > 0.02$, the error is less than 3 %) and hence,

$$MR = \frac{8}{\pi^2}\left\{\exp\left[-\left(\frac{\pi}{2H}\right)^2 D_{eff}\, t\right]\right\} \tag{2.27}$$

Taking the natural logarithm of the equation gives

$$\ln MR = \ln \frac{8}{\pi^2} - \left(\frac{\pi}{2H}\right)^2 D_{eff}\, t \tag{2.28}$$

that is

$$\ln MR = \ln (0.81057) - 2.4674 \left[\frac{D_{eff}\, t}{H^2}\right] \tag{2.29}$$

Hence, in the study, the effective moisture diffusivity D_{eff} will be determined by plotting the experimental data in terms of ln (MR) against drying time (t) and then using the slope in equation given

$$D_{eff} = \frac{-slope}{\left[\frac{2.4674}{H^2}\right]}$$
(2.30)

Solutions of the Fickian second law equation are summarized in table 2.4;

Table 2.1: Solutions of Fick's second law of Diffusion for some simple geometry

Geometry of the material	Boundary conditions	Dimensionless average free moisture content
Flat plate of thickness 2b	t=0;-b<z<b; M=M$_o$ $t > 0; z = \pm b; M = M^*$	$M = \frac{8}{\pi^2} \sum_{n=1}^{\infty} \frac{1}{(2n-1)} \exp\left[-(2n-1)^2 \frac{\pi^2}{4b}\left(\frac{D_L t}{b}\right)\right]$
Infinitely long cylinder of radius R	t=0;0<r<R; M=M$_o$ $t > 0; r = R; M = M^*$	$M = 4 \sum_{n=1}^{\infty} \frac{1}{R^2 \alpha_n^2} \exp(-D_L \alpha_n^2 t)$ Where α_n are positive roots of the equation $J_0(R\alpha_n) = 0$
Sphere of radius R	t =0;0<r<R; M=M$_o$ t > 0; r=R; M=M*	$M = \frac{6}{\pi^2} \sum_{n=1}^{\infty} \frac{1}{n^2} \exp\left[\frac{-n^2\pi^2}{R}\left(\frac{D_L t}{R}\right)\right]$

(Source: Pakowski and Mujumdar, 1995)

2.20.2 Activation energy of the drying process

The activation energy and rate of a reaction are related by the following Arrhenius type equation:

$$k = A \exp(- E_a / RT)$$ (2.30)

where k is the rate constant, A is a temperature-independent constant (often called the frequency factor), E_a is the activation energy, R is the universal gas constant, and T is the temperature.

This relationship was derived by Arrhenius in 1899. Because the relationship of reaction rate to activation energy and temperature is exponential, a small change in temperature or activation energy causes a large change in the rate of the reaction.

Activation energies are usually determined experimentally by measuring the reaction rate k at different temperatures T, plotting the logarithm of k against $1/T$ on a graph, and determining the slope of the straight line that best fits the points. If the activation energy in a reaction is low, a greater proportion of the collisions between reactants will result in reactions. If the temperature of the system is increased, the average heat energy is increased, a greater proportion of collisions between reactants result in reaction, and the reaction proceeds more rapidly. A catalyst increases the reaction rate by providing a reaction mechanism with lower activation energy, so that a greater proportion of collisions result in reaction.

In drying process the effective moisture diffusivity (D_{eff}) is analogous to the rate constant(k).

According to Suarez et al. (1980) and Roberts et al. (2008), temperature dependence of the effective moisture diffusivity can be presented by an Arrhenius relationship.

$$D_{eff} = D_o exp\left[-\frac{E_a}{RT}\right] \quad\quad (2.31)$$

where: D_o is the pre-exponential factor of the Arrhenius equation in m^2/s,

Ea is the activation energy in kJ/mol,   R is the universal gas constant (8.314 × 10-3 kJ/mol K),   T is the absolute air temperature (°K).

Linearizing the equation by taking the natural logarithm gives

$$\ln D_{eff} = \ln D_o - \frac{E_a}{R}\cdot\frac{1}{T} \quad\quad (2.32)$$

The pre-exponential factor of the Arrhenius equation and the corresponding activation energy were determined by using the data of effective moisture diffusivities and absolute air temperatures to plot ln (D_{eff}) against 1/T.

The Activation energy Ea is calculated using the slope of the line as follows

$$E_a = -\text{ (slope x R)} \quad\quad (2.32)$$

The correlation Coefficient is used to determine the validity of the equation

2.20.3 Convective heat transfer coefficient

The convective heat transfer coefficient in open sun drying can be determined using the expression for Nusselt Number (Nu)

$$Nu = \frac{h_c X}{K_v} = C(Gr.Pr)^n \qquad (2.33)$$

Hence

$$h_c = \frac{K_v}{X} C(Gr.Pr)^n \qquad (2.34)$$

The rate of heat utilized to evaporate Moisture is given as

$$Q_e = 0.016 h_c \left[P(T_c) - \gamma P(T_e) \right] \qquad (2.35)$$

Substituting gives

$$Q_e = 0.016 \frac{K_v}{X} C(Gr.Pr)^n \left[P(T_c) - \gamma P(T_e) \right] \qquad (2.36)$$

The moisture evaporated can be given by the following equation

$$M_{ev} = \frac{Q_e}{\gamma} t.A_t \qquad (2.37)$$

Where M_{ev} = moisture evaporated

γ = latent heat of vaporization of water, $\qquad$ A_t = area of the tray, $\qquad$ x = constant

$\qquad$ T = time interval (Anil anad Tiwari, 2006; Tribeni and Tiwari, 2008)

On substituting

$$M_{ev} = 0.016 \frac{K_v}{\gamma X} C(Gr.Pr)^n \left[P(T_c) - \gamma P(T_e) \right] t A_t \qquad (2.38)$$

Let

$$Z = 0.016 \frac{K_v}{\gamma X} \left[P(T_c) - \gamma P(T_e) \right] t A_t \qquad (2.39)$$

Substituting and rearranging gives

$$\frac{M_{ev}}{Z} = C(Gr.Pr)^n \qquad (2.40)$$

Taking natural logarithm of both sides

56

$$ln\left[\frac{M_{ev}}{Z}\right] = \ln C + n \ln(Gr.Pr) \tag{2.41}$$

Hence, the values of C and n can be determined by linear regression regression analysis

because this equation represents a linear equation of the form $Y = mX_o + C_o$

Where $Y = ln\left[\frac{M_{ev}}{Z}\right]$, $m = n$, $X_o = \ln [Gr.Pr]$, $C_o = \ln C$

The physical properties of humid air such as specific heat (C_v), thermal conductivity

(K_v), density (ρ_v), partial pressure P(T) can be determined using the following equations

where T_1 is taken as the average of crop temperature (T_c) and the temperature just above

the crop surface (T_e)

$$P(T) = \exp\left[25.317 - \frac{5144}{(T_1 + 273.15)}\right] \tag{2.42}$$

$$\rho_v = \frac{353.44}{T_1 + 273.15} \tag{2.43}$$

$$K_v = 0.0244 + 0.6773 \; x \; 10^{-4}T_1 \tag{2.44}$$

$$C_v = 999.2 + 0.143T_1 + 1.101 \; x \; 10^{-4}T_1^2 - 6.758 \; x \; 10^{-8}T_1^3 \tag{2.45}$$

$$\mu_v = 1.718 \; x \; 10^{-5} + 4620 \; x \; 10^{-8}T_1 \tag{2.46}$$

(Anil & Tiwari, 2006; Tribeni & Tiwari, 2008)

2.20.4. Efficiency of Dryers

There are different ways of measuring the efficiency of a dryer. These include thermal

efficiency, dryer efficiency, pick-up efficiency. In solar dryers such terms as collection

efficiency and system drying efficiency are common. Generally, drying efficiency is

defined as the ratio of the energy required to evaporate the moisture to the heat supplied to the dryer (Igbeka, 2013). It is a measure of the overall effectiveness of the drying system.

2.20.4.1. System drying efficiency

The system drying efficiency (η_p) describes how effectively the input energy to the drying system is used in the product drying. For dryers, the heat supplied to the dryer is the solar radiation incident on the plane of the collector. The system drying efficiency is calculated using equation

$$\eta_p = \frac{M_e.L}{A_c.I_c.t} \qquad (2.47)$$

Where

M_e is the moisture content,   L is the latent heat of vaporization

A_c is drying area, I_c is solar radiation,   t is time interval

For solar dryer, the transmittance of the solar collector increases the efficiency of the solar dryer

$$\eta_p = \frac{M_e.L}{A_c.I_c.t.\tau} \qquad (2.48)$$

Where τ = the transmittance of the solar collector

2.20.4.2. Thermal efficiency

The thermal efficiency of the dryer is the ratio of temperature input to the temperature utilized in drying. It is mathematically expressed as follow:

$$E_{ff} = \frac{T_p - T_{out}}{T_p - T_a} \qquad (2.49)$$

Where, T_p is Plenum air temperature (hot air entering into the drying chamber) ^oC

T_{out} is Out let air temperature (air leaving through the chimney), ^oC,

T_a is Ambient temperature, ^oC

2.20.5. Specific Energy Consumption (SEC)

Specific Energy Consumption is the energy required to eliminate 1 kg of water (moisture) from wet materials during heated-air drying. The total energy consumption, E_t was calculated using the relation

$$E_t = (A.V.\rho_a.C_a.\Delta T).t \qquad (2.50)$$

Where

A is the area of drying tray, V is the drying air speed, ρ_a is the air density, C_a is the specific heat capacity of air, ΔT is the temperature difference and t is the time of drying. (Motevali *et al.,* 2012; Mohsen, 2016).

The Specific Energy consumption, SEC, was calculated using the relation

$$SEC = \frac{E_t}{M} \qquad (2.51)$$

Where M is the mass of water removed (Motevali *et al.,* 2012)

2.21 Review of related works on drying

Dhanore & Jibhakate (2014) used "A Solar Tunnel Dryer for Drying Red Chilly as an Agricultural Product". The solar tunnel dryer consists of different parts such as drying chamber, collector area and chimney. The solar tunnel dryer is designed, developed & commissioned at Kavikulguru Institute of Technology and Science, Ramtek of Nagpur District in Maharashtra. The drying chamber is covered with UV-stabilized polythene sheet, which is available at the local market. The solar tunnel dryer having semi-cylindrical shape for increasing absorption of solar radiation. The dryer are made to open and close easily for the functions of spreading the drying product at the beginning of the day and cleaning the absorber surface and trays. Base of the tunnel dryer is covered with thermal insulation of one inch, in order to reduce the heat loss. The initial moisture content of the red chilly was 75% and the drying starts with 5kg of the chillies. The ambient temperature during the drying varied from a minimum of 33.7^{o}C to a maximum of 44.5^{o}C with the corresponding average temperature inside the solar tunnel dryer ranging from 40.46^{o}C to 62.9^{o}C. On an average, a total drying time of 24 hours (3 days) are required for solar tunnel dryer to reduce the moisture content of chilly from 75% to a final moisture content of 5% while the open sun drying required on an average 40 hours (5 days) to obtain same level of moisture content which showed a net saving in drying time. The system drying efficiency is defined as the ratio of the

energy required to evaporate the moisture to the energy supplied to the dryer. Solar drying achieves higher drying rates compared with sun drying.

Weerachet (2011) studied the "kinetics and temperature dependent moisture diffusivities of pumpkin seeds during drying". He used both a tray drier and a fluidized bed dryer (FBD) at drying temperatures of 60, 70 and 80°C. Both dryers were operated in the batch mode with an air velocity of 1.8 m/s and a bed depth of 3cm for the FBD and an air velocity range of 0.23 to 0.28 m/s for the tray drier. The seeds were dried until the moisture content was below 5% w.b. The seeds were collected at specified time interval and the moisture content was determined using the oven method. Hence, the moisture ratio was calculated. The data from the drying experiments were fitted into six mathematical models by a non-linear regression procedure. The statistical validity of the models was evaluated and compared using the coefficient of determination (R^2) and the root mean square error (RMSE). The closer the R^2 value is to unity and the lower the RMSE, the better and more acceptable the model. The result showed that the Page model and the Two-compartment model were the best drying models. Furthermore, at the same drying temperature, the drying rates of pumpkin seeds in the FBD were visibly faster than those from tray drying. The Effective moisture diffusivities was determined using the analytical solution of Fick's second law of diffusion for slab-shaped material with the assumptions of moisture transfer by diffusion. The effective moisture diffusivities of pumpkin seeds with hulls during drying in the FBD and the tray dryer were in the range 37.62×10^{-11} to 50.96×10^{-11} m^2/s and 7.69×10^{-11} to 36.40×10^{-11}

m^2/s, respectively. They increased with increasing drying temperature. The effective moisture diffusivities were higher for drying in the FBD. The activation energy (E_a in KJ/mol) was determined using temperature dependency of the Arrhenius relation. The activation energies of pumpkin seeds were 15 and 62.12 KJ/mol for the FBD and the tray dryer respectively, indicating that the minimum energy required to start moisture diffusion during drying in the FBD was lower than that for tray drying. Sensory test was carried out using the nine-point Hedonic scale on appearance, colour, aroma, taste, texture, overall liking. According to the sensory test results, the pumpkin seed samples dried in the present study were acceptable to the consumers to a comparable level with products sold in the supermarket.

Kulsum et al (2014) investigated the "Mathematical Modelling of Thin Layer Drying Kinetics of Biodegradable Pellets". The pellets were from Paddy husk, Potato peels and Banana peels. The Pellets were prepared by extrusion technology using glycerol and cashew nut shell liquid as plasticizers and were dried in a chamber with constant air circulation 1.5 m/sec. The drying experiments carried out in a tray dryer at selected three air drying temperatures (60, 70 and 80°C) to study the drying characteristics of the pellets. The drying cabinet was equipped with an electrical heater, a fan, and temperature indicators. The drying took place in the falling rate period and the drying rate decreased continuously throughout the drying period. Some mathematical models were used to describe the drying rate and the best selection was based on higher value of correlation coefficient (R^2), lower values of chi-square (X^2) and lower value of Root

mean square error (RMSE). Based on these, the study revealed that the Midilli model was the best mathematical model. Arrhenius equation was used to determine the activation energy which indicated that the maximum activation energy was 96.63 KJ/mol for Paddy husk, 31.65KJ/mol for Banana peel and 45.92 KJ/mol for Potato peel.

Paulo et al (2006) carried out a research on "Drying characteristics and kinetics of coffee Beny" using a laboratory scale mechanical drier under the drying air temperatures of 40^0, 50 and 60^0 and corresponding Relative Humidity of 22%,14% and 7%. For monitoring the drying process, samples of 30g were taken after 0.5,1,2,4,6,8 and 10 hours after the drying operation started. The moisture content was determined in air oven until constant weight was achieved. The objective of their work was to verify the temperature effect on coffee fruit drying, to obtain and to model the thin layer drying, also for determining the effective diffusivity coefficient and the activity energy during the coffee drying under different drying air temperature and relative humidity conditions. An Analytical method of determining the equilibrium moisture content X_e was developed using the moisture content x obtained at different times of drying. The dependency of the effective Diffusivity coefficient on temperature for coffee fruit thin drying was evident as the values increase from 2.91 x 10^{-10} , 3.57 x 10^{-10} and 4.96 x 10^{-10} ms^{-1} as temperatures increased from 40 to 50 and 60^0C respectively. It can also be observed that the activation energy for water diffusion in the coffee fruits during their drying process was 22.619KJ mol^{-1} . The mathematical modeling of the drying process was conducted using the values of coefficient of Determination (R^2), the mean relative

error (P) and the estimated errors (SE) for the different model equations. The page model was selected as the best model based on its R^2 being higher than 98%, its simplicity and the number of coefficients. Equally, in the page model, the drying content "K" decreased exponentially as the drying air temperature increases. Also, it was verified that the page model coefficient 'n' increased linearly with the increase of the drying air temp which could be estimated through the following expression   n = 0.4008 + 0.0069T

Saeid *et al.,* (2011) investigated the thin layer drying behavior of sour pomegranate arils using microwave, vacuum, and infrared methods as well as convection drying (three treatments including control and microwave pretreatments at 100 and 200 W) was studied. Effect of these drying methods on drying rate, effective moisture diffusion and activation energy was analyzed. It was observed that microwave pretreatment increases drying rate and effective moisture diffusion while it decreases activation energy. The highest values of drying rate and effective moisture diffusion were 0.965 g/min and 7.709×10^{-10} m^2/s obtained with pretreatment power of 200 W at air temperature and velocity of 70 °C and 1.5 m/s. while the lowest values were 0.082 g/min and 0.856×10^{-10} m^2/s for the control samples at 45 °C temperature and 0.5 m/s air velocity. Effective diffusion coefficient of pomegranate arils was in the range of 6.77×10^{-10} to 52.5×10^{-10} m^2/s, 3.43×10^{-10} to 29.19×10^{-10} and 4×10^{-10} to 32×10^{-10} m^2/s for vacuum, microwave and IR dryers, respectively. Activation energy for pomegranates in the vacuum dryer was 52.83 kJ, while in the microwave dryer it was 23.563(W/g). Activation energy in

the microwave dryer was calculated using the Arrhenius exponential model. A comprehensive comparison of the various dryers revealed that microwave pretreatment combined with convective drying performed best for the drying of pomegranate arils taking into consideration the drying rate, effective moisture diffusion and activation energy.

Amin *et al.,* (2001) studied the thin-layer drying kinetics of bell pepper in a laboratory scale convective dryer. Experiments were performed at air temperatures of 40, 50, 60, 70, and 80ºC and constant air velocity of 2 m/s. In order to select a suitable form of the drying curve, 12 different thin layer drying models were fitted to experimental data. The high values of coefficient of determination and the low values of reduced chi-square and root mean square error indicated that the Logarithmic model could satisfactorily illustrate the drying curve of bell pepper. The Logarithmic model had the highest value of R^2 (0.9929), the lowest $\chi 2$ (0.00003497) and RMSE (0.00481743). The Logarithmic model was found to satisfactorily describe the drying behavior of bell pepper. Fick's second law was used to calculate the Effective moisture diffusivity. The moisture diffusion coefficient varied between 1.7×10^{-9} and 11.9×10^{-9} m^2/s for the given temperature range and corresponding activation energy was 44.49 kJ/mol.

Amiri *et al.,* (2011) reported his work on the thin layer drying characteristics of high moisture corn under fixed, semi fluidized and fluidized bed conditions with high initial moisture content (66.82% wb) in a laboratory fluidized bed convective dryer at air temperatures of 50, 65, 80 and 95°C. In order to find a suitable drying curve, seven thin

layer-drying models were fitted to the experimental data of moisture ratio. Among the applied empirical models, Midilli *et al.* model was the best for drying behavior prediction in corn thin layer drying. This model presented high values for correlation coefficient (R^2). Fick´s second law was used to compute moisture diffusivity with some simplifications. Computed values of moisture diffusivity varied at the boundary of 4.87 x 10^{-11} – 2.90 x 10^{-10} m2 s^{-1} and 1.02 x 10^{-10} – 1.29 x 10^{-9} m2 s^{-1} during the first and second drying falling-rate, respectively. Values of effective moisture diffusivity for corn were also increased as input air temperature was increased. Value of activation energy varied from a minimum of 18.57 to a maximum of 50.74 kJ mol^{-1} from 50 to 95°C with drying conditions of fixed to fluidized bed. Specific energy consumption (SEC) for thin-drying of high moisture corn was found to be in the range of 0.33×10^6 – 1.52×10^6 kJ kg^{-1} from 50 to 95°C with drying condition of fluidized and fixed bed, respectively. Increase in air temperature in each air velocity caused decrease in SEC value. These corn properties would be necessary to design the best dryer system and to determine the best point of drying process.

The thin layer drying behaviour of ginger slices in a laboratory dryer was examined by Tinuade et al (2014). The slices of 5 mm, 10 mm and 15 mm thicknesses were dried using heated ambient air at temperatures from 40 to 70 ºC and air velocity of 1.5 m/s. The effects of drying air temperature and slice thickness on the drying characteristics, drying time and energy requirement of drying process was determined. The results have shown that an increase in the drying air temperature causes shorter drying times.

Thinner slices also causes a shorter drying time. The effective moisture diffusivity values increased from 3.36814×10^{-10} m2/s to 5.82524×10^{-9} m2/s while the activation energy values for different slice thickness of ginger varied from 196.15 to 198.79 kJ/mol. The total needed energy varied from 735.3 to 868.5 kWh while the value of specific energy requirement varied from 3676.6 to 4342.4 kWh/kg respectively.

Afolabi & Tunde studied the "effect of drying conditions on energy utilization during cocoyam drying". Cocoyam samples soaked in sodium metabisulphite (SM) and water blanched (WB) were oven dried at 50, 60 and 70°C and microwave power levels of 385, 540 and 700 W while untreated samples were sun dried. The effects of drying on selected properties of cocoyam were studied. The drying time generally reduced with increase in drying temperature and power level used. The use of SM pretreatment resulted in lower drying times compared with WB pretreatment. Effective moisture diffusivity values (D_{eff}) for all the drying conditions varied from 5.27×10^{-8} to 2.07×10^{-6} m^2/s and SM samples had higher values than WB samples. Activation energy values for oven drying were 37.41 kJ/mol and 61.79 kJ/mol and that for microwave drying were 38.59 and 41.91 W/g for SM and WB samples respectively. The energy consumption varied from 30 to 50 kWh for oven drying and 308 to 396.7 Wh for microwave drying while that of specific energy requirement varied from 86.2 to 106.5 kWh/kg and 1.49 to 2.03 kJ/kg water for oven drying and microwave drying respectively.

Nwajinka *et al.,* (2014) reported on the "study of thin layer drying characteristics of cocoyam (X. Sagittifolium) slices" using hot air convective dryer. The drying experiments were performed at five different drying temperatures of 65, 70, 75, 80 and 85ºC at air velocity of 2 m/s with relative humidity of 50, 40, 39.5, 33.8 and 22.2% respectively. Non linear regression analysis was used to model the drying of the cocoyam slices. Drying pattern was observed to be in the falling rate period. Out of the four thin-layers drying models investigated (Newton, Page, Henderson and Pabis and Logarithmic), Logarithmic model best described the drying parameters of cocoyam slices with high values of coefficient of determination of 0.973, 0.988, 0.991, 0.999 and 0.99. The moisture diffusivities at the drying temperatures varied from 2.53×10^{-5} m^2/s to 1.09×10^{-5} m^2/s. The results compared well with works on similar materials.

Samira et al (2015) studied the "mathematical modeling of drying of potato slices in a forced convective dryer based on important parameters". The effect of air temperature, air velocity, and sample shapes (circle and square with the same cross-sectional area) on kinetic drying of potato slices in a tunnel dryer was investigated experimentally and a suitable drying model was developed. The experiments of drying of potato slices were conducted at an air temperature of 45–70°C with an air velocity 1.60 and 1.81 m/sec. Results showed that drying temperature was the most effective parameter in the drying rate. The influence of air velocity was more profound in low temperature. The time for drying square slices was lower compared to the circle ones. Furthermore, drying data were fitted to different empirical models. Among the models, Midilli–Kucuk was the

best to explain the single layer drying of potato slices. The parameters of this model were determined as functions of air velocity and temperature by multiple regression analysis for circle and square slices. Various statistical parameters were examined for evaluating the model.

Amiri (2012) studied the "Modeling Some Drying Characteristics of High Moisture Potato Slices in Fixed, Semi Fluidized and Fluidized Bed Conditions". Drying properties of high moisture potato slices with initial moisture content of about 4.06 (db) under thin layer fixed, semi fluidized and fluidized bed conditions were studied. Drying air temperatures of 40, 50, 60 and 70°C were applied in experiments using a laboratory fluidized bed convective dryer. In order to predict the drying behavior of potato slices, seven thin layer drying models were applied from where finally Midilli et al. model was selected as the suitable one, based on comparative indices. Effective moisture diffusivity of the potato slices varied between 4.29×10^{-9} and 15.70×10-9 m^2 s^{-1} for fixed and fluidized bed conditions, respectively. Moisture diffusivity values of the slices were increased as the drying air temperature levels increased. Activation energy values varied between 15.88 and 24.95 kJ/mol. Minimum and maximum values of activation energy were obtained at minimum fluidized and fixed bed conditions, respectively. Consumption of specific energy for thin layer drying of high moisture potato slices was obtained between 0.45×10^5 and 1.64×10^5 (kJ kg-1). Increase in the drying air temperature in each bed condition caused increase in energy consumption. The maximum value of energy consumption was obtained at fluidized bed conditions.

Dagde & Nmegbu (2014) investigated the "The mathematical model of a batch tray dryer for the drying of potato chips using hot air medium". During this processes, the conservation principle was applied to the fundamental quantities of mass of moisture in Potato, mass of moisture (humidity) in air and energy of potato and energy in air. The model equations were solved using the fourth order Rungekutta algorithm and implemented in a visual basic program. The results from the program shows that the air temperature initially drops as it enters into the dryer due to the high moisture content in the potato but later starts to increase and stabilized as the time in the dryer progresses and also the temperature of the potato increases as the time in the dryer increases. From the results it was also found out that as the time spent in the dryer increases, the moisture content in the food decreases while the air humidity increases. These predictions are in agreement with cited available literature. Functional parameters in the dryer such as quantity of heat supplied and air flow rate were also simulated for process control and optimization.

2.22 Surface Response Methodology

Response surface methodology (RSM) is an empirical statistical technique employed for multiple regression analysis by using quantitative data obtained from properly designed experiments to solve multivariate equations simultaneously. A full factorial design, which includes all possible factor combinations in each of the factors, is a powerful tool for understanding complex processes for describing factor interactions in multifactor systems. (Rajeshkannan *et al.,* 2010). The relationships which link inputs with outputs

are complex and difficult to describe with elemental mathematical models. Therefore, the need arises for tools that are capable of more complex modeling and that achieve maximum refinement of the role of each variable in the system as well as the synergetic and/or antagonistic interrelationships between the same variables. The Response Surface Methodology (RSM) emerged in the 1950s within the context of Chemical Engineering in an attempt to construct empirical models able to find useful statistical relationships between all the variables making up an industrial system. This methodology is based on experimental design with the final goal of evaluating optimal functioning of industrial facilities, using minimum experimental effort. Here, the inputs are called factors or variables and the outputs represent the response that generates the system under the causal action of the factors. Afterwards, the use of the RSM was shown in the design of new processes and products. In recent years it is being applied successfully in other scientific fields such as biology, medicine, and economy. Myers *et al.,* (2004) has exhaustively reviewed the literature in the sense, describing the developments and applications of this methodology. Very recently, RSM has been used even to validate new experimental methods (Jurado *et al.,* 2003)

Response Surface Methodology is a collection of mathematical and statistical techniques used for the modeling and analysis of problems in which a response of interest is influenced by several variables and the objective is to optimize the response (output variable) which is influenced by several independent variables (input variables or factors). Different levels or values of the operating conditions comprise the factors in each experiment (Russell, 2009). Some may be categorical (e.g., the supplier of raw

material) and others may be quantitative (feed rates, temperatures, time, etc). In practice, categorical variables must be handled separately by comparing our best operating conditions with respect to the quantitative variables across different combinations of the categorical ones. The fundamental methods for quantitative variables involve fitting first-order (linear) or second-order (quadratic) functions of the predictors to one or more response variables, and then examining the characteristics of the fitted surface to decide what action is appropriate (Russell, 2009).

The designs of the response surface methodology (RSM) are those in which problems are modeled and analyzed; in these problems the response of interest is influenced by different variables. The RSM is widely used as an optimization, development, and improvement technique for processes based on the use of factorial designs — that is, those in which the response variable is measured for all the possible combinations of the levels chosen of the factors.

Two major Response Surface optimization designs are the Central Composite Design (CCD) and Box-Behnken Design (BBD). They are available to generate standard response-surface designs. The most popular response-surface design is the central-composite design (CCD), of Box and Wilson. The blocks in a CCD are of two types----one type, called a "cube" block, contains design points from a two-level factorial or fractional factorial design, plus center points; the other type, called a "star" block, contains axis points plus center points.

2.23 Artificial Neural Network

An Artificial Neural Network (ANN) is an information processing paradigm that is inspired by the way biological nervous systems, such as the brain, process information. Artificial neural networks are mathematical tools whose functioning is inspired by that of the human brain (Assidjo *et al.*, 2008). The key element of this paradigm is the novel structure of the information processing system. It is composed of a large number of highly interconnected processing elements (neurones) working in unison to solve specific problems. An outstanding feature of neural network is the ability to learn the solutions of problems from a set of examples, and to provide smooth and reasonable interpolations for new data. Also, in the field of food process engineering, it is a good alternative for conventional empirical modeling based on polynomial, and linear regressions (Ngankham and Ram, 2011). ANNs, in an appropriate form, can also provide reasonable solutions in the event of technological faults. An ANN has the ability of relearning to improve its performance if new data are available. One advantage of ANN modeling is that it can accommodate multiple input variables to predict multiple output variables even without prior knowledge of the process relationships (Mojtaba *et al.*, 2012).

Neural network modeling is essentially black box in nature. The capability of neural network to learn non-parametric or structure-free approximations is its strength, but this is also its weakness. In order to promote neural networks, many different ways have been employed. Many new learning algorithms have been designed and developed to train neural networks. The certain ways focus mainly on the size of the neural network,

namely the number of hidden layers and its corresponding number of neurons (Mousavi and Javan, 2009).

Recently, there is an upsurge in the application of ANN in optimizing the drying of agricultural products. ANN has been applied in drying of Carrot cubes (Aghbashlo *et al.,* 2011), Pistachio nuts (Omid *et al.,* 2009), coconut (Assidjo et at, 2008), apple (Mousavi and Javan, 2009), rough rice (Mousavi and Javan, 2009).

2.24 Hedonic Scale

The most widely used scale for measuring food acceptability is the 9-point hedonic scale. David Peryam and colleagues developed the scale at the Quartermaster Food and Container Institute of the U.S. Armed Forces, for the purpose of measuring the food preferences of soldiers. The scale was quickly adopted by the food industry, and now is used not just for measuring the acceptability of foods and beverages, but also of personal care products, household products, and cosmetics (Juyun *et al.,* 2009).

The 9-point hedonic scale, also known as degree-of-liking scale, is the most common hedonic scale for measuring product liking by consumers. Differently coded samples are presented to consumer panelists one at a time and they are asked to rate their hedonic response on the scale that can be in a vertical or horizontal line without affecting results (Juyun *et al.,* 2009).

3.24.1 Properties of Hedonic scale

The 9-point hedonic scale is a balanced bipolar scale around neutral at the center with four positive and four negative categories on each side. The categories are labeled with phrases representing various degrees of effect and those labels are arranged successively

to suggest a single continuum of likes and dislikes. The descriptors are intended to help not only subjects to respond accordingly but also to help experimenters interpret the mean value of responses in terms of degree of liking/disliking. One of the concerns about the scale during its development was whether its presentation format, i.e., long vs. short lines, vertical vs. horizontal orientation, or beginning with like vs. dislike, had effects on subjects' responses (Juyun, 2011).

3.24.2 Advantages of Hedonic scale

The primary reason for the wide acceptance of the 9-point hedonic scale is that, compared to other scaling methods (e.g., magnitude estimation), its categorical nature and limited choices make it easy for both study participants and researchers to use. Its simplicity further makes the 9-point hedonic scale suitable for use by a wide range of populations without an extensive training (Sukanya and Michael, 2014).

For researchers, data handling of the 9-point hedonic scale is also easier than other techniques which require measuring lines or recording magnitude estimates that may include fractions, although this practical matter is of diminishing importance given the development of computerized programs. More importantly, it has been shown that simple category scales are as sensitive as other scaling techniques. Therefore, when the primary concern of a study is measuring hedonic differences among foods, beverages, and consumer products and predicting their acceptance, the 9-point hedonic scale has proven itself to be a simple and effective measuring device (Juyun *et al.,* 2009).

CHAPTER THREE

MATERIALS AND METHODS

3.1 Preparation of samples

The cocoyam and potato were purchased from source in Awka South, Anambra State, Nigeria and properly identified by the Department of Botany, Nnamdi Azikiwe University, Awka. Other chemicals used were also obtained from Ananbra State, Nigeria and were of analytical grade. The cocoyam and potato tubers were washed, sliced to the appropriate thickness and then washed again to remove dirt.

3.2 Experimental procedure of the drying process

3.2.1 Determination of the diameter, surface area and sphericity:

In order to determine some physical properties of the food materials, 10 samples were picked. For each individual sample, three principal dimensions, namely major diameter (L), intermediate diameter (W) and minor diameter (T) will measured using an electronic micrometer (model QLR digit-IP54, China) with an accuracy of 0.001 mm. Because of the irregular shape of the materials, only the greatest values of both width and thickness were taken.

3.2.2 Instrumentation

The surface morphology was evaluated using the Scanning Electron Microscopy while the functional groups present were determined using the Fourier Transform Infra-Red. Temperature readings were taken with LCD Multi-Thermometer (Mextech) with mean

deviation of $\pm$ 1°C, + 2°F. All the mass measurements were obtained using LabTech BL7501 Electronic Compact Scale with mean deviation of $\pm$ 0.1g. Measurements involving length were carried out using Raider Digital Caliper with mean deviation + 0.1mm. The Oven drying experiment was carried out using Lab-Tech Oven 14 by 14 with Serial Number 03108 and rating 500 Watts.

3.2.3 Determination of Moisture content

The moisture content determinations were conducted in duplicate by the oven method in accordance with AOAC (2000) at a temperature of 120°C for 10 hours. This method was used for both cocoyam and potato in all the methods for proximate analysis for proximate analysis.

$$MC = \frac{M_1 - M_2}{M_1} \; x \; 100 \tag{3.1}$$

Where

    MC is the moisture content of the sample after drying.

    M_1 is the initial mass before drying

    M_2 is the mass after oven drying

For any weight of the sample at any time, the moisture content at that weight is determined using equation 3.2:

$$M_{t(db)} = M_o \%_{(db)} - \left(\frac{100(W_o - W_t)}{(1 - M_{o(wb)})W_o} \right) \tag{3.2}$$

Where,

$M_{t(db)}$ is Moisture content at any time %(db), M_o% (db) is initial moisture content % (db), M(db) is initial moisture content % (wb), W_t is weight of sample at any time, g and W_o is initial weight of sample, g

After each drying experiment, the sample moisture content was determined and termed the final moisture content. The total percentage of moisture removed which is the percentage of moisture content in the sample is calculated using equation 3.3

$$m = \frac{m_i - m_f}{m_i} \; x \; 100 \qquad\qquad (3.3)$$

Where m_i is initial moisture content and m_f is final moisture content

3.3 Sun drying

A sample of the different food crops each weighing 100g was spread on a paper plate on a concrete floor in the sun. Thermometer was used to measure the peak temperature of drying every day. Hygrometer was used to measure the wet and dry bulb temperatures of the surrounding. Using psychometric chart, the relative humidity of the surrounding and oven were known. The sample was sun dried between 9.00 a.m. and 3.00 p.m. every day. At the end of the drying period every day, some quantities of the sample were taken and placed in the oven for 16 hours with the oven temperature set at 103 ^{o}C to determine the moisture content in the sample until the moisture content was reduced considerable to about $6 - 8$ %

3.4 Oven drying

Triplicate samples of the food crops, each weighing 100 g were placed in the sample container and then placed in the oven with the oven temperature set at 35 ^{0}C with known initial moisture content. Hygrometer was used to measure the wet and dry bulb temperatures of the surrounding. Using psychometric chart, the relative humidity of the surrounding and oven were known. At every 15 minutes, each sample weight was known and recorded and the corresponding moisture content determined. This experiment was continued until the moisture contents of the samples were reduced to about 6 - 8 %. The experiment was repeated with oven temperatures set at 40 ^{0}C, 50 ^{0}C, 60 ^{0}C and 70 ^{0}C each time. The equilibrium moisture content (E.M.C.) for each drying temperature was determined by drying until relatively, no further change in weight of the samples was observed.

3.5 Solar drying

The solar dryer consists of the solar collector, the drying chamber, the air blower for regulating the speed of air, etc.

One of the essential components of the solar collector is the transparent glass cover. The solar collectors are usually called Flat plate collectors. Solar collectors usually have one or more glass covers. Glass easily transmits short-wave radiation. This implies that it poses no interference to incoming solar radiation. Once the sun's energy has passed through the glass, it will be absorbed by the material inside, usually painted black. The

heat cannot be radiated back outside the solar collector. The glass acts like a heat trap that traps heat energy into the drying chamber.

The food crops were sliced and appropriate weighed samples (between 100g to 400g) used. These were kept for drying in three replications. The weighed slices were taken in paper plates and kept inside the solar dryer platform. Observations on loss in weight and colour change in each sample were recorded at the particular interval of 15 minutes in solar drying.

Temperature and relative humidity in the solar drying was recorded throughout the drying period using hygrothermometer or Hygrometer was used to measure the wet and dry bulb temperatures of the surrounding and then using psychometric chart, the relative humidity of the surrounding and the solar dryer were known.

3.6 Conventional hot-air dryer

The variable parameters to be considered in the experiments were the moisture content, drying air velocity, relative humidity and temperature. The experiments were conducted at five air flow rates (1.0, 1.5, 2.0, 2.5 and 3.0 m/s).

Three replicates each, of the experiments, were conducted to reduce experimental error. 100g of the sample was used for each run of the experiments. The fan and heater were started and the drying temperature and air flow were allowed to run without load until stabilized condition was observed, when all the indicators are steady at a set value. Thereafter, the drying chamber was loaded with the samples for the experiments. The sample was weighed every fifteen minutes for the first one hour, then every thirty minutes for subsequent measurements until steady weights were observed in two or more consecutive weighing. The initial weight of the trays was subtracted from the weight of sample plus drying trays at each interval to note the weight loss of the sample.

Drying was continued until the moisture content of the sample reached equilibrium with the drying air. This state was observed when two or three consecutive weighing showed no significant variation or change in value. The average moisture content of the samples for each weighing period was calculated based on the initial mass and final moisture content of the samples.

The drying air temperatures, drying air velocity and sample weight were continuously measured and recorded every 30 min during the drying experiments. The speed of the

air was measured by a speed meter (hot wire anemometer, model 20004 AHYK), with the precision of 0.01m/s, while the temperature was measured by series of digital thermometers inserted at various points in the dryer. The sensing bulb of the digital thermometers were covered by wick and constantly kept wet for measurement of wet bulb temperature. The experiments were carried out under varying conditions of the drying air. There were four temperature levels (50°C, 60°C, 70 ^{o}C, and 80 ^{o}C) and five air velocities (1.0, 1.5, 2.0, 2.5 and 3.0 m/s). The data were analyzed and used for determination of the drying parameters.

3.7 Proximate analysis

Proximate analyses were carried out on the samples to determine the compositions of carbohydrate content, ash content, crude fibre, moisture content etc. according to (AOAC, 1984).

3.7.1 Moisture content determination

The moisture content was determined as outlined already using equation 3.4

$$\% \, MC = \frac{W_1 - W_2}{weight \ of \ sample} \qquad (3.4)$$

Where W_1 is weight of petridish and sample before drying

   W_2 is weight of petridish and sample after drying.

3.7.2 Ash content determination

Principle: The ash of foodstuff is the inorganic residue remaining after the organic matter has been burnt away. It should be noted, however, that the ash obtained is not necessarily of the composition as there may be some from volatilization.

   i.   Empty platinum crucible was washed, dried and the weight was noted.

   ii.   Exactly 2g of wet sample was weighed into the platinum crucible and placed in a muffle furnace at 500°c for 3 hours.

   iii.   The sample was cooled in a dessicator after burning and weighed.

The ash content is then given by

$$\% \; Ash \; content = \frac{W_3 - W_1}{W_2 - W_1} \qquad (3.5)$$

Where W_1 is weight of empty platinum crucible; W_2 is weight of the sample in the crucible before burning and W_3 is weight of the sample after burning.

3.7.3 Crude Fibre determination

   i.   Defat about 2g of material with petroleum ether (if the fat is more than 10%)

   ii.   Boil under reflux for 30 minutes with 200ml of a solution containing 1.25g of H2504 per 100ml of solution

   iii.   Filter the solution through linen or several layers of cheese cloth on a fluted funnel

   iv.   Wash with boiling water until the washings are no longer acid.

v.   Transfer the residue to a beaker and boil for 30 minutes with 200ml of a solution containing 1.25g of carbonate free NaOH per 100ml

vi.   Filter the final residue through a thin but close pad of washed and ignited asbestos in a Gooch crucible

vii.   Dry in an electric oven and weigh

viii.   Incinerate, cool and weigh

The loss in weight after incineration x 100 is the percentage of crude fibre.

$$\%Crude\ fibre = \frac{weight\ of\ fibre}{weight\ of\ sample}\quad x\quad 100 \qquad (3.6)$$

3.7.4 Crude fat determination

Soxhlet Fat Extraction Method

This method is carried out by continuously extracting a food with non- polar organic solvent such as petroleum ether for about 1 hour or more.

i.   Dry 250ml clean boiling flasks in oven at $105 - 110\ ^oC$ for about 30 minutes.

ii.   Transfer into a dessicator and allow to cool.

iii.   Weigh correspondingly labeled, cooled boiling flasks.

iv.   Fill the boiling flasks with about 300ml of petroleum ether (boiling point 40 - 60°C).

v.   Plug the extraction thimble lightly with cotton wool.

vi.   Assemble the soxhlet apparatus and allow to reflux for about 6 hours.

vii.   Remove thimble with care and collect petroleum ether in the top container of the set - up and drain into a container for re - use.

viii.   When flask is almost free of petroleum ether, remove and dry at 105 ^{o}C - 110 ^{o}C for 1 hour.

ix.   Transfer from the oven into a dessicator and allow to cool; then weigh.

3.7.5 Crude Protein determination

The method is the digestion of sample with hot concentrated sulphuric acid in the presence of a metallic catalyst. Organic nitrogen in the sample is reduced to ammonia, This is retained in the solution as ammonium sulphate. The solution is made alkaline, and then distilled to release the ammonia. The ammonia is trapped in dilute acid and then titrated.

Exactly 0.5g of sample was weighed into a 30ml Kjehdal flask (gently to prevent the sample from touching the walls of the side of each and then the flasks were stoppered and shaken. Then 0.5g of the Kjedahl catalyst mixture was added. The mixture was heated cautiously in a digestion rack under fire until a clear solution appeared.

The clear solution was then allowed to stand for 30 minutes and allowed to cool. After cooling about 100ml of distilled water was added to avoid caking and then 50ml was transferred to the kjedahl dstillation apparatus.

A 100ml receiver flask containing 5ml of 2% boric acid and indicator mixture containing 5 drops of Bromocresol blue and 1 drop of methlene blue was placed under a

condenser of the distillation apparatus so that the tap was about 20cm inside the solution. The 5ml of 40% sodium hydroxide was added to the digested sample in the apparatus and distillation commenced immediately until 50 drops gets into the receiver flask, after which it was titrated to pink colour using 0.01N hydrochloric acid.

% Nitrogen = Titre value   x   0.01   x   14   x   4   (3.7)

% Protein =   % Nitrogen   x   6.25   (3.8)

3.7.6 Carbohydrate determination: (Differential method)

% Carbohydrate = 100 - (%Protein + % Moisture + %Ash + %Fat + %Fibre)   (3.9)

3.8 Determination of Moisture ratio

In determining moisture ratio, it is assumed that the material layer is thin enough or the air velocity is high so that the conditions of the drying air (humidity and temperature) are kept constant throughout the material. Moisture ratio values can be calculated for the drying using the moisture contents at the initial time, equilibrium time and at that particular time:

$$MR = \frac{M_t - M_e}{M_i - M_e}$$ (3.10)

where,   MR is the moisture ratio (dimensionless), M_t is the moisture content at any given time (kg water/ kg solids), M_e is equilibrium moisture content (kg water/kg solids) and M_i is the initial moisture content.

The value of M_e is relatively small compared with M_t and M_o especially for food materials (Junling *et al.,* 2008; Agarry and Aworanti, 2012; Mohammed *et al.,* 2013).

Therefore, M_e can be assumed zero, hence the MR can be simplified to equation below.

$$MR = \frac{M_t}{M_o} \qquad\qquad (3.11)$$

3.8.1 Determination of Drying Rate (D_r)

Drying rate of the agricultural products can be calculated using the following equation (Akpinar et al., 2003);

$$D_r = \frac{M_{t+dt} - M_t}{dt} \qquad\qquad (3.12)$$

Where D_r is the drying rate (g/mins), dt is the time interval

The drying rate was obtained by calculating the time to remove a given quantity of moisture from the food products. The drying rate normally decreases with an increase in the drying time and an increase with temperature.

3.9 Determination of Drying Kinetic Models

Most of the models are of relevance to the falling rate period. The drying models are generally classified into three categories which are: the empirical, the semi-empirical and the theoretical models. More often, the models use the moisture ratio M_r which is defined as

$$M_r = \frac{M - M_e}{M_{cr} - M_e} \qquad (3.13)$$

M is the moisture content in dry basis (g water/g dry matter); M_e is the equilibrium moisture content. Several modeling curves have been investigated by researchers. The drying curve:

$$M_r = f(t) \qquad (3.14)$$

is obtained from the experimental moisture content data. This experimental curve is then fitted to a thin-layer drying model, by using a suitable function. In the case of empirical modeling, an empirical fitting function is investigated. A typical example is the Wang and Singh (Wang, 1978) model, used for rice drying. A wide range of semi-empirical models were investigated. One of them is the logarithmic model expressed as:

$$M_r = a.\,exp(-Kt) + C \qquad (3.15)$$

Where,

$$M_r = \frac{M - M_e}{M_i - M_e} \qquad (3.16)$$

When the final moisture is reasonably small to be significant (ie. $M_f \cong M_e$),

It can simply be expressed as:

$$M_r = \frac{M}{M_i} \qquad (3.17)$$

Where, M_i is the initial moisture content and M_f is the final moisture content.

Using the moisture ratio calculated, different drying kinetic models can be tested. The kinetic models are based on time as the independent variable while the moisture ratio

88

was considered as the dependent variable. There are many statistical-based models correlating experimentally obtained moisture data with time (t) in the literature. The most common among these used for food drying are tabulated in the Table 3.1.

Table 3.1: Standard thin layer drying models

S/No:	Model Name	Model
1	Newton	$MR = \exp(-kt)$
2	Page	$MR = \exp(-kt^n)$
3	Modified Page	$MR = \exp[-(kt)^n]$
4	Henderson & Pabis	$MR = A.\exp(-kt)$
5	Logarithmic	$MR = A.\exp(-kt)+c$
6	Two Term	$MR = A.\exp(k_0t)+b\exp(-k_1t)$
7	Two Term exponential	$MR = A.\exp(-kt)+(1-)\exp(-At)$
8	Wang & Singh	$MR = 1+at+bt^2$
9	Approximation of diffusion	$MR = A.\exp(-kt) + (1-a)\exp(-kbt)$
10	Verma et al.	$MR = A.\exp(-kt)+(1-a)\exp(-gt)$
11	Modified Henderson & Pabis	$MR = A.\exp(-kt)+b\exp(-gt)+ c\exp(-ht)$
12	Simplified Fick's Diffusion	$MR = A.\exp[-c(t/L2)]$
13	Modified Page II	$MR = \exp[-k(t/L2)^n]$
14	Midilli&Kucuk	$MR = A.\exp(-ktn)+bt$

(Sources: Wang, et al. 2007, Diamante and Munro 1993, Akpınar and Bicer 2003, Toğrul and Pehlivan 2002, Midilli, et al. 2002)

Where a, b, c, k and n are constant of models.

Based on the moisture ratio, these different kinetic models will be evaluated and the errors in their estimation determined.

The statistical validity of the models was evaluated and compared using three different criteria: Correlation Coefficient (R^2); Chi-squared ($\chi 2$), and Root Mean Square Error, (*RMSE*). The most suitable model for describing drying characteristics would be a model with the highest R^2 and the lowest $\chi 2$ and RMSE values.

$$R^2 = 1 - \frac{\sum_1^n (M R_{exp,i} - M R_{pre,i})^2}{\sum_1^n (M R_{exp} - M R_{pre,i})^2} \tag{3.13}$$

$$x^2 = \frac{\sum_{i=1}^N (M R_{exp,i} - M R_{pre,i})^2}{N - n} \tag{3.14}$$

$$RMSE = \sqrt{\frac{\sum_{i=1}^N (M R_{pre,i} - M R_{exp,i})^2}{N}} \tag{3.15}$$

3.10 Determination of effective moisture diffusivity

The effective moisture diffusivity was determined using the equation 3.16

$$\ln MR = ln\frac{8}{\pi^2} - \left(\frac{\pi}{2H}\right)^2 D_{eff} t \tag{3.16}$$

that is

MR = the moisture ratio at time, t

H = half thickness of the slice (m)

Hence, by plotting the experimental data in terms of ln (MR) against drying time (t) the

effective moisture diffusivity D_{eff} was determined using the slope in equation 3.17

$$D_{eff} = \frac{-slope}{\left[\frac{2.4674}{H^2}\right]} \qquad (3.17)$$

3.11 Determination of Activation energy

According to Suarez et al. (1980) and Roberts et al. (2008), temperature dependence of

the effective moisture diffusivity D_{eff} can be presented by an Arrhenius relationship as

in equation 3.18.

$$D_{eff} = D_o \; exp\left[-\frac{E_a}{RT}\right] \qquad (3.18)$$

where: D_o is the pre-exponential factor of the Arrhenius equation in m2/s,

E_a is the activation energy in kJ/mol,   R is the universal gas constant (8.314 $\times$

10-3 kJ/mol K),   T is the absolute air temperature (°K).

Linearizing the equation by taking the natural logarithm gives

$$\ln D_{eff} = \ln D_o - \frac{E_a}{R}.\frac{1}{T} \qquad (3.19)$$

Using the data of effective moisture diffusivities and absolute air temperatures to plot ln

(D_{eff}) against 1/T, the activation energy E_a will be determined using the slope of the plot

as:

$$E_a = - \; (slope \; x \; R) \qquad (3.20)$$

The correlation coefficient is used to determine the validity of the equation

3.12 Determination of Convective heat transfer coefficient

The convective heat transfer coefficient in drying can be determined using the equation 3.21.

$$h_c = \frac{K_v}{x} C (G_r . P_r)^n \qquad (3.21)$$

Where

hc is convective heat transfer coefficient,   Gr is Grasshof number

Pr is Prandtl number,   Kv is Thermal conductivity

3.13 Determination of Thermal efficiency

The thermal efficiency of the dryer is the ratio of temperature input to the temperature utilized in drying. It is mathematically expressed as follow:

$$E_{eff} = \frac{T_p - T_{out}}{T_p - T_a} \qquad (3.22)$$

Where, T_p is Plenum air temperature (hot air entering into the drying chamber) ^{o}C

T_{out} is Out let air temperature (air leaving through the chimney), ^{o}C,

T_a is Ambient temperature, ^{o}C

3.14 Optimization of the drying process

The drying process will also be optimized using Response Surface Methodology where the three independent variables will be slice thickness, air velocity and temperature and

the response will be moisture content. The Artificial Neural Network was also used to validate the optimization and predict the drying process.

3.14.1 Central Composite Design

The drying process was optimized using Central Composite Design (CCD). This was done to determine the best conditions for optimum drying of the cocoyam products. Equally, this helps to examine the interactive effects of the three important factors. The factors considered were time, air speed and slice thickness for the Solar cabinet dryer while for the Hot air conventional dryer, the factors were time, air speed and temperature. These factors were the independent variables while the mass remaining (g) and the moisture content (%db) were the dependent variables or responses.

Using the CCD involves varying the independent variables at five different levels (-α, -1, 0, +1, +α). In this work, a set of 34 experiments were performed which consist of 16 core points, 12 star like points and 6 centre points or null points. This is because the replicates of factorial points and the replicates of axial (star) points were two to increase the accuracy of the experiment. The distance of the star like point α used was 1.316. The experiments were performed in random to avoid systematic error. The coded values of the process parameters were determined by the following equation 3.23: (Rajeshkannan *et al.,* 2012)

$$x_i = \frac{X_i - X_o}{\Delta X} \qquad (3.23)$$

where x_i – coded value of the ith variable, X_i – uncoded value of the ith test variable and X_o – uncoded value of the ith test variable at center point.

The range and levels of individual variables are given in Table 2. The regression analysis was performed to estimate the response function as a second order polynomial:

A statistical program package, Design Expert 8.7.0.1 was used for regression analysis of the data obtained and to estimate the coefficient of the regression equation. The equations were validated by the statistical tests called the ANOVA analysis. The significance of each term in the equation is to estimate the goodness of fit in each case. Response surfaces were drawn to determine the individual and interactive effects of the test variable on the moisture content.

The optimal values of the test variables were first obtained in coded units and then converted to the uncoded units. Using four factor variable and six centre points will give the CCD design in Tables 3.2 and 3.3.

Table 3.2: Factors levels of independent variables for the Solar cabinet dryer

Independent Factors	-α	Low level (-)	Medium level (0)	High level (+)	+α
Time (mins)	99.6	120.0	150.0	180.0	200.5
Air speed, (m/s)	1.2	1.5	2.0	2.5	2.8
Slice thickness (mm)	1.66	2.00	2.50	3.00	3.34

Table 3.3: Factors levels of independent variables for the hot air dryer

Independent Factors	-α	Low level (-)	Medium level (0)	High level (+)	+α
Time (mins)	64.2	80.0	130.0	180.0	195.8
Air speed, (m/s)	0.60	1.00	2.25	3.50	3.90
Temperature, (^{o}C)	55.3	60.0	75.0	90.0	94.7

3.14.2 Artificial Neural Network

Artificial Neural Networks (ANNs) are mathematical models that loosely approximate the function of biological neural networks. The network was trained with Levenberg-Marquardt (LM) back propagation algorithm which is one of the Multi-Layer Perceptron (MLP). It consists of three or more layers of neurons, with the first layer of neurons representing the independent variable inputs. Each of the neurons in the first layer is connected to one or more layers of hidden neurons that represent nonlinear activation functions. These neurons are in turn connected to a final level of output neurons and, through the use of learning algorithms, the relative influence of each input neuron and their complex interactions on the observed result can be discerned. An MLP was developed in MATLAB software with three input neurons representing the drying time, air speed and slice thickness for Solar cabinet drying and drying time, air speed

and temperature for hot air drying, a single hidden layer of neurons, and an output neuron representing the moisture content. A representation of the MLP architecture can be observed in Fig. 3.2. The number of neurons required in the hidden layer was determined by trial and error to minimise the deviation of predictions from experimental results and reduce the possibility of over-fitting the model. A total of 26 (75%) of experimental results were used to train the network, with the remaining results split evenly between network validation and testing.
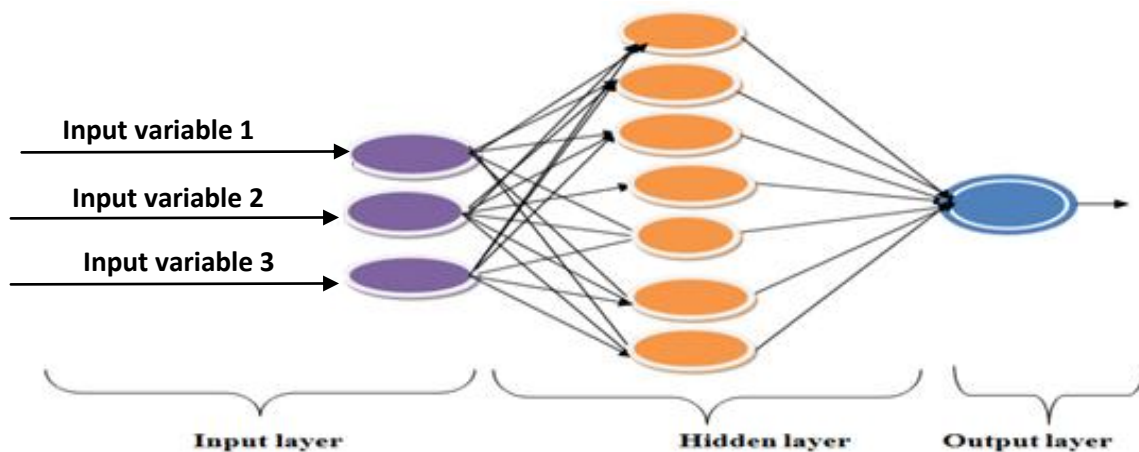
Fig 3.2: The ANN architecture for the drying process

3.15 Hedonic sensory analysis

The hedonic scale is based on equal interval, which is important in the assignment of numerical values to the response choices (from 1 = "dislike extremely" to 9 = "like extremely") and to the use of parametric statistics in analysis of the data. It was

physically administered to 50 untrained panelists who use flour for different purposes. The panelists were of different age and gender. Each panelist was supplied with a questionnaire, a pen and the flour samples and had unlimited time to complete the testing. The questionnaire was administered and collected immediately after it was completely filled hence there was no case of unreturned questionnaire.

9-Point Hedonic Scale

Like Extremely

Like Very Much

Like Moderately

Like Slightly

Neither Like nor Dislike

Dislike Slightly

Dislike Moderately

Dislike Very Much

Dislike Extremely

The sensory tests were conducted on the food materials by the panelists are general appearance, colour, aroma, texture. The analysis was done using SPSS software.

CHAPTER FOUR

RESULTS AND DISCUSSION

4.1 Physical properties of potato and cocoyam

4.1.1 Roundness

Roundness is a measure of the sharpness of the corners of the food crop. Roundness ratio is given by the formular.

$$Roundness\ ratio = \frac{r}{R} \qquad (4.1)$$

Where

R = the mean radius of the object

r = radius of curvature of the sharpest corner

The use of radius of curvature determines the roundness or flatness of the crop. Table 4.1 shows the roundness ratio of both the undried and dried potato and cocoyam. The roundness ratio for potato ranged from 0.021 to 0.133 from undried potato (UDP) to Solar cabinet dried potato (PDC) while it ranges from 0.027 to 0.165 for cocoyam.

4.1.2 Sphericity

Sphericity expresses the characteristic shape of a solid object relative to that of a sphere of the same volume. The equation for estimating the sphericity of food samples is

$$sphericity = \frac{D_i}{D_c} \qquad (4.2)$$

Where D_i = diameter of largest inscribed circle

D_c = diameter of smallest circumscribed circle   (Luther et al, 2003)

The sphericity of the crops area shown in Table 4.1. It is seen that the undried cocoyam with sphericity of 0.923 is the one that most closely approximates to a sphere. The closer the value approximates to unity, the closer it approximates to a sphere.

4.1.3 Surface area

Surface area is useful in estimating the amount of wax applied to fruit and food, amount of packaging film to wrap crops and rate of heating, cooling, freezing and drying. It is related to size but also depends on particle shape. Sample surface area is important in heating and cooling operation since heat transfer is proportional to surface area. As expected, the surface area of potato was much greater than that of cocoyam (Table 4.1)

Table 4.1   Physical Properties of potato and cocoyam

Material	Roundness Ratio	Sphericity of product	Surface Area (mm^2)
UDP	0.021	0.0867	16.10
UDC	0.027	0.923	12.17
SDP	0.091	0.667	9.41
CDP	0.125	0.643	11.25
PDP	0.133	0.628	9.41
ODP	0.067	0.58	9.05
SDC	0.096	0.777	5.26
CDC	0.146	0.584	4.39
PDC	0.165	0.76	4.02
ODC	0.089	0.503	3.80

4.2 Density

The density of a product measures the ratio of the mass to the volume of that product. Three categories of density were analysed and reported.

4.2.1 True density

The density (also called the true density) of foods and food products is used in numerous situations involving heat transfer and is a critical parameter affecting the functional properties of the powder (Hamed and Bahareh, 2013). The variation of the density of the food crops with different drying techniques is shown in Fig 4.1 and 4.2. The true density of the undried potato and cocoyam are 1.15 and 1.33g/cm^3 respectively. Vasiliki et al (2011) obtained true density values of 1.504 g/cm^3 for rice, 1.543 g/cm^3 for potato and 1.591 g/cm^3 for strawberry. The density generally decreased for the dried products. This should enhance the durability of the products since product density influences the amount and strength of packaging material. The density of processed product also dictates the characteristics of its container or package. Equally, food density influences its texture or mouth feel (Luther et al, 2003).
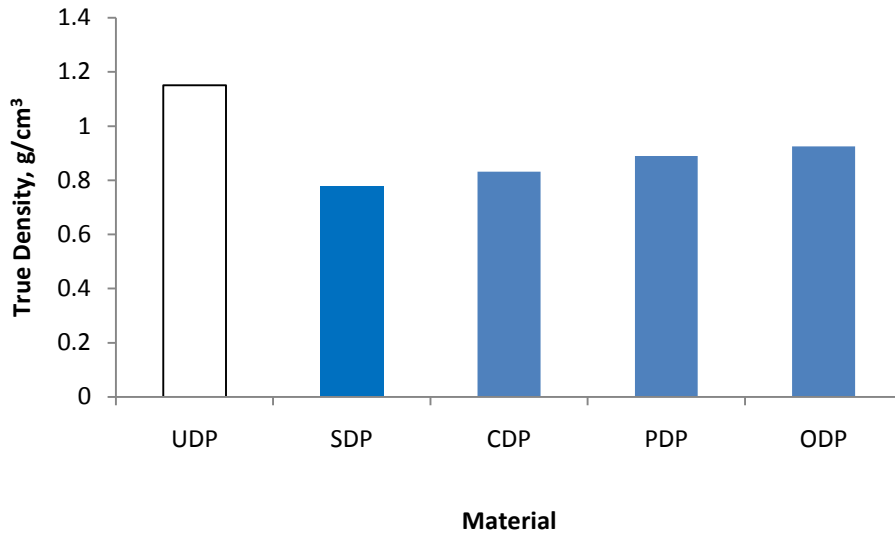
Fig 4.1: Variation of true density with different techniques for drying of potato
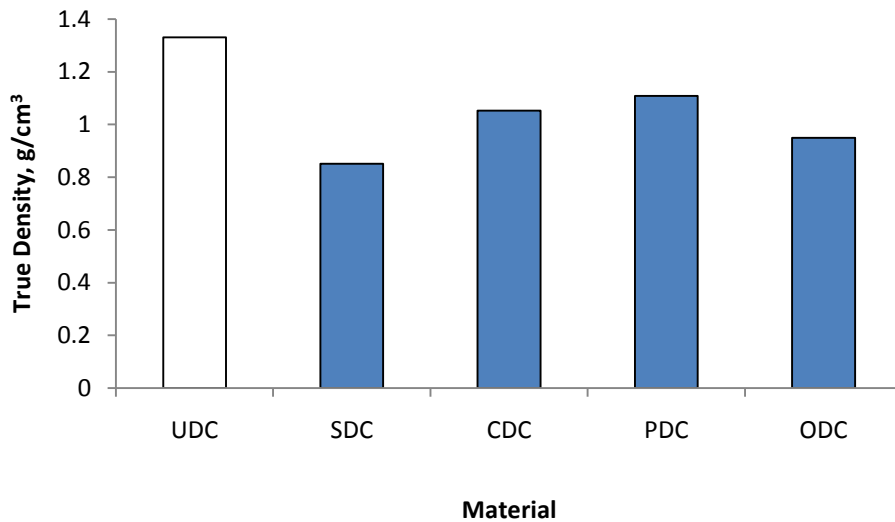
Fig 4.2: Variation of true density with different techniques for drying of cocoyam

4.2.2. Bulk Density

Fig. 4.3 and 4.4 shows the variation of bulk density with different drying techniques.

Bulk density is the mass of a group of individual particles divided by the space occupied

by the entire mass including the air space (Luther et al, 2003). The bulk densities were lower than the true densities. This is because there is relatively no air space in the powder product giving rise to smaller volume. The bulk density depends on the attractive inter-particles forces, particles size and number of contact positions (Peleg and Bagley, 1983). The lowest bulk density was observed in the hot-air convective dried products with a value of 0.508 g/cm^3 for potato and 0.480 g/cm^3 for cocoyam. Using freeze-drying, Vasiliki et al (2011) reported bulk density values of between 0.15 to 0.25 g/cm^3 at different applied pressures while the bulk density of Nigerian cassava ranged from 0.171 to 0.551 g/cm^3 (Nwabanne, 2009). The drying techniques employed were seen to affect the bulk density. As expected, the bulk densities of the dried products were lower than the dried products. Singh et al (2010) observed that the bulk density of seed gum powder is primarily dependent on particle size, particle distribution and particle shape.
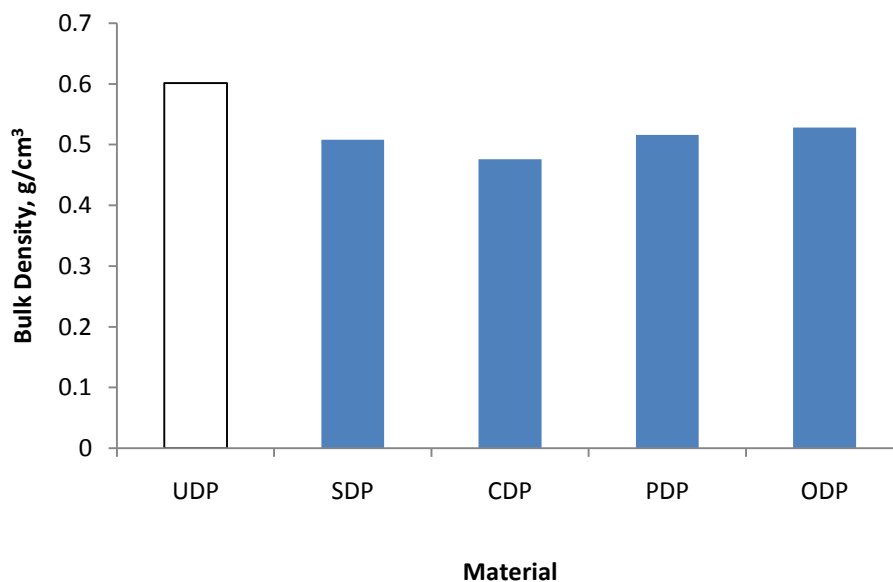
Fig 4.3: Effect of the different techniques for drying of potato with bulk density
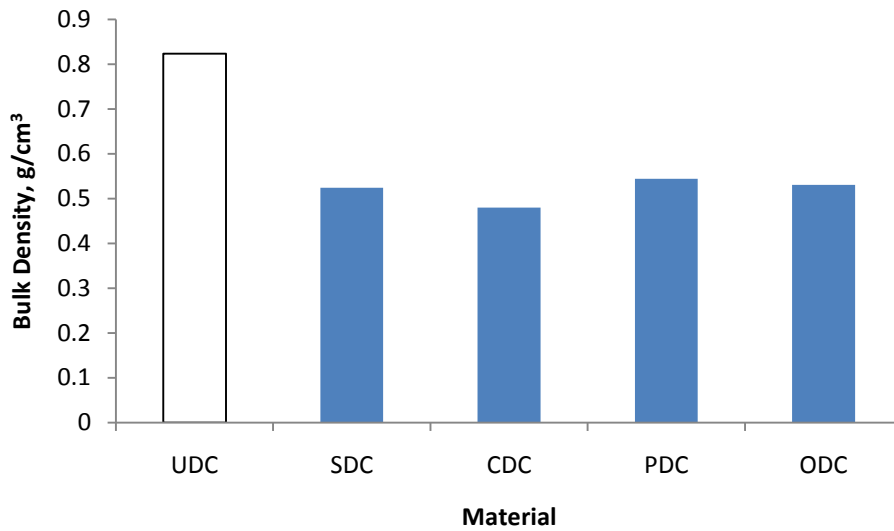
Fig 4.4: Effect of the different techniques for drying of cocoyam with bulk density

4.2.3 Tapped Density

The tapped density is one of the main characteristics of a power which is the maximum packing of a powder achieved under the influence of well defined, externally applied forces (Hamed and Bahareh, 2013). Fig 4.5 and 4.6 revealed the variation of the tapped densities with different drying techniques. The hot-air conventionally dried product was discovered to have the lowest tapped densities of 0.664 g/cm^3 for CDP and 0.692 for CDC while the oven dried products gave the highest tapped densities. Hamed and Bahareh (2013) equally reported that among four different drying methods, the oven dried product gave the highest tapped density for Durian seed gum. The tapped density indicates the volume of a mass of sample after inducing a closer packing of particles by tapping the container. According to Goldfarb and Ramachandrum (2003), there are two

crucial reasons for measuring the tapped density. First, the tapped density is more reproducible than the bulk value. Secondly, the flow characteristics of a powder are inferred from the ratio of these two densities. It should be noted that the total volume of the inter-particles voids can change with drying and packaging process hence the need for tapped density measurement to rectify that (Hamed and Bahareh, 2013). The bulk and tapped densities provide a perspective from the packing and rearrangement of the particles and the compaction profile of a material (Kumar et al, 2010).
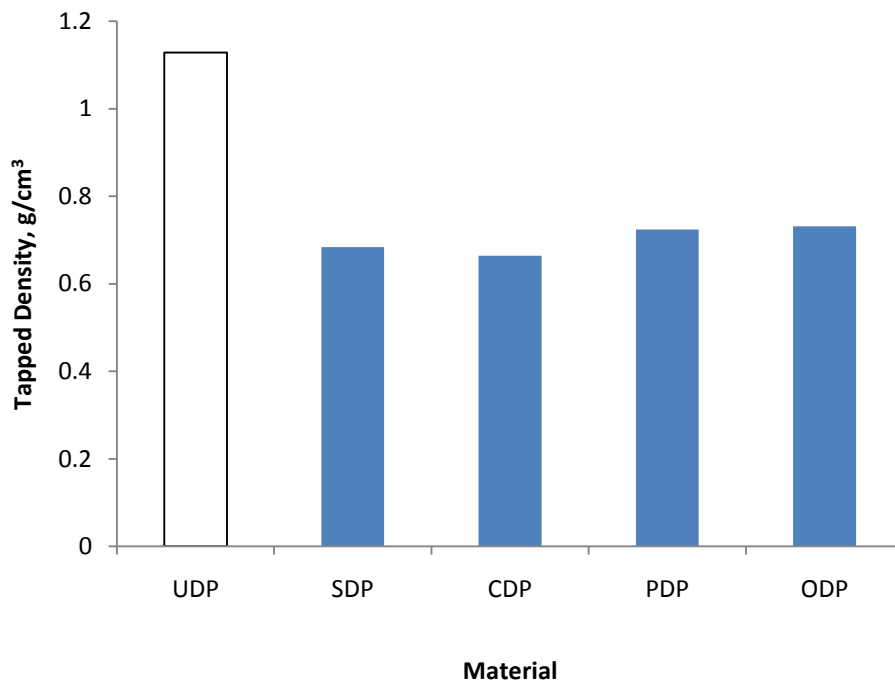
Fig 4.5: Variation of true density with different techniques for drying of potato
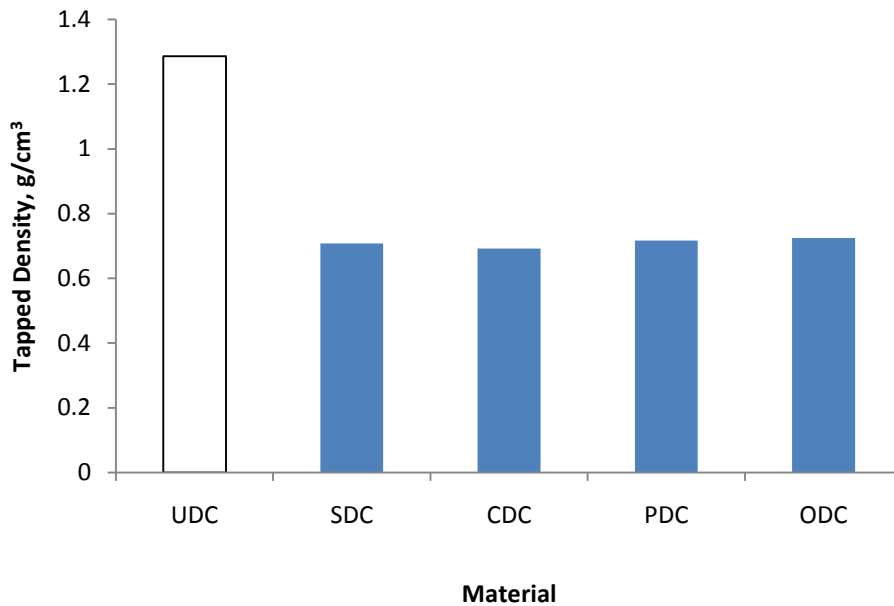
Fig 4.6: Variation of tapped density with different techniques for drying of cocoyam

4.3 Porosity

Porosity is the percentage of air between the particles compared to a unit volume of particles. It was estimated using the equation reported by Vasiliki et al, (2001)

$$\varepsilon = 1 - \frac{\rho_b}{\rho_{ts}} \qquad (4.3)$$

Where ρ_b is bulk density (gcm^{-3})

ρ_{ts} is true density (gcm^{-3})

Fig 4.7 and 4.8 indicated the effect of the different drying techniques on the porosity of the products. The porosity values obtained ranged from 0.38 to 0.54. Vasiliki et al (2001) reported porosity values of 0.45 to 0.70 in freeze-drying of rice kernels. The porosity decreased slightly for dried potato but increased for dried cocoyam which may

have accounted for the faster drying rate in cocoyam. With high porosity, air flows easily through the crop bed, drying is faster and the power required by fans and pumps are low (Luther et al, 2003).
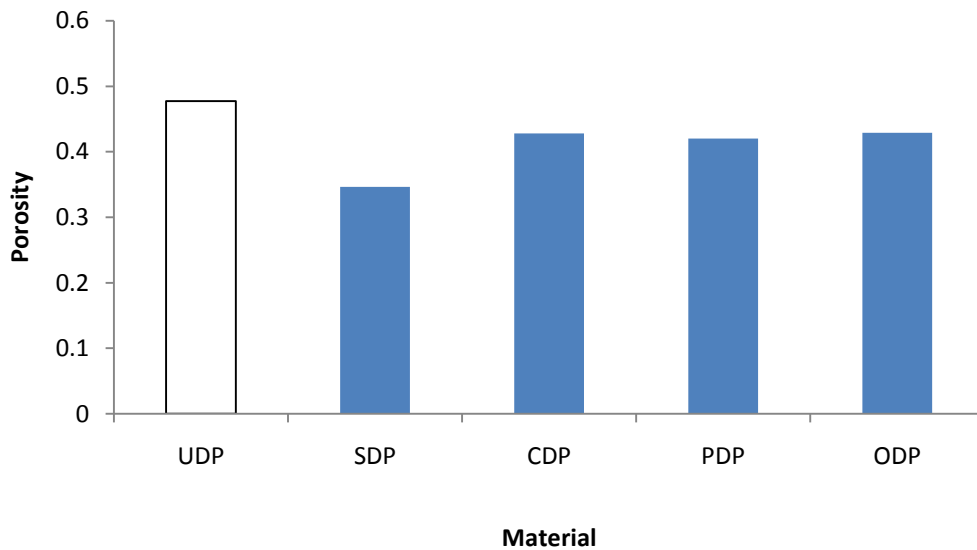
Fig 4.7: Variation of porosity values with different techniques for drying of potato
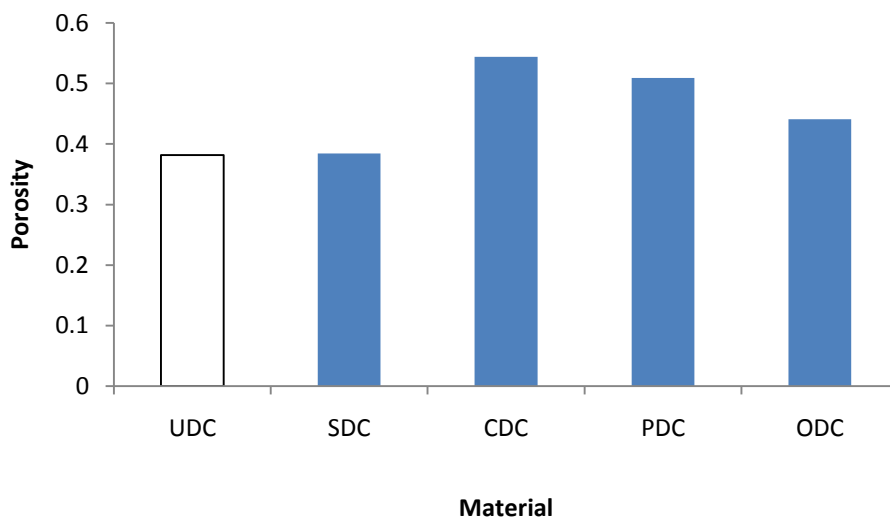
Fig 4.8: Variation of porosity values with different techniques for drying of cocoyam

4.4 Compressibility Index

The compressibility index is used to assess the excellent or poor flowability characteristics of the powder. It was calculated by the formular given by equation 4.4.

$$compressibility\ Index\ (\%) = \frac{Tapped\ density - Bulk\ density}{Tapped\ density}\ x\ 100 \qquad (4.4)$$

It is dimensionless since it is only a ratio of the difference in tapped and bulk densities and the tapped density. The effect of the different drying methods on the compressibility index is Fig 4.9 and 4.10. If the characteristics is less than 10%, it shows excellent flow. When the compressibility index is between 21 – 25%, it shows passable flow characteristics while between 26% – 31% indicates poor flow characteristics. Above 32%, suggests very poor flow characteristics (Hamed and Bahareh, 2013). Hence the different dried products have different flow characteristics. The compressibility index of the products indicated that the PDC, the SDP and the SDC have passable flow characteristics with compressibility index of about 25%. The UDP and UDC are seen to have very poor flow characteristics.
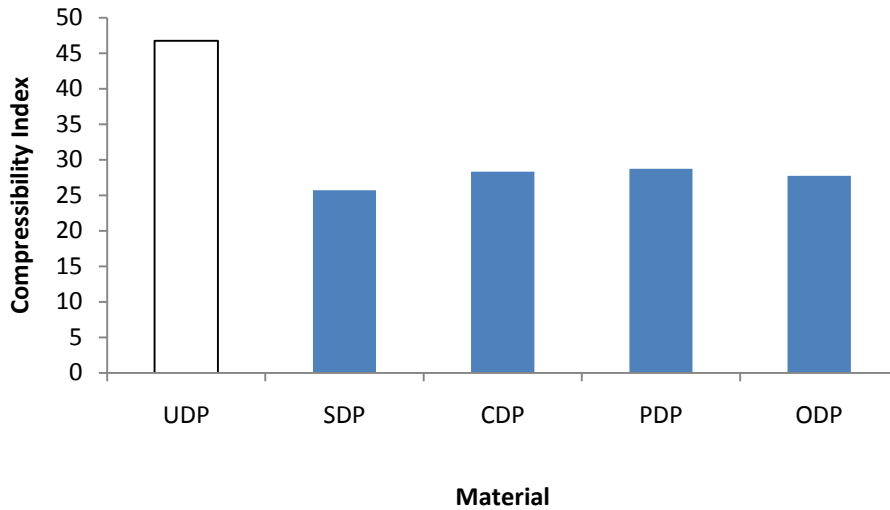
Fig 4.9: Effects of different techniques for drying of potato with compressibility index
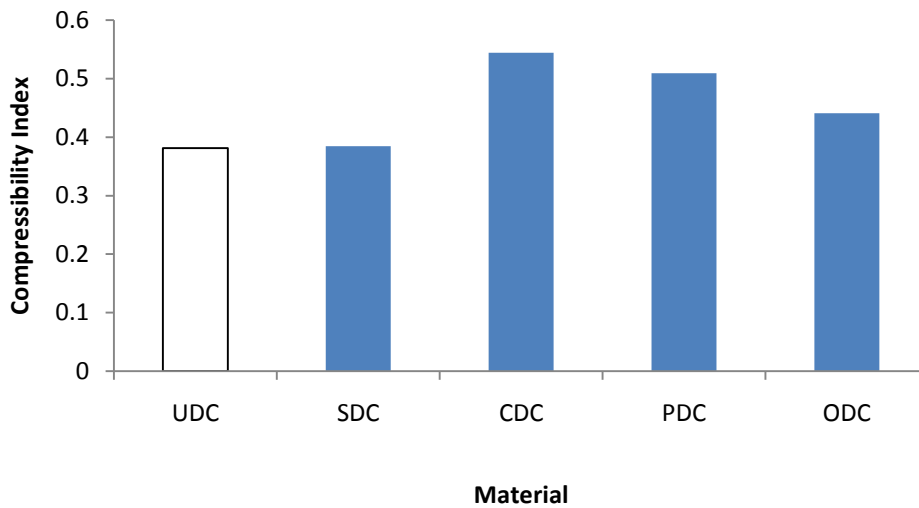
Fig 4.10: Effects of different techniques for drying of cocoyam with compressibility index

4.5 Proximate Analysis

The result of the proximate analysis is shown in Table 4.2. While water content has the highest composition for the undried products, carbohydrate content has the highest composition for the dried products. As expected, the water content decreased for the

dried products. The range of fibre content varied from 7.1 to 11.15 for cocoyam and 5.1 to 5.65 for potato. Nwabanne (2009) in the analysis of fermented ground cassava reported fibre content values of between 5.10 to 5.40. It is observed that ash content, crude fibre and carbohydrate content increased significantly for dried product while the protein content and fat content only slightly increased. All the products had low protein content. Luther et al (2002) showed similar values for various fruit products. The potato products had more protein content and fat content than the cocoyam products. The difference in drying rate has been explained by Nwabanne (2009) to be as a result of difference in the chemical composition of the cultivars.

Table 4.2: Proximate analysis of potato and cocoyam

Material	WC	AC	PC	CF	FC	CC
UDP	68.4	4.95	1.87	5.1	4.05	15.18
UDC	72.8	5.45	1.09	7.1	2.1	11.46
SDP	24.65	12.85	2.1	5.4	5.5	49.5
CDP	25.8	9.7	2.8	5.3	5.2	46.2
PDP	24.45	7.45	3.65	5.2	5.9	46.36
ODP	25.2	13.25	2.05	5.65	4.85	49.0
SDC	26.55	13.85	1.35	10.75	3.05	44.45
CDC	27.35	12.35	1.75	10.45	2.85	45.25
PDC	26.7	11.95	1.95	10.4	3.15	45.85
ODC	27.15	14.75	1.3	11.15	2.6	43.05

Where   WC = Water content;   AC = Ash content;   PC = Protein content
CF = Crude Fibre;   FC = Fats content;   CC = Carbohydrate Content
K = Thermal conductivity;   Cp = Specific heat capacity
α = Thermal diffusivity

4.6. Thermal Properties

The knowledge of the thermal properties of food materials is very important in the design of dryers for drying them. Such thermal properties include specific heat capacity, thermal conductivity and diffusivity.

4.6.1 Specific Heat capacity

Fig. 4.11 and 4.12 show the effects of drying technique on the heat capacity of the product. Generally, the specific heat capacity decreased for the dried products. The oven-dried products were observed to have the smallest specific heat capacity of 1.981 KJ/kg K for potato and 2.007 KJ/kg K for cocoyam. Ademiliyu et al (2006) reported values of between 1.085 to 1.284 KJ/KgK for specific heat capacity of bone dry fermented ground cassava cultivars. The specific heat capacity of sundried potato is slightly higher than that for hot-air conventionally dried potato while the reverse is the case for cocoyam. It is noted that the specific heat capacity of cocoyam is slightly higher than that of potato. This is probably because of its higher water content since water has the greatest effect upon specific heat capacity among other constituents (Luther et al, 2003).
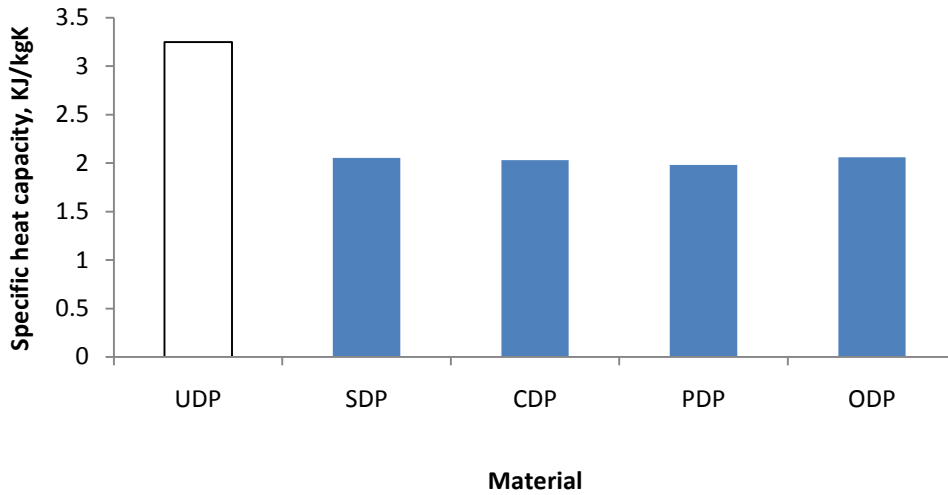
Fig. 4.11   Effects of different drying techniques on the specific heat capacity of potato at initial moisture content of 210 db and temperature range of 60 - 70 ^{o}C
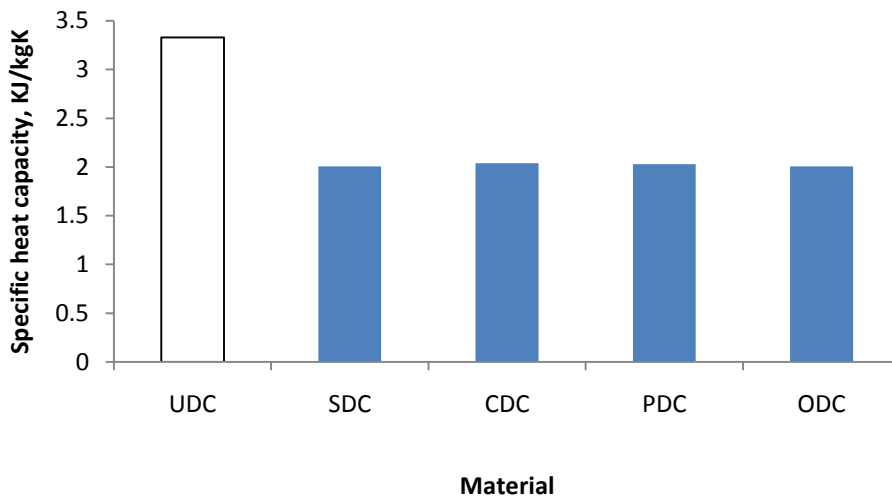
Fig. 4.12 Effects of different drying techniques on the specific heat capacity of cocoyam at initial moisture content of 290 db

4.6.2   Thermal conductivity

Thermal conductivity is a measure of the ease with which heat flows through a material.

The variation of the thermal conductivity on the different drying methods is shown in

Fig 4.13 and 4.14. The values ranged from 0.282 to 0.451 W/mK for potato products while it ranged from 0.291 to 0.463 W/mK for cocoyam. In drying of cassava, Nwabanne (2009) reported thermal conductivity values of 0.24 W/mK. The thermal conductivity decreased for dried products. For potato, the lowest thermal conductivity was observed in PDP while for cocoyam, it was the SDC.

The thermal conductivity of most food materials is in a relatively narrow range of between 0.2 to 0.5 W/mK (Luther et al, 2003). Thermal conductivity is strongly influenced by a material's water content.
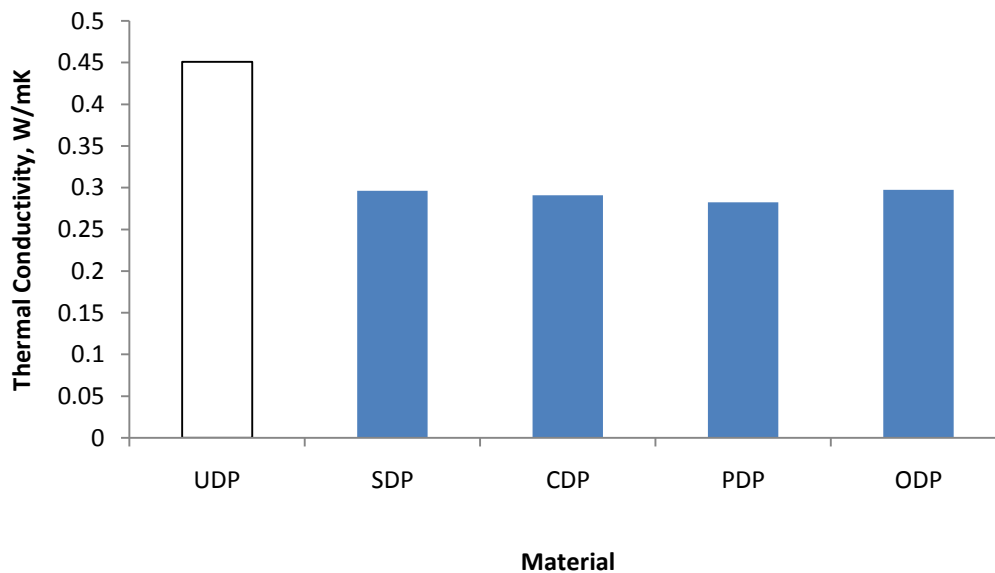
Fig. 4.13   Effects of different drying techniques on the thermal conductivity of potato at initial moisture content of 210 db and temperature range of 60 - 70 $^\circ$C
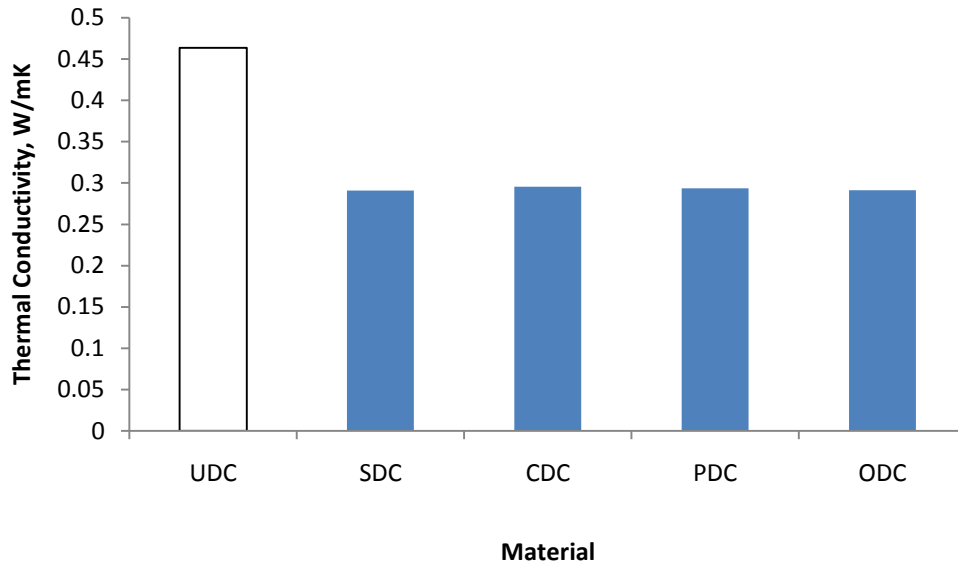
Fig. 4.14   Effects of different drying techniques on the thermal conductivity of cocoyam at initial moisture content of 290 db and temperature range of 60 - 70 $^{\circ}$C

4.6.3 Thermal diffusivity

Fig 4.15 and 4.16 shows the thermal diffusivity of the dried and undried products where it is seen that the type of drying affects the thermal diffusivity. The thermal diffusivity increased with drying for the products ranging from 1.21×10^{-4} to 1.85×10^{-4} m^2/s for potato and from 1.04×10^{-4} to 1.7×10^{-4} m^2/s for cocoyam. The Thermal diffusivity of ground cassava has been reported to be between 9.0×10^{-4} to 2.0×10^{-4} (Nwabanne, 2009). The SDP exhibited the highest Thermal diffusivity for potato. Thermal diffusivity is a measure of how fast heat propagates or diffuses through a material. Thermal diffusivity is very relevant in transient heat transfer where temperature varies time and location and it is a combination of three basic thermal properties which are thermal conductivity, density and specific heat capacity (Luther et al, 2003).
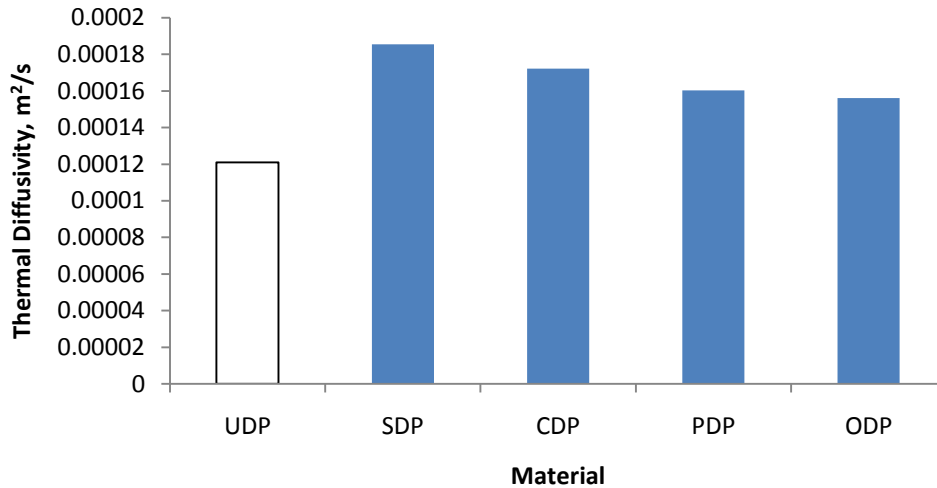
Fig 4.15: Variations of thermal diffusivity with different techniques for drying of potato at initial moisture content of 210 db and temperature range of 60 - 70 ^{o}C
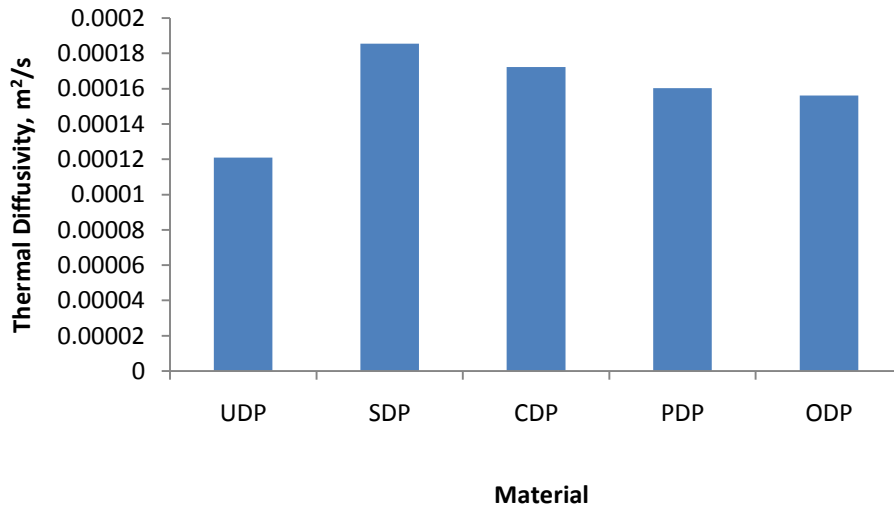
Fig 4.16: Variations of thermal diffusivity with different techniques for cocoyam drying at initial moisture content of 290 db and temperature range of 60 - 70 ^{o}C

4.7 Moisture Content variation

4.7.1 Effect of slice thickness on water content

The effect of slice thickness on the moisture content and the moisture ratio of the food samples are given in Fig 4.17 to 4.20.

The moisture content was seen to decrease with time as expected because drying removes the water molecules in the food samples (John et al, 2008). The rate of moisture content and moisture ratio decrease was found to be dependent on the thickness of the sample because the moisture content decreases with increase in slice thickness. With the 2mm thick slices, SDP and SDC attained equilibrium moisture content at 330 minutes and 300 minutes respectively while for the 4mm thick slice, a time of 390 minutes and 420 minutes was needed to attain equilibrium moisture content for SDP and SDC respectively. When a bigger slice thickness of 6mm was used, it took a time of 480 minutes and 420 minutes to reach equilibrium moisture content. This is because at low slice thickness, the free moisture can be easily removed from the surface. The thicker the slice, the slower the approach to equilibrium moisture content and the slower the drying rate (Etoamaihe and Ibeawuchi, 2010). Furthermore, at fixed temperature, the drying time increases as the product becomes thicker mainly because as the product's thickness increases, the moisture dissipation inside the product and finally its departure from the product would face more resistance, hence prolonging the drying time (Mohammad et al, 2013). Aremu et al (2013) when investigating the effect of slice thickness on drying kinetics of mango reported that the drying time increased as the slice thickness increase. This is in agreement with the findings of Etoamaihe and Ibeawuchi (2010) in drying different slices of cassava. Slice thickness is one of the main factors affecting the drying characteristics.
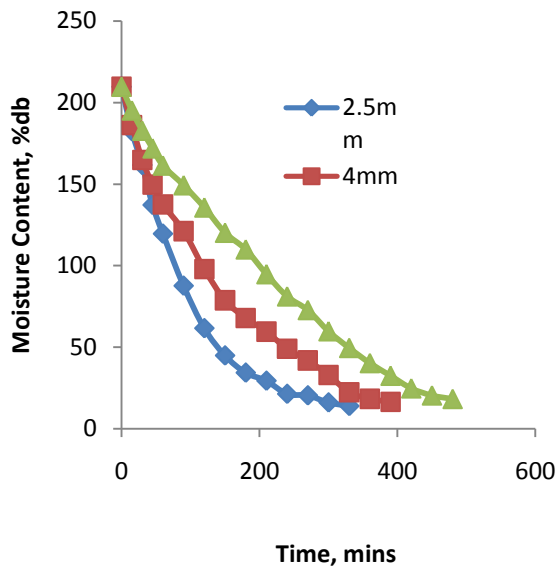
Fig 4. 17: Effect of slice thickness on moisture Content against time for SDP
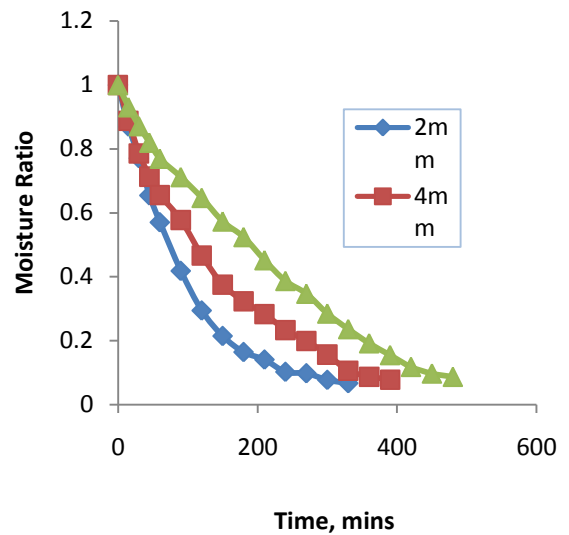
Fig 4. 18: Effect of slice thickness on moisture ratio against time for SDP
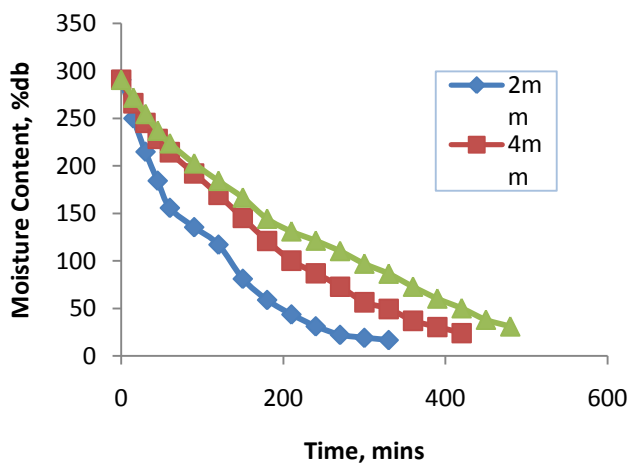
Fig 4. 19: Effect of slice thickness on moisture Content against time for SDC
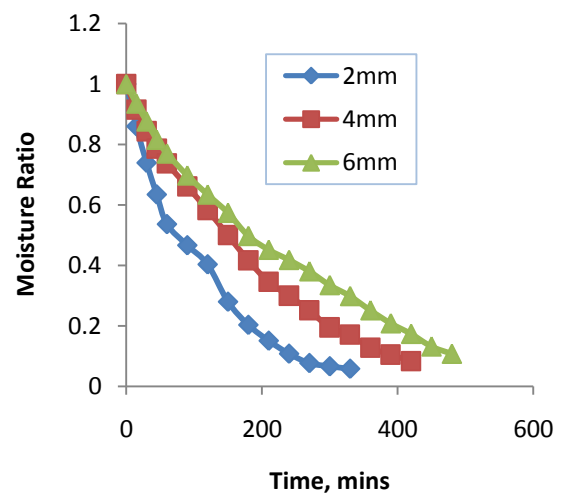
Fig 4. 20: Effect of slice thickness on moisture ratio against time for SDC

116

4.7.2 Effect of Initial mass on drying time

Fig 4.21 to 4.24 shows the variation between initial mass and the moisture content and moisture ratio. The moisture ratio was found to decrease as time increases from its initial moisture ratio of 1.0. The increase in initial mass slightly increased the drying time. This is probably because of the surface area of the drying chamber not being large chamber. The internal mass transfer occurred by diffusion indicating that the drying process occurred in falling rate period just like most of other agricultural products (Ndukwu, 2009; Aremu et al, 2013). The drying of SDP and SDC exhibited the characteristics moisture desorption behaviour, that is, an initial high rate of moisture removal was followed by slower moisture removal in the latter stages. Wankhade et al (2012) reported that the rate of decrease of moisture content was highest at the first hour of drying and then the moisture content loss was slowed down in the subsequent drying periods. As the drying process progressed, the moisture ratio was observed to decrease non-linearly with increase in drying time for all the samples. Tunde and Afon, (2009) reported similar trend in drying of cassava.
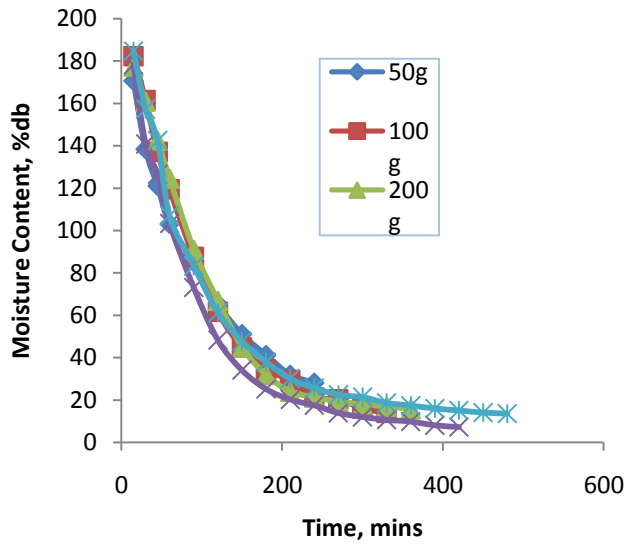
Fig 4. 21: Effect of initial mass on moisture content against time for SDP
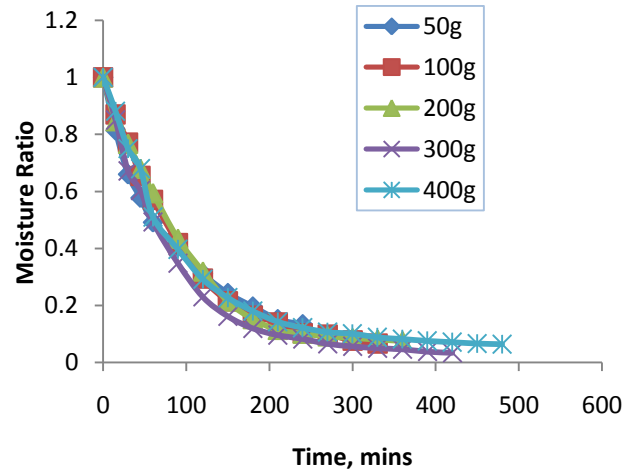
Fig 4. 22: Effect of initial mass on moisture ratio against time for SDP
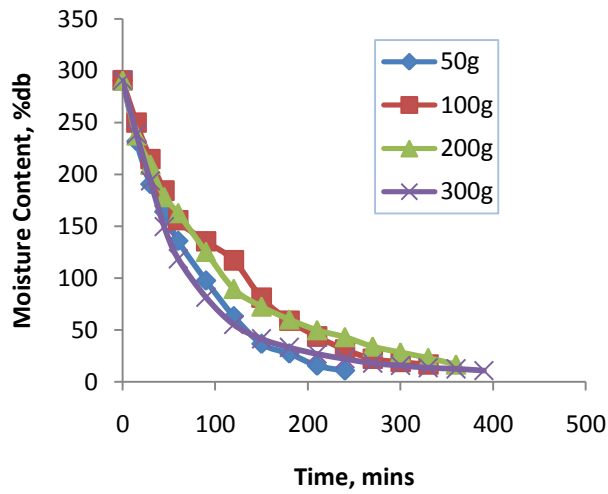
Fig 4. 23: Effect of initial mass on moisture content against time for SDC
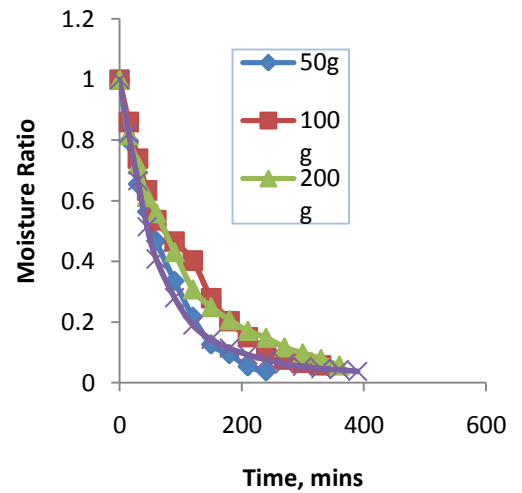
Fig 4. 24: Effect of initial mass on moisture ratio against time for SDC

4.7.3 Effect of drying air speed on moisture content

The effect of air speed on the different drying mechanism was investigated as reported in Fig 4.25 to 4.28. The air speed used varied from 1.5 to 3.5 m/s. With increase in the air speed, there is an increase in the drying rate of the products. This is because one of the requirements of drying is that the air must be moving. When the hot dry air absorbs water from the surface of the drying product, it needs to be quickly moved on so that another set of air can repeat the process. The faster this process, the higher the drying rate will be. Hence, it is seen that the drying time is decreased as the air speed increased.

With an air speed of 1m/s, a drying time of 225 minutes was required for PDP while a drying time of just 165 minutes was required when the air speed was increased to 3.5 m/s, both achieving an equilibrium moisture content of about 15% to 16% db.

In thin layer drying model, the rate of change in material moisture content in the falling rate drying period is proportional to the instantaneous difference between material moisture content and the expected moisture content when it comes into equilibrium with the drying air (Mohammad et al, 2013). The combination of higher temperature, movement of the air and lower humidity in a solar dryer increases the rate of drying. The moisture content decreases continuously with drying time (Wankhade et al, 2012).
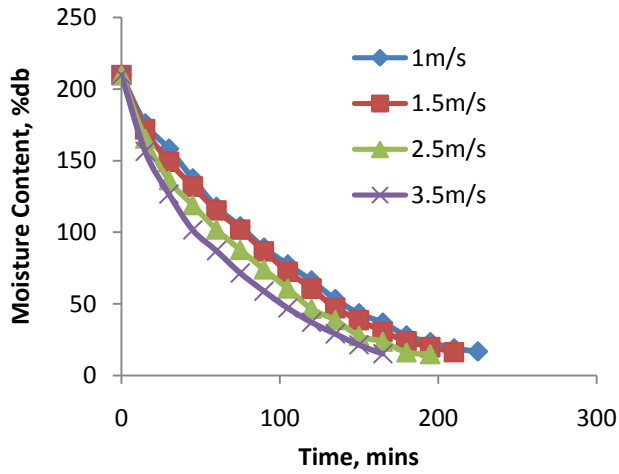
Fig 4. 25: Effect of speed on moisture content against time for PDP at 4mm
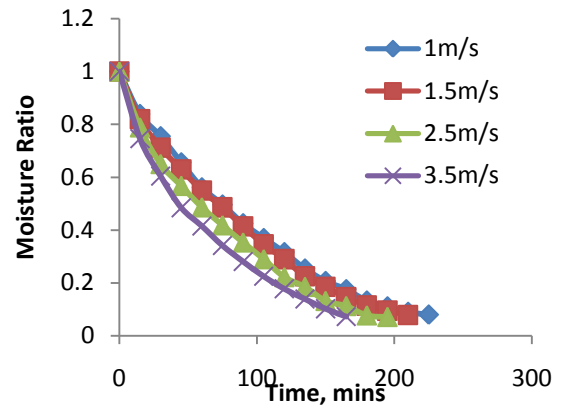
Fig 4. 26: Effect of speed on moisture ratio against time for PDP at 4mm
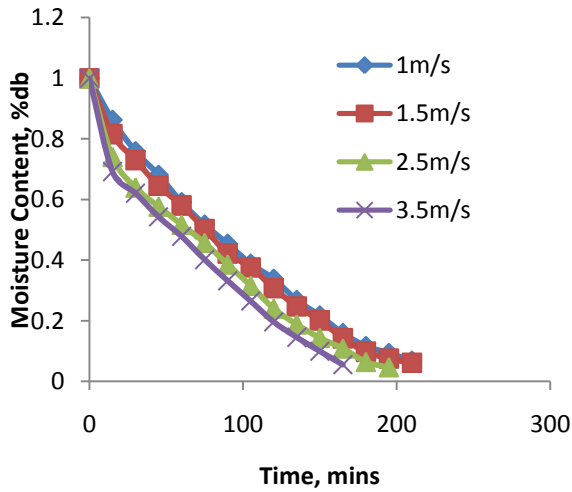
Fig 4. 27: Effect of speed on moisture content against time for PDC at 4mm
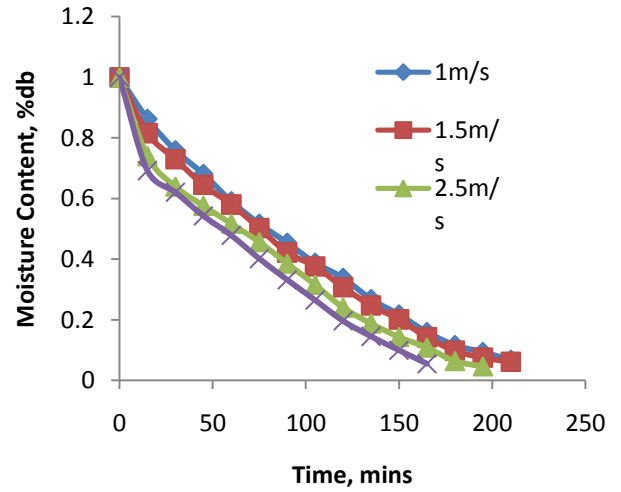
Fig 4. 28: Effect of speed on moisture ratio against time for PDC at 4mm

4.7.4 Effect of temperature on drying rate using Oven dryer

Fig 4.29 to 4.32 reveal the effect of temperature on the drying process. It was done using the oven dryer for temperatures in the range of 60 ^{o}C and 90 ^{o}C. This temperature was used because using a very high temperature may cause the food item to be hardened on the surface (Adu et al, 2012). The results indicated that the drying time was decreased as the temperature increased. This is due to the fact that as the temperature increased, the average kinetic energy of the moisture increases making it easier for the moisture to diffuse out of the products. It was seen that higher temperature drying did not so much affect the drying time as would have been expected. This is probably because the air circulation inside the Oven is not sufficient. In the drying of ODP and ODC, as the drying temperature reduces from 90 ^{o}C to 60 ^{o}C, the time taken to reach the equilibrium moisture content in the product increased from 210 and 240 minutes to 360 and 390 minutes for ODP and ODC respectively.

Wankhade et al (2012) and Saeed et al (2008) reported that air temperature had a significant effect on the moisture content of samples. Increasing the temperature brings about a decrease in drying time because both the thermal gradient inside the object and the evaporation rate of the product increase (Mohammad et al, 2013).
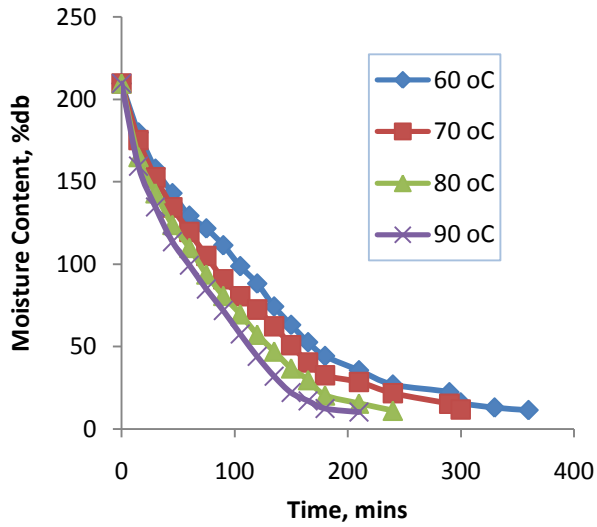
Fig 4. 29: Effect of Temperature on moisture content against time for ODP at 4mm and 1.5m/s
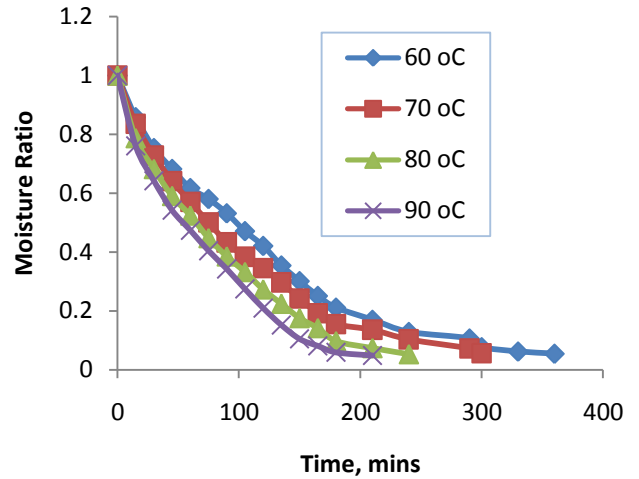
Fig 4. 30: Effect of Temperature moisture ratio against time for ODP at 4mm and 1.5m/s
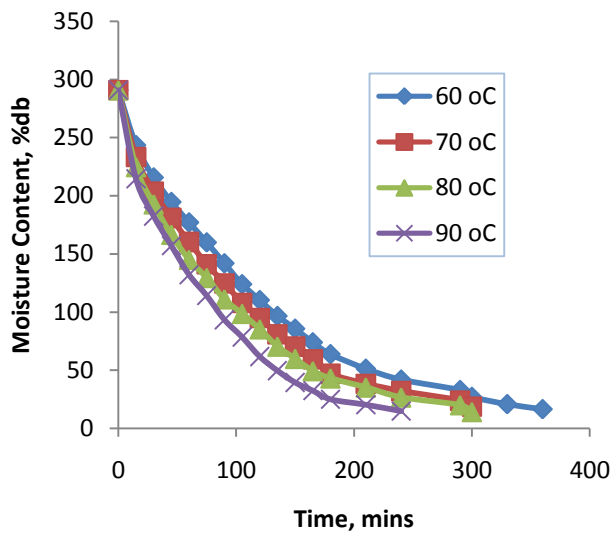
Fig 4. 31: Effect of Temperature on moisture content against time for ODC at 4mm and 1.5m/s
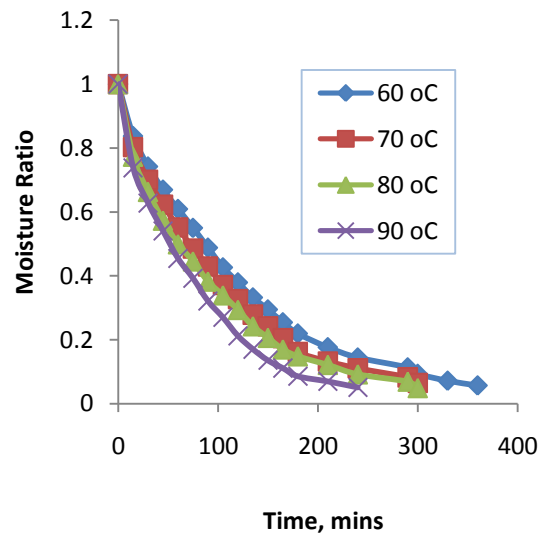
Fig 4. 32: Effect of Temperature on moisture ratio against time for ODC at 4mm and 1.5m/s

4.7.5 Effect of temperature and air speed on hot air conventional dryer

The hot-air conventional dryer was used to investigate the effects of temperature and air speed on the drying process (Fig 4.33 to 4.44). The CDP at 209.597% db and CDC at 290.625 % db initial moisture content were dried at different temperatures at 50 $^{\circ}$C, 60 $^{\circ}$C, and 70 $^{\circ}$C with air speeds of 2.0, 2.5, 3.0, 3.5 and 4.0 m/s. In the drying of CDP, the drying process took just 120 minutes to attain equilibrium moisture content when dry at an air speed of 4.0 m/s and temperature of 70 $^{\circ}$C while it took 210 minutes to dry at 2.0 m/s and 50 $^{\circ}$C. Increased temperature of drying caused a faster attainment of equilibrium moisture content and hence increased drying rate (Etoamaihe and Ibeawuchi, 2009). The drying time of both CDP and CDC decreased as the temperature, air speed and time are important parameters in drying. Equally, drying occurs initially at the outer layer. Hence when the product is dried, its permeability is decreased and the surface is hardened. This hardened layer imposes a barrier against dissipation of moisture across the product's surface and hence prolongs its departure from the product (Mohammad et al, 2013; Motevali et al, 2012)
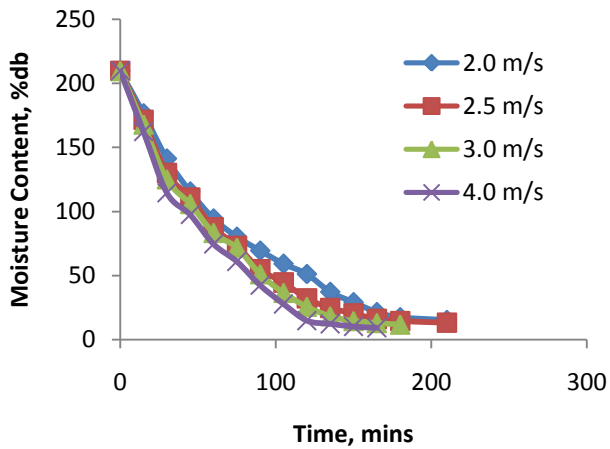
Fig 4.33: Effect of air flow rate on moisture content for CDP at 50°C
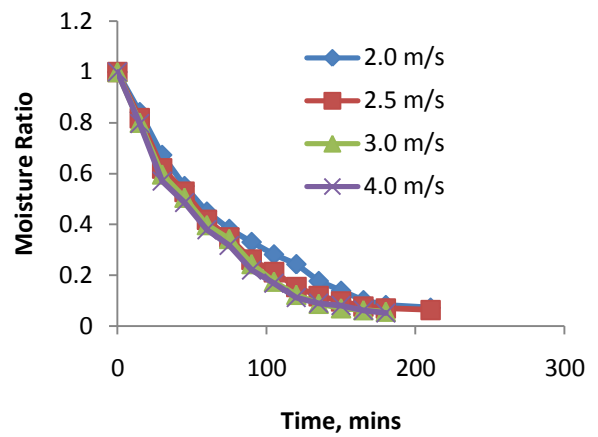
Fig 4.34: Effect of air flow rate on moisture ratio for CDP at 50 ^{o}C
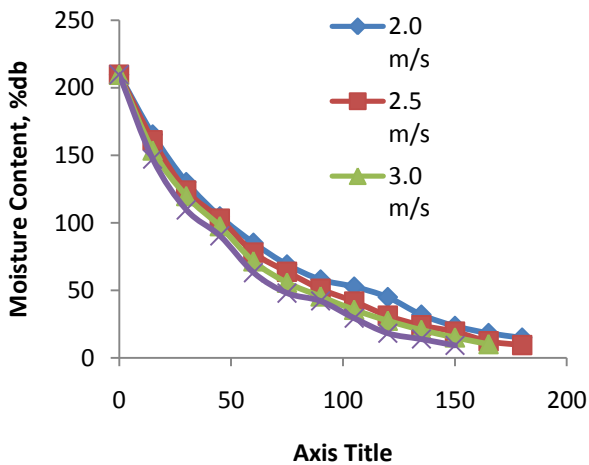
Fig 4.35: Effect of air flow rate on moisture content for CDP at 60°C
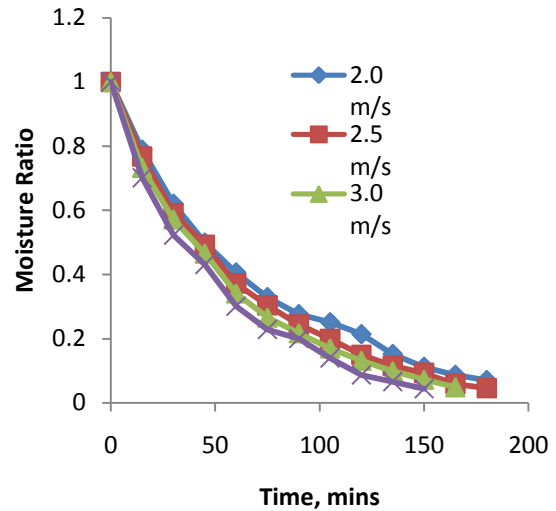
Fig 4.36: Effect of air flow rate on moisture ratio for CDP at 60 ^{o}C
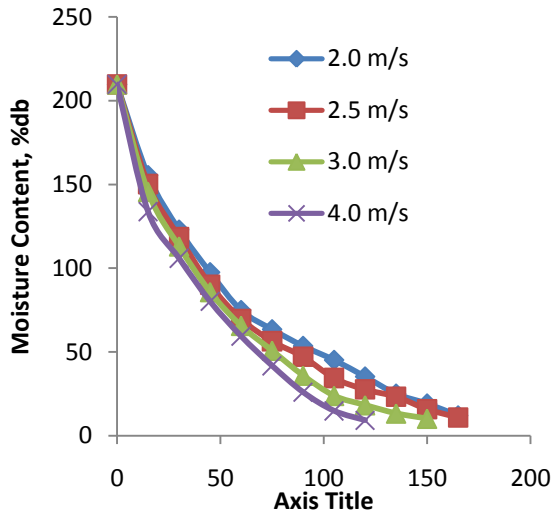
Fig 4.37: Effect of air flow rate on moisture content for CDP at 70 °C
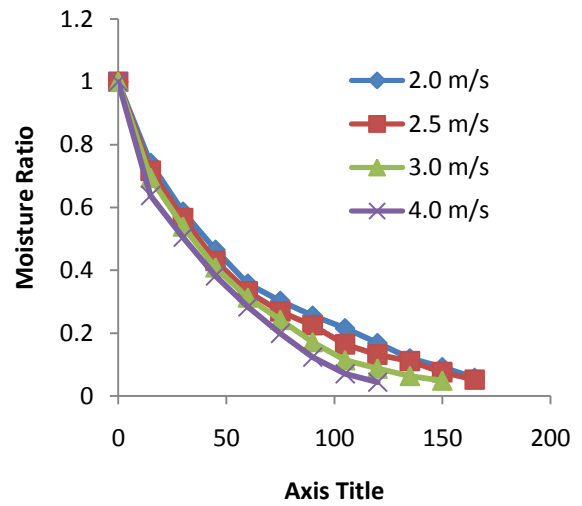
Fig 4.38: Effect of air flow rate on moisture ratio for CDP at 70 °C
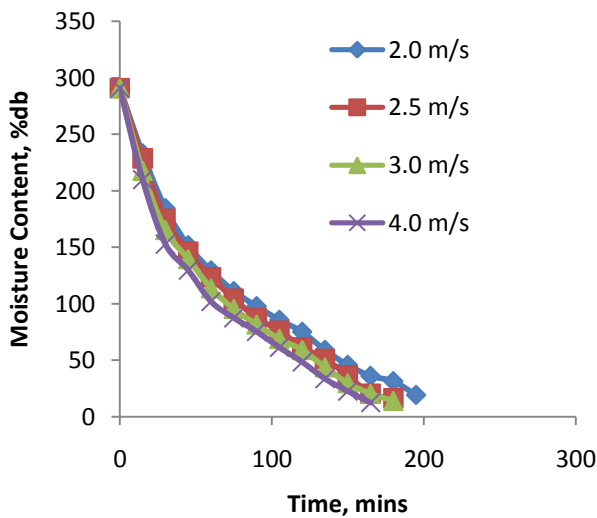
Fig 4.39: Effect of air flow rate on moisture content for CDC at 50°C
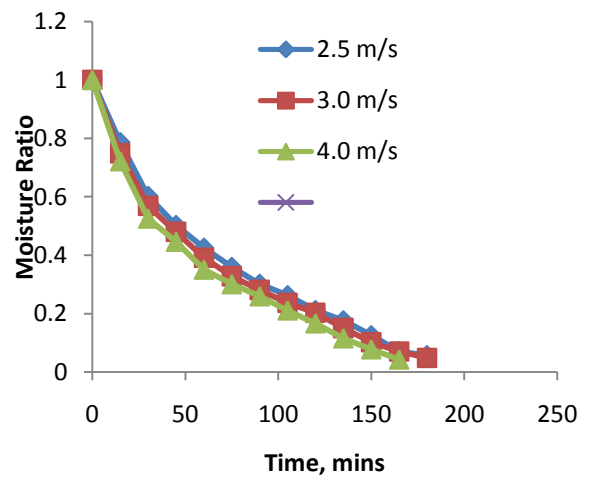
Fig 4.40: Effect of air flow rate on moisture ratio for CDC at 50 °C

Fig 4.42: Effect of air flow rate on moisture ratio for CDC at 60 °C
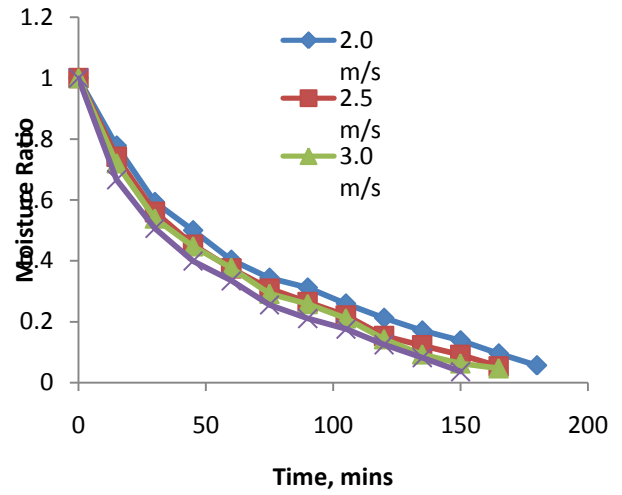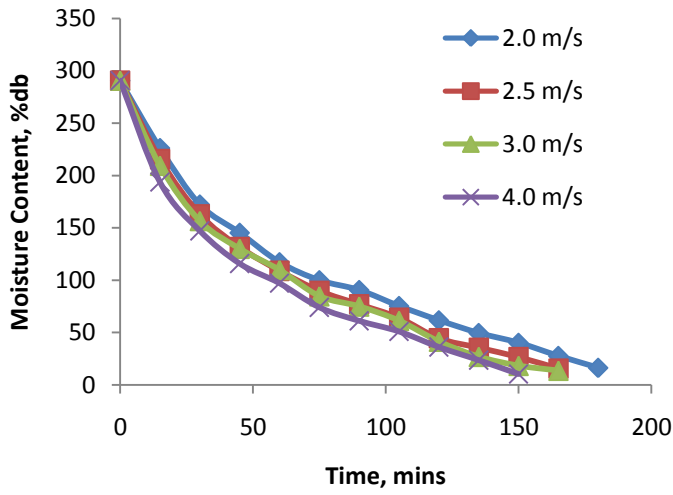
Fig 4.41: Effect of air flow rate on moisture

content for CDC at 60°C
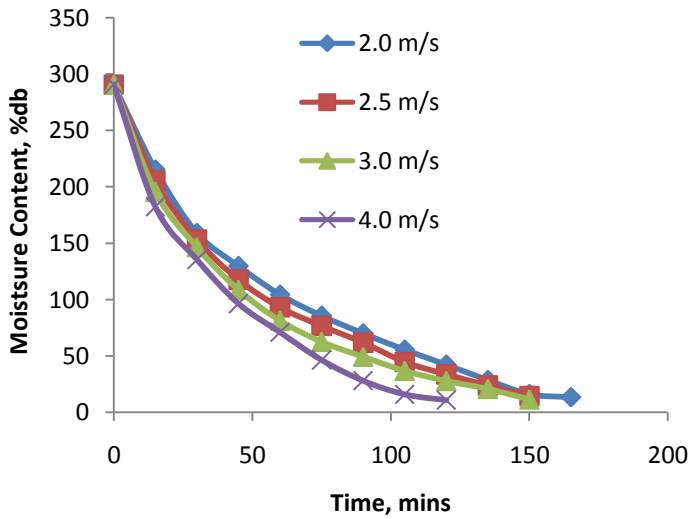
Fig 4.43: Effect of air flow rate on moisture

content for CDC at 70°C
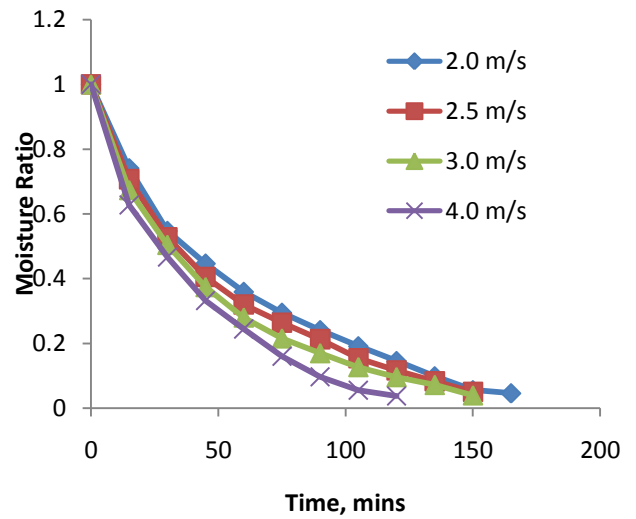
Fig 4.44: Effect of air flow rate on moisture

ratio for CDC at 70 °C

4.7.6 Temperature difference between Ambient and drying Chamber Temperature

The Photovoltaic dryer functioning as a solar dryer absorbs energy from the sun which is used in the drying chamber to dry the products. Fig 4.45 to 4.48 shows the difference in the temperature of the drying chamber and the ambient. This is expected because solar dryers operate by raising the temperature of the air in the drying chamber. This is enhanced by the transmittance of the glass used in the collector bed. Domenec and Natalie (2014) reported that with efficient insulation, the temperatures of the drying chamber will more than double the ambient temperature. The temperature just at the exit of the drying chamber is lower than the temperature of the drying chamber but higher than the ambient temperature.
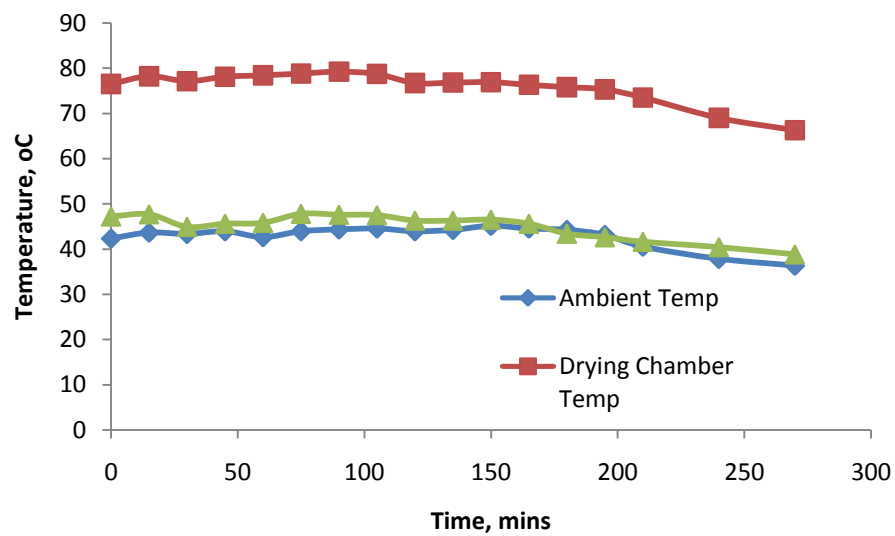
Fig. 4.45   Temperature variation in the first month
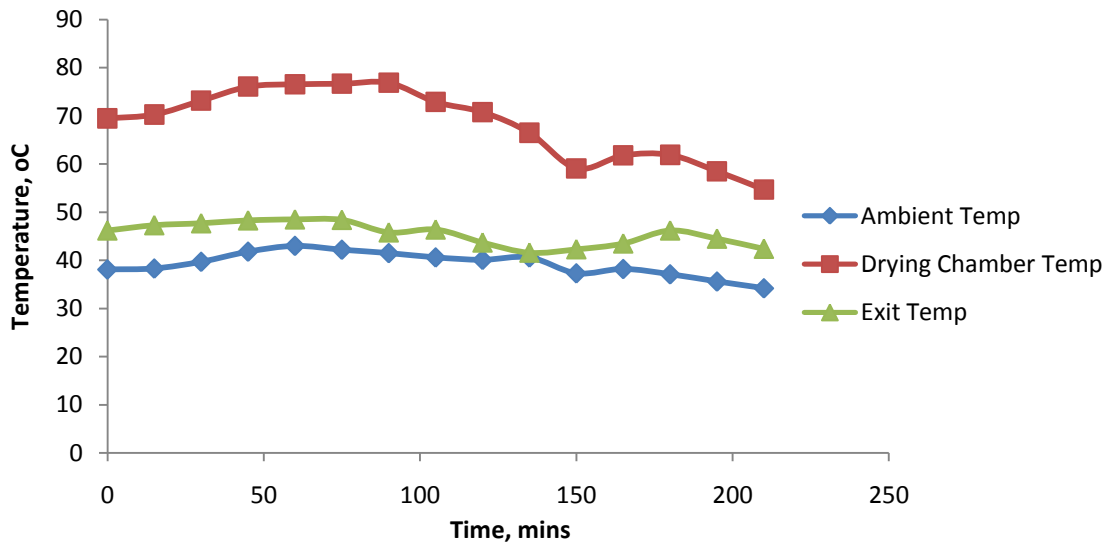
Fig. 4.46   Temperature variation in the second month
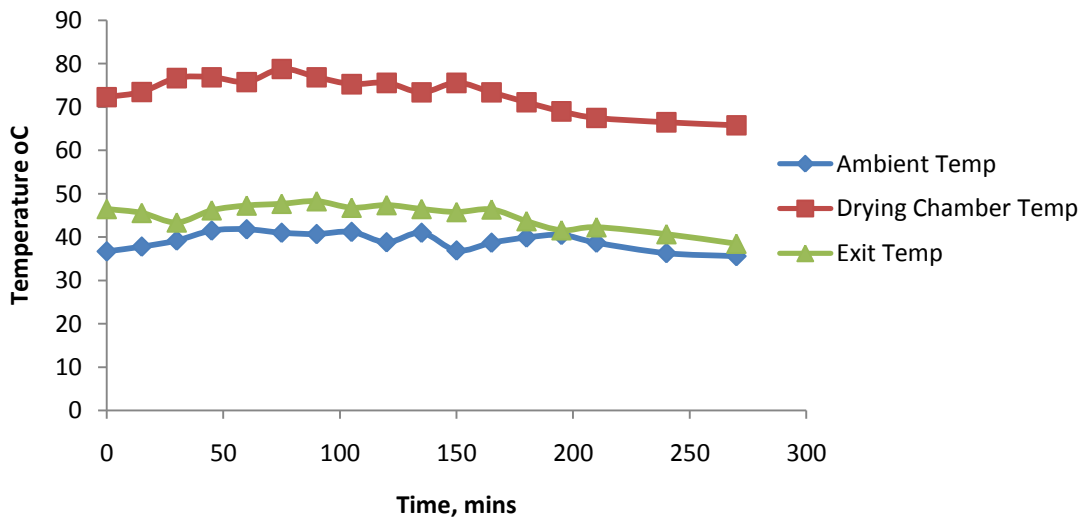
Fig. 4.47   Temperature variations in the third month
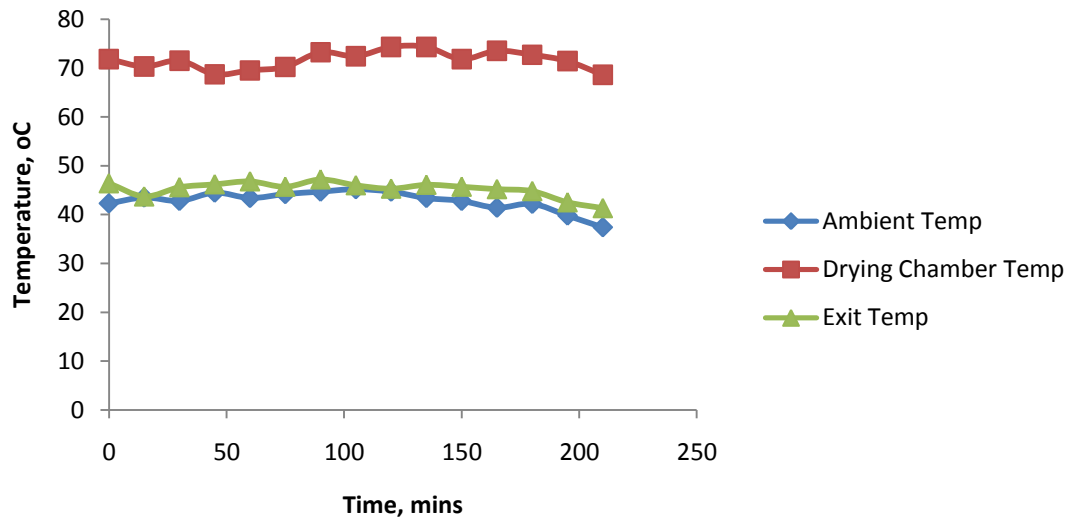
Fig. 4.48   Temperature variation in the fourth month

4.8   Mass Shrinkage Ratio

The mass shrinkage ratio is the most important structural variation. This is due to the weight loss (Saeed et al, 2008). The variation of the mass shrinkage ratio with time for the different drying techniques is shown in Fig 4.49 to 4.64. Most of the shrinkage was observed to have occurred in the early stages of the drying and seen to be tending towards a constant value in the later stages. This is because towards the end of the drying, the surface became drier than the centre making the surface stiff and hence limits the shrinkage (Bao-meng et al, 2013). To minimize shrinkage, low-temperature drying should be employed so that moisture gradients throughout the products are minimized. Moisture gradient occurring inside the food during drying generates stresses

in the cellular structure of the food resulting in the structural collapse which responds to the physical changes of shape and dimension or the volume change of material (Amira et al, 2014).
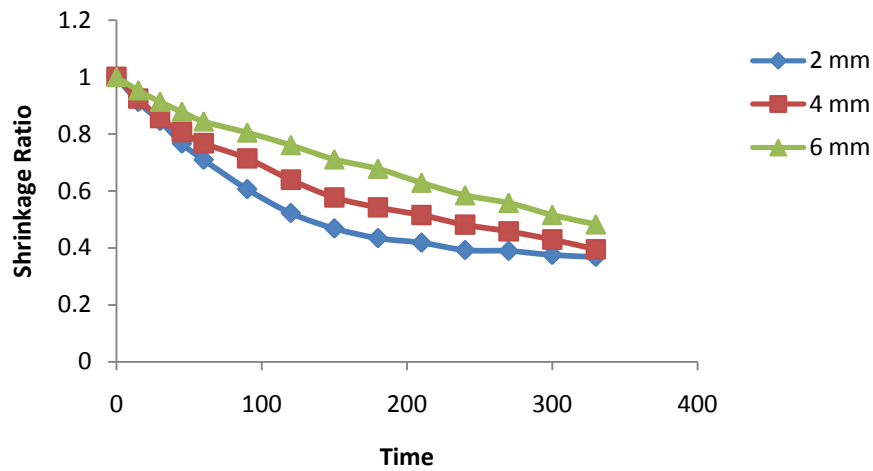
Fig 4.49 Plot of time against shrinkage ratio at different slice thickness for SDP
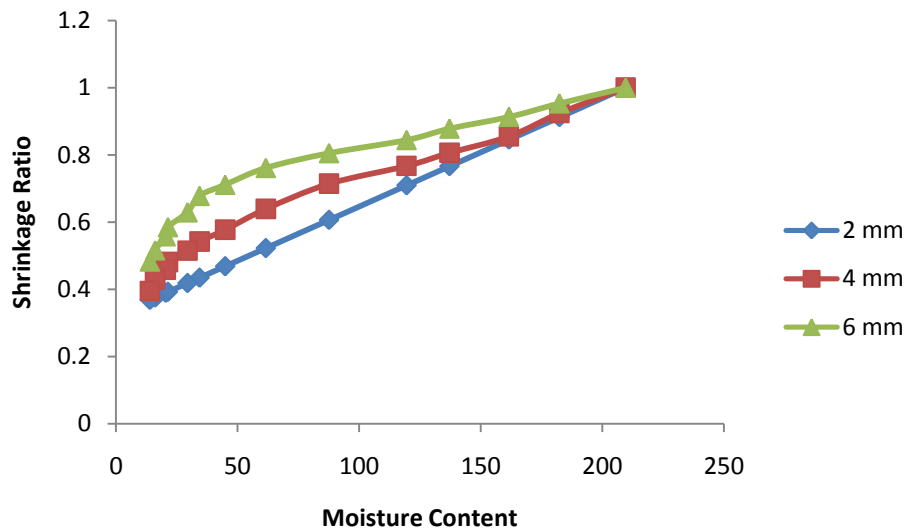
Fig 4.50 Plot of moisture content against shrinkage ratio at different slice thickness for SDP
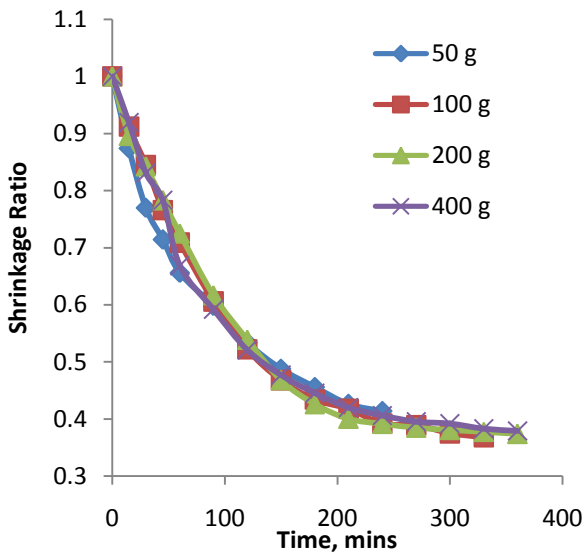
Fig 4.51 Plot of time against shrinkage ratio at different initial masses for SDP
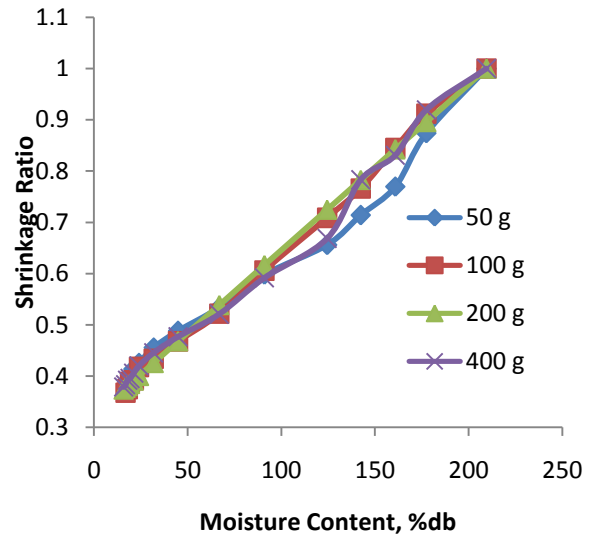
Fig 4.52   Plot of moisture content against shrinkage ratio at different initial masses for SDP
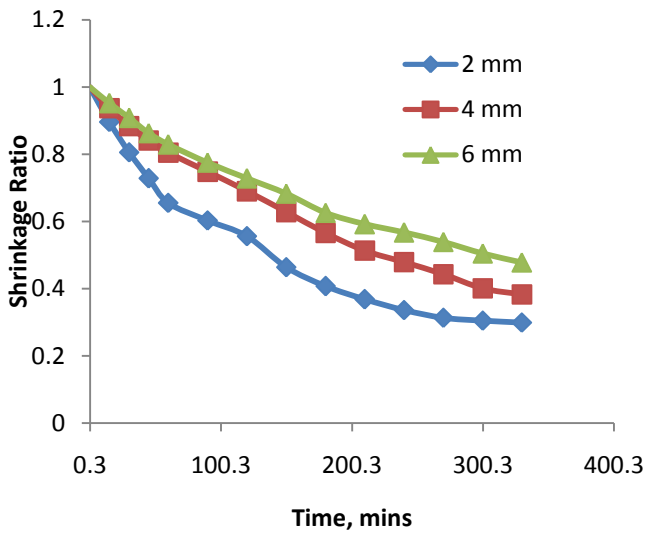
Fig 4.53 Plot of time against shrinkage ratio at different slice thickness for SDC
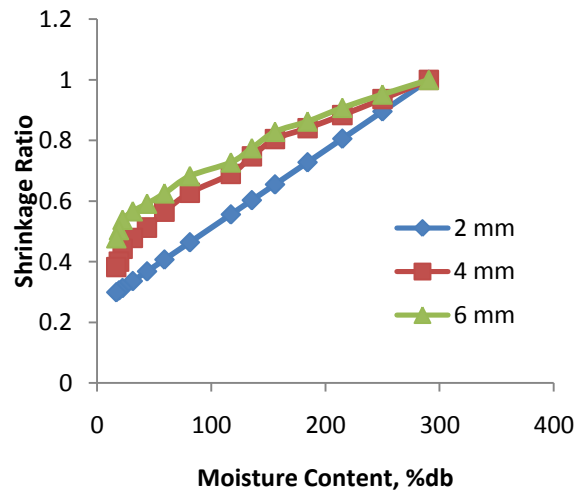
Fig 4.54   Plot of moisture content against shrinkage ratio   at different slice thickness for SDC
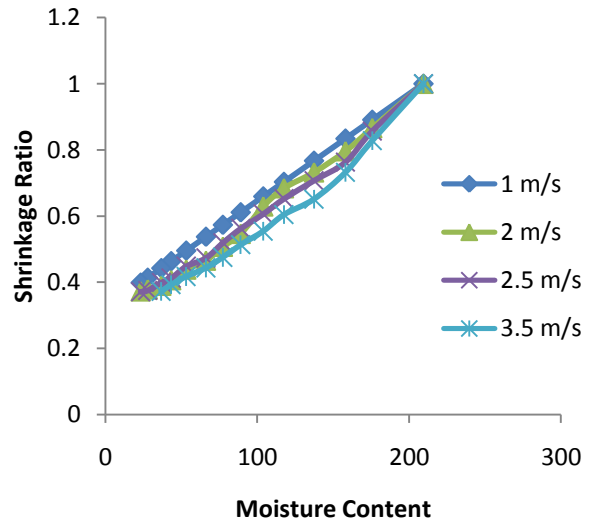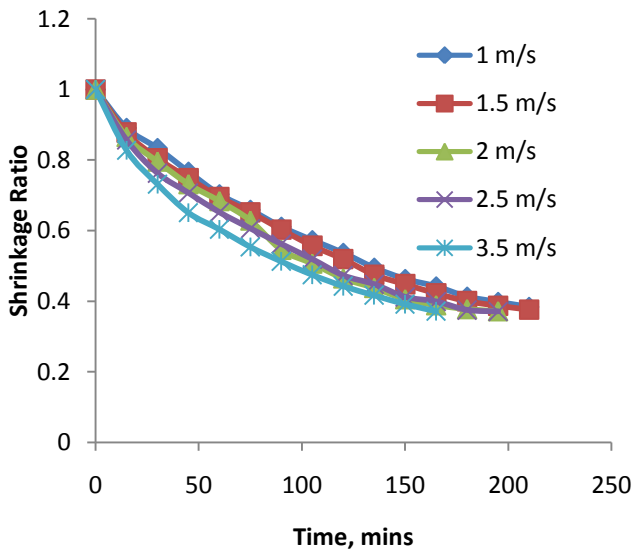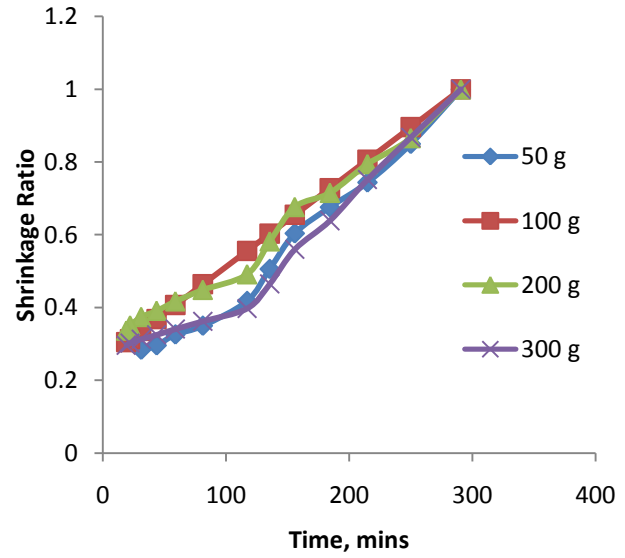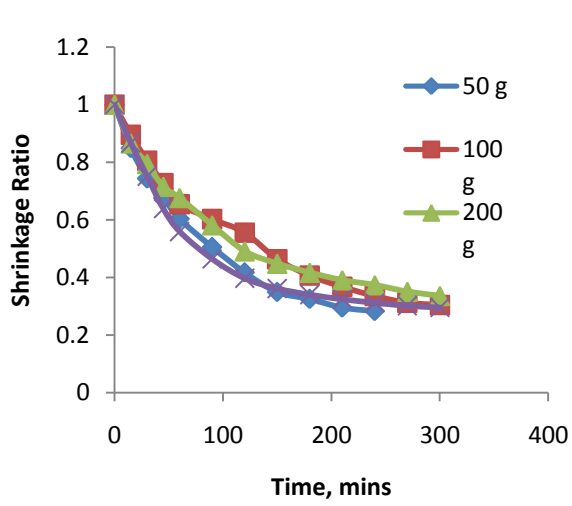
ge ratio at

Fig 4.57 Plot of time against shrinkage ratio at different air speeds for PDP

Fig 4.58   Plot of moisture content against shrinkage ratio at different air speeds for PDP

132
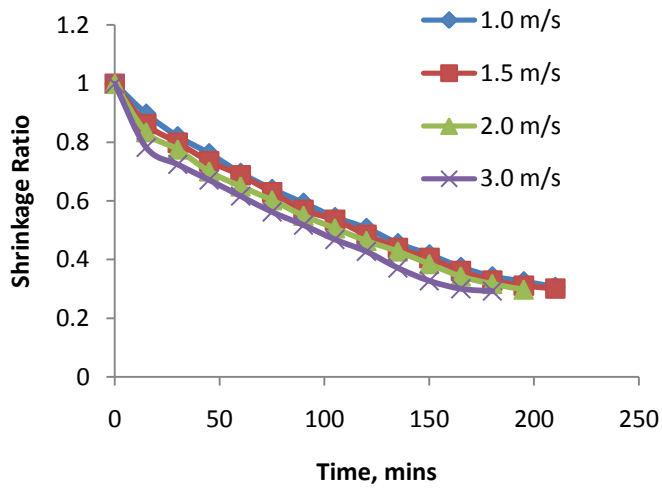
Fig 4.59 Plot of time against shrinkage ratio at different air speeds for PDC
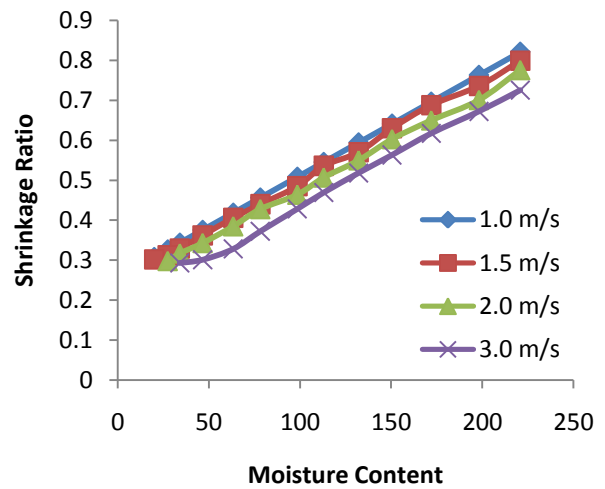
Fig 4.60   Plot of moisture content against shrinkage ratio at different air speeds for PDC
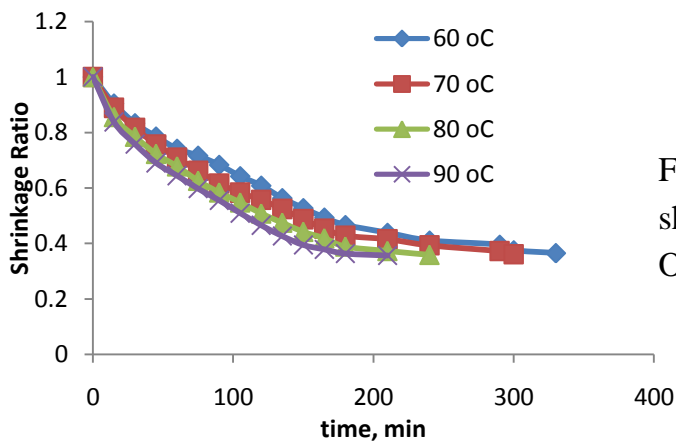
Fig 4.61 Plot of time against shrinkage ratio at different temperature for ODP
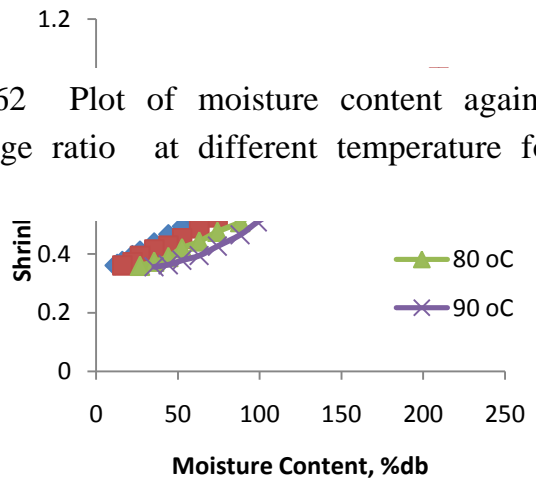
Fig 4.62   Plot of moisture content against shrinkage ratio   at different temperature for ODP

133
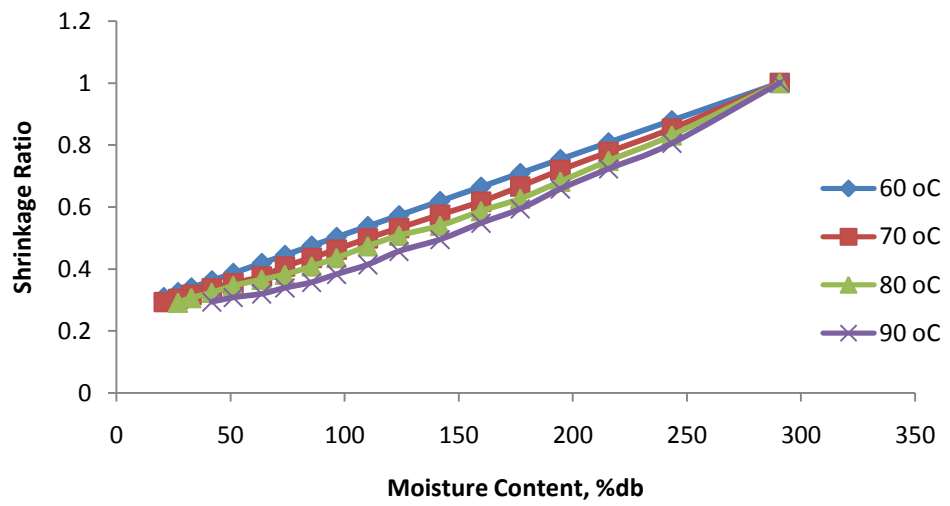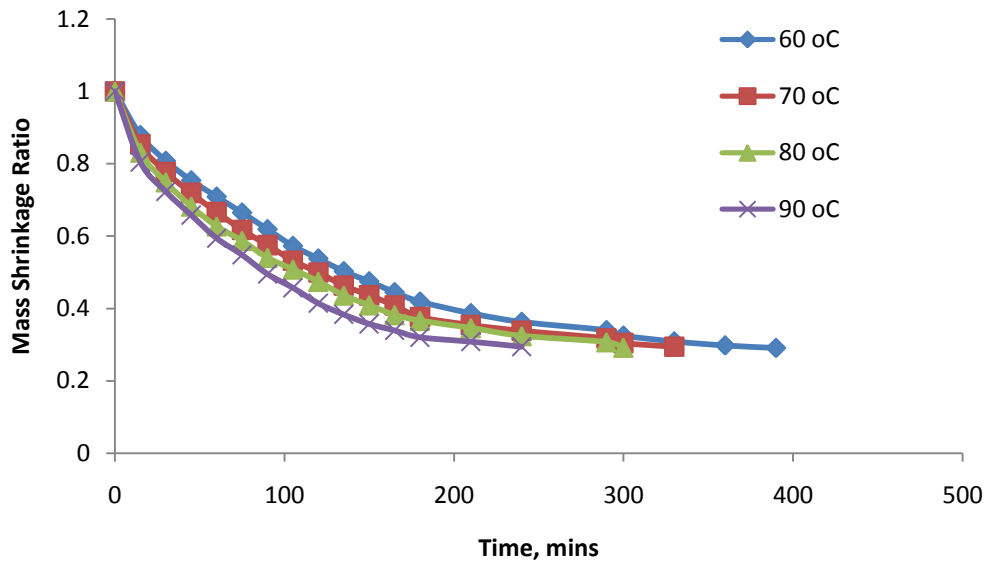
Fig 4.64 Plot of moisture content against shrinkage ratio at different temperature

4.9 Drying rate

The drying rate was evaluated as the decrease of the water concentration during the time interval between two subsequent measurements divided by time interval (Anna et al, 2014). Many factors were discovered to affect the drying rate.

4.9.1 Effect of thickness and initial mass on drying rate

Fig 4.65 to 4.72 reveals the effects of slice thickness and initial mass on the drying rate of ODP and ODC. The drying rate was obtained by calculating the time required to remove a given quantity of moisture from the product. The drying rate decreased as the slice thickness increased. After 15 minutes, the drying rate of the 2 mm slice thickness was 0.586 g/g.min while for 4 mm and 6 mm slice thickness, the drying rate were 0.507 and 0.313 g/g.min. The main factor that controls the drying rate is the rate at which moisture can move from the interior of a piece of food to the surface. Therefore the shorter the distance that moisture has to travel, the faster the drying rate will be. Equally, reducing the size also increases the surface area of the food in relation to the volume of the pieces which increases the rate at which water can be evaporated from the food. During the initial period, drying rate is high. This is due to the fact that the energy required to evaporate the surface moisture is low (Sajith and Muraleedharan, 2014). With moisture content, the drying rate decreases as the moisture content decreases. This is probably because the amount of moisture removed depends on the quantity of moisture in the product.
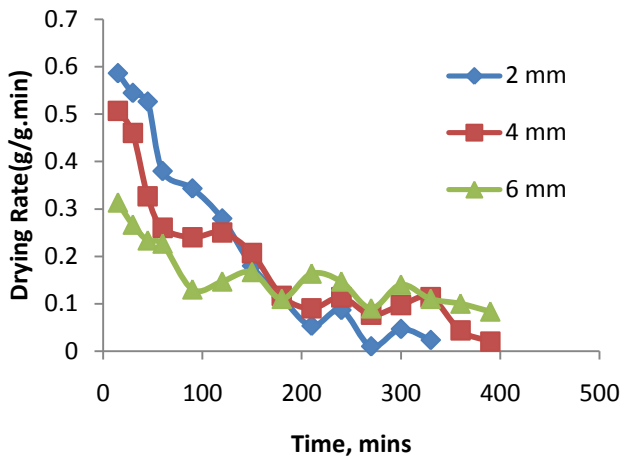
Fig 4.65 Plot of drying rate against time at different slice thicknesses for SDP
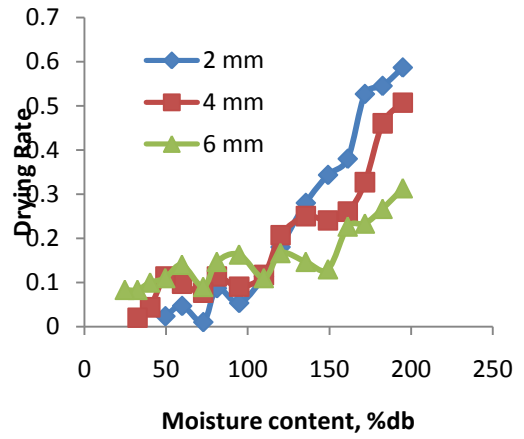
Fig 4.66 Plot of drying rate against moisture content at different slice thicknesses for SDP
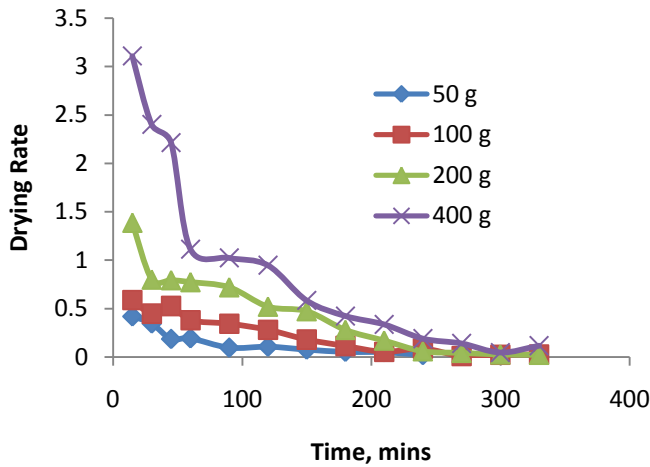
Fig 4.67 Plot of drying rate against time at different initial masses for SDP
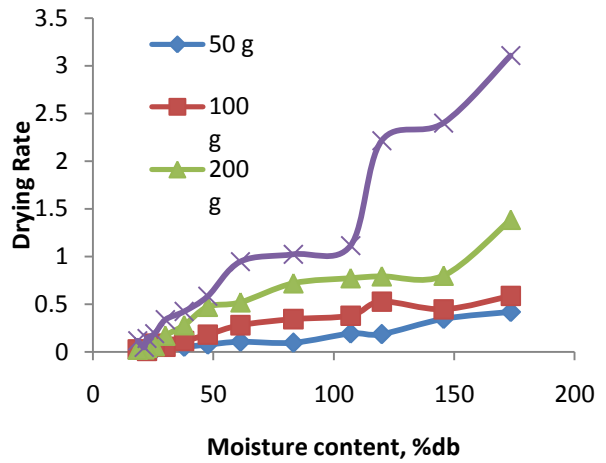
Fig 4.68 Plot of drying rate against moisture content at different initial masses for SDP

Fig 4.70 Plot of drying rate against moisture content at different slice thickness for SDC
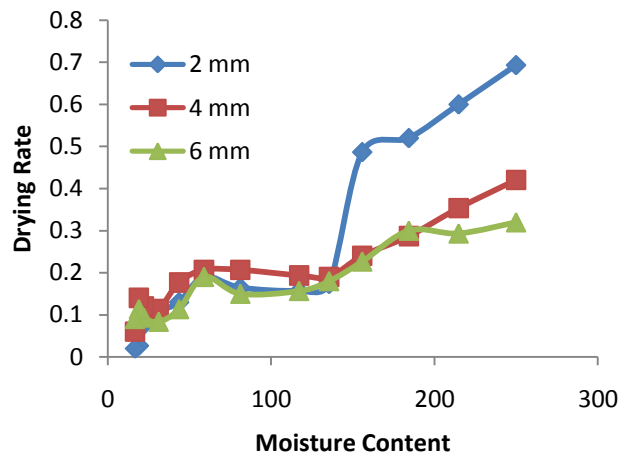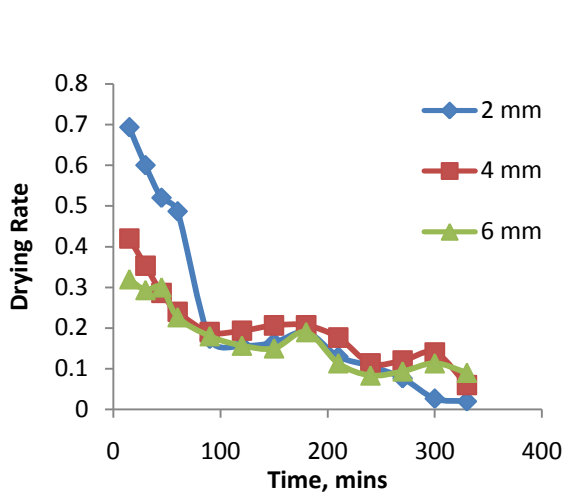
Fig 4.69 Plot of drying rate against time at

different slice thickness for SDC
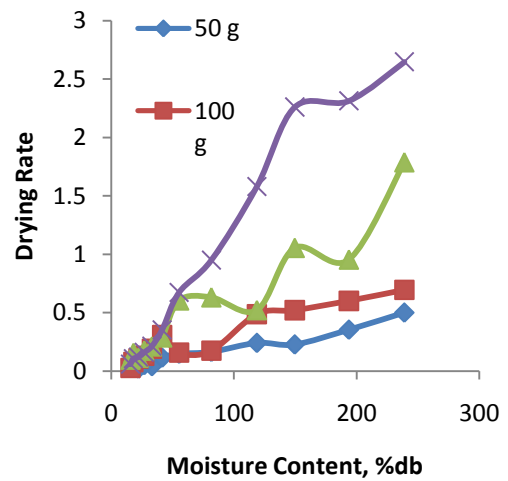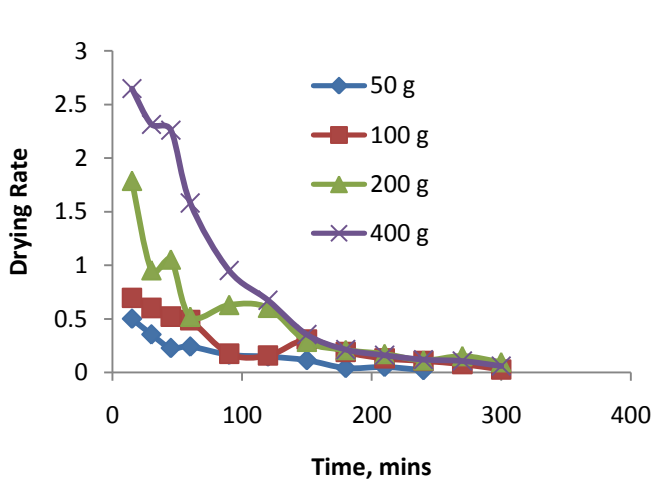
Fig 4.71 Plot of drying rate against time at   Fig 4.72 Plo

different initial masses for SDC   content at dif

4.9.2 Effect of air speed on the drying rate

The variation of different air speed on the drying rate is given in Fig 4.73 to 4.76. It is seen that increase in air speed leads to a relative increase in the drying rate. At a time of 30 minutes, the drying rate was seen to be 0.38, 0.467, 0.573 and 0.64 g/g.min for air speed of 1.0, 2.0, 3.0 and 3.5 m/s respectively. Nicholas (2012) reported also an increase in drying rate as air speed increases from 1.8 to 3.8 m/s. Mirzaee et al (2009) reported similar trend. The drying rate of PDC was seen to be initially higher than that of the PDP.

It is apparent that the drying rate is higher at the beginning of the drying process and decreases continuously with the drying time (Mirazaee et al, 2009). According to Wankhade et al (2012), the drying rate goes on decreasing with decrease in moisture content. The rate of drying also has an important effect on the quality of the dried food products. The rate of drying in the Solar cabinet dryer is higher than that in the open sun drying. This is in agreement with the investigations of Ajao and Adedeji (2008).
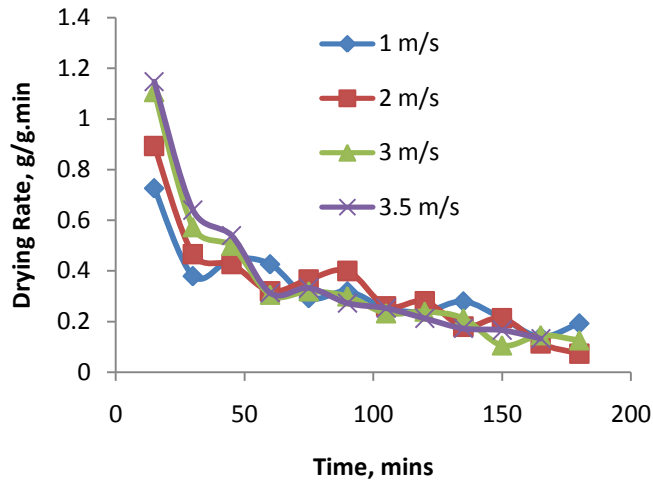
Fig 4.73 Plot of drying rate against time at different air speeds for PDP
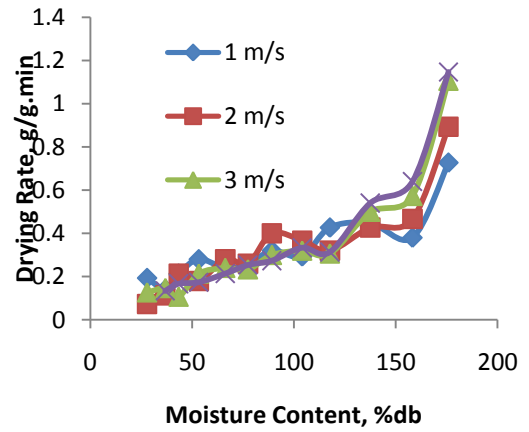
Fig 4.74 Plot of drying rate against moisture content at different air speeds for PDP
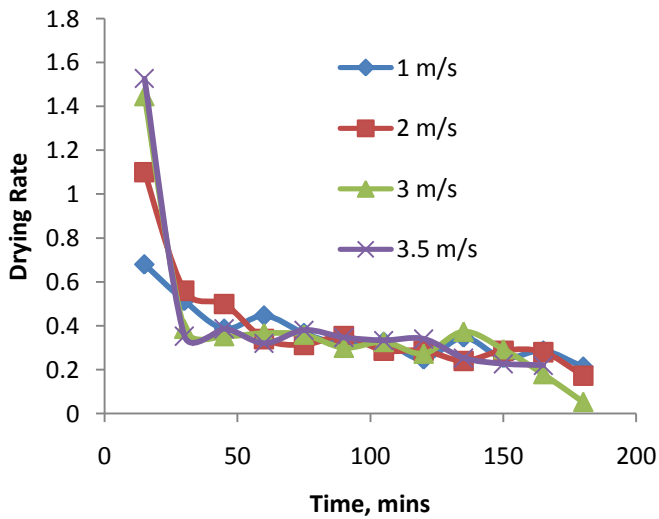
Fig 4.75 Plot of drying rate against time at different air speeds for PDC
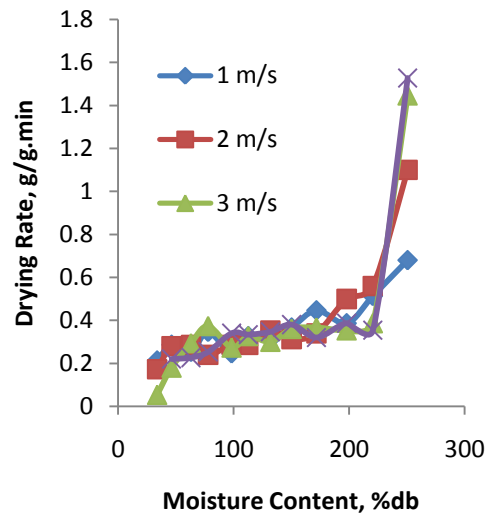
Fig 4.76 Plot of drying rate against moisture content at different air speeds for PDC

4.9.3 Effect of temperature on drying rate

The effects of temperature on the drying rate were given in Fig 4.77 to 4.80. It is seen that for both the oven dryer and the hot-air conventional dryer that increase in temperature increases the rate of drying. This is attributed to increased evaporation of water both on the surface and in the products due to the increased temperature (Junling et al, 2008). As the drying process continues, less free water on the product's surface is available and hence, the drying rate starts to decrease. The high drying rate at high drying temperature could be due to more heating energy which speeds up the movement of water molecules and results in higher moisture diffusivity (Junling et al, 2008).

The curve of the drying rate was seen not to be a perfect curve. The curve was in agreement with the work of Divine et al (2013). This could be due to the nature of the drying products and the diffusion mechanism inside the products as the drying progresses.
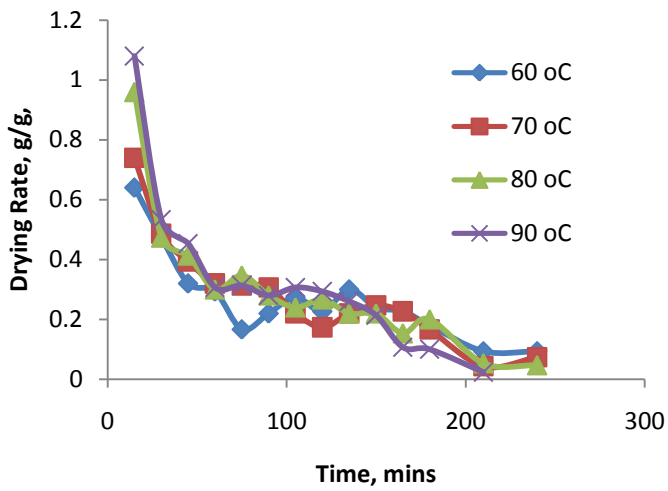
Fig 4.77   Effect of temperature on drying rate against time for ODP
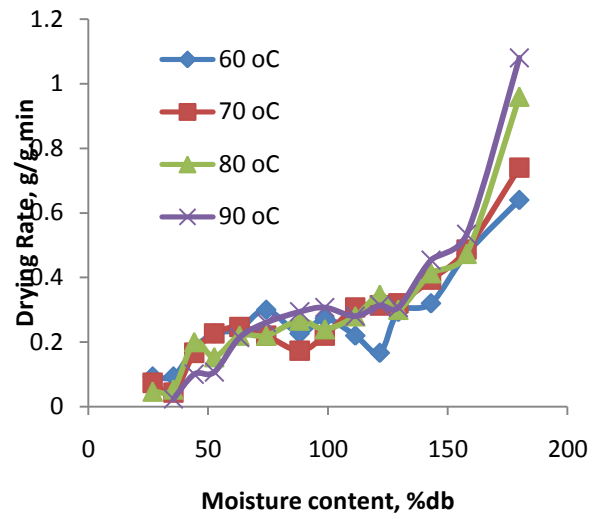
Fig 4.78   Effect of temperature on drying rate against moisture content for ODP
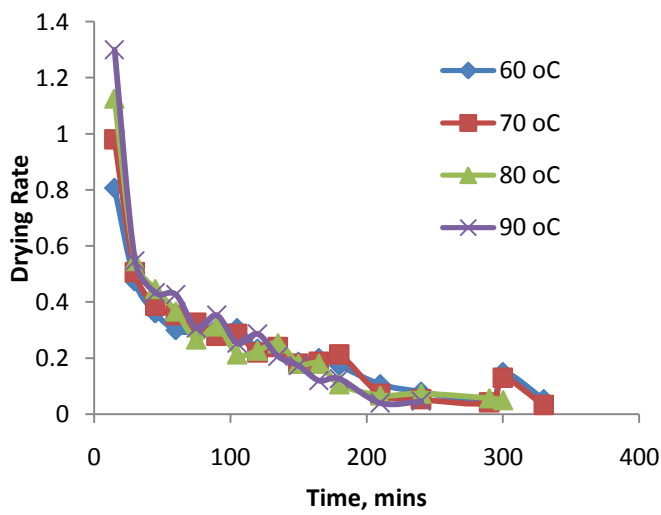
Fig 4.79   Effect of temperature on drying rate against time for ODP
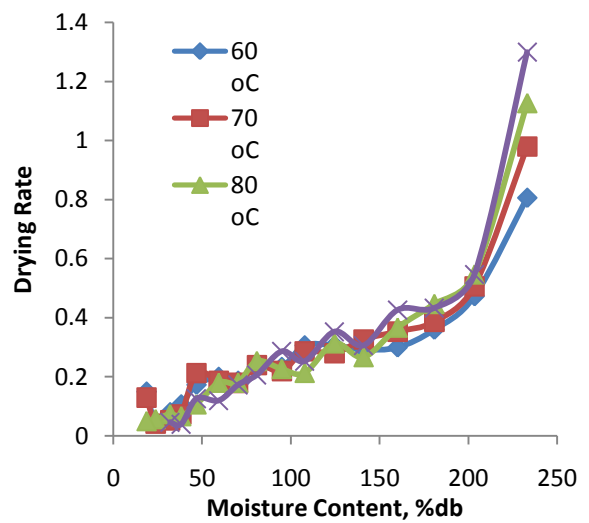
Fig 4.80   Effect of temperature on drying rate against moisture content for ODP

4.9.4 Variation of drying rate in the hot-air dryer

The hot-air conventional dryer shows the combined effects of air speed and temperature on the drying rates of CDP and CDC (Fig 4.81 to 4.90). The air speed used in the dryer ranged from 2.0 m/s to 4.0 m/s while the temperature was between 50 ^{o}C and 70 ^{o}C. It is seen that there is more significant difference as the temperature changes from 50 ^{o}C to 70 ^{o}C than when the air speed increased from 2.0 to 4.0 m/s. In thin-layer drying, the effect of temperature on drying time is more significant relative to the air speed (Mirzaee et al, 2009; Divine et al, 2013). The drying process that occurs at higher air speed and higher temperature reached the equilibrium moisture content more quickly than others. Ndukwu (2009) reported the same observation. The drying rates were higher at the beginning of the drying operation and later decreases with decreasing moisture content (Anna et al, 2014; Ndukwu, 2009). The drying rate helps to determine the time the food should spend in the dryer before the moisture content is low enough to prevent spoilage by micro-organisms. The high drying rate at high drying temperature could be due to more heating energy which speeds up the movement of water molecules and results in higher moisture diffusivity (Junling et al, 2008).
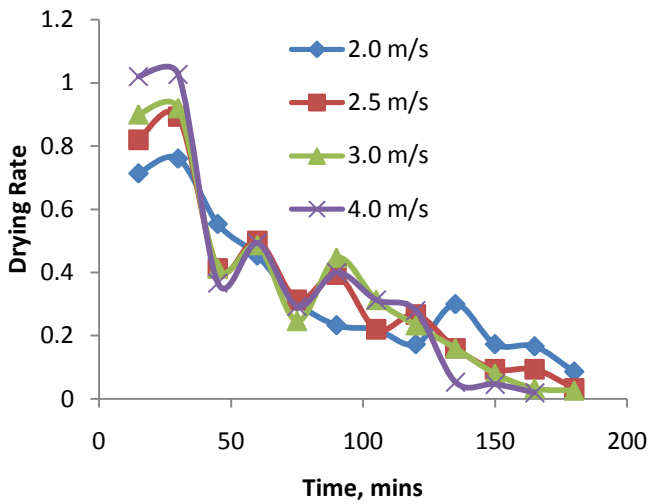
Fig 4.81 Effect of air speed on drying rate against time for ODP at 50 $^\circ$C
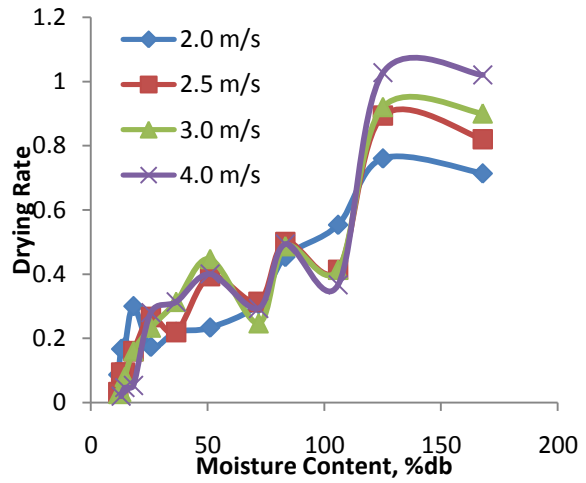
Fig 4.82 Effect of air speed on drying rate against moisture content for ODP at 50 $^\circ$C
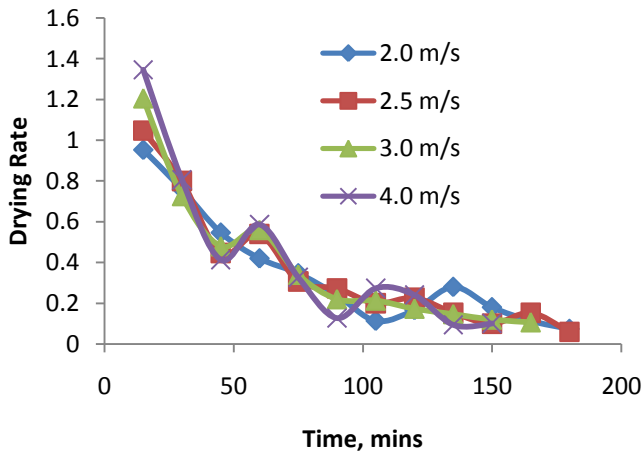
Fig 4.83 Effect of air speed on drying rate against time for ODP at 60 $^\circ$C
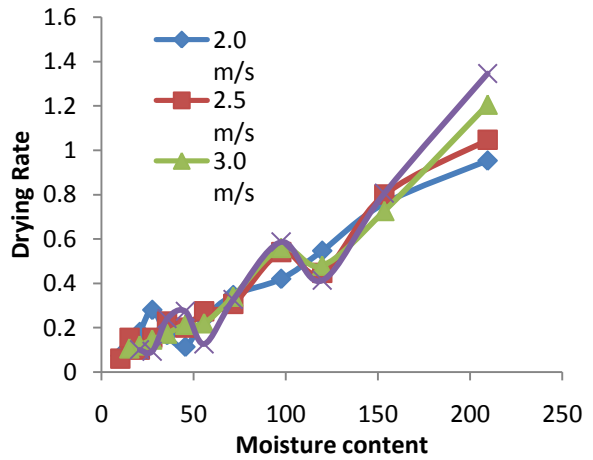
Fig 4.84 Effect of air speed on drying rate against moisture content for ODP at 60 $^\circ$C
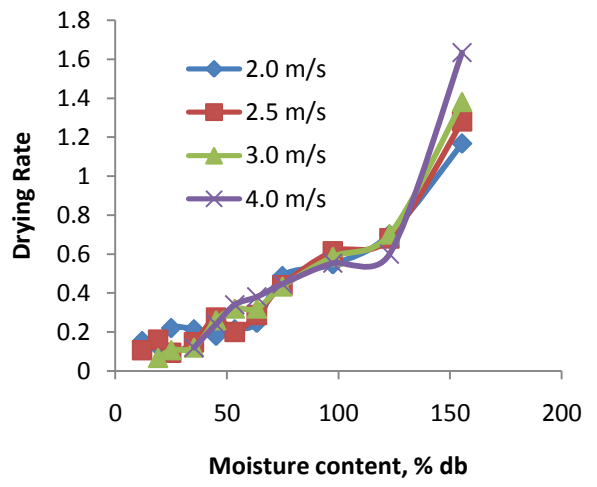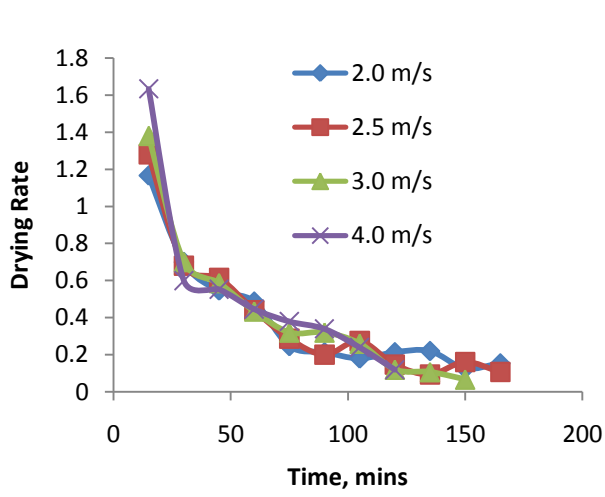
Fig 4.85 Effect of air speed on drying rate against time for ODP at 70 $^{\circ}$C
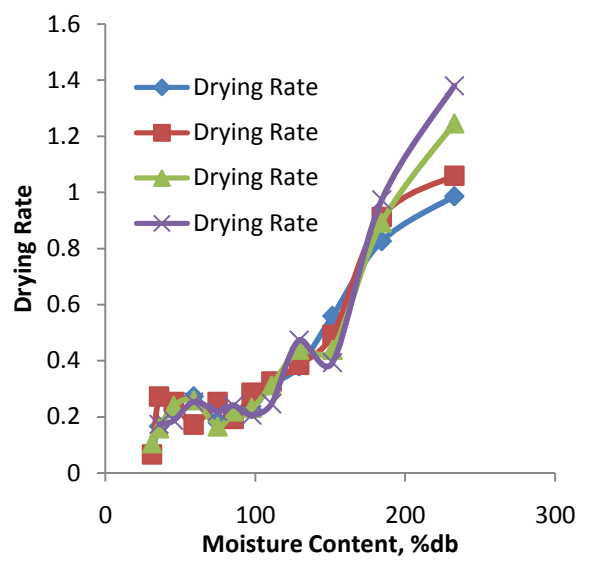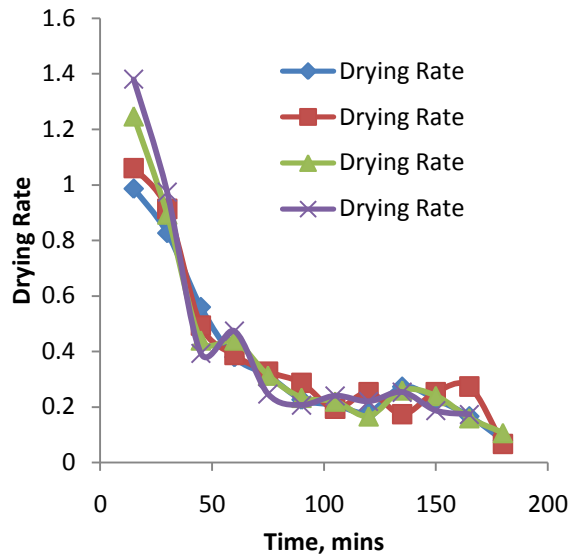
Fig 4.87 Effect of air speed on drying rate against time for ODC at 50 $^{\circ}$C

Fig 4.88 Effect of air speed on drying rate against moisture content for ODC at 50 $^{\circ}$C
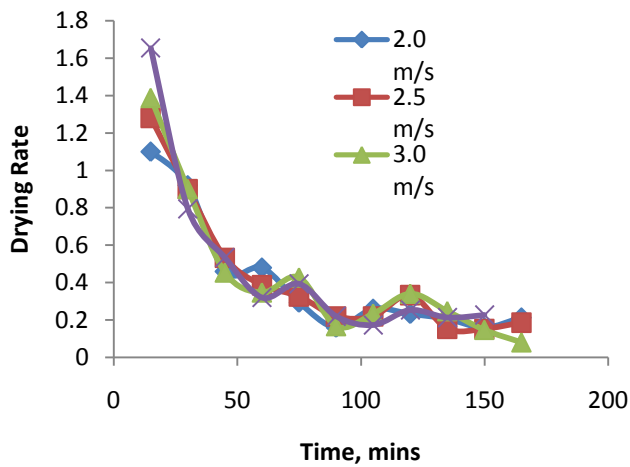
Fig 4.89   Effect of air speed on drying rate against time for ODC at 60 $^{\circ}$C
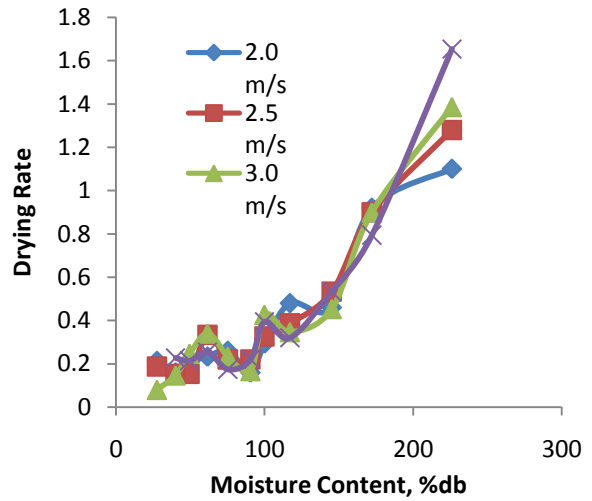
Fig 4.90   Effect of air speed on drying rate against moisture content for ODC at 60 $^{\circ}$C
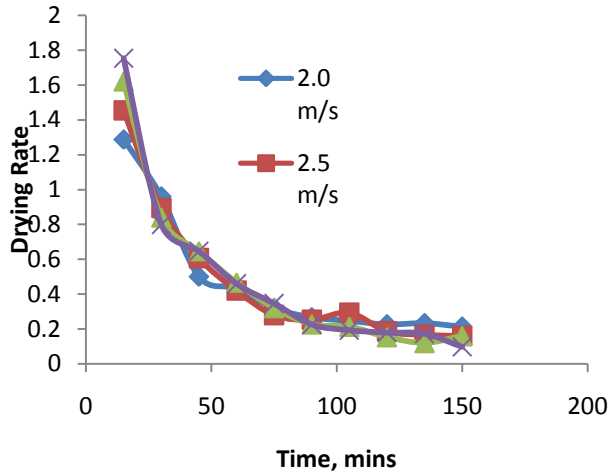
Fig 4.91   Effect of air speed on drying rate against time for ODC at 70 $^{\circ}$C
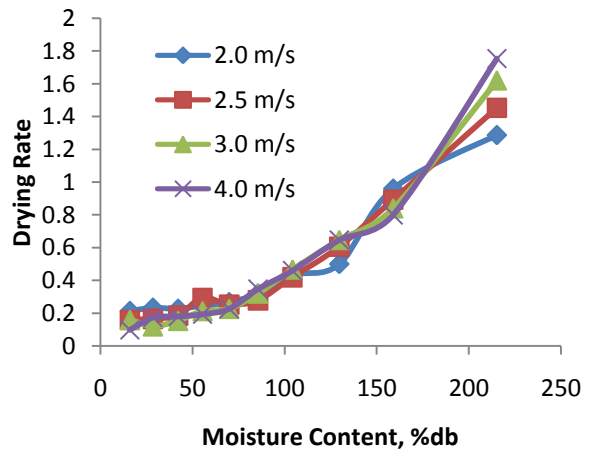
Fig 4.92   Effect of air speed on drying rate against moisture content for ODC at 70 $^{\circ}$C

145

4.10   Water activity and estimated mold-free shelf life

The water activity of a food material is not the same thing as its moisture content. There is the water in food crop which is not bound to food molecules and which can support the growth of bacteria, yeasts and molds (fungi). The term water activity (a_w) refers to this unbound water. The water activity was calculated by the formular given by Olaoye et al (2012) and depicted in Fig 4.93 and 4.94. The samples which were not dried have water activity of more than 0.9 which supports the growth of most micro organisms. It is seen that the water activity decreased significantly after drying to less than 0.6 which do not support most micro organisms (Appendix A). The water activity of cocoyam was higher than that of potato. The least water activity was observed in the oven dried products. The estimated mold-free shelf life (MFSL) was equally calculated by the formular given by Man and Jones (2000) as shown in appendix A and presented in Fig 4.95 and 4.96. It is observed that the dried products have an estimated MFSL of not less than 600. This means that it is estimated that the food products, which before drying could not last long before spoiling, can be preserved for an estimated period of 2 years and above. The MFSL was found to be dependent on the water activity in such a way that the MFSL decreases with water activity.
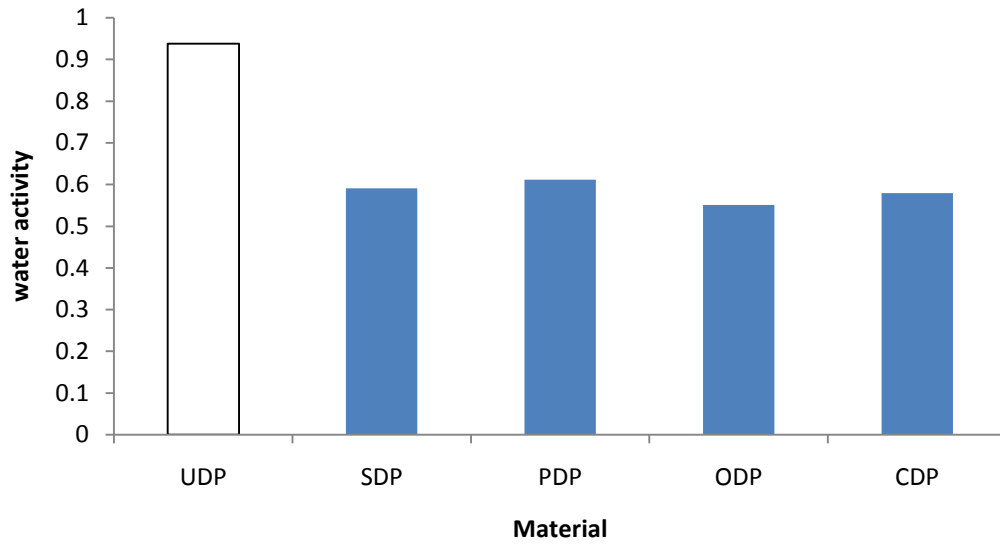
Fig 4.93 Variation of water activity with different drying methods of potato
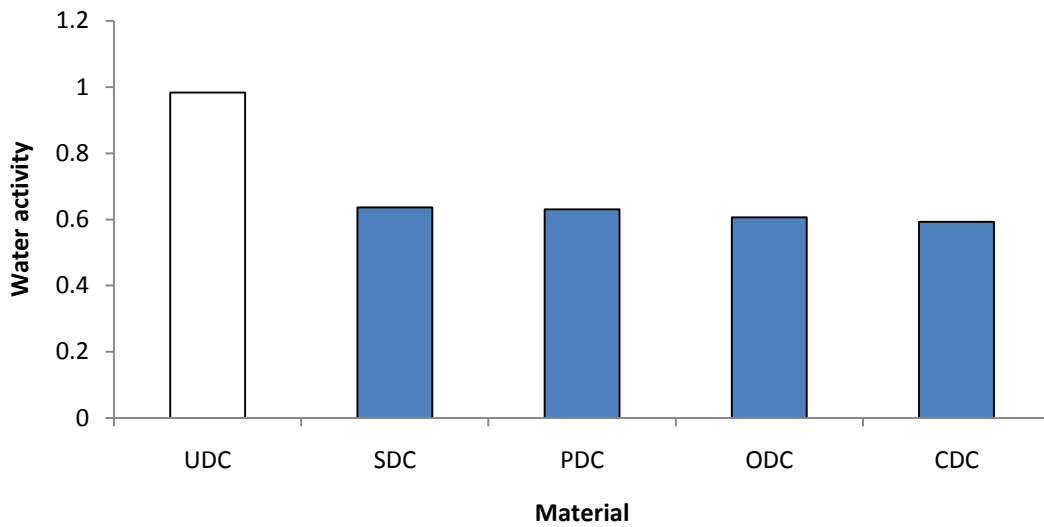
Fig 4.94 Variation of water activity with different drying methods of cocoyam
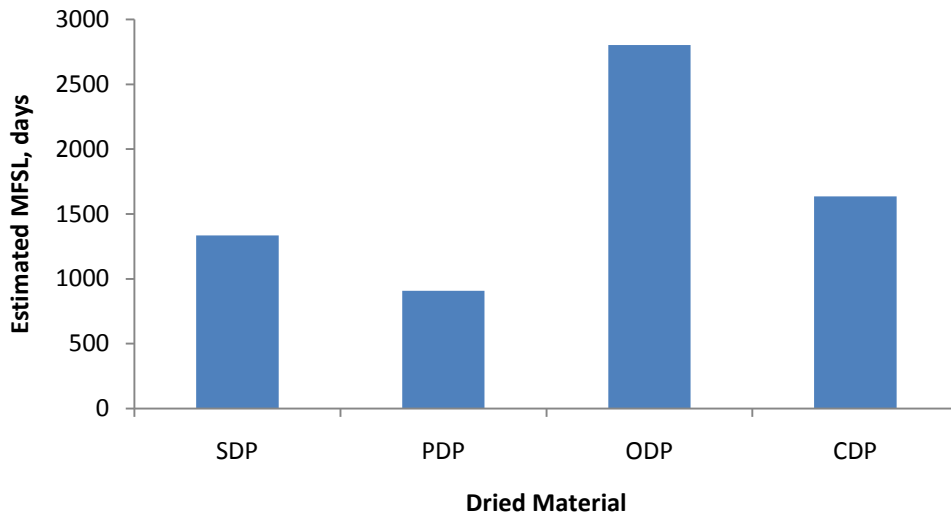
Fig 4.95 Effects of the different drying methods on the estimated mold-free shelf life obtained in dried potato
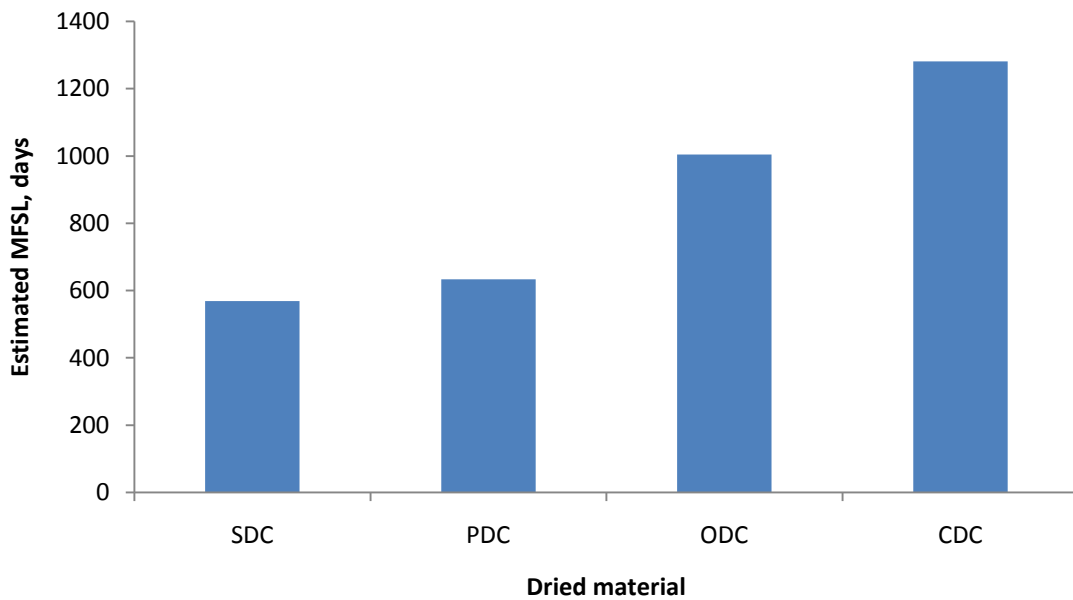
Fig 4.96 Effects of the different drying methods on the estimated mold-free shelf life obtained in dried cocoyam.

4.11. Scanning Electron Microscope analysis

Scanning Electron Microscope (SEM) analysis was used to show the morphology or texture, crystalline structure and surface topography of a material. It is highlighted as a powerful tool for the advanced characterization of a heterogeneous structured material (Sturm et al, 2012). The SEM analysis was done using discrete particles ranging from 30 μm to 100 μm at magnifications of between 500 – 2500x.

The results of the SEM analysis of the undried samples and the samples dried using the various drying methods are presented in Plates 4.1 to 4.10. The result indicate that the drying processes made the particles to form agglomerates that was not seen in the undried particles. This observation is similar to that reported in the SEM analysis of Durian fruit seed by Hamed and Bahareh (2013) who reported that there are some agglomerations which have taken place during the drying process. Their surface morphologies and texture after drying are characterized by ragged and rough surfaces while prominent interspatial pores can also be observed within the matrix of the undried samples.

The four different methods used for the drying of the samples do not show much significant changes in the micro-structure of the particles. This is in agreement with the work of Houben et al, (2013) who reported that there is no major differences in the visible damage (amount of cracks) of the micro structure of dried samples using air drying, oven drying or freeze drying.

The samples dried by oven and the hot air conventional driers (Plates 4.4, 4.6, 4.8 and 4.10) indicated slight significant agglomerates more than the others. This is probably due to the intensity of the heat energy experienced in these dryers. The dried samples also show evidence of particle deposition on the surface and cracked lines on their matrices as observed in Plate 4.9. This is probably because of the moisture which has left the interlayer spaces of the dried samples. According to the micrographs, it seems that the cavities on the surface resulted from the evaporation of the moisture during the drying, taking the space previously occupied by moisture (Devarly et al, 2008). These results revealed that the surface texture of the samples before drying were drastically affected after the drying.

Plate 4.1: SEM analysis of UDP
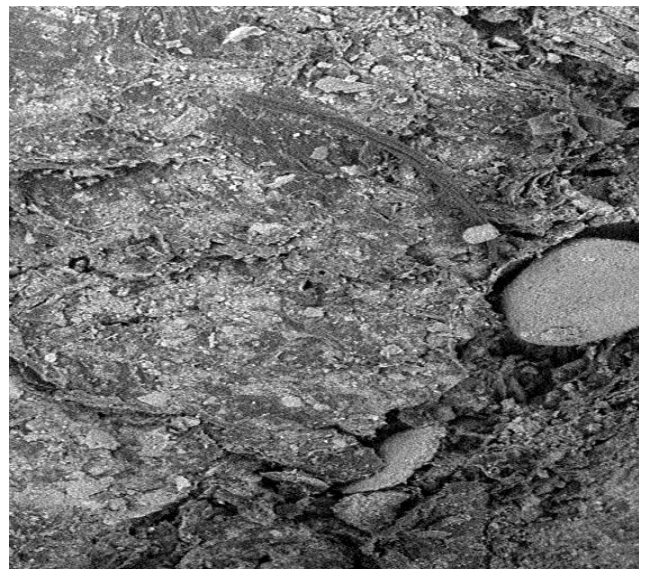
Plate 4.2: SEM analysis of UDC
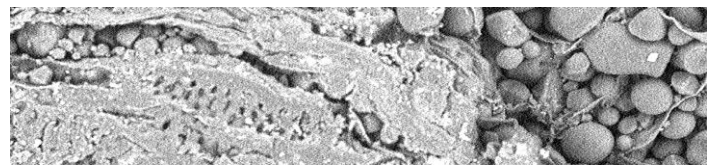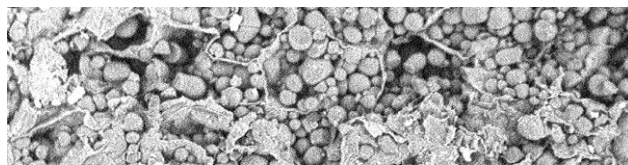
Plate 4.5: SEM analysis of PDP
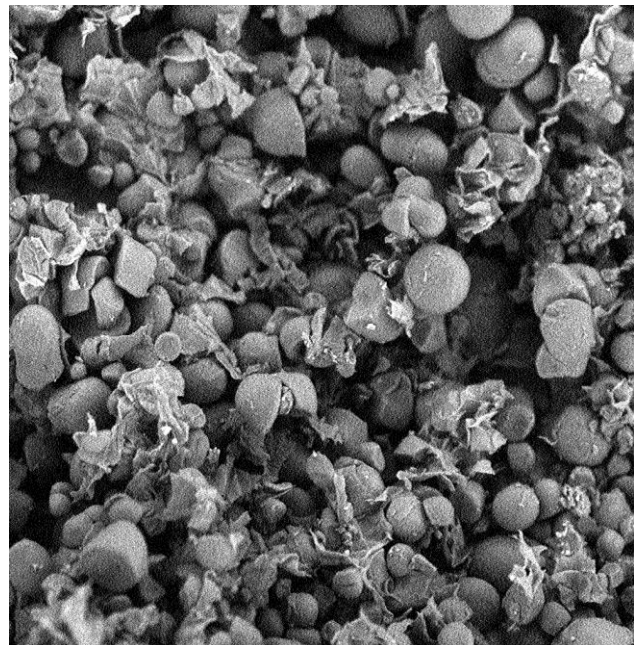
Plate 4.6: SEM analysis of ODP
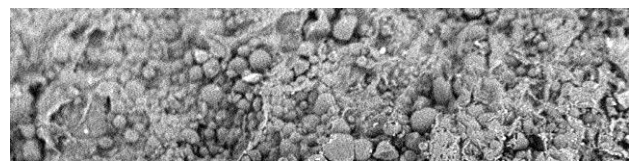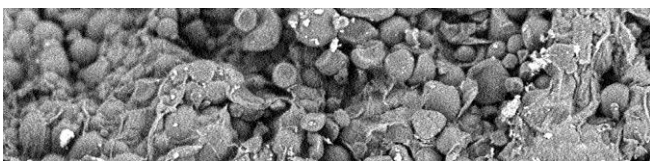
4.12　Fourier Transform Infrared Spectrometer (FTIR)

The FTIR technique is an important tool to identify the characteristic functional groups and the various forms of the minerals present in the samples under consideration.

The major functional groups on the food materials (before and after drying) were identified by the FTIR spectroscopy in the range of $600cm^{-1}$ to $4000cm^{-1}$ as shown in Tables 4.3 to 4.12. Foods are complex mixtures, with the main components being water, proteins, fats and carbohydrates (Stuart, 2004). The results displayed certain discernable spectral peaks which were used to predict the nature and assign some of the functional groups notably present on the food materials with regards to its region of transmittance and notional structure.

These FTIR spectra results were compared with known signature of identified materials in the FTIR library (Stuart, 2004; Vyazovkin, 2012). For samples UDP and CDP (Tables 4.3 and 4.6), their lowest transmission were at transmittance of about 75 while for samples UDC, PDC and ODP (Tables 4.4, 4.11 and 4.8), their lowest transmission were at transmittance as low as 30. The FTIR spectra revealed that generally, the prevalent functional groups were the carbohydrates, proteins, fats, ethers and water. Generally, the transmittance tends to decrease as the wave number decreases though the trend is not so significant. There were not much noticeable changes in the functional group after the drying.

Table 4. 3 Fourier Transform Infrared Spectrometer of UDP

Absorption Wavelength (cm^{-1})	Transmittance	Intensity	Assignment	Class of compounds
3805	91.66	s	O-H stretch	Carboxylic acid
3142	87.7	s	C-H stretch	Carbohydrates
2370	88.7	m	H-C =O stretch	Ethers
2322	88.7	w	H-C =O stretch	Ethers
1982	89.7	vs	Amide I	Proteins
1736.9	89.1	m	C =O- stretch	Fats
1341.8	86.5	s	Couples stretch	Carbohydrates
1013	88.9	s	Coupled Bend	Carbohydrates

Table 4. 4 Fourier Transform Infrared Spectrometer of UDC

Absorption Wavelength (cm^{-1})	Transmittance	Intensity	Assignment	Class of compounds
3272	64.7	s	≡C—H stretch	Carbohydrates
2929	76.0	m	C—H stretch	Fats
1636	82.5	s	Amide I	Protein
1420	79.6	m	C—H stretch	Carbohydrates
995	30.4	vs	C=C—H bend	Fats

861	67.1	s	C—H bend	Aromatic
760	62.9	m	≡C—H bend	Alkynes

Table 4. 5 Fourier Transform Infrared Spectrometer of SDP

Absorption Wavelength (cm^{-1})	Transmittance	Intensity	Assignment	Class of compounds
2931	73.5	m	C—H stretch	Carbohydrates
2386	86.3	w	H—C=O stretch	Ether
1953	50.4	m	C=O stretch Amide	Protein
1674	82.3	s	H—O—H stretch	Water
1333	78.5	s	H—O—H bend	Carbohydrates
1025	72.5	m	C—O—C stretch	Ethers
953	68.7	m	C=C—H bending	Fats
755	62.2	s	—(CH$_2$) bend	Alkanes

Table 4. 6 Fourier Transform Infrared Spectrometer of CDP

Absorption	Transmittance	Intensity	Assignment	Class of

Wavelength (cm^{-1})	ce	ity		compounds
3276	87.7	m	O—H stretch	Water
2927	85.9	s	H—C=O stretch	Aldehydes
2027	94.0	s	C≡N stretch	Nitriles
1744	91.3	m	C=O stretch	Fats
1457	89.9	vs	Couples stretch	Carbohydrates
1148	84.7	ms	N—H bend	Amides
995	70.9	s	C=C—H bend	Fats
861	85.9	s	C—H bend	Aromatic

Table 4. 7 Fourier Transform Infrared Spectrometer of PDP

Absorption Wavelength (cm^{-1})	Transmittance	Intensity	Assignment	Class of compounds
2945	60.1	m	C—H stretch	Carbohydrates
2865	89.3	s	=C —H stretch	Carbohydrates
2367	73.5	s	H —C=O stretch	Ethers
1897	68.5	w	C=O stretch amide	Protein
1685	72.8	s	H —O —H stretch	Water
1427	57.6	m	C-H bend	Alkane
1005	63.5	s	C=C —H bend	Fats
840	53.1	s	C —H bend	Aromatic

Table 4. 8   Fourier Transform Infrared Spectrometer of ODP

Absorption Wavelength (cm^{-1})	Transmittance	Intensity	Assignment	Class of compounds
3272	60.1	wm	N —H symmetric	Amides
2926	69.2	vs	C —H stretch	Fats
1744	85.3	w	C=O stretch	Aldehydes
1420	74.8	s	C —H bend	Alkyls
1338	71.8	m	CH$_3$C —H bend	Alkyls
1077	48.7	m	Coupled stretch	Carbohydrates
857	62.7	s	C —Cl stretch	Alkyl halides

Table 4. 9   Fourier Transform Infrared Spectrometer of SDC

Absorption Wavelength (cm^{-1})	Transmittance	Intensity	Assignment	Class of compounds
3432	84.3	s	O —H stretch	Water
2887	81.4	s	C —H stretch	Carbohydrates
2240	89.3	s	C ≡C bend	Alkynes
2001	72.5	m	C ≡N stretch	Nitriles

1871	68.3	w	C=O stretch Amide	Protein
1733	71.8	m	C=O stretch	Fats
1522	62.4	m	Coupled bend	Carbohydrates
981	58.1	w	C=C —H bend	Fats

Table 4. 10   Fourier Transform Infrared Spectrometer of CDC

Absorption Wavelength (cm^{-1})	Transmittance	Intensity	Assignment	Class of compounds
3652	88.4	s	O —H stretch	Carboxylic acids
3097	83.8	wm	=C —H stretch	Alkenes
2855	83.0	m	C —H stretch	Carbohydrates
2113	84.1	s	C ≡N stretch	Nitiles
1774	82.7	s	C —H —S stretch	Fats
1509	79.4	ms	N-H bend	Amides
1438	78.7	ms	Ring C=C stretch	Aromatic
1013	76.6	s	C —O —C stretch	Ethers

Table 4. 11   Fourier Transform Infrared Spectrometer of PDC

Absorption	Transmitta	Intensity	Assignment	Class of

Wavelength (cm^{-1})	nce				compounds
3283	73.3	s		O —H stretch	Water
2926	80.9	m		C —H — stretch	Carbohydrates
1640	75.5	m		C —H stretch Amides	Protein
1420	81.2	s		C —H bend	Alkane
995	45.1	m		C=C —H bend	Fats
859	74.5	ms		C —H bend	Aromatic
760	69.6	w		-(CH$_2$)$_n$ bend	Alkanes
700	64.0	s		≡C —H bend	Alkynes

Table 4. 12   Fourier Transform Infrared Spectrometer of ODP

Absorption Wavelength (cm^{-1})	Transmittance	Intensity	Assignment	Class of compounds
2932	70.3	s	C —H stretch	Carbohydrates
2856	78.4	s	C —H stretch	Carbohydrates
2240	72.9	s	C ≡C —	Alkynes
2103	63.4	m	C ≡N	Nitriles
1879	65.5	m	C=O stretch	Protein
1444	57.4	s	C —H bend	Alkyls
1021	54.3	m	Coupled	Carbohydra

			stretch		tes
870	43.4	w	C　　—Cl stretch		Ethers

S = strong;　　m = medium;　　　　w = weak;　　　vs = very strong

4.13　Effective Moisture Diffusivity

Drying process of food materials generally occurs in the falling rate period. The effective moisture diffusivity also called effective moisture diffusion coefficient was obtained by plotting the logarithm of moisture ratio (ln MR) against time of drying in seconds using Fick's second law. Drying rate constant (K_o) was the slope of the regression line from which the effective moisture diffusivity (D_{eff}) was calculated using

$$D_{eff} = \frac{4L^2 K_o}{\pi} \qquad\qquad (4.5)$$

Where L is the half slice thickness in meters

To calculate the effective moisture diffusivity using Fick's law, the following assumptions were made.

(1) Moisture is initially distributed uniformly throughout the mass of a sample.

(2) Mass transfer is symmetric with respect to the center.

(3) Surface moisture content of the sample instantaneously reaches equilibrium with the condition of surrounding air.

(4) Resistance to the mass transfer at the surface is negligible compared to internal resistance of the sample.

(5) Mass transfer is by diffusion only.

(6) Diffusion coefficient is constant and shrinkage is negligible   (Amin et al, 2011)

The effective moisture diffusivity of a food material characterizes its intrinsic mass transport property of moisture which includes molecular diffusion, liquid diffusion, vapour diffusion, hydrodynamic flow and other possible mass transport mechanisms (Karathanos et al, 1990).

4.13.1 Effect of slice thickness and mass on Effective Moisture Diffusivity

The effective moisture diffusivity for SDP and SDC was calculated at different slice thicknesses and masses in sun drying and presented in Table 4.13 to 4.14. The plots gave high coefficients of determination indicating good correlation. The result showed that the moisture diffusivity values were in the range of 5.404 x 10^{-11} to 2.432 x 10^{-10} m^2/s which are generally within the range of 10^{-11} to 10^{-6} m^2/s given for food materials' moisture diffusion coefficient. (Moshen, 2016; Baballs and Belessiotis, 2014; Aghbashlo et al, 2008).

The Table 4.13 and 4.14 showed that the minimum value of effective moisture diffusivity was obtained at the minimum slice thickness used and that increase in slice thickness increases the value of effective moisture diffusivity at constant drying temperature. This trend is consistent with that reported by Tinuade et al, (2014). This is probably because the moisture gradient of the sample increased. The effective diffusion constant of a material is affected by the shorter distance that moisture needs to travel before the evaporation to the surroundings (Amira et al, 2014). The effective moisture diffusivity of SDP was slightly higher than that of SDC.

The mass used have only a slight effect on the effective moisture diffusivity as indicated by the Table 4.3.   This is because almost the same surface area is maintained for each individual sample in the drying.   There is no significant difference in the effective moisture diffusivity value of potato and that of cocoyam. At smaller mass, the effective moisture diffusivity of SDP was higher than that of SDC while as the mass increases, the effective moisture diffusivity of SDC became slightly higher. The effective moisture diffusivity of potato dried in the temperature range of 50 to 70 ^{o}C at constant air velocity of 2 m/s has been reported to be in the range of 2.53 x 10^{-11} to 1.76 x 10^{-10} m^{2}/s (Doymaz, 2011) which is similar to the values obtained in this work. The effective moisture diffusivity was reported by Nwajinka et al, (2014) to be in the range of 2.53 x 10^{-5} to 1.09 x 10^{-5}. This is different from the value obtained here which may be attributed to the fact that he used a cabinet dryer with electric-heater which is different from the sun drying used here.

Table 4.13   Effect of slice thickness on the effective moisture diffusivity

Potato		
Size	D_{eff} (m^2/s)	R^2
2 mm	5.404 x 10^{-11}	0.985
4 mm	1.621 x 10^{-10}	0.991
6 mm	2.432 x 10^{-10}	0.989
Cocoyam		
Size	D_{eff} (m^2/s)	R^2

2 mm	6.0793×10^{-11}	0.993
4 mm	1.351×10^{-10}	0.993
6 mm	1.8238×10^{-10}	0.998

Table 4.14   Effect of initial mass on the effective moisture diffusivity

Potato		
Mass (g)	D_{eff} (m^2/s)	R^2
50	2.1615×10^{-10}	0.990
100	2.4317×10^{-10}	0.996
200	2.7018×10^{-10}	0.994
300	3.242×10^{-10}	0.990
Cocoyam		
Mass (g)	D_{eff} (m^2/s)	R^2
50	2.1617×10^{-10}	0.990
100	2.1617×10^{-10}	0.989
200	2.9717×10^{-10}	0.978
300	3.5125×10^{-10}	0.996

4.13.2 Effects of air speed on Effective moisture diffusivity

The result of the effective moisture diffusivity calculated in the Photo voltaic dryer is presented in Table 4.15. It shows the effects of air speed (m/s) on the values of effective

diffusion constant for PDP and PDC. The coefficient of determination was high indicating that there is a good correlation.

The result revealed that the effective moisture diffusivity of cocoyam is generally greater than that of potato. The higher moisture diffusivity of cocoyam is expected because of the higher moisture content, texture and composition of cocoyam which reduces the transfer of moisture as compared to other food products (Nwajinka et al, 2014). The moisture diffusion constant ranged from 2.702×10^{-10} m^2/s to 3.783×10^{-10} m^2/s and 2.972×10^{-10} m^2/s to 4.053×10^{-10} m^2/s for PDP and PDC respectively as the air speed increased from 1.0 to 3.0 m^2/s. This is because there is greater absorption of moisture from the sample surface at higher air speed. This leads to an increase in the moisture content gradient of the sample and hence an increase in the effective moisture diffusivity. Motevali et al, (2012) and Mohsen (2016) reported similar trend of direct variation of velocity and effective moisture diffusivity in the thin-layer drying of jujube and apple slices respectively. The range of values obtained in this work is similar to the values of 4.54×10^{-10} m^2/s to 1.08×10^{-9} m^2/s obtained in the solar drying of basil leaves by Shahi et al (2014).

A linear regression of the relationship between drying air speed and effective moisture diffusivity is given as

For PDP : $D_{eff} = 6.0 \times 10^{-10} V + 2.0 \times 10^{-11}$

$R^2 = 0.9259$

For PDC : $D_{eff} = 5.0 \times 10^{-10} V + 2.0 \times 10^{-11}$

$R^2 = 0.9999$

Where V is the drying air speed (m/s)

Table 4.15   Effect of drying air speed on the effective moisture diffusivity

Potato		
Air speed (m/s)	D_{eff} (m^2/s)	R^2
1.0	2.7018×10^{-10}	0.989
1.5	2.9722×10^{-10}	0.989
2.0	3.5125×10^{-10}	0.990
3.0	3.7827×10^{-10}	0.993
Cocoyam		
Air speed (m/s)	D_{eff} (m^2/s)	R^2
1.0	2.9722×10^{-10}	0.969
1.5	3.2423×10^{-10}	0.961
2.0	3.5125×10^{-10}	0.955
3.0	4.0528×10^{-10}	0.947

4.13.3 Effect of temperature on Effective moisture diffusivity

The variation of temperature with the effective moisture diffusivity was investigated using the oven dryer and shown in Table 4.16.

The values ranged between 1.8967 x 10^{-10} m^2/s to 4.053 x 10^{-10} m^2/s for both ODP and ODC. The coefficients of determination were greater than 0.95 implying that there is a good fit correlation. These values are in the range reported by several authors. Minaei et al (2012) reported effective moisture diffusivity of pomegranate arils in the range of 3.43 x 10^{-10} m^2/s to 32.05 x 10^{-10} m^2/s for micro-wave drying. Tulek (2011) equally reported moisture diffusion constant between 9.619 x 10^{-10} m^2/s to 1.556 x 10^{-9} m^2/s in drying mushroom slices at the same temperature of 50°C to 70°C used in this work. The table also indicated that increase in temperature increases the effective moisture diffusivity for both ODP and ODC. This trend is in agreement with the results reported by severally authors for agricultural products such as melon seeds (Nwajinka et al, 2014b), kale (Mwithiga and Olwal, 2015) red chillies (Kaleemullah and Kailappan, 2006), mango (Aremu et al, 2013), basil leaves (Shahi et al, 2014), apricots (Mirzaee et al, 2009). This observation can be attributed to the fact there is increase in the activity of water molecules and a decrease in water viscosity as the temperature increases. These factors trigger off increased diffusion of water molecules in the object capillaries and hence increase the moisture diffusivity. In addition, the effect of drying air flow rate on moisture diffusivity can be seen where any increment in air flow rate increases the moisture diffusivity of the samples (Mohsen, 2016)

A linear regression of the relationship between drying air speed and effective moisture diffusivity is given as

For PDP : $\quad D_{eff} = 7.0 \times 10^{-12} T + 2.0 \times 10^{-10}$

$\qquad R^2 = 0.961$

For PDC : $\quad D_{eff} = 4.0 \times 10^{-12} T + 8.0 \times 10^{-11}$

$\qquad R^2 = 0.912$

Where T is the drying air Temperature (^{O}C)

Table 4.16   Effect of drying temperature on the effective moisture diffusivity

Potato		
Temperature (^{o}C)	D_{eff} (m^2/s)	R^2
60	2.15612×10^{-10}	0.988
70	2.43171×10^{-10}	0.993
80	3.24228×10^{-10}	0.989
90	4.05285×10^{-10}	0.981
Cocoyam		
Temperature (^{o}C)	D_{eff} (m^2/s)	R^2

60	1.89673×10^{-10}	0.995
70	2.15612×10^{-10}	0.992
80	2.43171×10^{-10}	0.992
90	3.24228×10^{-10}	0.995

4.13.4 Effective moisture diffusivity in the Hot-Air Conventional dryer

The hot air conventional dryer showed the effects of both drying air speed and drying temperature because both affect the drying process.

The result (Table 4.17 and 4.18) showed that the effective moisture diffusion constant values calculated ranged from 2.967×10^{-10} m^2/s to 7.295×10^{-10} m^2/s which is generally within the range of 10^{-11} to 10^{-6} m^2/s given for food materials effective moisture diffusivity (Aghbashlo et al, 2008). For CDP, the minimum effective moisture diffusivity was 6.76×10^{-10} m^2/s which was obtained at a temperature of 70°C and air speed of 4.0 m/s while for CDC, the maximum was 7.30×10^{-10} m^2/s obtained at the same conditions. The plots gave straight lines with high coefficients of determination ranging from 0.958 to 0.997 which shows good correlation. The effective moisture diffusion constant in the hot-air conventional dryer was slightly greater than that for the oven dryer. It was seen that both temperature and air speed do not inversely affect the effective moisture diffusivity. The same trend with both temperature and air speed was reported by Moshen (2016). The moisture diffusivity in these slices was affected by the drying temperature because the drying temperature affected the internal mass transfer during drying (Nwajinka et al, 2014). This is due to the increased heating energy which

168

would increase the activity of the water molecules leading to higher moisture diffusivity when samples were dried. Equally, effective moisture diffusion constant increases with temperature because at higher temperature, the water molecules are loosely bound to the food matrix and hence less energy is required to remove the moisture than at lower temperature (Amira et al, 2014). The knowledge of effective moisture diffusivity helps in designing a low cost but efficient dryer for drying agricultural products.

Table 4.17 Variation of effective moisture diffusivity with speed in the Hot air dryer for Potato

Temperature of 50 ^{o}C		
Air speed (m/s)	D_{eff} (m^2/s)	R^2
2.0	3.5178 x 10^{-10}	0.990
2.5	4.0528 x 10^{-10}	0.996
3.0	4.5878 x 10^{-10}	0.989
4.0	5.3984 x 10^{-10}	0.982
Temperature of 60 ^{o}C		
Air speed (m/s)	D_{eff} (m^2/s)	R^2
2.0	3.7773 x 10^{-10}	0.958
2.5	4.3284 x 10^{-10}	0.972
3.0	4.8634 x 10^{-10}	0.991
4.0	5.9500 x 10^{-10}	0.947
Temperature of 70 ^{o}C		
Air speed (m/s)	D_{eff} (m^2/s)	R^2

2.0	4.0529×10^{-10}	0.928
2.5	4.5878×10^{-10}	0.964
3.0	5.3984×10^{-10}	0.961
4.0	6.7602×10^{-10}	0.949

Table 4.18   Variation of effective moisture diffusivity with speed in the Hot air dryer

for Cocoyam

Temperature of 50 ^{o}C		
Air speed (m/s)	**D_{eff} (m^2/s)**	**R^2**
2.0	2.9667×10^{-10}	0.992
2.5	3.7773×10^{-10}	0.969
3.0	4.0528×10^{-10}	0.976
4.0	4.3284×10^{-10}	0.967
Temperature of 60 ^{o}C		
Air speed (m/s)	**D_{eff} (m^2/s)**	**R^2**
2.0	3.5179×10^{-10}	0.989
2.5	4.3284×10^{-10}	0.982
3.0	4.5878×10^{-10}	0.978
4.0	4.8634×10^{-10}	0.958
Temperature of 70 ^{o}C		
Air speed (m/s)	**D_{eff} (m^2/s)**	**R^2**
2.0	4.3284×10^{-10}	0.992

2.5	4.5878 x 10⁻¹⁰	0.995
3.0	5.1390 x 10⁻¹⁰	0.997
4.0	7.2951 x 10⁻¹⁰	0.991

4.14 Activation Energy

The dependence of the effective moisture diffusion constant on drying air temperature was used in the linear Arrhenius-type relationship as given by Reza et al, (2013) in equation 4.33

$$Ln\, D_{eff} = Ln\, D_o - \frac{E_a}{R}\left(\frac{1}{T}\right) \tag{4.5}$$

Where

E_a is the activation energy in KJ/kg mol

R is the universal gas constant (8.314 KJ/kg mol K)

D_o is the frequency factor or the pre-exponential factor

T is the absolute drying temperature in Kelvin

4.14.1 Activation energy in the oven drying method

In the drying of agricultural products, the activation energy is a measure of the temperature sensitivity of the effective moisture diffusivity and it is equally the minimum amount of energy required to initiate moisture diffusion within the slice (Aremu et al, 2013; Shahi et al, 2012).

Hence, a straight line plot of ln D_{eff} against 1/T in figure 4.97 gave a slope from which the activation energy is calculated. The coefficients of determination for the two processes were 0.978 and 0.945 indicating good correlation.
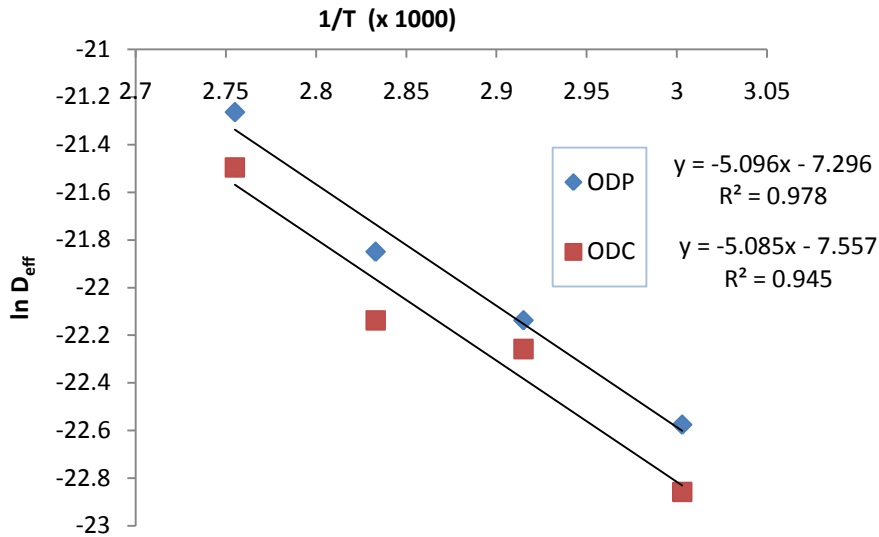
Figure 4.97: Plot of ln D_{eff} against 1/T for ODP and ODC

The activation energy was calculated as 42.368 KJ/mol and 42.277 KJ/mol for ODP and ODC respectively. The difference in the activation energy of ODP and ODC were almost insignificant. The values calculated were within the range of activated energy reported by many authors. In the drying of apricots, Mirzaee et al, (2009) reported activation energy values of between 29.35 KJ/mol to 33.78 KJ/mol while Aremu et al (2013) in the drying of mango, reported activation energy of 28.95 KJ/mol. In the drying of melon seeds, Nwajinka et al, (2014) reported activation energy values of between 39.7KJ/mol to 48.6 KJ/mol. The magnitude of the activation energy for

agricultural and food products has been generally reported to be between 12 KJ/mol to 110 KJ/mol (Reza et al, 2013; Mirzaee et al, 2009).

4.14.2 Activation energy in the hot-air conventional drying method

The variations of different air speed on the activation energy in the hot-air conventional dryer were obtained by plotting the graph of ln D_{eff} against 1/T as shown in Figures 4.98 and 4.99
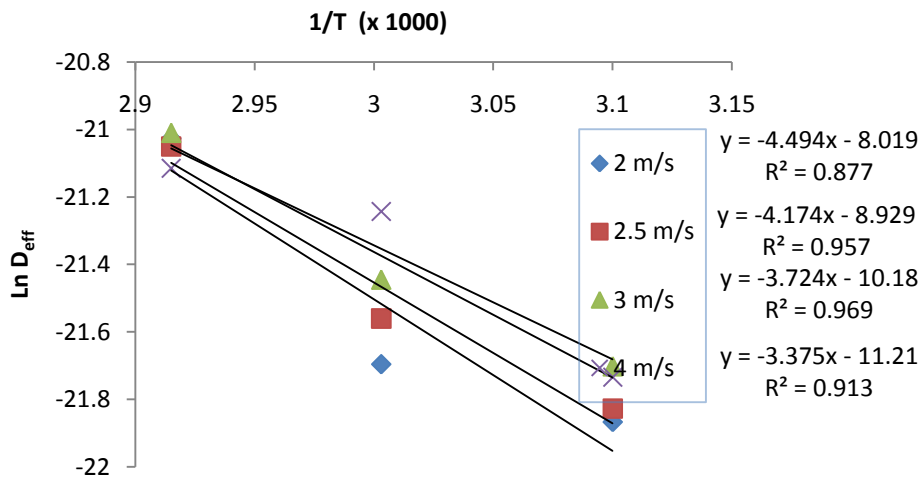
Figure 4.98:   Plot of ln D_{eff} against 1/T at different air speeds for CDP
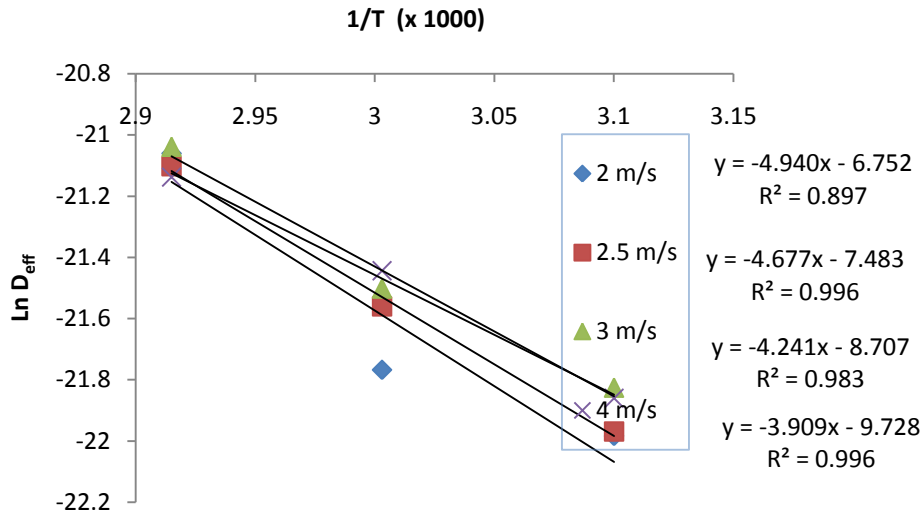
Figure 4.99: Plot of ln D_{eff} against 1/T at different air speeds for CDC

The coefficients of determination of the fitted lines with experimental data as seen from the plots were mostly very high indicating a good correlation. The activation energy of CDP and CDC were calculated and presented in Table 4.19. It was observed that the magnitude of the activation energy is affected by the drying air speed. The minimum activation energy for CDP was 28.06 KJ/mol while the maximum was 37.367 KJ/mol. For CDC, the minimum and maximum activation energy was 32.499 KJ/mol and 41.071 KJ/mol respectively. The magnitudes of activation energy were in agreement with the general range of activation energy of 12.7 KJ/mol to 110 KJ/mol reported for most food materials (Aghbashlo et al, 2008).

The study on the activation energy revealed that as the air speed increased, the activation energy progressively decreased. This is due to the fact that activation energy being energy that must be overcome before a process starts is reduced as the drying air speed increases. If the air speed of the system is increased, the average heat energy is

174

increased; a greater proportion of collision between reactants result in reaction and the reaction proceeds more rapidly. Nwajinka et al (2014) and Mirzaee et al (2009) reported similar trends in activation energy. In the thin-layer drying of Russian olive, the activation energy decreased from 63.83 KJ/mol to 48.18 KJ/mol as the drying air speed increased from 0.5 m/s to 1.5 m/s (Abbasazadeh et al, 2012). The values of the frequency factors calculated in Table 4.3 are similar to that reported by Amira et al (2014). This trend is consistent with the trend obtained in this work. The activation energy was higher in CDC than in CDP. This is probably because cocoyam has more moisture content than potato and its composition reduces the transfer of moisture (Nwajinka et al, 2014).

A linear regression of the relationship between drying air speed and activation energy is given as

For CDP : $E_a = -4.694V + 46.26$

$R^2 = 0.958$

For CDC : $E_a = -4.365V + 49.48$

$R^2 = 0.960$

Where V is the drying air speed (m/s)

Table 4.19 Activation Energy in Hot air conventional dryer

Potato			
Velocity (m/s)	R^2	**Activation Energy (KJ/mol)**	$D_o \times 10^{-3}$ (m^2/s)
2.0	0.887	37.363	0.329

2.5	0.957	34.703	0.133
3.0	0.969	30.961	0.0379
4.0	0.913	28.060	0.0135
Cocoyam			
Velocity (m/s)	R^2	**Activation Energy (KJ/mol)**	D_o x 10^{-3} (m^2/s)
2.0	0.897	41.071	1.17
2.5	0.996	38.885	0.563
3.0	0.983	35.261	0.165
4.0	0.996	32.449	0.0596

4.15 Total Energy consumption and Specific Energy consumption

The total energy consumption is the total energy that was used to remove the quantity of water that was removed during the drying while the Specific Energy consumption is the energy required to remove one kilogram of water from the surface of the food product.

The total energy consumption, E_t was calculated using the relation

$$E_t = (A.V.\rho_a.C_a.\Delta T).t \qquad (4.6)$$

Where

A is the area of drying tray, V is the drying air speed, ρ_a is the air density, C_a is the specific heat capacity of air, ΔT is the temperature difference and t is the time of drying. (Motevali et al, 2012; Mohsen, 2016).

The Specific Energy consumption, SEC, was calculated using the relation

$$SEC = \frac{E_t}{M} \qquad\qquad (4.7)$$

Where M is the mass of water removed.

4.15.1 Variations of Slice thickness with Total Energy consumption and Specific Energy consumption

The graphs of the total energy consumed in drying the slices at different thicknesses were presented in Fig 4.100 and 4.101 while the specific energy consumptions are seen in Figure 4.102 and 4.103. The total energy increased from 10.67 KWh to 14.89 KWh for SDP as the slice thickness increased. The maximum and minimum values of specific energy consumption were 166.72 KWh/kg and 232.70 KWh/kg respectively for SDP and 162.43 KWh/kg and 253.21 KWh/kg respectively for SDC. The highest total energy needed was obtained for the thickest slice samples while the lowest energy was observed least thick sample. This is probably due to the fact that the energy utilized to transfer heat to the internal regions of the slice is higher since the heat transfer distance is higher (Tinuade et al, 2014).
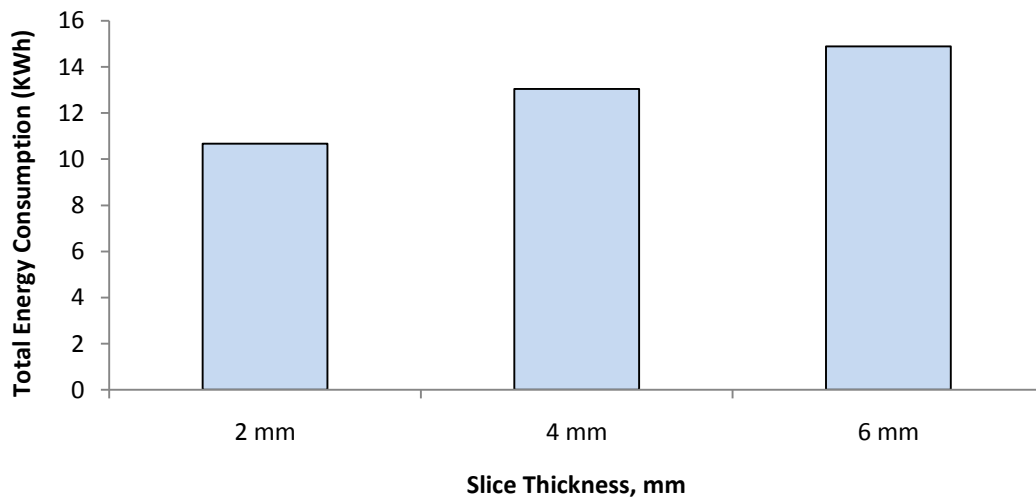
Fig 4.100 Effect of slice thickness on the total energy consumption of SDP
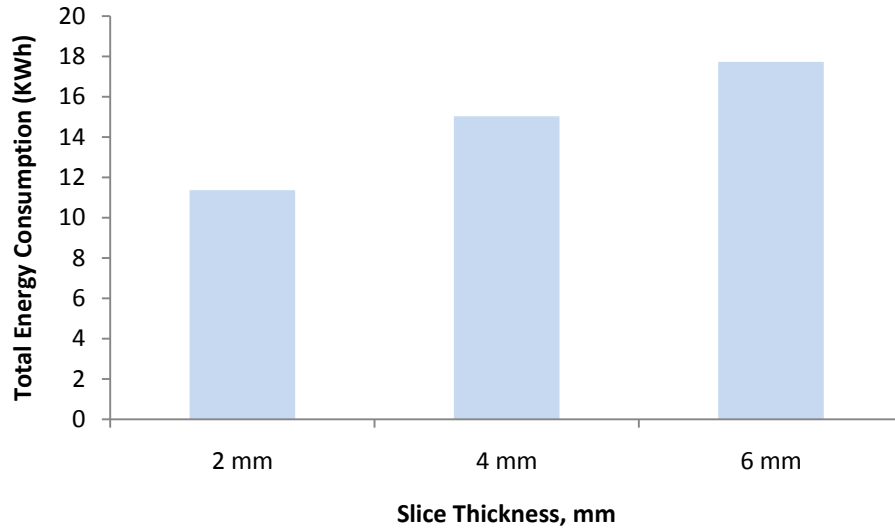
Fig 4.101 Effect of slice thickness on the total energy consumption of SDC
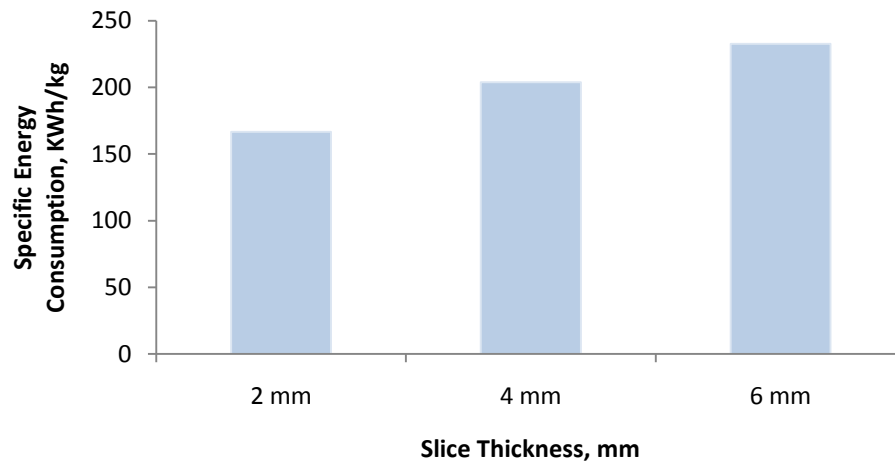
Fig 4.102 Effect of slice thickness on the specific energy consumption of SDP
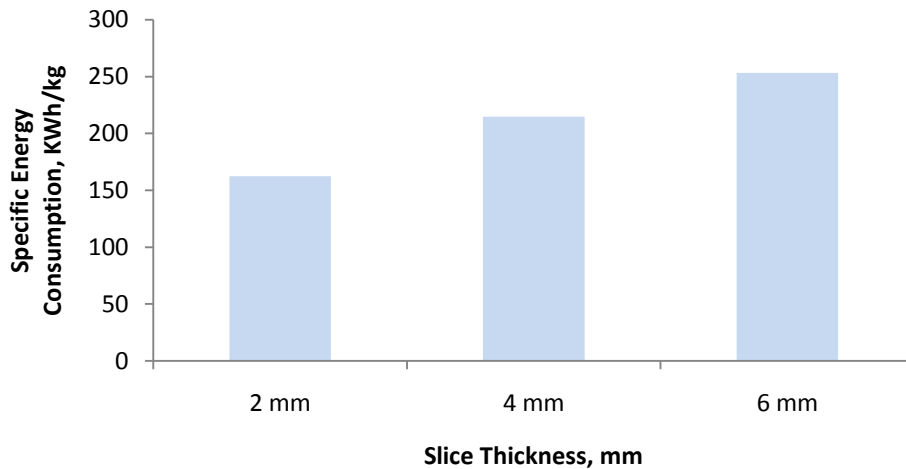
Fig 4.103 Effect of slice thickness on the specific energy consumption of SDC

4.15.2 Variation of Air speed with Total Energy consumption and Specific Energy consumption

The effects of air speed on the total energy consumption and specific energy consumption were evaluated using the Photovoltaic dryer and given in Figure 4.104 to 4.107. The total energy consumption ranged from 18.017 KWh to 67.295 KWh for the products. This is within the range reported by some authors. Moshen (2016) in drying apple slices calculated a total energy consumption ranging from 13.89 KWh to 23.94 KWh while Abbaszadeh et al (2012) in thin layer drying of Russian Olive reported total energy consumption between 16.34 KWh to 75.04 KWh. The specific energy consumption increased from 257.387 KWh/kg to 961.356 KWh/kg as the air speed increased 1.0 m/s to 3.5 m/s. The trend is in agreement with the results reported for thin-layer drying of Jujube

(Motevali et al, 2012) and Russian Olive (Abbaszadeh et al, 2012). This is because vapour pressure decreases with increasing air speed, thereby the product moisture faces less resistance to evaporation (Motevali et al, 2012).
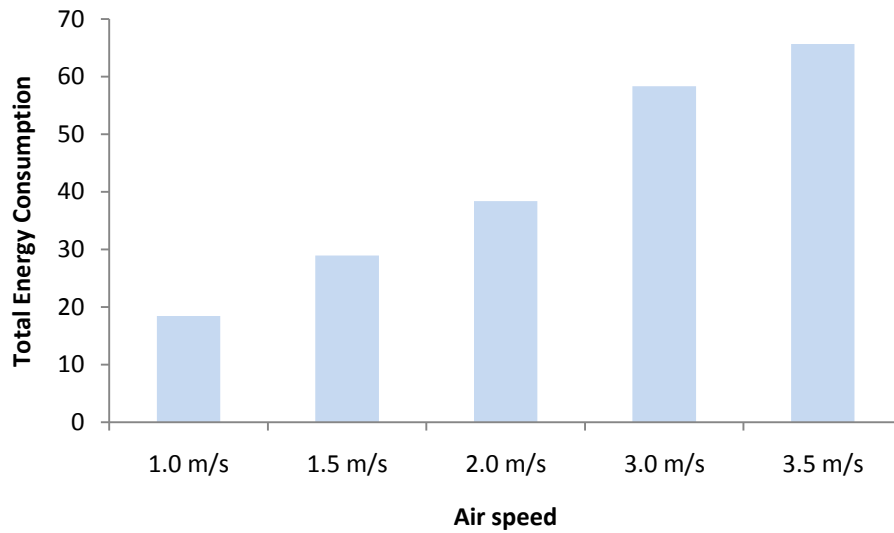
Fig 4.104   Effect of air speed on the total energy consumption of PDP
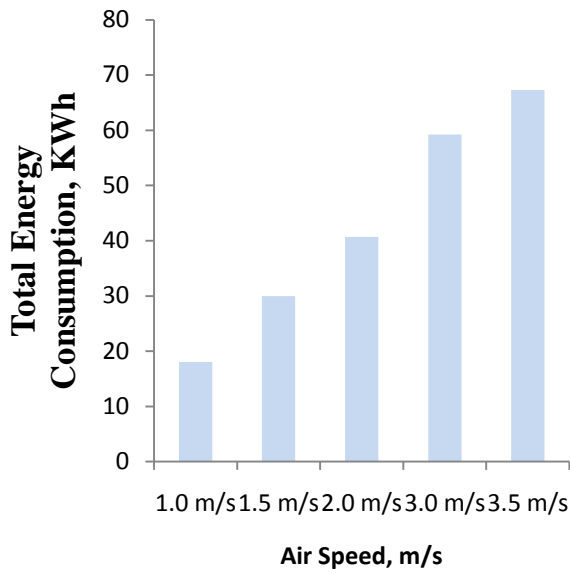
Fig 4.105   Effect of air speed on the total energy consumption of PDC
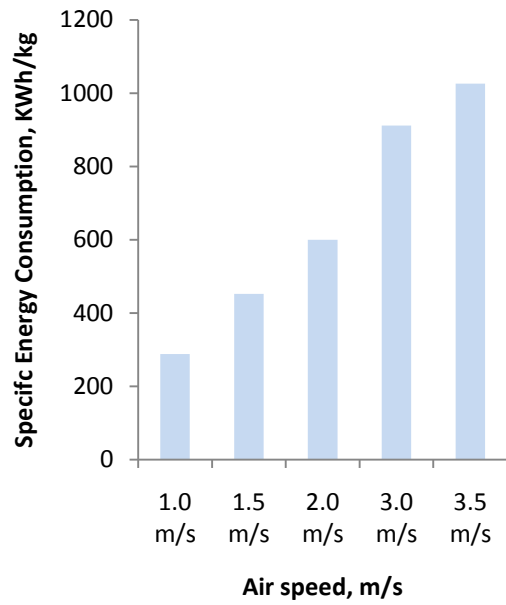
Fig 4.106   Effect of air speed on the specific energy consumption of PDP
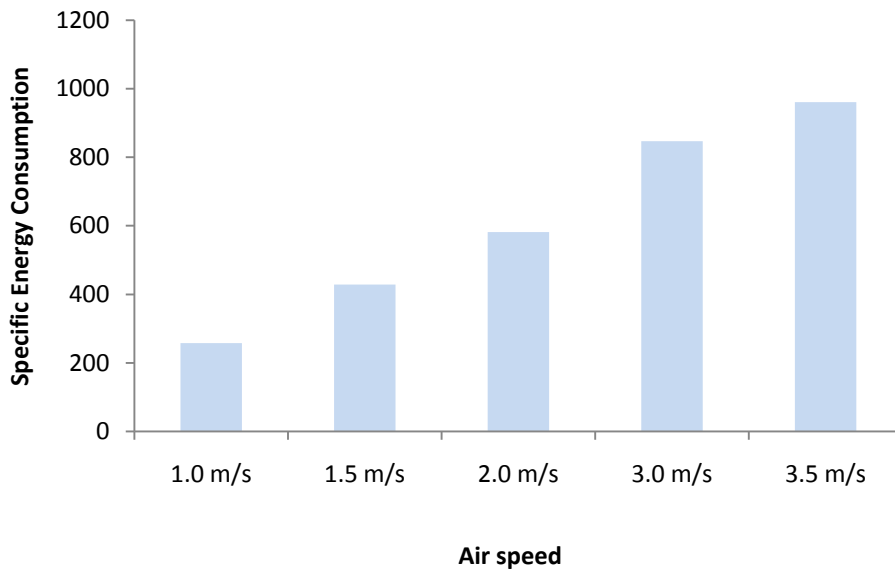
Fig 4.107   Effect of air speed on the specific energy consumption of PDC

4.15.3 Variation of Temperature with Total Energy consumption and Specific Energy consumption

The total energy consumption and the Specific Energy consumption were also seen to vary with different drying temperature as shown in Fig. 4.108 to 4.111. The total energy consumption of ODP and ODC were seen to be only slightly different. It is seen that energy consumption of the drying process decreases with increasing air temperature.

The total energy consumption and Specific Energy consumption increased from a minimum of 14.552 KWh and 220.54 KWh/kg to a maximum of 17.54 KWh and 259.90 KWh/kg respectively as the temperature decreased from 90°C to 60°C. This is because with increasing temperature, the drying time reduces due to increased thermal gradients inside the material and consequently, increased the product drying time (Motevali et al, 2012). This phenomenon can also be attributed to the fact that greater heat transfer and water vapour pressure deficit that occurs during drying is done at higher temperature. This gave rise to a greater uptake of air and evaporation is achieved in a shorter time thus reducing the amount of energy needed (Rayaguru and Routray, 2012; Tinuade et al, 2014).
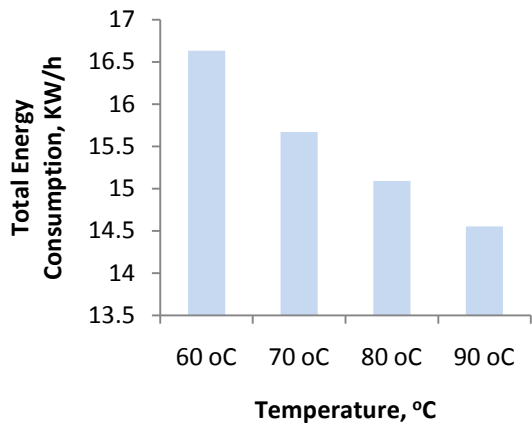
Fig 4.108   Effect of temperature on the

total energy consumption of ODP
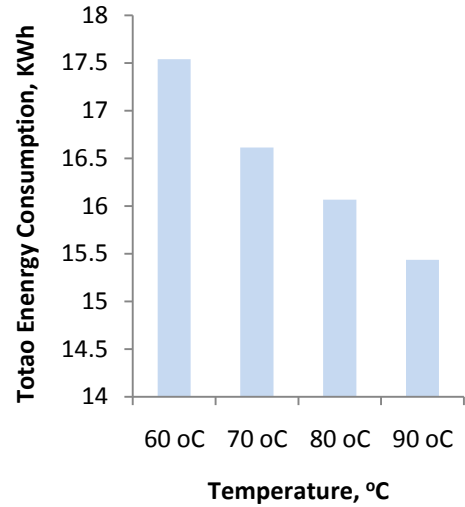
Fig 4.109   Effect of temperature on the

total energy consumption of ODC
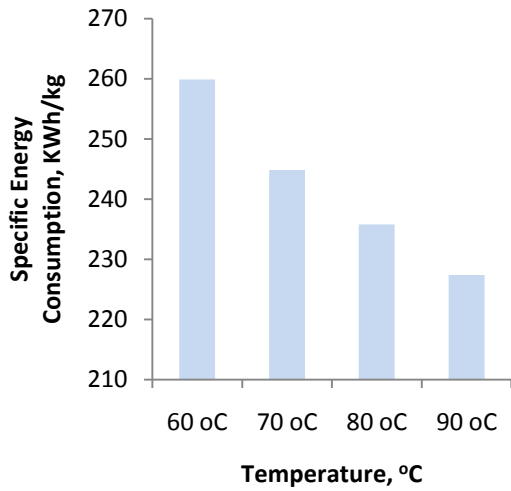
Fig 4.110   Effect of temperature on the

specific energy consumption of ODP
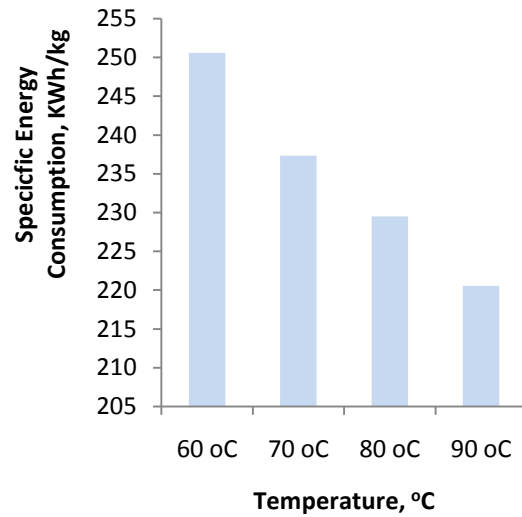
Fig 4.111   Effect of temperature on the

specific energy consumption of ODC

4.16 Convective heat transfer coefficient

The relative humidity (γ) and the average of the crop temperature (T_c) and the temperature above the crop surface (T_e) were calculated at hourly interval for corresponding moisture evaporated and used to determine the physical properties of air. The physical properties were used to calculate the values of the Grashof Number (Gr) and the Prandtl Number (Pr) which were used in linear regression analysis to determine the values of the constants C and n. The values of C and n obtained in this present work were 1.759 and 0.249 respectively for open sun drying of 400g of potato while for 300g of potato, the values were 2.396 and 0.262 respectively. These values of C and n are similar to those values reported by some authors. For open sun drying of 600 g of onion flasks, Anwar and Tiwari (2001) reported the values of C and n as 1.00 and 0.31 respectively while for open sun drying of corn kernels, Ravinder et al (2013) reported values of 0.99 and 0.24 for C and n respectively. The variations seen are attributed to the nature of the product, the drying hours used in the experiment and the different environmental conditions (Anil and Tiwari, 2006).

The convective heat transfer coefficient h_c, for drying of potato ranges from 4.0m to 9.0 W $m^{-2}\,{}^oC^{-1}$ and from 4.0 to 13.0 W $m^{-2}\,{}^oC^{-1}$ for cocoyam as seen in Tables 4.20 to 4.32. These observations are quite similar to the convective heat transfer coefficient reported by some authors. In the drying of fish, Tribeni and Tiwari (2008) reported convective heat transfer coefficient ranging from 1.23 to 9.20 W $m^{-2}\,{}^oC^{-1}$ while Anil and Tiwari (2006) in the drying of onion flakes calculated a value of 1.04 to 3.08 W $m^{-2}\,{}^oC^{-1}$. Ravinder (2014) reported that the convective heat transfer coefficient of some food products ranges from 3.71 to 25.98 W $m^{-2}\,{}^oC^{-1}$. The convective heat transfer coefficient

vary from commodity to commodity which is due to differences in porosity, moisture content, shape and size of the commodity (Ici-Turk, 2005).

Table 4. 20 Convective heat transfer coefficient for potato slices at 2mm

Time, h	$T_c(^oC)$	$T_e(^oC)$	$T_i(^oC)$	M_e (kg)	R.H	n	C	h_c (W m^{-2} $^oC^{-1}$)
1	33.5	39.2	36.35	0.0303	0.313	0.032	0.712	4.698392
2	34.5	39.8	37.15	0.0187	0.285	0.032	0.712	4.695566
3	35.3	41.2	38.25	0.0088	0.268	0.032	0.712	4.722881
4	37.8	43.7	40.75	0.0042	0.253	0.032	0.712	4.748262
5	36.1	40.9	38.5	0.0017	0.243	0.032	0.712	4.694322
6	35.6	40.4	38.0	0.0007	0.258	0.032	0.712	4.689277

Table 4. 21 Convective heat transfer coefficient for potato slices at 4mm

Time, h	$T_c(^oC)$	$T_e(^oC)$	$T_i(^oC)$	M_e (kg)	R.H	n	C	h_c (W m^{-2} $^oC^{-1}$)
1	32.8	40.5	36.65	0.0233	0.323	0.111	1.763	11.52393
2	35.1	40.3	37.7	0.0128	0.282	0.111	1.763	11.04725
3	34.9	42.4	38.65	0.0097	0.266	0.111	1.763	11.51944
4	37.3	42.8	40.05	0.0061	0.258	0.111	1.763	11.14927
5	36.5	41.3	38.9	0.0052	0.253	0.111	1.763	10.96616
6	36.8	42.1	39.45	0.0047	0.247	0.111	1.763	11.09514
7	34.3	39.7	37	0.0031	0.255	0.111	1.763	11.0838

Table 4.22 Convective heat transfer coefficient for potato slices at 6mm

Time, h	$T_c(^oC)$	$T_e(^oC)$	$T_i(^oC)$	M_e (kg)	R.H	n	C	h_c (W m^{-2} $^oC^{-1}$)
1	33.1	39.7	36.4	0.0156	0.317	0.083	1.19	7.730516
2	35.6	40.8	38.2	0.0083	0.275	0.083	1.19	7.600654
3	35.3	41.8	38.55	0.0083	0.267	0.083	1.19	7.747013
4	38.1	42.5	40.3	0.0093	0.253	0.083	1.19	7.520822
5	36.7	43.1	39.9	0.0069	0.248	0.083	1.19	7.753516
6	37.4	42.4	39.9	0.0063	0.239	0.083	1.19	7.596268
7	35.9	40.8	38.35	0.005	0.245	0.083	1.19	7.565049
8	34.7	39.2	36.95	0.0021	0.279	0.083	1.19	7.495166

Table 4. 23 Convective heat transfer coefficient for cocoyam slices at 2mm

Time, h	$T_c(^oC)$	$T_e(^oC)$	$T_i(^oC)$	M_e (kg)	R.H	n	C	h_c (W m^{-2} $^oC^{-1}$)
1	33.5	39.2	36.35	0.0345	0.313	0.04	0.753	4.947229
2	34.5	39.8	37.15	0.0139	0.285	0.04	0.753	4.941019
3	35.3	41.2	38.25	0.0109	0.268	0.04	0.753	4.973537
4	37.8	43.7	40.75	0.0071	0.253	0.04	0.753	4.999146
5	36.1	40.9	38.5	0.0031	0.243	0.04	0.753	4.935198
6	35.6	40.4	38	0.0018	0.258	0.04	0.753	4.930115

Table 4. 24 Convective heat transfer coefficient for cocoyam slices at 4mm

Time, h	$T_c(^oC)$	$T_e(^oC)$	$T_i(^oC)$	M_e (kg)	R.H	n	C	h_c (W m^{-2} $^oC^{-1}$)
1	32.8	40.5	36.65	0.019	0.323	0.106	1.719	11.25039
2	35.1	40.3	37.7	0.0141	0.282	0.106	1.719	10.80685
3	34.9	42.4	38.65	0.0098	0.266	0.106	1.719	11.24874
4	37.3	42.8	40.05	0.0087	0.258	0.106	1.719	10.90503
5	36.5	41.3	38.9	0.0078	0.253	0.106	1.719	10.73253
6	36.8	42.1	39.45	0.005	0.247	0.106	1.719	10.85372
7	34.3	39.7	37	0.0033	0.255	0.106	1.719	10.84013

Table 4. 25 Convective heat transfer coefficient for cocoyam slices at 6mm

Time, h	$T_c(^oC)$	$T_e(^oC)$	$T_i(^oC)$	M_e (kg)	R.H	n	C	h_c (W m^{-2} ^{o}C^{-1})
1	33.1	39.7	36.4	0.0171	0.317	0.094	1.27	8.213861
2	35.6	40.8	38.2	0.0123	0.275	0.094	1.27	8.052934
3	35.3	41.8	38.55	0.0078	0.267	0.094	1.27	8.227819
4	38.1	42.5	40.3	0.0059	0.253	0.094	1.27	7.951668
5	36.7	43.1	39.9	0.0062	0.248	0.094	1.27	8.231953
6	37.4	42.4	39.9	0.0062	0.239	0.094	1.27	8.043131
7	35.9	40.8	38.35	0.0058	0.245	0.094	1.27	8.009825
8	34.7	39.2	36.95	0.0049	0.279	0.094	1.27	7.929775

Table 4. 26 Convective heat transfer coefficient for 50 g cocoyam slices

Time, h	$T_c(^oC)$	$T_e(^oC)$	$T_i(^oC)$	M_e (kg)	R.H	n	C	h_c (W m^{-2} ^{o}C^{-1})
1	32.4	37.5	34.95	0.0198	0.305	0.069	0.86	5.50523
2	33.7	38.1	35.9	0.0093	0.287	0.069	0.86	5.458483
3	34.5	38.8	36.65	0.0046	0.262	0.069	0.86	5.456961
4	33.1	39.2	36.15	0.0021	0.238	0.069	0.86	5.585356

Table 4. 27 Convective heat transfer coefficient for 100 g cocoyam slices

Time, h	$T_c(^oC)$	$T_e(^oC)$	$T_i(^oC)$	M_e (kg)	R.H	n	C	h_c (W m^{-2} ^{o}C^{-1})
1	33.1	37.6	35.35	0.0345	0.317	0.09	1.377	8.604343
2	34.3	38.5	36.4	0.0136	0.298	0.09	1.377	8.564627
3	34.5	38.4	36.45	0.0112	0.301	0.09	1.377	8.508334
4	34.7	39.7	37.2	0.0071	0.275	0.09	1.377	8.710559
5	34.2	38.3	36.25	0.0031	0.252	0.09	1.377	8.544142
6	32.9	38.3	35.6	0.0016	0.259	0.09	1.377	8.749996

Table 4. 28 Convective heat transfer coefficient for 200 g cocoyam slices

Time, h	$T_c(^oC)$	$T_e(^oC)$	$T_i(^oC)$	M_e (kg)	R.H	n	C	h_c (W m^{-2} $^oC^{-1}$)
1	33.4	36.8	35.1	0.0647	0.302	0.293	2.14	10.53179
2	35.1	37.3	36.2	0.037	0.284	0.293	2.14	9.262595
3	36.3	37.8	37.05	0.0149	0.253	0.293	2.14	8.273863
4	36.8	39.6	38.2	0.0086	0.245	0.293	2.14	9.925246
5	35.9	39.3	37.6	0.0075	0.235	0.293	2.14	10.51115
6	34.7	38.5	36.6	0.0059	0.238	0.293	2.14	10.86784
7	33.2	37.2	35.2	0.0021	0.253	0.293	2.14	11.04455

Table 4. 29 Convective heat transfer coefficient for 300 g cocoyam slices

Time, h	$T_c(^oC)$	$T_e(^oC)$	$T_i(^oC)$	M_e (kg)	R.H	n	C	h_c (W m^{-2} $^oC^{-1}$)
1	33.2	38.5	35.85	0.132	0.314	0.262	2.396	13.67989
2	34.8	38.8	36.8	0.0487	0.298	0.262	2.396	12.70231
3	36.5	38.7	37.6	0.017	0.283	0.262	2.396	10.85694
4	36.9	38.9	37.9	0.0084	0.265	0.262	2.396	10.58782
5	36.3	37.6	36.95	0.005	0.245	0.262	2.396	9.461675
6	35.1	37.9	36.5	0.0024	0.238	0.262	2.396	11.57058
7	34.3	37.2	35.75	0.0013	0.247	0.262	2.396	11.68126
8	33.7	36.5	35.1	0.0009	0.258	0.262	2.396	11.57764

Table 4. 30 Convective heat transfer coefficient for 50 g potato slices

Time, h	$T_c(^oC)$	$T_e(^oC)$	$T_i(^oC)$	M_e (kg)	R.H	n	C	h_c (W m^{-2} $^oC^{-1}$)
1	33.4	37	35.2	0.0172	0.307	-0.055	0.4	2.828921
2	34.2	38.1	36.15	0.0061	0.283	-0.055	0.4	2.824929
3	34.8	38.8	36.8	0.0039	0.262	-0.055	0.4	2.826763
4	34.6	39.2	36.9	0.0021	0.238	-0.055	0.4	2.805997

Table 4. 31 Convective heat transfer coefficient for 100 g potato slices

Time, h	$T_c(^oC)$	$T_e(^oC)$	$T_i(^oC)$	M_e (kg)	R.H	n	C	h_c (W m^{-2} $^oC^{-1}$)
1	33.6	37.6	35.6	0.0291	0.313	0.061	0.636	4.036923
2	34.6	38.5	36.55	0.0187	0.298	0.061	0.636	4.037723
3	35.2	38.7	36.95	0.0088	0.301	0.061	0.636	4.014098
4	35.7	39.7	37.7	0.0042	0.275	0.061	0.636	4.052483
5	33.8	38.3	36.05	0.0017	0.252	0.061	0.636	4.069391
6	33.2	38.3	35.75	0.0011	0.259	0.061	0.636	4.098323

Table 4. 32 Convective heat transfer coefficient for 400 g potato slices

Time, h	$T_c(^oC)$	$T_e(^oC)$	$T_i(^oC)$	M_e (kg)	R.H	n	C	h_c (W m^{-2} $^oC^{-1}$)
1	34.5	38.8	36.65	0.1325	0.317	0.249	1.759	9.607727
2	35.8	38.8	37.3	0.0591	0.295	0.249	1.759	8.782319
3	36.7	38.7	37.7	0.0302	0.283	0.249	1.759	7.938032
4	36.7	38.9	37.8	0.0158	0.265	0.249	1.759	8.128441
5	36.5	37.6	37.05	0.0056	0.245	0.249	1.759	6.841383
6	35.8	37.9	36.85	0.0051	0.238	0.249	1.759	8.037013
7	34.6	37.2	35.9	0.003	0.247	0.249	1.759	8.478308
8	33.7	36.5	35.1	0.0019	0.258	0.249	1.759	8.638211

4.16.1 Variation of convective heat transfer coefficient with mass and thickness

The variations of the convective heat transfer coefficient with mass and slices thickness is presented in Fig. 4.3 to 4.5. It was observed that the 50g mass gave the lowest convective heat transfer coefficient for both cocoyam and potato drying. The values of convective heat transfer coefficient were seen to increase as the mass increases. This is in agreement with Anil and Tiwari (2006) who reported that in the drying of onion

slices that convective heat transfer coefficient increases from 1.25 to 2.48 W m^{-2} ^{o}C^{-1} as the mass of the slices increased from 300 g to 900 g. The convective heat transfer coefficient significantly depends on the mass and thickness of the layer of the slices. This may be attributed to non exposure of some flakes due to higher layer thickness. Hence, the increase in the convective heat transfer coefficient (Anil and Tiwari, 2006). Equally, it has been observed that the rate of moisture transfer plays an important role in convective heat transfer coefficient (Ravinder, 2014). Convective heat transfer coefficient is influenced by both temperature difference and the absolute temperature value of the temperature. The calculation of convective heat transfer coefficient is a key requirement in any design problem in which heating or cooling is involved (Coulson and Richardson, 2004).
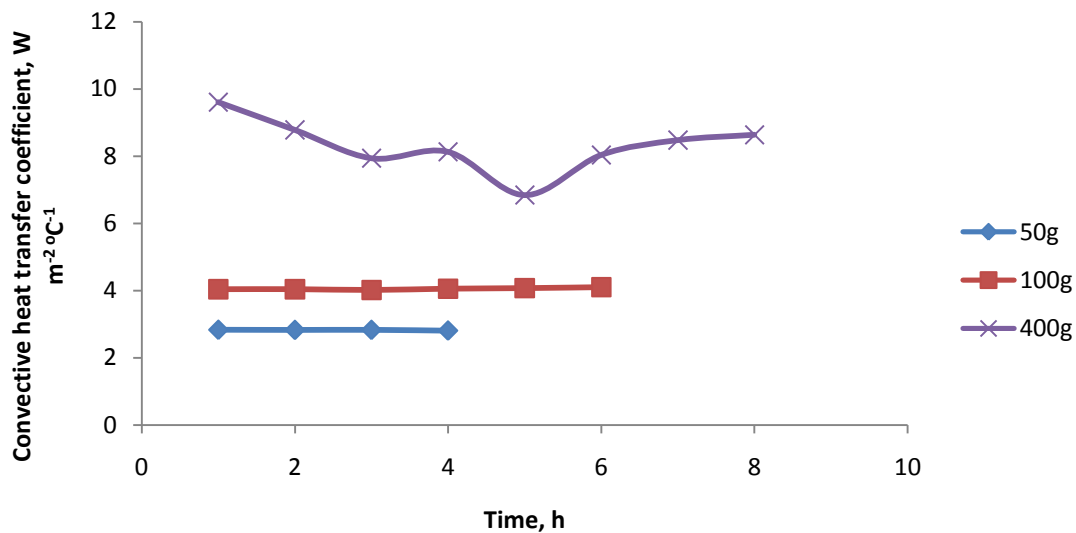
Fig 4.112 Variation in convective heat transfer with mass for potato drying
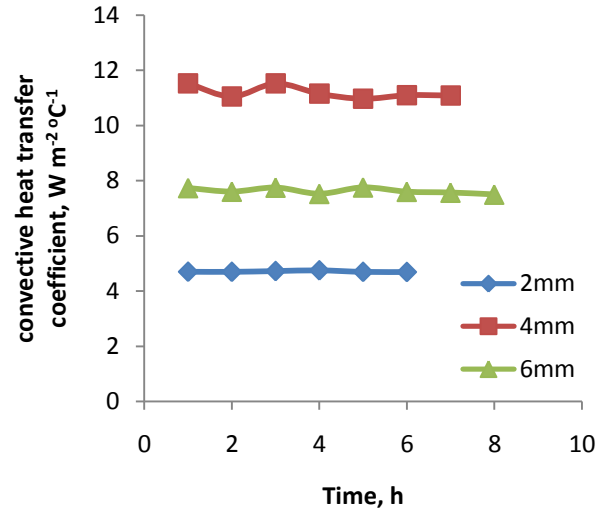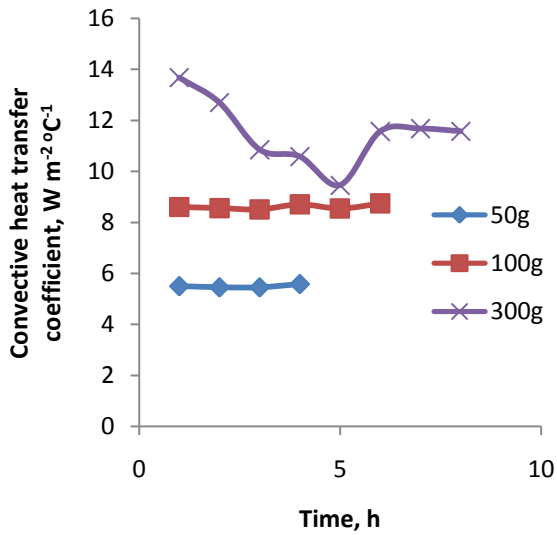
Fig 4.114   Variation in convective heat transfer with slice thickness for potato drying
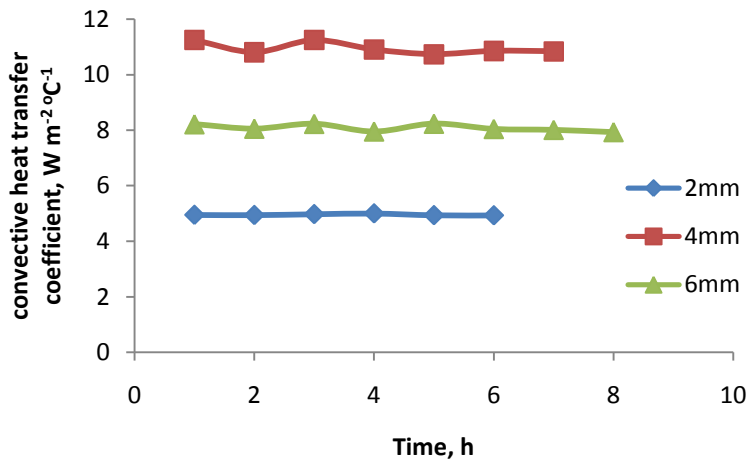
Fig 4.115   Variation in convective heat transfer with slice thickness for cocoyam

191

4.17   Efficiency of dryers

The efficiencies of the dryers involved include system drying efficiency and the thermal efficiency.

4.17.1 System Drying Efficiency

The system drying efficiency is defined as the ratio of the energy required to evaporate the moisture to the energy supplied to the dryer (Igbeka, 2013; Senadeera and Kalugalage, 2004). It describes how effectively the input energy to the drying system is used in the product drying. The variations of the system drying efficiency with slice thickness for both sun drying and photovoltaic drying is given in Fig 4.115 to 4.118. The system drying efficiency decreased with time probably because as the time of drying increases, the moisture content decreases. This observation is in agreement with the trend reported by Navale et al (2015).

Initially, the least slice thickness gave the highest efficiency but as the drying nears its completion, the least slice thickness gave the least drying efficiency. This can be explained by the fact that due to the small distance that the moisture has to travel before getting to the surface, it is quickly removed and as the drying time continues, there is just little moisture to be removed. For the drying of 2 mm slice potato, the average system drying efficiency was 24.3 % for open sun drying and 30.8% for photovoltaic drying. Generally, the efficiency obtained in the photovoltaic dryer was higher than that obtained in the open sun drying and this leads to reduction in its drying period. This is because there is better energy utilization in the photovoltaic dryer (Navale et al, 2015).
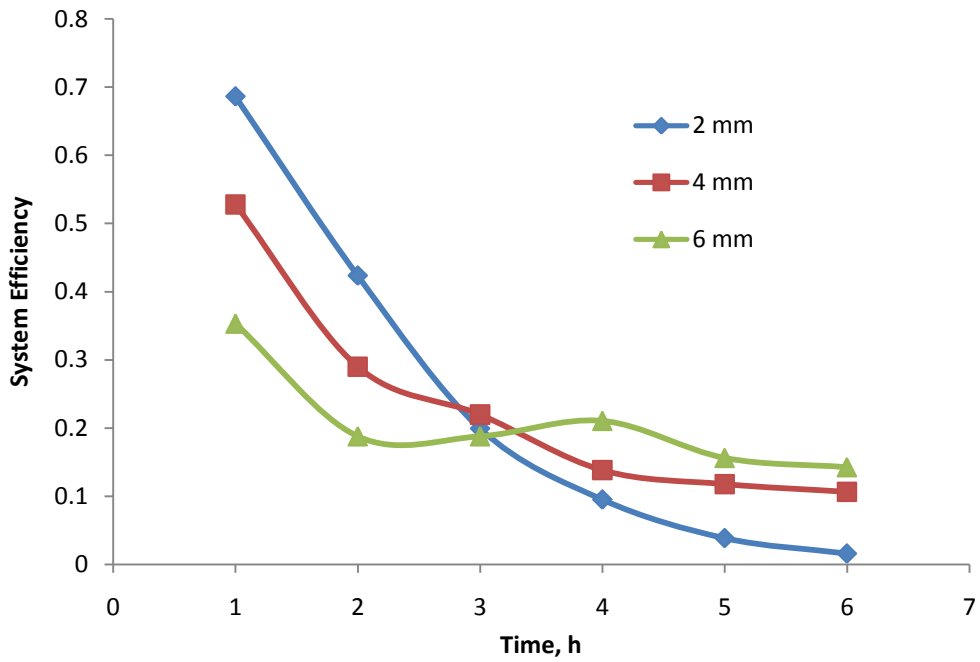
Fig 4.115 Effect of slice thickness on System efficiency for sun drying of potato
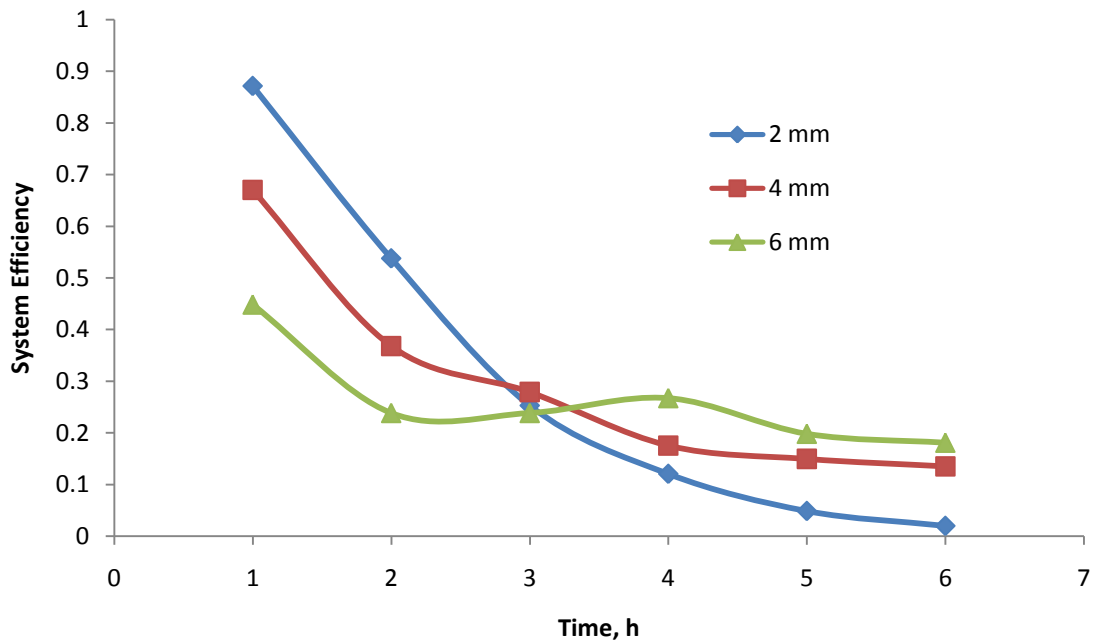
Fig 4.116 Effect of slice thickness on System efficiency for Solar cabinet dryer of potato
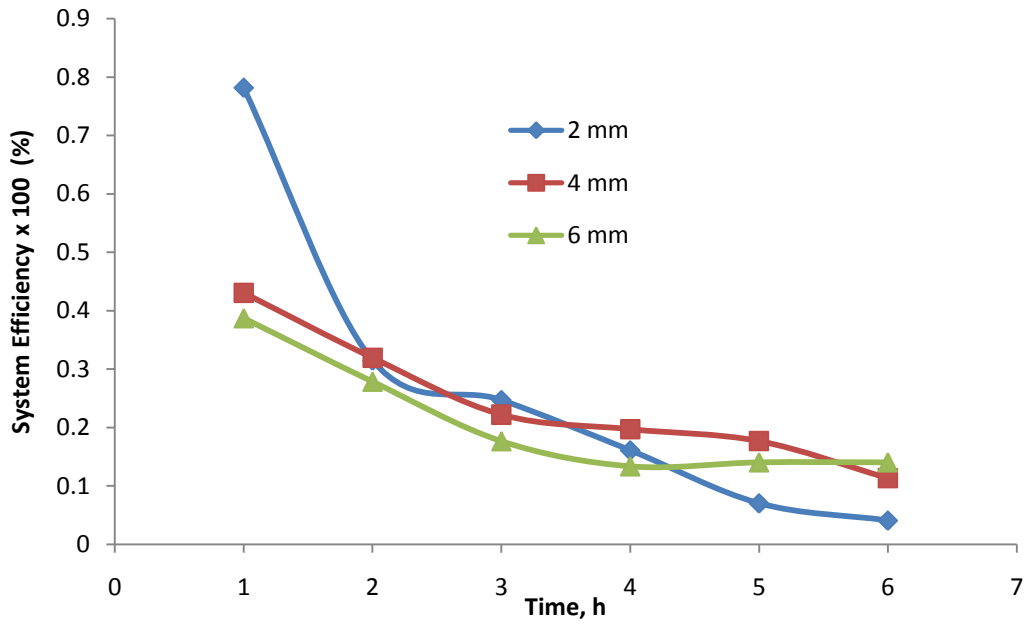
Fig 4.117 Effect of slice thickness on System efficiency for sun drying of cococyam
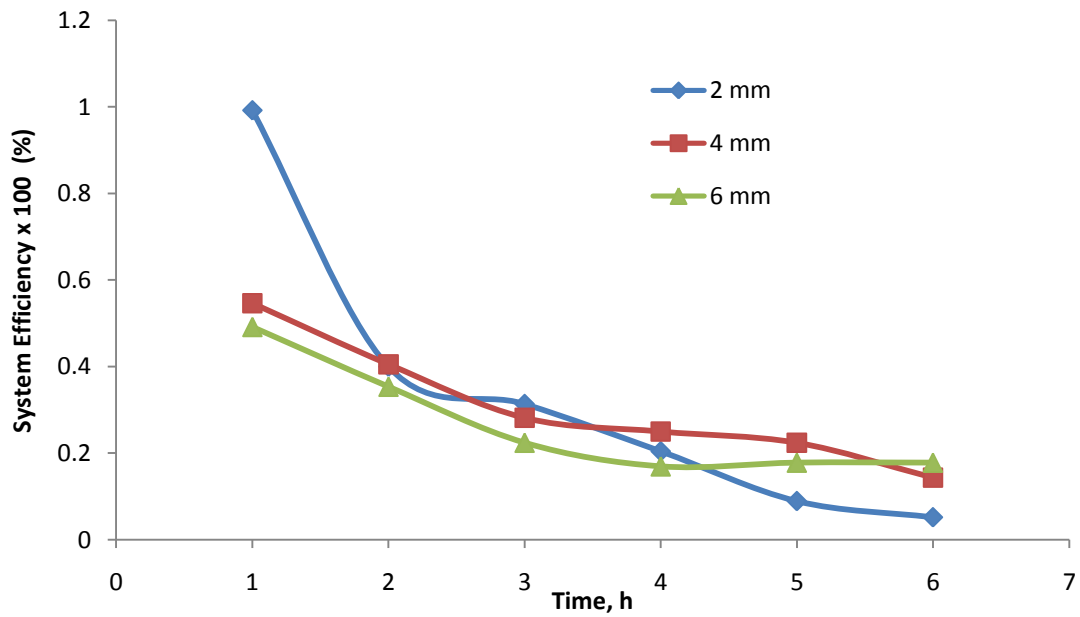
Fig 4.118   Effect of slice thickness on System efficiency for Photovoltaic dryer of cocoyam

4.17.2 Thermal Efficiency

The average thermal efficiency in photovoltaic dryer, hot-air conventional dryer and the oven dryer are presented in Fig 4.119. The thermal efficiency is the ratio of heat input to the heat utilized in the drying. The result indicates that the thermal efficiency is highest in the photovoltaic dryer with a value as high as 90%. This is mainly due to the transmittance of the glass which greatly increased the temperature in the solar collector far above the ambient temperature.
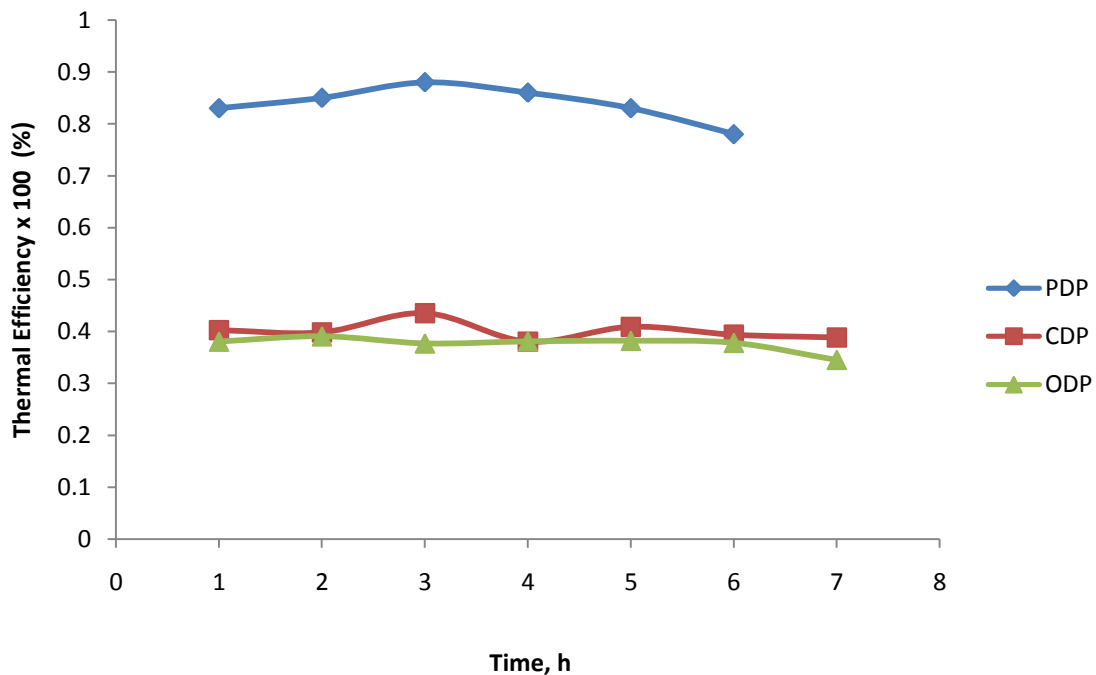
Fig 4.119   Average thermal efficiency for the different dryers

4.18   Mathematical modeling and kinetics of drying curves.

The experimental data of moisture ratio verses drying time were fitted with fourteen (14) different drying kinetic models. Non-linear regression analyses using MATLAB software was employed for the statistical modeling of the drying curves through selecting the General Equation option from curve fitting toolbox 1.1. The acceptability of the drying models was determined by the correlation coefficient first and then by the root – mean – square error (RMSE) and the sum of square errors (SSE). Only the results of the best drying kinetic models were presented. To select the best model for describing the drying curve, the criteria is that the value of correlation coefficient (R^2) should be high while the RMSE should be low. The results of the statistical analysis are given in Table 4.3 to 4.9. For SDP, the Modified Page I model was the best model while the Logarithmic was the best model for SDC. As seen in the case of the photovoltaic dryer, the Logarithmic and the Approximation Diffusion models show the best suitability in describing the drying kinetics of potato and cocoyam. The Two-Term model and the Logarithm model described the experimental data of ODC and CDC. The Modified Page I model was the best model for curve fitting of the experimental data in drying of potato using both the oven and hot-air conventional dryer. This may be due to the fact that the modified page 1 model is an empirical modification and has corrected the shortcomings of other theoretical and semi-theoretical models (Anna et al, 2014).

Table 4.33 Kinetic analysis for different mathematical models for SDP

Model Name	R^2	Adj R^2	SSE	RMSE
Newton	0.9976	0.9976	0.00335	0.0161
Page	0.9976	0.9974	0.00334	0.0167
M. Page I	0.9978	0.9974	0.00335	0.0167
Logarithmic	0.8927	0.1642	0.973	0.2974
Two Term	0.8089	1.352	2.489	0.4988
Wang and Singh	0.9871	0.986	0.01776	0.0385
A. Diffusion	0.9977	0.997	0.0032	0.0178
Midilli & Kucuk	0.1659	-0.08436	1.148	0.3387

Table 4.34   Kinetic analysis for different mathematical models for SDC

Model Name	R^2	Adj R^2	SSE	RMSE
Newton	0.9395	0.9215	0.1326	0.349
Page	0.9920	0.9832	0.0163	0.0084
M. Page I	0.9023	0.8828	0.0033	0.0087
Logarithmic	0.9960	0.9634	0.0084	0.0804
Two Term	0.9960	0.9721	0.0193	0.1156

Wang and Singh	0.9909	0.9811	0.0085	0.0848
A. Diffusion	0.8720	0.8211	0.0034	0.0125
Midilli & Kucuk	0.8077	0.7399	0.0092	0.0798

Table 4.35 Kinetic analysis for different mathematical models for PDP

Model Name	R^2	Adj R^2	SSE	RMSE
Newton	0.9824	0.967	0.00319	0.05511
Page	0.9934	0.795	0.00072	0.02553
M. Page I	0.9919	0.979	0.0072	0.0013
Logarithmic	0.9941	0.991	0.000555	0.0217
Two Term	0.0.9936	0.985	0.00056	0.0056
Wang and Singh	0.8721	0.7111	0.0857	0.5223
A. Diffusion	0.0.9965	0.9951	0.0057	0.0177
Midilli & Kucuk	-0.525	0.874	1.434	4.003

Table 4.36 Kinetic analysis for different mathematical models for PDC

Model Name	R^2	Adj R^2	SSE	RMSE
Newton	0.9353	0.9211	0.0041	0.0159
Page	0.9412	0.9400	0.0023	0.0079
M. Page I	0.9018	0.897	0.0034	0.0027
Logarithmic	0.9929	0.9792	0.00037	0.0152
Two Term	0.9369	0.9111	0.00228	0.0273
Wang and Singh	0.9638	0.9434	0.00871	0.0497
A. Diffusion	0.941	0.922	0.00034	0.03821
Midilli & Kucuk	0.8251	0.8005	0.00521	0.875

Table 4.37   Kinetic analysis for different mathematical models for ODP

Model Name	R^2	Adj R^2	SSE	RMSE
Newton	0.9112	0.894	0.0097	0.0963
Page	0.996	0.963	0.0046	0.0203
M. Page I	0.997	0.982	0.0064	0.0083
Logarithmic	0.9807	0.9591	0.00821	0.0542
Two Term	0.9920	0.979	0.0134	0.0374
Wang and Singh	-0.1342	-0.4856	0.0873	0.00457

A. Diffusion	0.9534	0.9138	0.0042	0.0345
Midilli & Kucuk	0.5382	0.5004	0.8315	0.432

Table 4.38 Kinetic analysis for different mathematical models for ODC

Model Name	R^2	Adj R^2	SSE	RMSE
Newton	0.9573	0.9453	0.00635	0.0561
Page	0.9805	0.9773	0.00934	0.0137
M. Page I	0.9128	0.8991	0.00835	0.0767
Logarithmic	0.9813	0.9721	0.91973	0.2274
Two Term	0.9952	0.9815	2.889	0.4988
Wang and Singh	0.9911	0.9781	0.05776	0.0385
A. Diffusion	0.8937	0.7777	0.0072	0.0178
Midilli & Kucuk	0.6118	0.516	1.5148	0.3387

Table 4.39 Kinetic analysis for different mathematical models for CDP

Model Name	R^2	Adj R^2	SSE	RMSE

Newton	0.8785	0.8502	0.0047	0.0363
Page	0.9943	0.9781	0.0016	0.0703
M. Page I	0.9977	0.9825	0.0024	0.0023
Logarith mic	0.9785	0.9518	0.00221	0.0342
Two Term	0.9944	0.9799	0.0434	0.0974
Wang and Singh	0.9955	0.778	0.0273	0.00457
A. Diffusion	0.8311	0.8222	0.0042	0.0745
Midilli & Kucuk	0.8923	0.8793	0.08315	0.432

Table 4.40 Kinetic analysis for different mathematical models for CDC

Model Name	R^2	Adj R^2	SSE	RMSE
Newton	0.9521	0.9411	0.0326	0.0349
Page	0.9491	0.9403	0.0463	0.00384
M. Page I	0.9398	0.9187	0.00733	0.00387
Logarith mic	0.9645	0.9481	0.0024	0.00804
Two Term	0.9441	0.9275	0.0493	0.01156
Wang and Singh	0.9311	0.9200	0.0085	0.03848
A.	0.9623	0.9491	0.0034	0.0125

Diffusion				
Midilli & Kucuk	0.9001	0.8823	0.0092	0.0798

4.19 Optimization of the drying of potato

The design matrix and output responses for the drying processes were given in Tables 4.41 and 4.42. The responses obtained from various runs are significantly exceptional which implies that each of the factors have substantial effect on the response.

Table 4.41: Optimization Results for the drying of PVDP

Run Order	Time (mins)	Air Speed (m/s)	Slice Thickness (mm)	Mass (g)	Moisture Content (%db)
1	120.0	1.5	2.00	54.2	67.8
2	120.0	1.5	2.00	54.1	67.5
3	180.0	1.5	2.00	42.5	31.6
4	180.0	1.5	2.00	42.4	31.3
5	120.0	2.5	2.00	45.9	42.1
6	120.0	2.5	2.00	45.6	41.1
7	180.0	2.5	2.00	36.2	12.1
8	180.0	2.5	2.00	36.3	12.4
9	120.0	1.5	3.00	54.1	67.5
10	120.0	1.5	3.00	54	67.2
11	180.0	1.5	3.00	45.5	40.9
12	180.0	1.5	3.00	45.7	41.5
13	120.0	2.5	3.00	52.8	63.5
14	120.0	2.5	3.00	52.8	63.5
15	180.0	2.5	3.00	43.3	34.1
16	180.0	2.5	3.00	43.4	34.4
17	99.6	2.0	2.50	57.6	78.3
18	99.6	2.0	2.50	57.6	78.0
19	200.5	2.0	2.50	38.2	18.3
20	200.5	2.0	2.50	38.2	17.9
21	150.0	1.2	2.50	49.0	51.7
22	150.0	1.2	2.50	49.0	51.7
23	150.0	2.8	2.50	43.1	33.4
24	150.0	2.8	2.50	43.0	33.1
25	150.0	2.0	1.66	41.1	27.9
26	150.0	2.0	1.66	41.3	27.6
27	150.0	2.0	3.34	48.7	50.8
28	150.0	2.0	3.34	48.7	50.8

202

29	150.0	2.0	2.50	45.5	40.9
30	150.0	2.0	2.50	45.3	40.2
31	150.0	2.0	2.50	45.4	40.5
32	150.0	2.0	2.50	45.4	40.6
33	150.0	2.0	2.50	45.4	40.6
34	150.0	2.0	2.50	45.3	40.2

Table 4.42: Optimization Results for the drying of HVDP

Run Order	Time (mins)	Air Speed (m/s)	Temperature (^{o}C)	Mass (g)	Moisture Content (%db)
1	80.00	1.00	60.0	61.5	90.40195
2	80.0	1.00	60.0	61.0	88.85397
3	180.0	1.00	60.0	45.0	39.31836
4	180.0	1.00	60.0	45.0	39.31836
5	80.0	3.50	60.0	55.3	71.20691
6	80.0	3.50	60.0	55.5	71.8261
7	180.0	3.50	60.0	42.7	32.19762
8	180.0	3.50	60.0	42.6	31.88802
9	80.0	1.00	90.0	53.9	66.87254
10	80.0	1.00	90.0	53.7	66.25335
11	180.0	1.00	90.0	43.2	33.74561
12	180.0	1.00	90.0	43.5	34.6744
13	80.0	3.50	90.0	47.0	45.51031
14	80.0	3.50	90.0	47.3	46.43911
15	180.0	3.50	90.0	38.4	18.88493
16	180.0	3.50	90.0	38.0	17.64654
17	64.2	2.50	75.0	57.3	77.39886

203

18	64.2	2.50	75.0	57.3	77.39886
19	195.8	2.50	75.0	43.6	34.984
20	195.8	2.50	75.0	43.5	34.6744
21	130.0	0.60	75.0	51.3	58.82301
22	130.0	0.60	75.0	51.6	59.7518
23	130.0	3.90	75.0	44.0	36.22239
24	130.0	3.90	75.0	44.2	36.84158
25	130.0	2.25	55.3	49.6	53.55985
26	130.0	2.25	55.3	49.4	52.94065
27	130.0	2.25	94.7	42.6	31.88802
28	130.0	2.25	94.7	42.7	32.19762
29	130.0	2.25	75.0	48.0	48.60629
30	130.0	2.25	75.0	47.2	46.12951
31	130.0	2.25	75.0	49.0	51.70226
32	130.0	2.25	75.0	48.4	49.84468
33	130.0	2.25	75.0	47.7	47.6775
34	130.0	2.25	75.0	48.0	48.60629

4.19.1 Analysis of Variance

The Analysis of Variance (ANOVA) was used to interpret the Central Composite Design. The detailed table of statistics compares the Sequential P-value, the Lack of fit P-value, the Adjusted R-squared and the Predicted R-squared values. The summary of

P-values indicates that a quadratic model fitted the ANOVA analysis and hence it was suggested. The linear and 2FI models were not suggested. The Cubic model is always aliased because the CCD does not contain enough runs to support a full cubic model. A significance level of 95% was used hence all terms whose P-value are less than 0.05 are considered significant. The model summary test, the sequential model sum of squares and the lack of fit test for the drying process were also presented in Appendix.

4.19.2 ANOVA analysis and model fitting

The F-value tests were performed using the ANOVA to calculate the significance of each type of model. Based on the results of F-value, the highest order model with significant terms which shows the most accurate relationship between parameters would be chosen. The Sequential Model Sum of squares of PVDP, the Linear vs Mean, the Quadratic vs 2FI, the 2FI vs Linear and the Cubic vs Quadratic models have significant F-value of 1443.24, 18.06, 8.64 and 22.37. Equally, for HADP, the F-value of the Quadratic vs 2FI was 43.13.

Besides evaluating the significance, the adequacy of the models was evaluated by applying the lack-of-fit test. This test is used in the numerator in an F-test of the null hypothesis and indicates that a proposed model fits well or not. The test for lack-of-fit compares the variation around the model with pure variation within replicated observations. This test measured the adequacy of the different models based on response surface analysis (Lee et al., 2006, Pishgar et al., 2012). Hence, the Quadratic model with the lowest insignificant model of lack of fit is suggested. The high

significant results of lack of fit for linear, cubic and 2FI models showed that these models are not adequate to use.

Equally, the R-squared values for the quadratic and cubic models have the best value of 0.9899 and 0.9986 respectively for PVDP and 0.9938 and 0.9979 respectively for HADP when compared to the other models (2FI and linear). The measure of how efficient the variability in the actual response values can be explained by the experimental variables and their interactions is given by the R-Squared value. The coefficient of regression R^2 was used to validate the fitness of the model equation. For PVDP, the R^2 has a high value of 0.9899 showing that 98.99% of the variability in the response can be explained by the model while for HADP, the R^2 has a value of 0.9938 showing that 99.38% of the variability in the response can be explained by the model. This implies that the prediction of experimental data is quite satisfactory.

The closer the R^2 value is to unity, the better the model predicts the response. Adjusted-R^2 is a measure of the amount of variation around the mean explained by the model, adjusted for the number of terms in the model.

The adjusted-R^2 decreases as the number of terms in the model increases, if those additional terms don't add value to the model. Predicted-R^2 is a measure of the amount of variation in new data explained by the model. The adjusted R^2 (PVDP = 0.9860; HADP = 0.9915) is in close agreement with the predicted R^2 (PVDP = 0.9780; HADC = 0.9879). The predicted-R^2 and the adjusted-R^2 should be within 0.20 of each other.

Otherwise there may be a problem with either the data or the model (Taran and Aghaie, 2015).

Table 4.43   ANOVA Table for PVDP

Source	Sum of Squares	df	Mean Square	F Value	p-value Prob> F
Model	10130.44		1125.60	160.10	< 0.0001
A-Time	7221.669		7221.669	1668.74	< 0.0001
B-Air Speed	1108.90		1108.90	256.24	< 0.0001
C-Slice Thickness	1240.64		1240.64	286.68	< 0.0001
AB	3.45		3.45	0.80	0.3808
AC	26.10		26.10	6.03	0.0217
BC	295.24		295.24	68.22	< 0.0001
A^2	205.31		205.31	47.44	< 0.0001
B^2	23.46		23.46	5.42	0.0287
C^2	0.38		0.38	0.087	0.7703
Residual	103.86	4	4.33		
Lack of Fit	102.54		20.51	293.86	< 0.0001

Pure Error	1.33	9	0.070		
Cor Total	10234.30	3			

Std. Dev. = 2.08;   Mean = 43.55;   C.V. = 4.78%;   PRESS = 225.44

R-Squared = 0.9899   Adj R-Sq = 0.9860;   Pred R-Sq = 0.9780;   Adeq Precision = 58.902

Table 4.44   ANOVA Table for HADP

Source	Sum of Squares	f	Mean Square	F Value	p-value Prob> F
Model	11139.		1237.70	428.95	<

Source	Sum of Squares	df	Mean Square	F Value	p-value
	32				0.0001
A-Time	7393.94		7393.94	2562.52	< 0.0001
B-Air Speed	1472.35		1472.35	510.27	< 0.0001
C-Temperature	1587.86		1587.86	550.30	< 0.0001
AB	59.91		59.91	20.76	0.0001
AC	220.84		220.84	76.54	< 0.0001
BC	31.06		31.06	10.76	0.0032
A^2	254.71		254.71	88.27	< 0.0001
B^2	0.61		0.61	0.21	0.6488
C^2	132.80		132.80	46.03	< 0.0001
Residual	69.25	4	2.89		
Lack of Fit	47.11		9.42		0.0003
Pure Error	22.14	9			
Cor Total	11208.57	3			

Std. Dev. = 1.70; Mean = 49.24; C.V. = 3.45%; PRESS = 135.96

R-Squared = 0.9938   Adj R-Sq = 0.9915;   Pred R-Sq = 0.9879;   Adeq Precision = 74.451

The ANOVA tables were given in Tables 4.45 and 4.46. A significance level of 5% (0.05) was used hence all terms whose P-value are less than 0.05 are considered significant. From the Tables 4.51 and 4.52, the regression F-values of 260.10 (PVDP) and 428.95 (HADP) implies that the model is significant which was validated by the P-values being less than 0.0005. There is only a 0.05% chance that a "Model F-Value" this large could occur due to noise. The tests for adequacy of the regression models, significance of individual of model coefficients and the lack of fit test were performed using the same statistical package. The P-values were used as a tool to check the significance of each of the coefficients, which in turn are necessary to understand the pattern of the mutual interactions between the test variables (Shrivastava et al, 2008). The larger the magnitude of F-test value and the smaller the magnitude of P-values, the higher the significance of the corresponding coefficient (Alam et al, 2008).

The adequate precision measures the signal to noise ratio and compares the range of the predicted value at the design points to the average prediction error. The adquate predicion ratio above 4 indicates adequate model efficacy (Kumar et al, 2007). Hence, the adquate precision ratios of 48.902 (PVDP) and 74.451 (HADP) indicates adquate signal. This indicates that an adequate relationship of signal to noise ratio exists. Also, a PRESS value of 225.44 (PVDP) and 135.96 (HADP) indicates an adquate signal implying that the models can be used to navigate the design space.

The C.V called coefficient of variation which is defined as the ratio of the standard deviation of estimate to the mean value of the observed response is independent of the unit. It is also a measure of reproducibility and repeatability of the models (Chen et al., 2010; Chen et al., 2011). The calculations indicated the C.V value of 4.78% (PVDP) and 3.45% (HADP) which showed that the model can be considered reasonably reproducible (because its CV was not greater than 10%) (Chen et al., 2011).

The quadratic model equations generated for the PVDP and HADP in terms of actual factors are

$(M.C)_{PVDP}$ = + 329.15668 - 1.82264 * Time - 76.66334 * Air Speed - 31.06976 * Slice Thickness + 0.030960 * Time * Air Speed + 0.085139 * Time * Slice Thickness + 17.18266 * Air Speed * Slice Thickness + 3.35288E-003 * Time^2 + 4.07982 * Air Speed^2 - 0.51746 * Slice Thickness^2   (4.8)

$(M.C)_{HADP}$ = + 144.38212 - 1.26991 * Time - 4.22455 * Air Speed + 1.14196 * Temperature + 0.030960 * Time * Air Speed + 4.95356E-003 * Time * Temperature -0.074303 * Air Speed * Temperature + 1.80607E-003 * Time^2 - 0.14183 * Air Speed^2 - 0.014490 * Temperature^2   (4.9)

In terms of coded factors

$(M.C)_{PVDP}$ = + 40.41 - 16.26 * A - 6.37 * B + 6.74 * C + 0.46 * A * B + 1.28 * A * C + 4.30 * B * C + 3.02 * A^2 + 1.02 * B^2 - 0.13 * C^2   (4.10)

$(M.C)_{HADP}$ = + 48.55 - 17.96 * A - 8.01 * B - 8.32 * C + 1.93 * A * B + 3.72 * A * C - 1.39 * B * C + 4.52 * A^2 - 0.22 * B^2 - 3.26 * C^2   (4.11)

The equation in terms of coded factors can be used to make predictions about the response for given levels of each factor. By default, the high levels of the factors are coded as +1 and the low levels of the factors are coded as -1. The coded equation is useful for identifying the relative impact of the factors by comparing the factor coefficients, while the equation in terms of actual factors can be used to make predictions about the response for given levels of each factor. Here, the levels are to be specified in the original units for each factor.

In a regression equation, when an independent variable has a positive sign, it means that an increase in the variable will cause an increase in the response while a negative sign will result in a decrease in the response (Kumur et al, 2008).

Values of P less than 0.05 indicate the model terms are significant. For PVDP, among the test variables used in the study, AB and C^2 are insignificant model terms while for HADP, the insignificant term is B^2. Therefore, eliminating the insignificant terms, the final model equations becomes as expressed in equations 4.12 to 4.15.

In terms of actual factors are

$(M.C)_{PVDP}$ =   +329.15668 - 1.82264 * Time - 76.66334 * Air Speed - 31.06976 * Slice Thickness + 0.085139 * Time * Slice Thickness + 17.18266   * Air Speed * Slice Thickness + 3.35288E-003 * Time^2 - 0.51746 * Slice Thickness^2   (4.12)

$(M.C)_{HADP}$ = + 144.38212 - 1.26991 * Time - 4.22455 * Air Speed + 1.14196 * Temperature + 0.030960 * Time * Air Speed + 4.95356E-003 * Time * Temperature -0.074303 * Air Speed * Temperature + 1.80607E-003 * Time^2 - 0.014490 * Temperature^2 (4.13)

In terms of coded factors

$(M.C)_{PVDP}$ = + 40.41 - 16.26 * A - 6.37 * B + 6.74 * C + 1.28 * A * C + 4.30 * B * C + 3.02 * A^2 - 0.13 * C^2 (4.14)

$(M.C)_{HADP}$ = + 48.55 - 17.96 * A - 8.01 * B - 8.32 * C + 1.93 * A * B + 3.72 * A * C - 1.39 * B * C + 4.52 * A^2 - 3.26 * C^2 (4.15)

The response values obtained by inserting the independent values are the predicted values of the model. These values are compared to the actual experimental values. The result of this comparison is shown in the Table 4.53 and 4.54. From the table, it is seen that there is a close correlation between the actual experimental response and the predicted response. This confirms the effectiveness of the model in predicting the drying process.

213

Table 4.47 Table of Experimental Vs Predicted Responses for PVDP

Run Order	Time (mins)	Air Speed (m/s)	Slice thickness (mm)	Experimental Response	Predicted Response
1	120.0	1.5	2.00	67.8	66.25071
2	120.0	1.5	2.00	67.5	66.25071
3	180.0	1.5	2.00	31.6	30.24716
4	180.0	1.5	2.00	31.3	30.24716
5	120.0	2.5	2.00	42.1	43.98716
6	120.0	2.5	2.00	41.1	43.98716
7	180.0	2.5	2.00	12.1	9.841201
8	180.0	2.5	2.00	12.4	9.841201
9	120.0	1.5	3.00	67.5	68.58434
10	120.0	1.5	3.00	67.2	68.58434
11	180.0	1.5	3.00	40.9	37.68916
12	180.0	1.5	3.00	41.5	37.68916
13	120.0	2.5	3.00	63.5	63.50345
14	120.0	2.5	3.00	63.5	63.50345
15	180.0	2.5	3.00	34.1	34.46586
16	180.0	2.5	3.00	34.4	34.46586
17	99.6	2.0	2.50	78.3	76.29441
18	99.6	2.0	2.50	78.0	76.29441
19	200.5	2.0	2.50	18.3	21.6015

					5
20	200.5	2.0	2.50	17.9	21.6015 5
21	150.0	1.2	2.50	51.7	54.0137 2
22	150.0	1.2	2.50	51.7	54.0137 2
23	150.0	2.8	2.50	33.4	32.5819 2
24	150.0	2.8	2.50	33.1	32.5819 2
25	150.0	2.0	1.66	27.9	28.7124 9
26	150.0	2.0	1.66	27.6	28.7124 9
27	150.0	2.0	3.34	50.8	51.3816 1
28	150.0	2.0	3.34	50.8	51.3816 1
29	150.0	2.0	2.50	40.9	40.4129 5
30	150.0	2.0	2.50	40.2	40.4129 5
31	150.0	2.0	2.50	40.5	40.4129 5
32	150.0	2.0	2.50	40.6	40.4129 5
33	150.0	2.0	2.50	40.6	40.4129 5
34	150.0	2.0	2.50	40.2	40.4129 5

Table 4.48 Table of Experimental Vs Predicted Responses for HADP

Run Order	Time (mins)	Air Speed (m/s)	Temperature (^{o}C)	Experimental Response	Predicted Response
1	80.00	1.00	60.0	90.40195	88.1302 8

2	80.0	1.00	60.0	88.85397	88.13028
3	180.0	1.00	60.0	39.31836	40.91437
4	180.0	1.00	60.0	39.31836	40.91437
5	80.0	3.50	60.0	71.20691	71.01973
6	80.0	3.50	60.0	71.8261	71.01973
7	180.0	3.50	60.0	32.19762	31.54377
8	180.0	3.50	60.0	31.88802	31.54377
9	80.0	1.00	90.0	66.87254	66.84257
10	80.0	1.00	90.0	66.25335	66.84257
11	180.0	1.00	90.0	33.74561	34.48734
12	180.0	1.00	90.0	34.6744	34.48734
13	80.0	3.50	90.0	45.51031	44.15927
14	80.0	3.50	90.0	46.43911	44.15927
15	180.0	3.50	90.0	18.88493	19.54398
16	180.0	3.50	90.0	17.64654	19.54398
17	64.2	2.50	75.0	77.39886	80.00119
18	64.2	2.50	75.0	77.39886	80.00119
19	195.8	2.50	75.0	34.984	32.73361
20	195.8	2.50	75.0	34.6744	32.73361
21	130.0	0.60	75.0	58.82301	58.7094
22	130.0	0.60	75.0	59.7518	58.7094
23	130.0	3.90	75.0	36.22239	37.61674

24	130.0	3.90	75.0	36.84158	37.6167 4
25	130.0	2.25	55.3	53.55985	53.8521 1
26	130.0	2.25	55.3	52.94065	53.8521 1
27	130.0	2.25	94.7	31.88802	31.9477 1
28	130.0	2.25	94.7	32.19762	31.9477 1
29	130.0	2.25	75.0	48.60629	48.5469 1
30	130.0	2.25	75.0	46.12951	48.5469 1
31	130.0	2.25	75.0	51.70226	48.5469 1
32	130.0	2.25	75.0	49.84468	48.5469 1
33	130.0	2.25	75.0	47.6775	48.5469 1
34	130.0	2.25	75.0	48.60629	48.5469 1

The Normal plot of Residuals and the Predicted vs Actual plots (Figures 4.120 to 125) were used to check whether the points will follow a straight line in which we conclude that the residuals follow a normal distribution. It is seen that the points were closely distributed to the stright line of the plot. This confirms the good relationship between the experimental values and the predicted values of the response though some small scatter like an "S" shape is always expected. This observation shows that the central composite design is well fitted into the model and thus can be used to perform the optimisation operation for the process.

From the diagram it could be concluded that the residuals followed a normal distribution pattern. The points of the normal distributions are seen to be mostly interlocked with the straight line with a few points lying outside the diagonal line in a moderately scattered manner.

These plots equally confirm that the selected model was adequate in predicting the response variables in the experimental values.
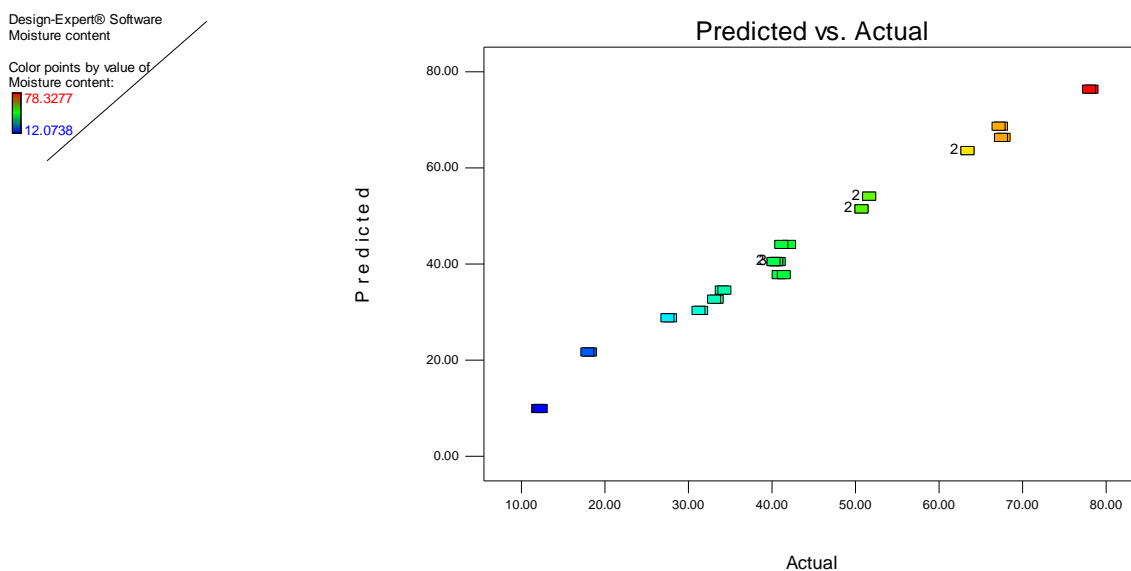
Figure 4.120 Linear correlation between Predicted vs. Actual values for PVDP
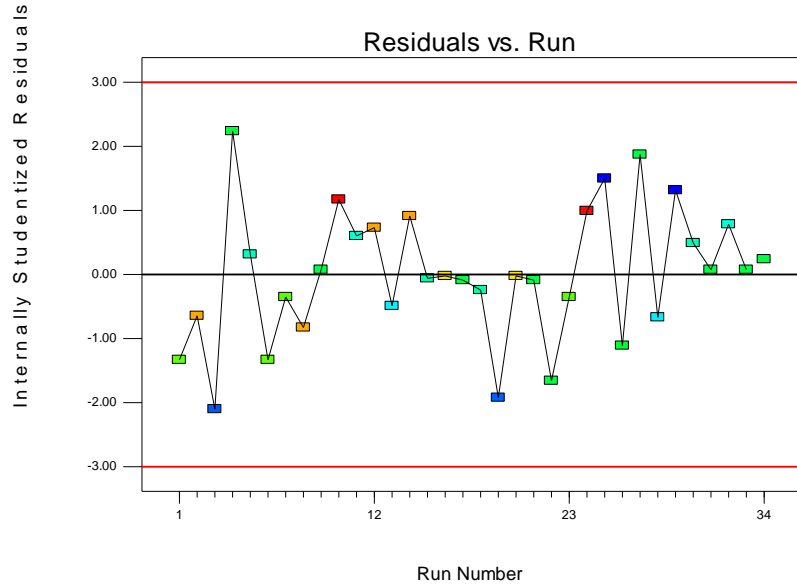
Fig 4.121 : Plot of Residuals vs Run order for PVDP
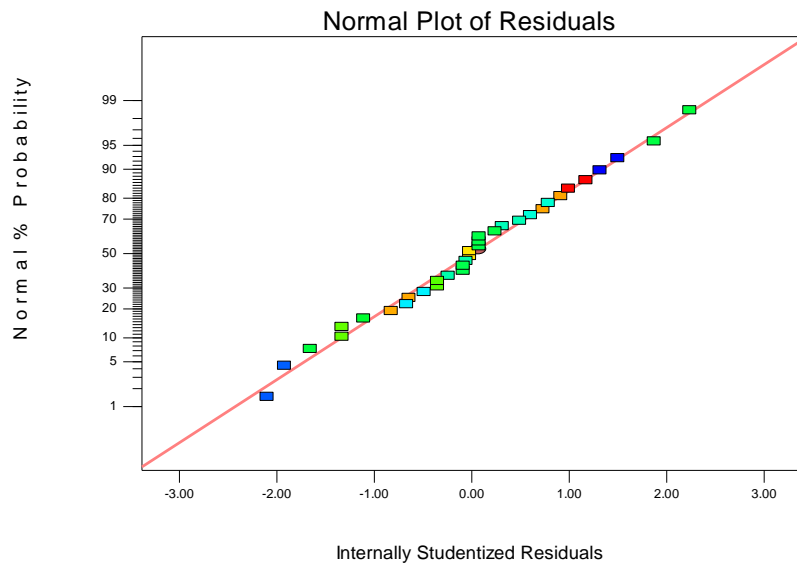
Figure 4.122   Normal probability plots of Residuals obtained from PVDP

Predicted vs. Actual
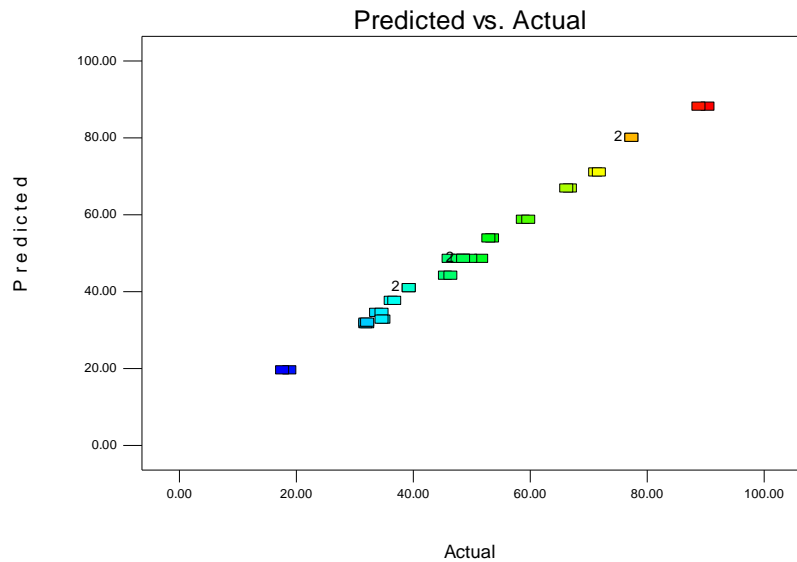
Figure 4.123 Linear correlation between Predicted vs. Actual values for HADP
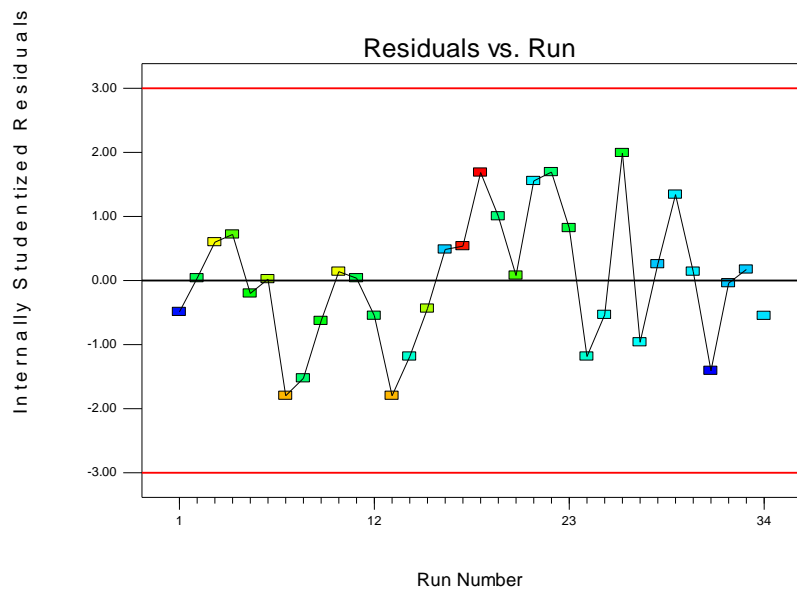
Residuals vs. Run

Fig 4.124 : Plot of Residuals vs Run order for HADP
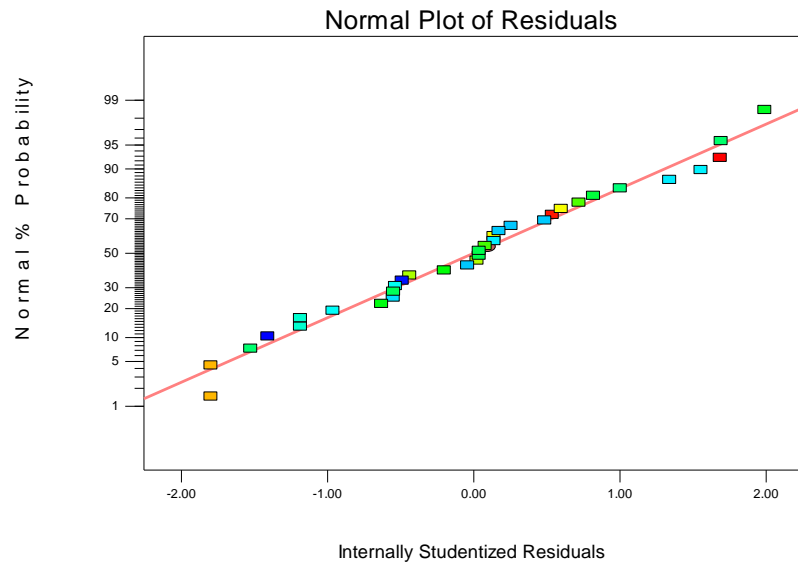
Figure 4.125   Normal probability plots of Residuals obtained from HADP

The Perturbation graph is shown in Fig 4.126 and 4.127. It shows the deviation from the reference point in terms of coded terms. The reference point of a deviation is the mean. For PVDP, the reference point is at a mointure content of 42% db while for HADP, the reference point is at moisture content of 48%db. From the figures, it is also seen that time has the greatest deviation from the reference point ranging from $60 - 27$%db for PVDP and $72 - 37$ %db for HADP as it ranged from -1 to +1. In HADP, temperature and air speed has almost the same deviation from the mean.
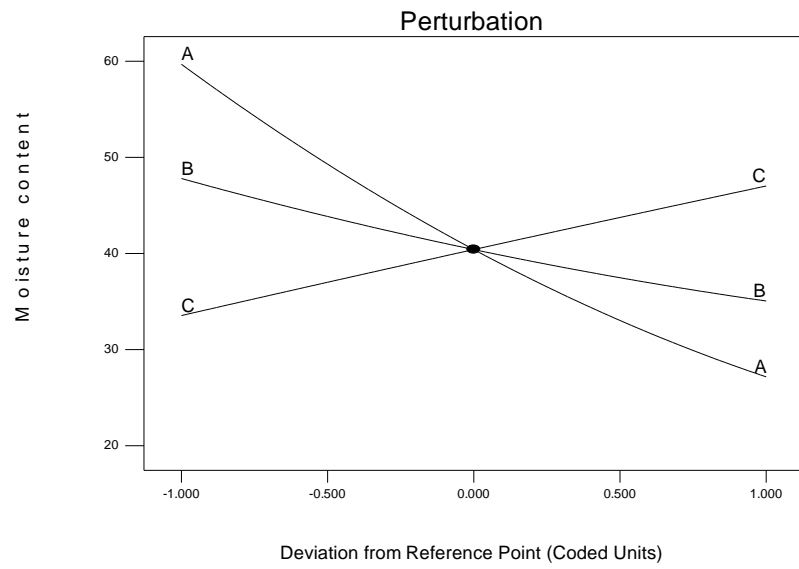
Fig 4.126   Perturbation plot showing deviation from the Reference point for PVDP
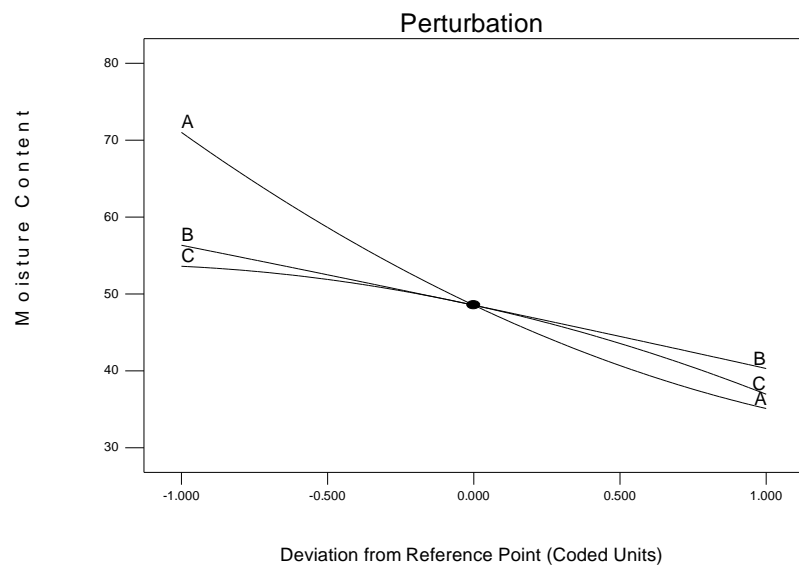
Fig 4.127   Perturbation plot showing deviation from the Reference point for HADP

4.19.3   Three Dimensional (3D) surface plots for EBT adsorption

The 3-D response surface plots for PVDP and HADP are presented in Figures 4.128 to 4.132. The 3-D response surface plots are graphical representation of the interactive effects of any two variables the factors.

Response surface estimation for minimum moisture content represents surface plots as a function of two factors at a time while maintaining all other factors at fixed levels. This is more helpful in understanding both the main and the interaction effects of these two factors. These plots can be easily obtained by calculating from the model, the values taken by one factor where the second varies with constraint of a given Y value. The response surface curves were plotted to understand the interaction of the variables and to determine the optimum level of each variable for maximum response.

The nature of the response surface curves shows the interaction between the variables. The elliptical shape of the curve indicates good interaction of the two variables and circular shape indicates no interaction between the variables (Box and Wilson, 1951; Box and Hunter, 1951). From figures 4.128 to 4.133, it was observed that the elliptical nature of the contour depicted the mutual interactions of all the variables. There was a relative significant interaction between every two variables, and there was a maximum predicted yield as indicated by the surface confined in the smallest ellipse in the contour diagrams. It can be seen from the graphs that there is a good interaction between the variables especially time and air speed. Equally, as time increased the moisture content decreased significantly till a time of about 150 minutes in which the significance reduces.
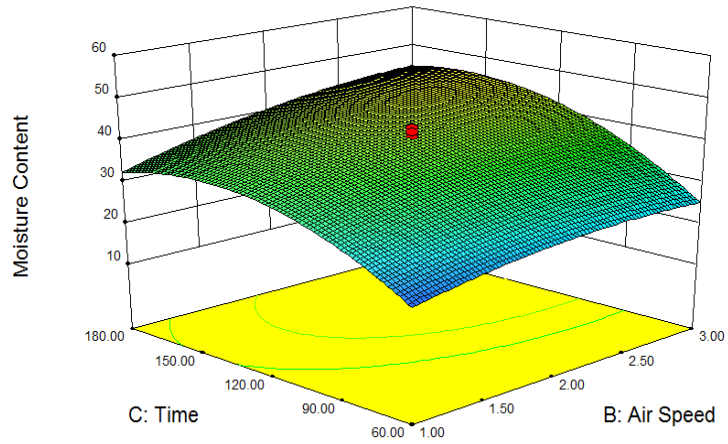
Fig 4.128   3D surface plot showing the combined effects of Time and Air Speed for PVDP
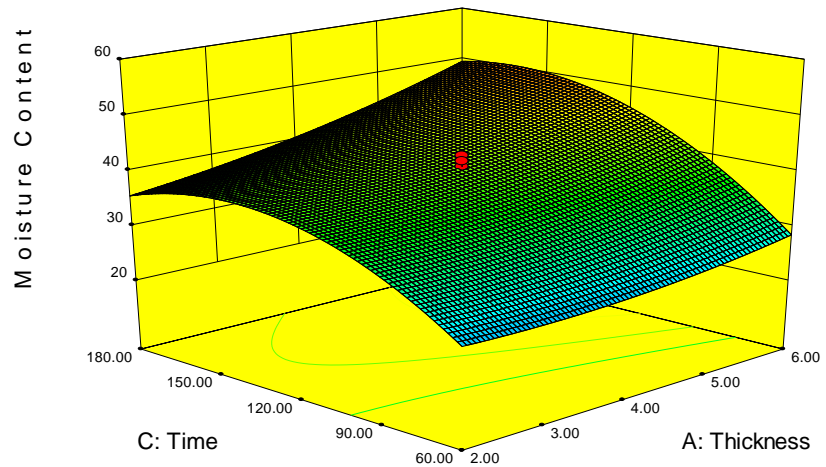
Fig 4.129   3D surface plot showing the combined effects of Time and Slice Thickness
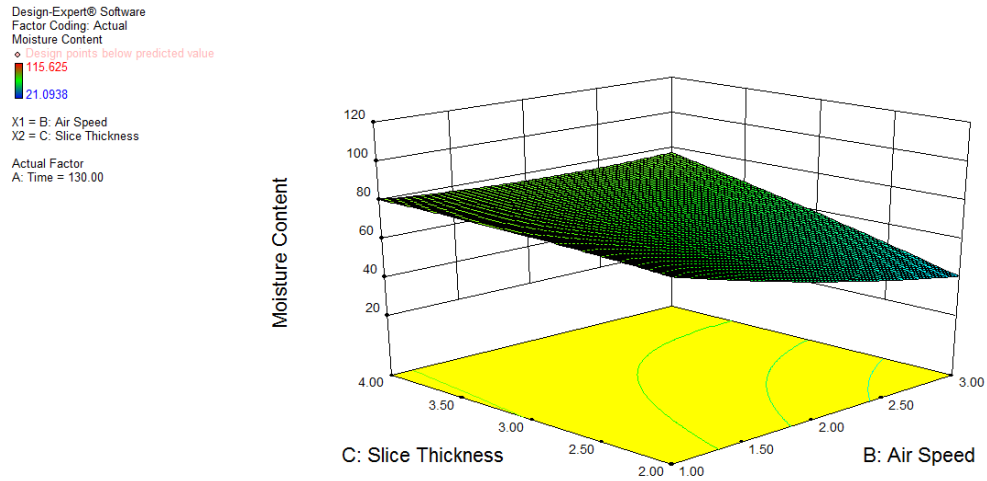
for PVDP

Fig 4.130   3D surface plot showing the combined effects of Slice Thickness and Air

Speed for PVDP
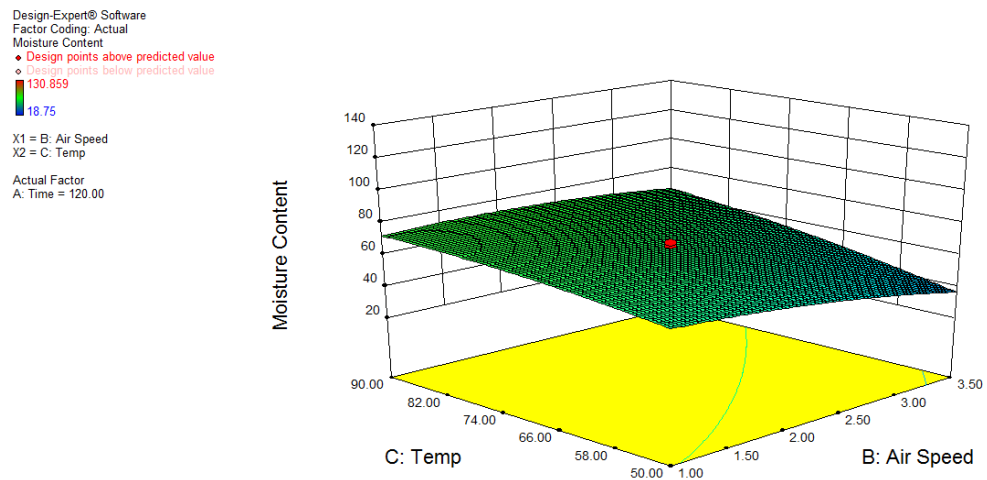
Fig 4.131 3D surface plot showing the combined effects of Temperature and Air Speed

for HADP
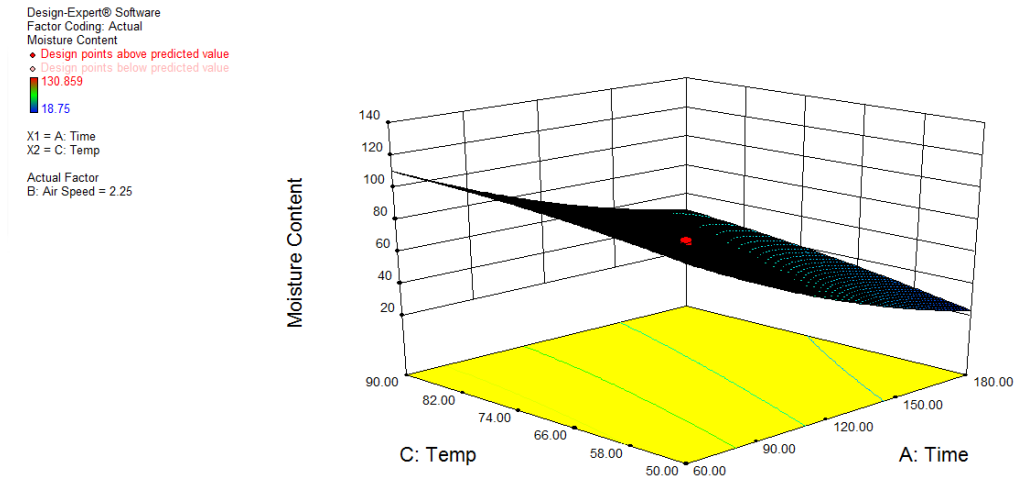
Fig 4.132 3D surface plot showing the combined effects of Time and Temperature for

HADP

The 3D surface plots show that the minimum moisture content of 12.4 %db was

obtained at a time of 180 minutes, an air speed of 2.5 m/s and slice thickness of 2.0 mm

for PVDP which is in accordance with the model. For HADP, the minimum moisture

content of 17.6 %db was obtained at a time of 180 minutes, an air speed of 3.5 m/s and

temperature of 90$^{\text{o}}$C.

From the plots of one factor (Fig 4.133 to 4.136), it is seen that the effect of the air

speed decreasing from 2.5 m/s to 1.5 m/s is that the moisture content reduced from

48%db to 35%db. As the slice thickness decreased from 3 mm to 2 mm, the moisture

content linearly decreased from 48 %db to 33 %db. This is because as the slice

thickness decreases, the moisture dissipation inside the product and finally its departure from the product would face less resistance (Mohammad et al, 2013). The thicker the slice, the slower the approach to equilibrium moisture content and the slower the drying rate (Etoamaihe and Ibeawuchi, 2010).
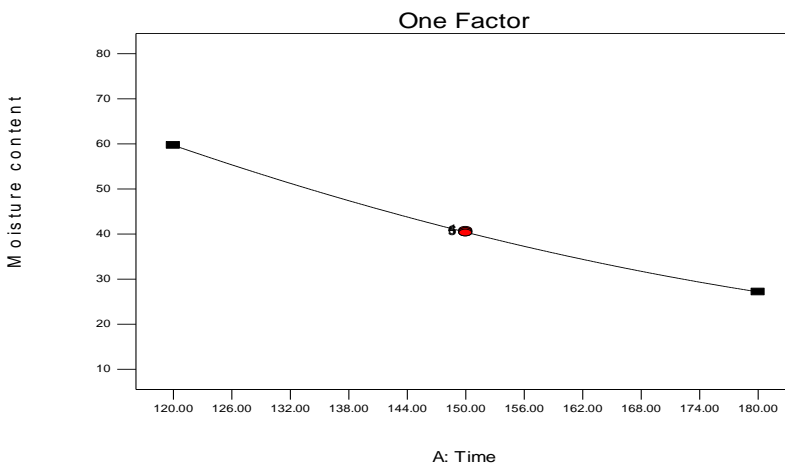
Fig 4. 133a   Plots for a one factor at a time of Moisture content and time for PVDP
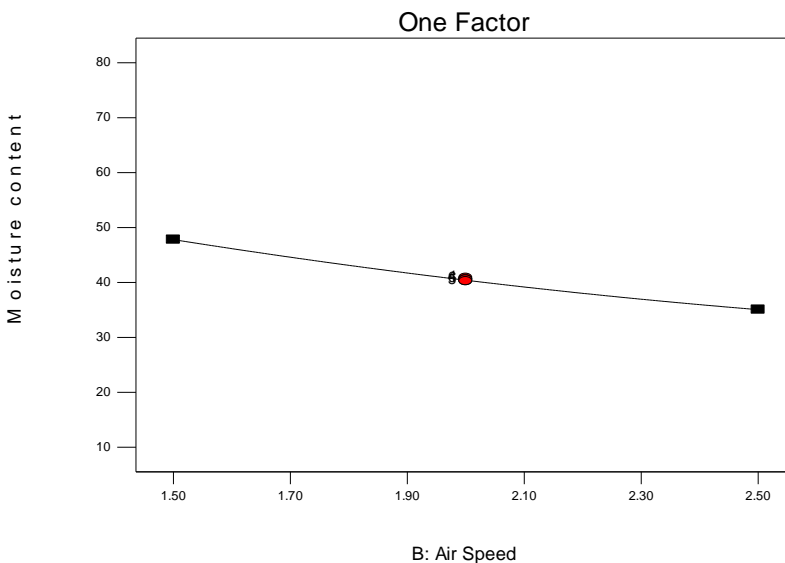
Fig 4. 133b   Plots for a one factor at a time of Moisture content and air speed for PVDP
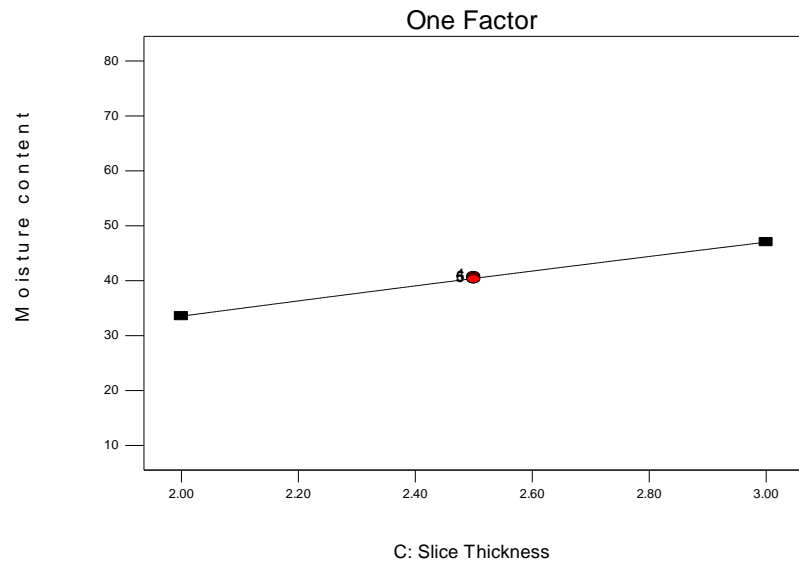
One Factor

Fig 4. 133c   Plots for a one factor at a time of Moisture content and slice thickness for
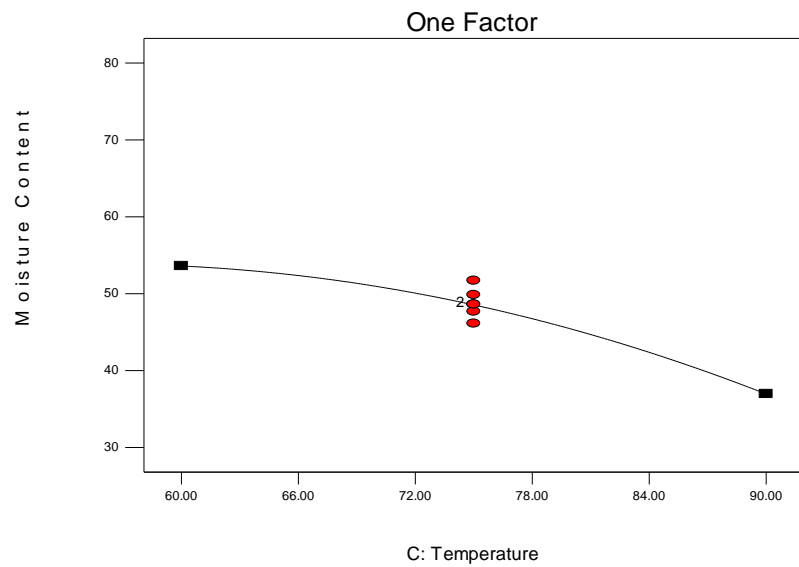
PVDP

One Factor

Fig 4. 133d : Plots for a one factor at a time of Moisture content and temperature for PVDP

4.19.4 Validation of Optimization Result for PVDP and HADP.

Investigation of the optimum process parameters for maximizing the removal efficiency of moisture is one of the primary objectives of the present study. From Table 4.55, it can be seen that, time of 180 mins, air speed of 2.5 m/s and slice thickness of 2.0 are the optimum conditions required for maximum drying of PVDP while for the maximum drying of HADP, a temperature of $90^{o}C$, air speed of 3.5 m/s and time of 180 minutes is required. Under these conditions, the predicted moisture content of PVDP was 9.8%db and 19.5%db for HADP. These are in good agreement with the experimental

value of 17.6%db and 12.1%db for HADP and HADP respectively, performed at the same optimum values of the process variables. The optimization was performed using the numerical method of the Design Expert by State Ease U.S.A.

Table 4.49a: The Predicted Optimum Conditions and Experimental Validation Result for PVDP

	Optimum Conditions Predicted			Predicted Moisture content (%)	Experimental Validation Result (%)
Material	**Time (mins)**	**Air Speed (m/s)**	**Slice Thickness (mm)**		
PVDP	180	2.5	2.0	12.1	9.8

Table 4.49b The Predicted Optimum Conditions and Experimental Validation Result for HADP

Material	Optimum Conditions Predicted			Predicted Moisture content (%)	Experimental Validation Result (%)
	Time (mins)	Air Speed (m/s)	Temperature (ºC)		
HADP	180	3.5	90	17.6	19.5

4.20 The Artificial Neural Network Function Analysis for PVDP and HADP

In fitting problem for the drying of PVDP and HADP, the neural network was required to map between a data set of numeric inputs of the various process parameters (such as time, slice thickness, air speed and temperature) influencing the drying process and a set of numeric targets. Artificial neural networks (ANN's) are inspired by biological neural systems. In this approach weighted sum of inputs arriving at each neuron is passed through an activation function (generally nonlinear) to generate an output signal (Manpreet *et al.,* 2011; Haykyn, 2003). Neural network function fitting is used to select data, create and train a network, and evaluate its performance using mean square error and regression analysis. Interest in using artificial neural networks (ANNs) for predicting has led to a tremendous surge in research activities in the past two decades (Omid *et al.,* 2009; Aghbashlo *et al.,* 2011).

A two-layer feed-forward network with sigmoid hidden neurons and liner output neurons, was used to fit the multi-dimensional mapping problems arbitrarily well, given consistent data and enough neurons in its hidden layer. The network was trained with Levenberg-Marquardt (LM) back propagation algorithm which is one of the Multi-Layer Perceptron (MLP) networks that is used for error minimization. If there was not

enough memory, the case scaled conjugate gradient back propagation was used. MLPs are normally trained with error back-propagation (BP) algorithm. It is a general method for iteratively solving for weights and biases (Nourbakhsh *et al.,* 2014). The network architecture was given as shown in the Figure 4.134 and 135
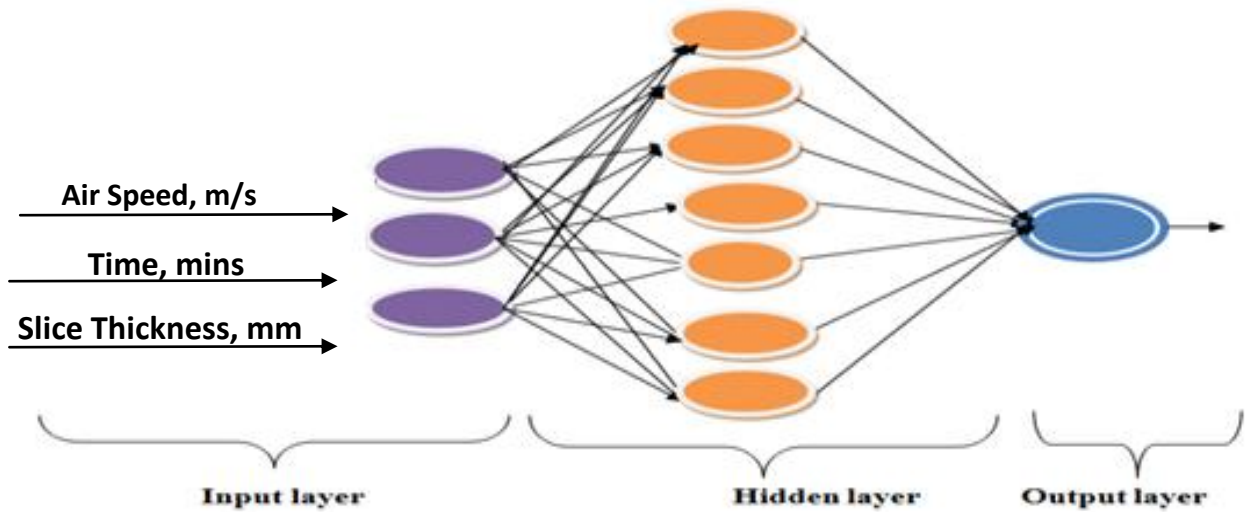

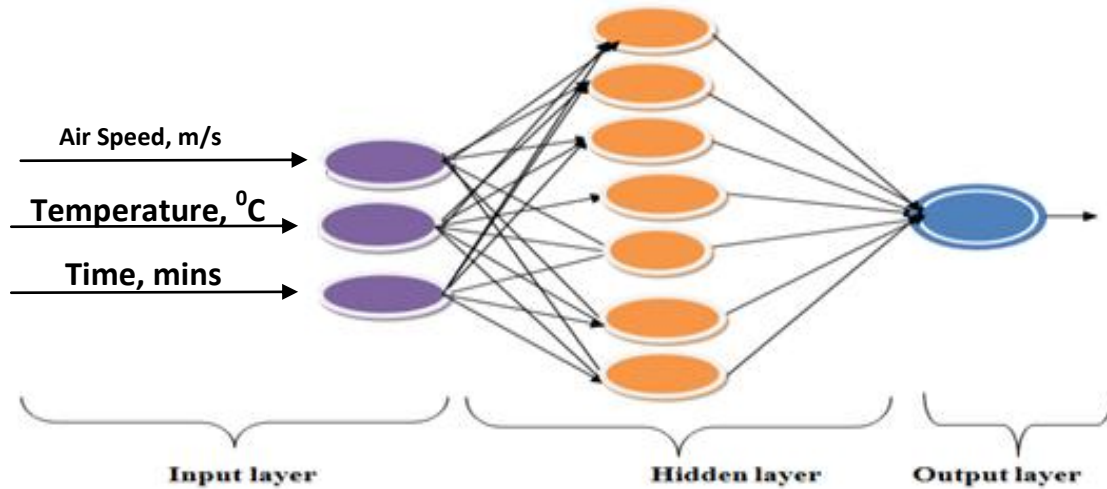Figure 4.134: The Neural Network Architecture of PVDP

Figure 4.135: The Neural Network Architecture of HADP

4.20.1   Artificial Neural Network Training, Validation and Testing.

For the drying of both PVDP and HADP, a total of 26 samples were set aside for training, 5 samples for testing and 3 samples for validation representing about 75% training, 15% testing and 10% validation. For the training, the network was trained and adjusted according to its error. In the validation, the network generalization was measured by network validation and halted when generalization stops improving to stop over fitting. The testing have no effect on training and so provide an independent measure of network performance during and after training.
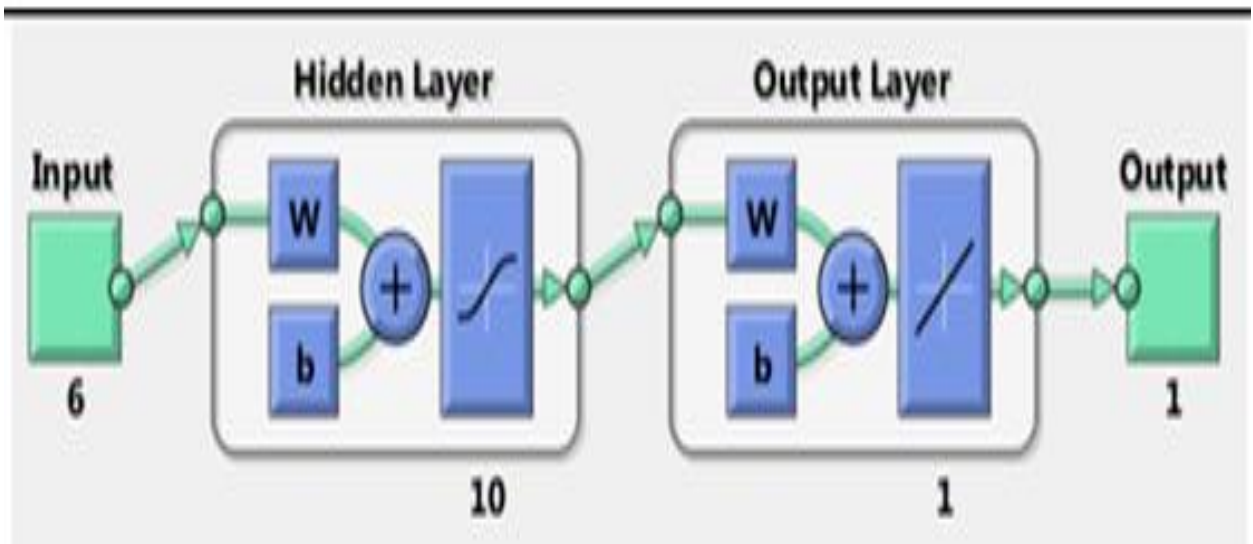
Fig 4.136 Flow diagram of the ANN network

The ANN model was evaluated for the network performance with different hidden neurons of 5, 10, 15 and 20 to define a fitting neural network model architecture.

Mean Square Error (MSE) is the average squared difference   between outputs and targets. Lower values are better. Zero means no error. Regression values (R) measures

the correlation between outputs and inputs. An R-value of 1 means a close relationship, 0 a random relationship. A close observation of the values revealed that the best performance was given by the network architecture of 20 hidden neurons for both PVDP and HADP.

After the selection of the hidden number of neurons, a number of trainings runs were performed to look out for the best possible weights in error back propagation framework and the final selected network architecture was trained for 10 iterations. The mean square error of the best trained networks were 0.0118 and 16.917 for PVDP and HADP respectively while the regression coefficients were 0.9998 and 0.9755 for PVDC and HADC respectively of the training.

4.20.2 Post-Training Analysis (Network Validation)

After the training, the network was analyzed to check the network performance and to determine if any changes needed to be made to the training process, the network architecture or the data sets. Figure 4.137 and 138 shows the plot of the training errors, validation errors, and testing errors.
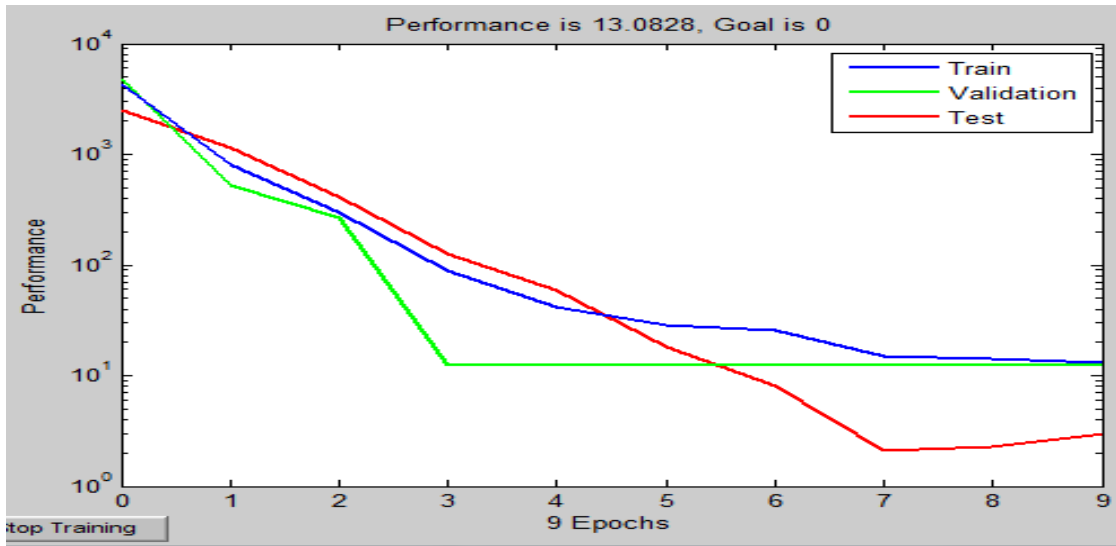
Figure 4.137: Plot of the network validation performance for PVDP
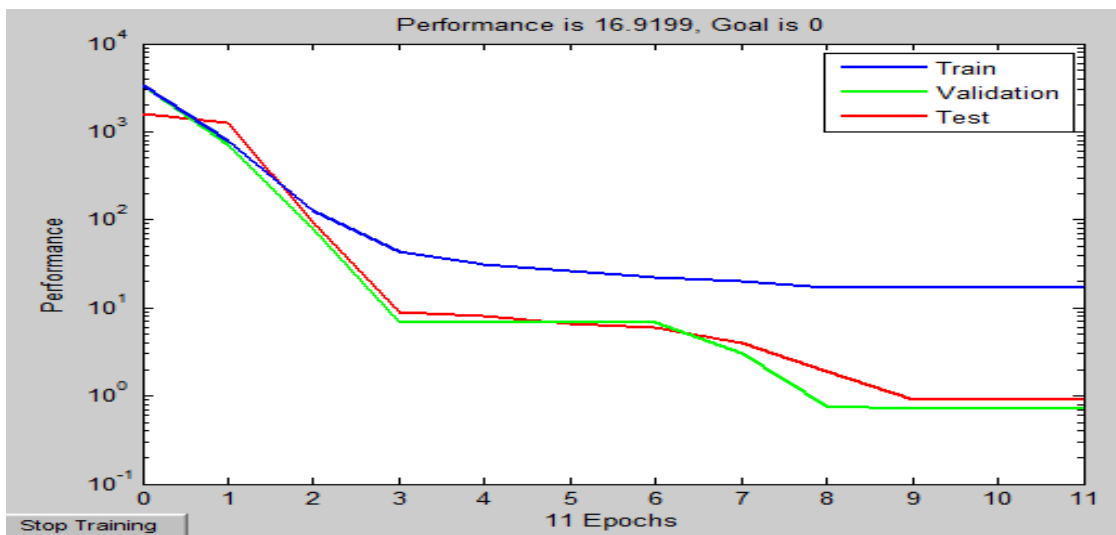
Figure 4.138: Plot of the network validation performance for HADP

The best training performance shows a training error of about 13.08 at Epoch 7 when the validation and testing error are at 3 and 7 respectively for PVDP. For HADP, the best training performance was at 16.92 at epoch 3. The validation and the test curves are similar with performance at 8 and 9 respectively.

The result is valid because of the following:

a) The final mean-square error is small.

b) The test set error and the validation set error has similar characteristics.

c) No significant overfitting has occurred by epoch 9 and 11 respectively for PVDP and HADP (where the validation performance occurs).

The figure does not indicate any major problems with the training. If the test curve had increased significantly before the validation curve increased, then it could be possible that some over fitting might have occurred.
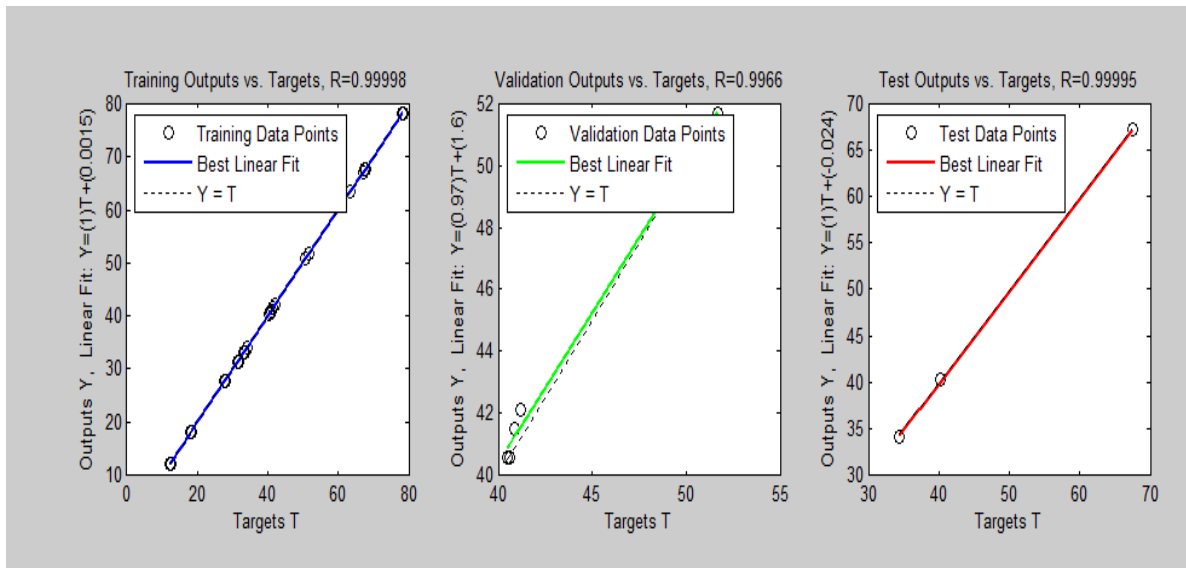
Figure 4.139 Regression plots showing outputs vs targets for training, validation and test of PVDP
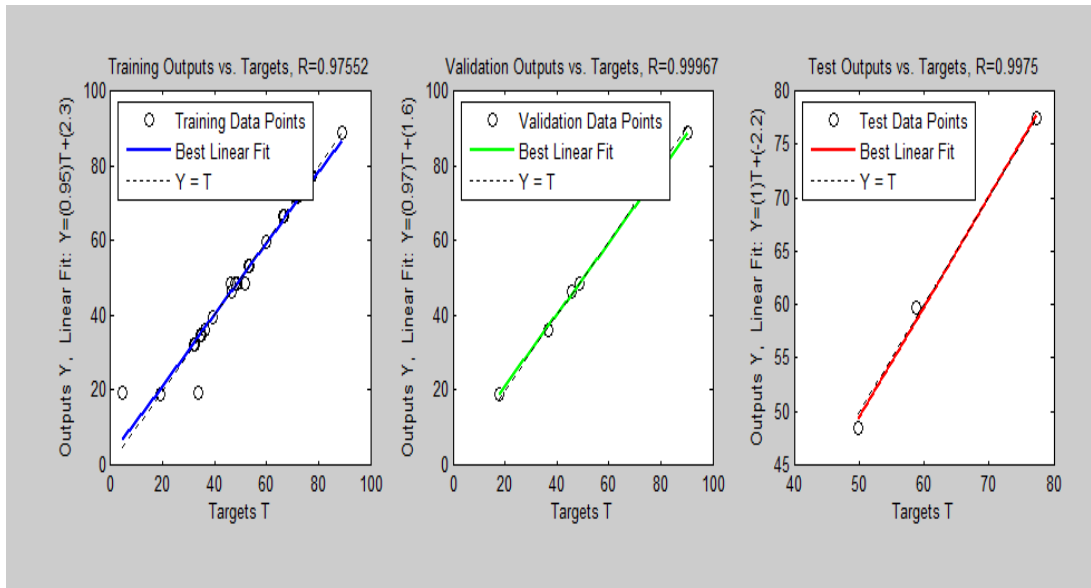
Figure 4.140 Regression plots showing outputs vs targets for training, validation and test of HADP

The regression plots in figure 4.139 and 4.140 displays the network outputs with respect to targets for training, validation, and test sets. The data fall reasonably along a 45 degree line, where the network outputs are equal to the targets. For this process, the fit is reasonably good for all data sets, with R values in each case were very close to unity.

4.20.3 Test of the network (Network evaluation) for PVDP and HADP

The MSE (PVDP = 0.0012; HADP = 16.917) and the R (PVDP = 0.9998; HADP = 0.9755) values are good, showing that the performance on the training set is good. But if the test performance was significantly worse, which could indicate over fitting, reducing

the number of neurons can improve the result. If training performance is poor, then the number of neurons will be increased.

The Network test/evaluation shows the output tracks the target very well for training, testing, and validation and the R-value is over 0.9000 for the responses. The output tracks the target very well since the R values and the MSE values show good network performance. Based on these performance values a satisfactory network response can be concluded. The model generated sets of output equation that relates the target to the output for training, testing, validation and the overall model output equation.

4.20.4 Comparison of RSM and ANN for the drying of potato

In order to establish the superiority of either of the models generated by the CCD and ANN, a couple of techniques are applied. These include;

1) Absolute Average Deviation (AAD) observed for both models;

2) Coefficient of determination for both models.

The AAD observed for both models give an indications of how accurate the model predictions can be. (Josh *et al.,* 2014).

$$\text{AAD (\%)} = \left(\frac{1}{n}\sum_{i=1}^{n}\left\{\frac{(R_{art.pred} - R_{art.exp})}{R_{art.exp}}\right\}\right) x \ 100 \qquad (4.16)$$

where n is the number of sample points, $R_{art,pred}$ is the predicted moisture content and $R_{art,exp}$ is the experimentally determined moisture content. (Josh *et al.,* 2014).
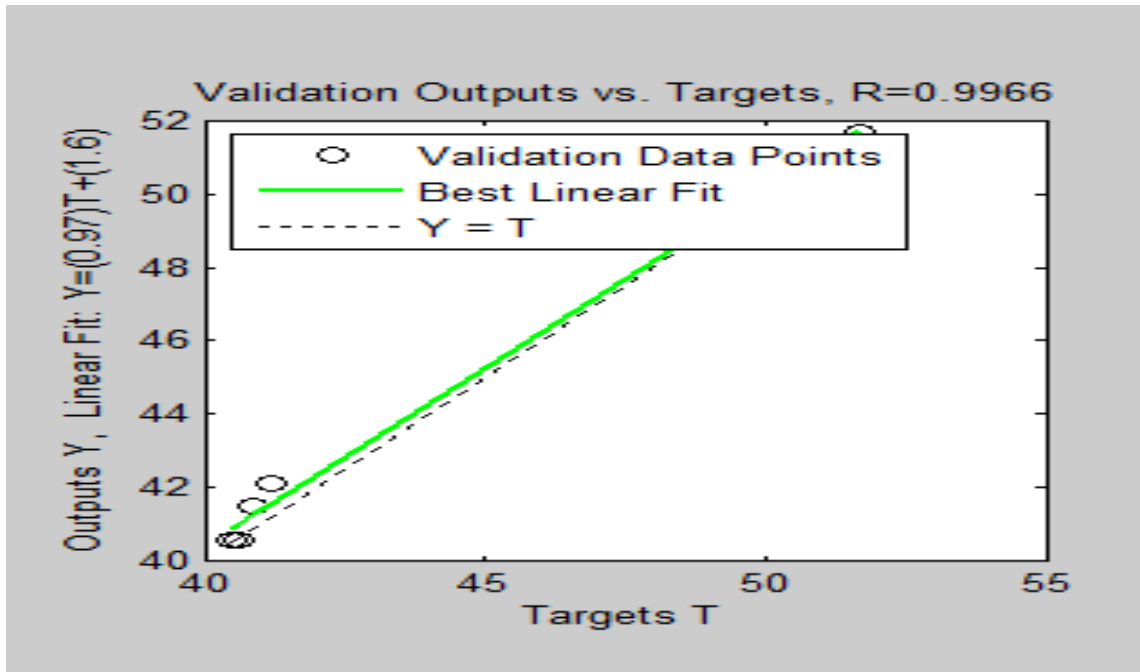
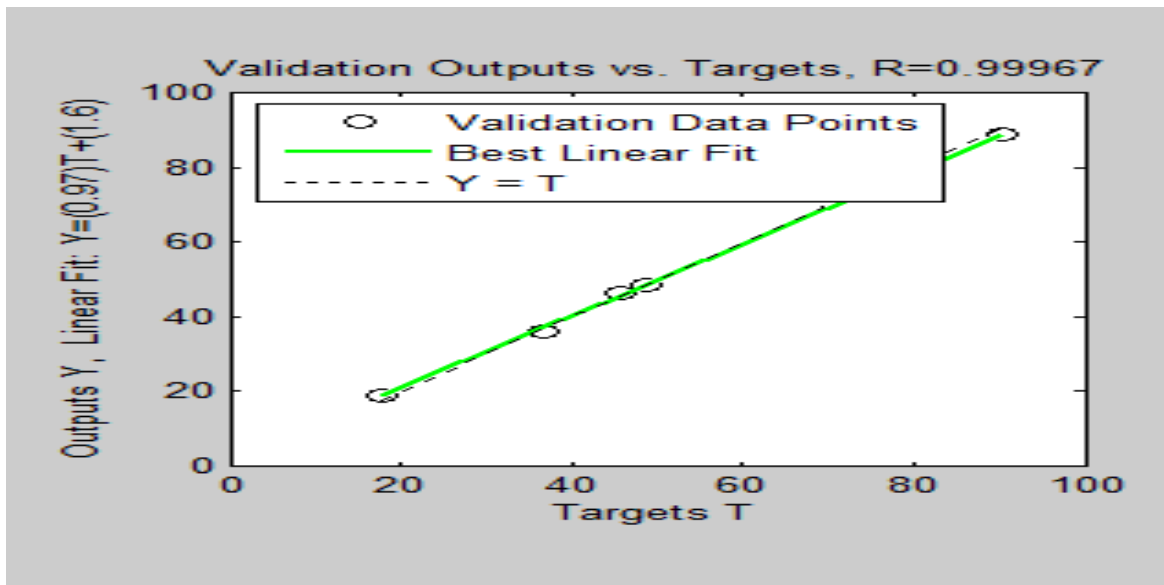Figure 4.141   Plot Validation output vs. Actual output for PVDP

Figure 4.142   Plot Validation output vs. Actual output for HADP

From Fig. 4.141 and 4.142, the linear fit model generated by validation outputs vs target plots are

For both PVDP and HADP,

$$Y = (0.97)T + (1.6) \qquad\qquad (4.17)$$

Where Y = the ANN model value,

T (Target) = the experimental value used to generate the corresponding ANN value.

These are used to predict the ANN model values.

These values are tabulated on Table 4.60 and compared with the values generated by the CCD. The graph of the correlation between the experimental values and the predicted values by CCD and ANN are shown on Fig. 4.143 and 4.144.

Table 4.50 Table of Comparison of model prediction

PVDP			HADP		
Experimental Value	**CCD**	**ANN**	**Experimental Value**	**CCD**	**ANN**
67.8	66.25071	67.366	90.40195	88.13028	89.28989
67.5	66.25071	67.075	88.85397	88.13028	87.78835
31.6	30.24716	32.252	39.31836	40.91437	39.73881
31.3	30.24716	31.961	39.31836	40.91437	39.73881
42.1	43.98716	42.437	71.20691	71.01973	70.6707
41.1	43.98716	41.467	71.8261	71.01973	71.27132
12.1	9.841201	13.337	32.19762	31.54377	32.83169
12.4	9.841201	13.628	31.88802	31.54377	32.53138
67.5	68.58434	67.075	66.87254	66.84257	66.46636
67.2	68.58434	66.784	66.25335	66.84257	65.86575
40.9	37.68916	41.273	33.74561	34.48734	34.33324
41.5	37.68916	41.855	34.6744	34.48734	35.23417
63.5	63.50345	63.195	45.51031	44.15927	45.745

63.5	63.50345	63.195	46.43911	44.15927	46.64594
34.1	34.46586	34.677	18.88493	19.54398	19.91838
34.4	34.46586	34.968	17.64654	19.54398	18.71714
78.3	76.29441	77.551	77.39886	80.00119	76.67689
78	76.29441	77.26	77.39886	80.00119	76.67689
18.3	21.60155	19.351	34.984	32.73361	35.53448
17.9	21.60155	18.963	34.6744	32.73361	35.23417
51.7	54.01372	51.749	58.82301	58.7094	58.65832
51.7	54.01372	51.749	59.7518	58.7094	59.55925
33.4	32.58192	33.998	36.22239	37.61674	36.73572
33.1	32.58192	33.707	36.84158	37.61674	37.33633
27.9	28.71249	28.663	53.55985	53.85211	53.55305
27.6	28.71249	28.372	52.94065	53.85211	52.95243
50.8	51.38161	50.876	31.88802	31.94771	32.53138
50.8	51.38161	50.876	32.19762	31.94771	32.83169
40.9	40.41295	41.273	48.60629	48.54691	48.7481
40.2	40.41295	40.594	46.12951	48.54691	46.34562
40.5	40.41295	40.885	51.70226	48.54691	51.75119
40.6	40.41295	40.982	49.84468	48.54691	49.94934
40.6	40.41295	40.982	47.6775	48.54691	47.84718
40.2	40.41295	40.594	48.60629	48.54691	48.7481

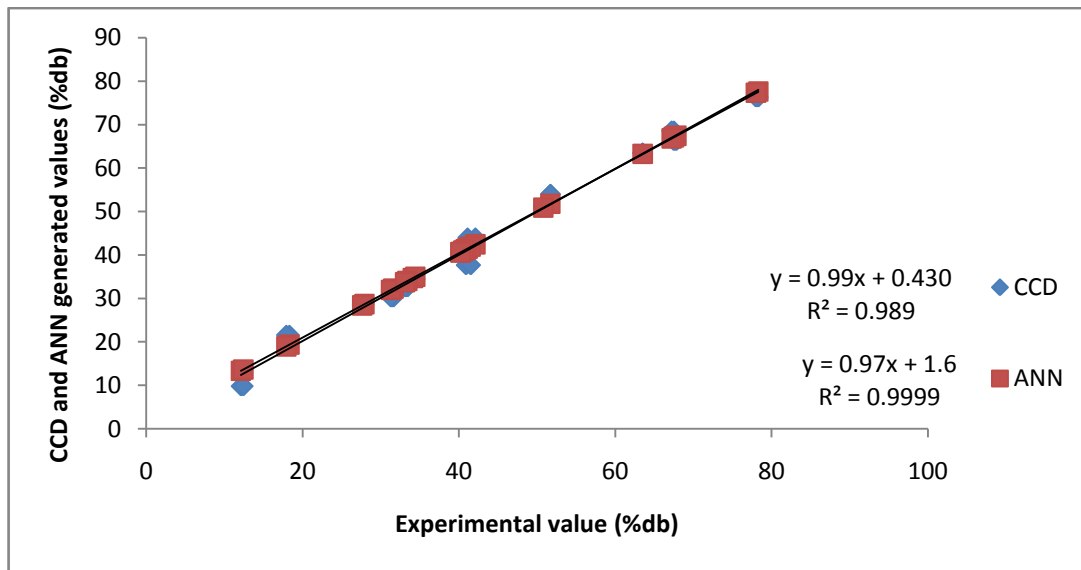y = 0.99x + 0.430
R² = 0.989

y = 0.97x + 1.6
R² = 0.9999

Figure 4.143 Interactive plot for RSM and ANN model appraisal of PVDP
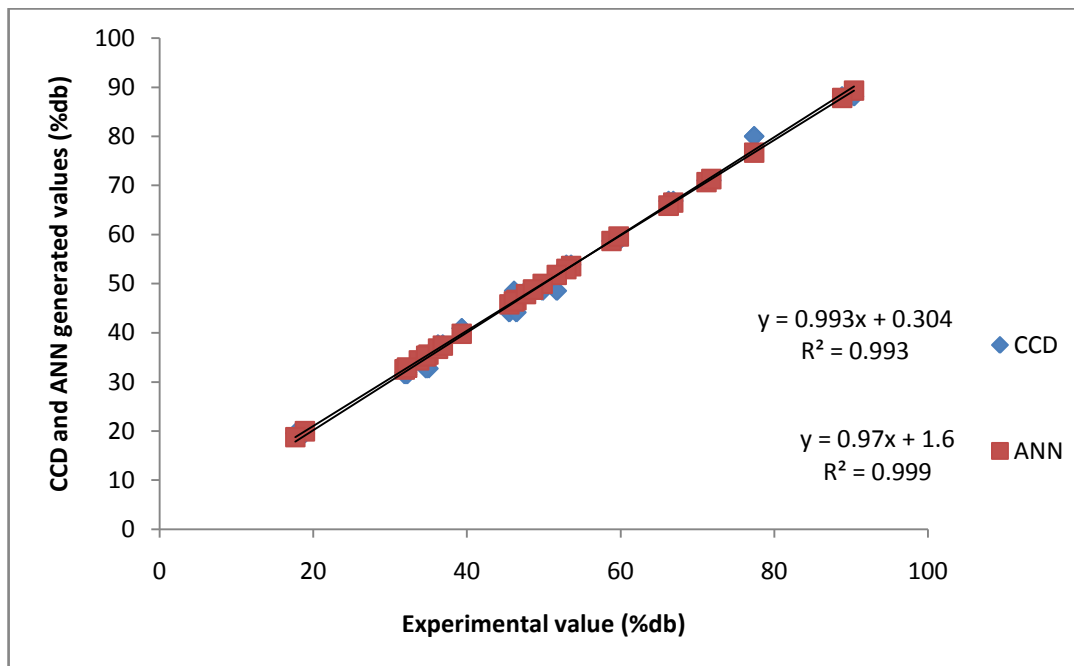

Figure 4.144 Interactive plot for RSM and ANN model appraisal of HADP

From the graphs on figure 4.143 and 4.144, it is observed that the correlation coefficient for the ANN model is close to unity, while that for the CCD is 0.989 (for PVDC) and 0.993 (for HADC). These values are a measure of how close the predicted value of the response is to the actual experimental values. The R^2 values of ANN being greater than CCD is as expected since the CCD model was generated using quadratic model.

The AAD analysis revealed that the deviated slightly more from the experimental value than the CCD. The AAD values generated in terms of absolute value for PVDP are 0.527 and 0.0479 for ANN and CCD respectively.

Since the ANN model has a higher R^2, then it could be concluded that the ANN model is accepted to produce a better prediction compared to the CCD model.

From these analyses it is evident that ANN model is superior to the CCD model and therefore the ANN model will be adopted for the optimization of the drying process.

4.21 Optimization of the drying process of cocoyam

These factors were the independent variables while the mass remaining (g) and the moisture content (%db) were the dependent variables or responses. In this work, a set of 34 experiments were performed which consist of 16 core points, 12 star like points and 6 centre points or null points. This is because the replicates of factorial points and the replicates of axial (star) points were two to increase the accuracy of the experiment. The design matrix and output responses for the drying processes were given in Tables 4.51 and 4.52. The responses obtained from various runs are significantly exceptional which implies that each of the factors have substantial effect on the response.

Table 4.51: Optimization Results for the drying of PVDC

Run Order	Time (mins)	Air Speed (m/s)	Slice thickness (mm)	Mass (g)	Moisture Content (%db)
1	80.0	1.00	2.00	52.4	104.69
2	80.0	1.00	2.00	52.7	105.86
3	180.0	1.00	2.00	40.2	57.03
4	180.0	1.00	2.00	40.2	57.03
5	80.0	3.00	2.00	43.3	69.14
6	80.0	3.00	2.00	43.1	68.36
7	180.0	3.00	2.00	31	21.09
8	180.0	3.00	2.00	31.1	21.48
9	80.0	1.00	4.00	53.3	106.30
10	80.0	1.00	4.00	53.1	106.02
11	180.0	1.00	4.00	42.9	67.58
12	180.0	1.00	4.00	42.8	67.19
13	80.0	3.00	4.00	51.8	102.34
14	80.0	3.00	4.00	51.9	102.73
15	180.0	3.00	4.00	41.3	61.33
16	180.0	3.00	4.00	41.5	62.11
17	64.2	2.00	3.00	55	114.84
18	64.0	2.00	3.00	55.2	115.63
19	195.8	2.00	3.00	36.5	42.58
20	195.8	2.00	3.00	36.8	42.97
21	130.0	0.68	3.00	47.8	86.71
22	130.0	0.68	3.00	47.7	86.33
23	130.0	3.32	3.00	41.6	62.50
24	130.0	3.32	3.00	41.4	61.72
25	130.0	2.00	1.68	39.2	53.13
26	130.0	2.00	1.68	39.9	55.86
27	130.0	2.00	4.32	46.3	80.86
28	130.0	2.00	4.32	46.2	80.47
29	130.0	2.00	3.00	42.5	66.01
30	130.0	2.00	3.00	42.6	66.41
31	130.0	2.00	3.00	42.6	65.63
32	130.0	2.00	3.00	42.4	65.63
33	130.0	2.00	3.00	42.4	65.63
34	130.0	2.00	3.00	42.5	66.02

Table 4.52: Optimization Results for the drying of HADC

Run Order	Time (mins)	Air Speed (m/s)	Temperature (^oC)	Mass (g)	Moisture Content (%db)
1	60.0	1.00	50.0	57.3	122.656
2	60.0	1.00	50.0	57.8	122.656
3	180.0	1.00	50.0	42	64.0625
4	180.0	1.00	50.0	41.6	64.0625
5	60.0	3.50	50.0	50.8	99.2188
6	60.0	3.50	50.0	51.3	99.2188
7	180.0	3.50	50.0	38.5	48.4375
8	180.0	3.50	50.0	38.5	48.4375
9	60.0	1.00	90.0	48.8	91.4063
10	60.0	1.00	90.0	49.3	91.4063
11	180.0	1.00	90.0	38.5	48.4375
12	180.0	1.00	90.0	38.6	48.4375
13	60.0	3.50	90.0	43.4	67.9688
14	60.0	3.50	90.0	43.8	67.9688
15	180.0	3.50	90.0	34.7	36.7187
16	180.0	3.50	90.0	35.3	36.7187
17	41.0	2.50	70.0	53.7	107.031
18	41.0	2.50	70.0	53.2	107.031
19	198.9	2.50	70.0	39.4	52.3438
20	198.9	2.50	70.0	39.4	52.3438
21	120.0	0.60	70.0	47.4	83.5938
22	120.0	0.60	70.0	46.8	83.5938
23	120.0	3.90	70.0	41	60.1563
24	120.0	3.90	70.0	41.6	60.1563
25	120.0	2.25	43.7	45.9	79.6875
26	120.0	2.25	43.7	46.3	79.6875
27	120.0	2.25	96.3	38	48.4375
28	120.0	2.25	96.3	38.3	48.4375
29	120.0	2.25	70.0	44.2	71.875
30	120.0	2.25	70.0	44.7	67.9688
31	120.0	2.25	70.0	44.4	67.9688
32	120.0	2.25	70.0	44.4	67.9688
33	120.0	2.25	70.0	44.2	71.875
34	120.0	2.25	70.0	44.5	67.9688

4.21.1 Analysis of Variance

The Analysis of Variance (ANOVA) was used to interpret the Central Composite Design. The summary of P-values indicates that a quadratic model fitted the ANOVA analysis and hence it was suggested. The linear and 2FI models were not suggested. The Cubic model is always aliased because the CCD does not contain enough runs to support a full cubic model. A significance level of 95% was used hence all terms whose P-value are less than 0.05 are considered significant. The model summary test and the lack of fit test for the drying process were also presented in Tables 4.62 to 4.67.

4.21.2 Model Fitting of RSM for PVDC and HADC

The F-value tests were performed using the ANOVA to calculate the significance of each type of model. Based on the results of F-value, the highest order model with significant terms which shows the most accurate relationship between parameters would be chosen. The Sequential Model Sum of squares of PVDC, the Linear vs Mean, the Quadratic vs 2FI and the Quadratic vs 2FI models have significant F-value of 90.74, 14.02 and 13.99 respectively while the Cubic vs Quadratic models have 9.74 which relatively is not significant. Equally, for HADC, the F-value of the Quadratic vs 2FI was 77.0.

Besides evaluating the significance, the adequacy of the models was evaluated by applying the lack-of-fit test. This test is used in the numerator in an F-test of the null hypothesis and indicates that a proposed model fits well or not. The test for lack-of-fit compares the variation around the model with pure variation within replicated

observations. This test measured the adequacy of the different models based on response surface analysis (Lee *et al.,* 2006, Pishgar *et al.,* 2012). There was significant difference for PVDC in the F-value of the models (Linear = 470.22, 2FI = 251.28, Quadratic = 143.85 and Cubic = 231.38). It is equally seen that for HADC, the lack of fit was 6.41. Hence, the Quadratic model with the lowest insignificant model of lack of fit is suggested. The high significant results of lack of fit for linear, cubic and 2FI models showed that these models are not adequate to use.

The closer the R^2 value is to unity, the better the model predicts the response. Adjusted-R^2 is a measure of the amount of variation around the mean explained by the model, adjusted for the number of terms in the model.

The coefficient of regression R^2 was used to validate the fitness of the model equation. For PVDC, the R^2 has a high value of 0.9859 showing that 98.59% of the variability in the response can be explained by the model while for HADC, the R^2 has a value of 0.9665 showing that 96.65% of the variability in the response can be explained by the model. This implies that the prediction of experimental data is quite satisfactory.

The adjusted-R^2 decreases as the number of terms in the model increases, if those additional terms don't add value to the model. Predicted-R^2 is a measure of the amount of variation in new data explained by the model. The adjusted R^2 (PVDC = 0.9806; HADC = 0.9540) is in close agreement with the predicted R^2 (PVDC = 0.9714; HADC = 0.9298). The predicted-R^2 and the adjusted-R^2 should be within 0.20 of each other. Otherwise there may be a problem with either the data or the model, Taran and Aghaie (2015).

Table 4.53   ANOVA Table for PVDC

Source	Sum of Squares	df	Mean Square	F Value	p-value Prob> F
Model	18770.67		2085.63	186.23	< 0.0001
A-Time	12568.69		12568.69	1122.30	< 0.0001
B-Air Speed	2166.08		2166.08	193.42	< 0.0001
C-Slice Thickness	2414.65		2414.65	215.61	< 0.0001
AB	3.09		3.09	0.28	0.6042
AC	84.27		84.27	7.52	0.0113
BC	1063.88		1063.88	95.00	< 0.0001
A^2	357.26		357.26	31.90	< 0.0001
B^2	87.15		87.15	7.78	0.0102
C^2	19.50		19.50	1.74	0.1995
Residual	268.78		11.20		

		4			
Lack of Fit	261.86	.	52.37	143.85	< 0.0001
Pure Error	6.92	9	0.36		
Cor Total	19039. 45	. 3			

Std. Dev. = 3.35;   Mean = 72.20;   C.V. = 4.64%;   PRESS = 544.70

R-Squared = 0.9859   Adj R-Sq = 0.9806;   Pred R-Sq = 0.9714;   Adeq Precision = 48.274

Table 4.54   ANOVA Table for HADC

Source	Sum of Squares	f	Mean Square	F Value	p-value Prob> F
Model	17247.02		17247.02	841.61	< 0.0001
A-Time	11394.57		11394.57	5004.24	< 0.0001
B-Air Speed	1925.75		1925.75	845.75	< 0.0001
C-Temperature	2992.54		2992.54	1314.26	< 0.0001
AB	95.37		95.37	41.88	< 0.0001
AC	308.99		308.99	135.70	< 0.0001
BC	3.81		3.81	1.68	0.2079
A^2	374.01		374.01	164.26	< 0.0001
B^2	11.53		11.53	5.07	0.0338
C^2	157.43		157.43	69.14	<

					0.0001
Residual	54.65	4	2.28		
Lack of Fit	34.30		6.86	6.41	0.0012
Pure Error	20.35	9	1.07		
Cor Total	17301. 67	3			

Std. Dev. = 1.51;   Mean = 71.65;   C.V. = 2.11%;   PRESS = 99.02

R-Squared = 0.9968   Adj R-Sq = 0.9957;   Pred R-Sq = 0.9943;   Adeq Precision = 104.80

The ANOVA tables were given in Tables 4.53 and 4.54. A significance level of 5% (0.05) was used hence all terms whose P-value are less than 0.05 are considered

significant. From the Tables 4.53 and 4.54, the regression F-values of 186.23 (PVDC) and 841.61 (HADC) implies that the model is significant which was validated by the P-values being less than 0.0001. There is only a 0.01% chance that a "Model F-Value" this large could occur due to noise. The tests for adequacy of the regression models, significance of individual of model coefficients and the lack of fit test were performed using the same statistical package. The P-values were used as a tool to check the significance of each of the coefficients, which in turn are necessary to understand the pattern of the mutual interactions between the test variables (Shrivastava et al, 2008). The larger the magnitude of F-test value and the smaller the magnitude of P-values, the higher the significance of the corresponding coefficient (Alam et al, 2008).

The adequate precision measures the signal to noise ratio and compares the range of the predicted value at the design points to the average prediction error. The adquate predicion ratio above 4 indicates adequate model efficacy (Kumar et al, 2007). Hence, the adquate precision ratios of 48.278 (PVDC) and 104.80 (HADC) indicates adquate signal. This indicates that an adequate relationship of signal to noise ratio exists. Also, a PRESS value of 544.70 (PVDC) and 99.02 (HADC) indicates an adquate signal implying that the models can be used to navigate the design space.

The C.V called coefficient of variation which is defined as the ratio of the standard deviation of estimate to the mean value of the observed response is independent of the unit. It is also a measure of reproducibility and repeatability of the models (Chen *et al.,* 2010; Chen *et al.,* 2011). The calculations indicated the C.V value of 4.64% (PVDC)

and 2.11% (HADC) which illustrated that the models can be considered reasonably reproducible because their CV was not greater than 10%. (Chen et al., 2011).

The quadratic model equations generated for the PVDC and HADC in terms of actual factors are:

$(M.C)_{PVDC}$ = +217.18970 - 1.14451 * Time -43.60440 * Air Speed - 4.51766* Slice Thickness - 8.78906E-003 * Time * Air Speed +0.045898 * Time * Slice Thickness + 8.15430 * Air Speed * Slice Thickness + 2.13897E-003 * Time^2 + 2.64110 * Air Speed^2 - 1.24925 * Slice Thickness^2 (4.18)

$(MC)_{HADC}$ = +194.90998 - 1.06589 * Time - 15.37227 * Air Speed + 0.18779 * Temperature + 0.032552 * Time * Air Speed + 3.66211E-003 * Time * Temperature + 0.019531 * Air Speed * Temperature + 1.51982E-003 * Time^2 + 0.61492 * Air Speed^2 -8.87435E-003 * Temperature^2 (4.19)

In terms of coded factors

$(MC)_{PVDC}$ = +67.65 -23.41 * A - 9.72 * B +10.26 * C - 0.44 * A * B +2.29 * A * C +8.15 * B * C +5.35 * A^2 + 2.64 * B^2 - 1.25 * C^2 (4.20)

$(MC)_{HADC}$ = + 69.70 - 22.29 * A - 9.16 * B - 11.42 * C + 2.44 * A * B + 4.39 * A * C + 0.49 * B * C + 5.47 * A^2 + 0.96 * B^2 - 3.55 * C^2 (4.21)

The equation in terms of coded factors can be used to make predictions about the response for given levels of each factor. By default, the high levels of the factors are coded as +1 and the low levels of the factors are coded as -1. The coded equation is useful for identifying the relative impact of the factors by comparing the factor coefficients, while the equation in terms of actual factors can be used to make predictions about the response for given levels of each factor. Here, the levels are to be specified in the original units for each factor.

In a regression equation, when an independent variable has a positive sign, it means that an increase in the variable will cause an increase in the response while a negative sign will result in a decrease in the response (Kumur et al, 2008).

Values of P less than 0.05 indicate the model terms are significant. For PVDC, among the test variables used in the study, A*B and C^2 are insignificant model terms while for HADC, only B^2 is insignificant. Therefore, eliminating the insignificant terms, the final model equations becomes as expressed in equations 4.22 to 4.25.

In terms of actual factors are

$(M.C)_{PVDC}$ = +217.18970 - 1.14451 * Time - 43.60440 * Air Speed - 4.51766* Slice Thickness + 0.045898 * Time * Slice Thickness + 8.15430 * Air Speed * Slice Thickness +2.13897E-003 * $Time^2$ + 2.64110 * Air $Speed^2$ (4.22)

$(MC)_{HADC}$ = +194.90998 - 1.06589 * Time - 15.37227 * Air Speed + 0.18779 * Temperature + 0.032552 * Time * Air Speed + 3.66211E-003 * Time * Temperature

+ 0.019531 * Air Speed * Temperature + 1.51982E-003 * Time^2 - 8.87435E-003

* Temperature^2 (4.23)

In terms of coded factors

$(MC)_{PVDC}$ = +67.65 -23.41 * A - 9.72 * B + 10.26 * C + 2.29 * A * C + 8.15 * B * C

+ 5.35 * A^2 + 2.64 * B^2 (4.24)

$(MC)_{HADC}$ = + 69.70 - 22.29 * A - 9.16 * B - 11.42 * C + 2.44 * A * B + 4.39

* A * C + 0.49 * B * C + 5.47 * A^2 - 3.55 * C^2 (4.25)

The response values obtained by inserting the independent values are the predicted values of the model. These values are compared to the actual experimental values. The result of this comparison is shown in the Table 4.72 and 4.73. From the table, it is seen that there is a close correlation between the actual experimental response and the predicted response. This comfirms the effectiveness of the of the model in describing the drying process.

Table 4.55 Table of Experimental Vs Predicted Responses for PVDC

Run Order	Time (mins)	Air Speed (m/s)	Slice Thickness (mm)	Experimental Value	Predicted Value
1	80.0	1.00	2.00	104.69	107.27
2	80.0	1.00	2.00	105.86	107.27
3	180.0	1.00	2.00	57.03	56.73

4	180.0	1.00	2.00	57.03	56.73
5	80.0	3.00	2.00	69.14	72.40
6	80.0	3.00	2.00	68.36	72.40
7	180.0	3.00	2.00	21.09	20.11
8	180.0	3.00	2.00	21.48	20.11
9	80.0	1.00	4.00	104.30	106.90
10	80.0	1.00	4.00	103.52	106.90
11	180.0	1.00	4.00	67.58	65.54
12	180.0	1.00	4.00	67.19	65.54
13	80.0	3.00	4.00	102.34	104.65
14	80.0	3.00	4.00	102.73	104.65
15	180.0	3.00	4.00	61.33	61.53
16	180.0	3.00	4.00	62.11	61.53
17	64.2	2.00	3.00	114.84	107.73
18	64.0	2.00	3.00	115.63	107.73
19	195.8	2.00	3.00	42.58	464.10
20	195.8	2.00	3.00	42.97	46.10
21	130.0	0.68	3.00	86.71	85.02
22	130.0	0.68	3.00	86.33	85.02
23	130.0	3.32	3.00	62.50	59.54
24	130.0	3.32	3.00	61.72	59.43
25	130.0	2.00	1.68	53.13	51.98
26	130.0	2.00	1.68	55.86	51.98
27	130.0	2.00	4.32	80.86	78.99
28	130.0	2.00	4.32	80.47	78.99
29	130.0	2.00	3.00	66.01	67.65
30	130.0	2.00	3.00	66.41	67.65
31	130.0	2.00	3.00	65.63	67.65
32	130.0	2.00	3.00	65.63	67.65
33	130.0	2.00	3.00	65.63	67.65
34	130.0	2.00	3.00	66.02	67.65

Table 4.56 Table of Experimental Vs Predicted Responses for HADC

Run Order	Time	Air Speed	Tempera ture	Experime ntal Value	Predict ed Value
1	60.0	1.00	50.0	122.656	122.79
2	60.0	1.00	50.0	122.656	122.79
3	180.0	1.00	50.0	64.0625	64.53

4	180.0	1.00	50.0	64.0625	64.53
5	60.0	3.50	50.0	99.2188	98.6
6	60.0	3.50	50.0	99.2188	98.6
7	180.0	3.50	50.0	48.4375	50.11
8	180.0	3.50	50.0	48.4375	50.11
9	60.0	1.00	90.0	91.4063	90.18
10	60.0	1.00	90.0	91.4063	90.18
11	180.0	1.00	90.0	48.4375	49.5
12	180.0	1.00	90.0	48.4375	49.5
13	60.0	3.50	90.0	67.9688	67.94
14	60.0	3.50	90.0	67.9688	67.94
15	180.0	3.50	90.0	36.7187	37.03
16	180.0	3.50	90.0	36.7187	37.03
17	41.0	2.50	70.0	107.031	108.52
18	41.0	2.50	70.0	107.031	108.52
19	198.9	2.50	70.0	52.3438	49.84
20	198.9	2.50	70.0	52.3438	49.84
21	120.0	0.60	70.0	83.5938	83.43
22	120.0	0.60	70.0	83.5938	83.43
23	120.0	3.90	70.0	60.1563	59.3
24	120.0	3.90	70.0	60.1563	59.3
25	120.0	2.25	43.7	79.6875	78.59
26	120.0	2.25	43.7	79.6875	78.59
27	120.0	2.25	96.3	48.4375	48.52
28	120.0	2.25	96.3	48.4375	48.52
29	120.0	2.25	70.0	71.875	69.7
30	120.0	2.25	70.0	67.9688	69.7
31	120.0	2.25	70.0	67.9688	69.7
32	120.0	2.25	70.0	67.9688	69.7
33	120.0	2.25	70.0	71.875	69.7
34	120.0	2.25	70.0	67.9688	69.7

The Normal plot of Residuals and the Predicted vs Actual plots (Figures 4.145 to 4.150) were used to check whether the points will follow a straight line in which we conclude that the residuals follow a normal distribution. It is seen that the points were closely distributed to the striaght line of the plot. This confirms the good relationship between

the experimental values and the predicted values of the response though some small scatter like an "S" shape is always expected. This observation shows that the central composite design is well fitted into the model and thus can be used to perform the optimisation operation for the process.

The diagnostics analysis which is completed by normal probability plots of residuals for investigations are shown on Figure 4.19.2. From the diagram it could be concluded that the residuals followed a normal distribution pattern. The points of the normal distributions are seen to be mostly interlocked with the straight line with a few points lying outside the diagonal line in a moderately scattered manner.

These plots equally confirm that the selected model was adequate in predicting the response variables in the experimental values.
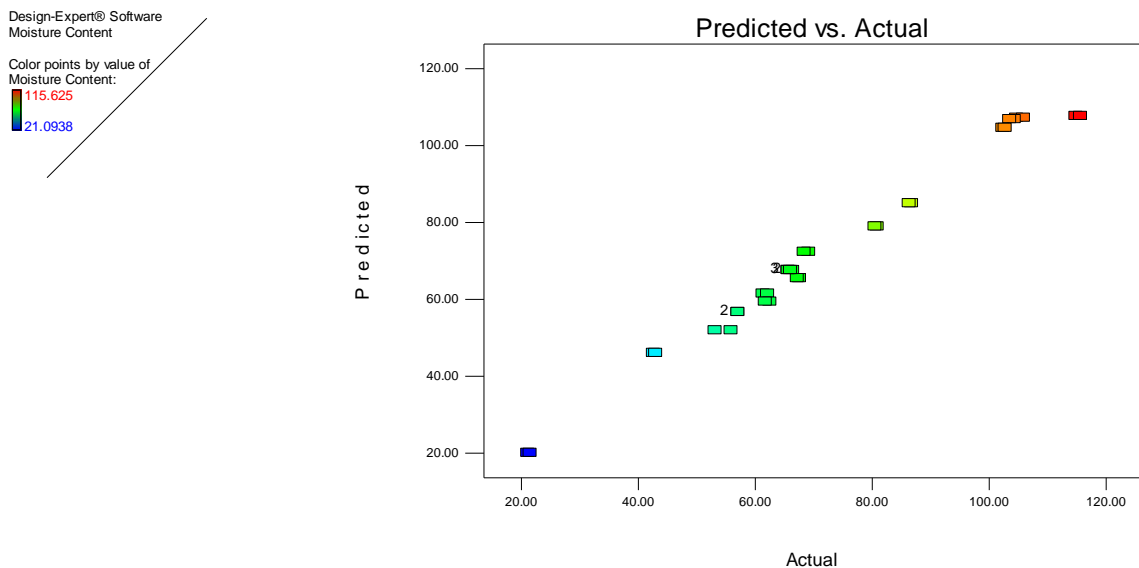
Figure 4.145 Linear correlation between Predicted vs. Actual values for PVDC
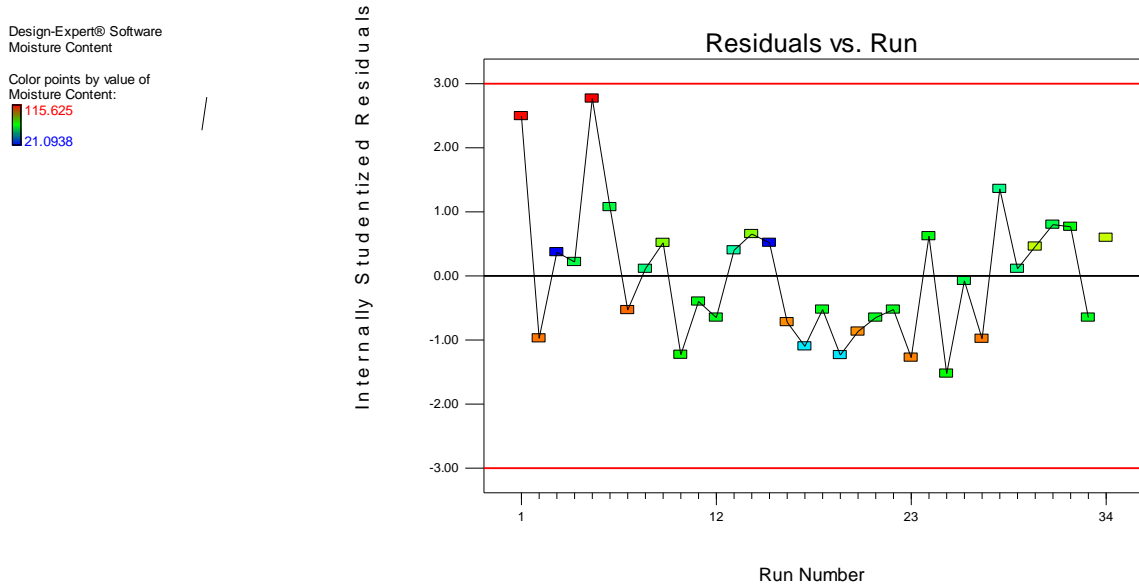
Fig 4.146: Plot of Residuals vs Run order for PVDC
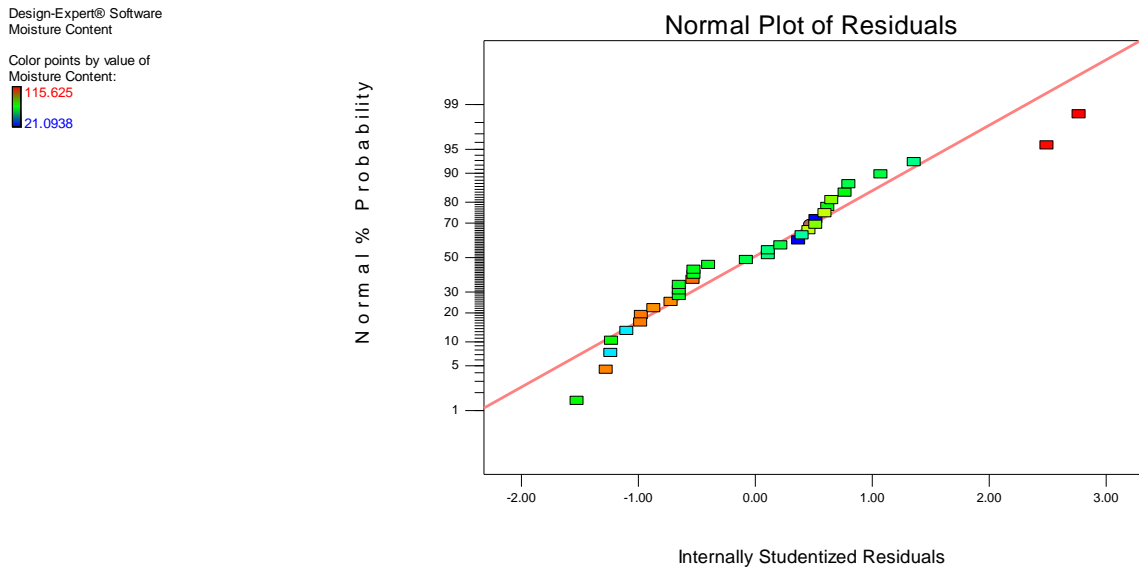
Figure 4.147   Normal probability plots of Residuals obtained from PVDC

Predicted vs. Actual
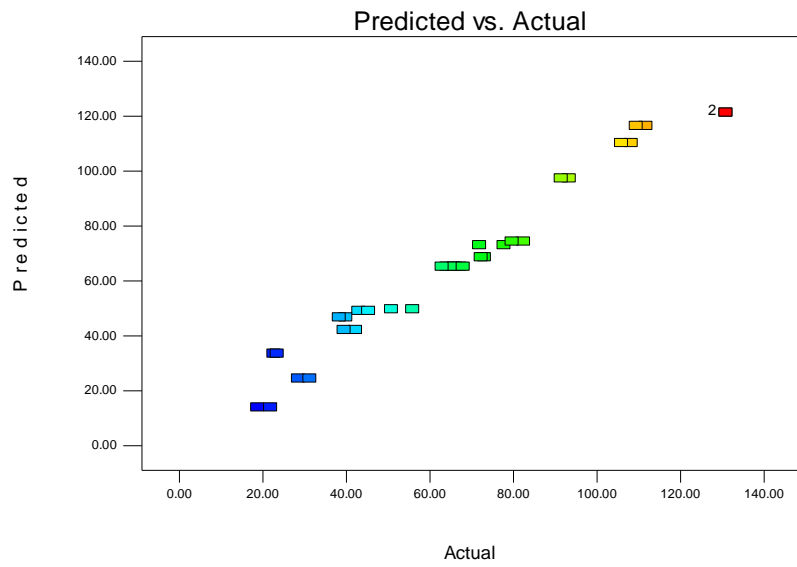
Figure 4.148   Linear correlation between Predicted vs. Actual values for HADC
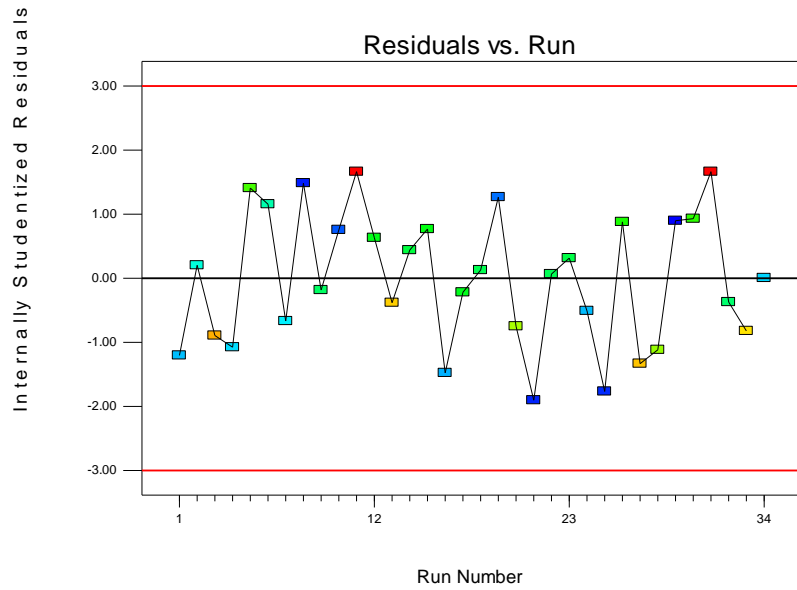
Residuals vs. Run

Fig 4.149:   Plot of Residuals vs Run order for HADC
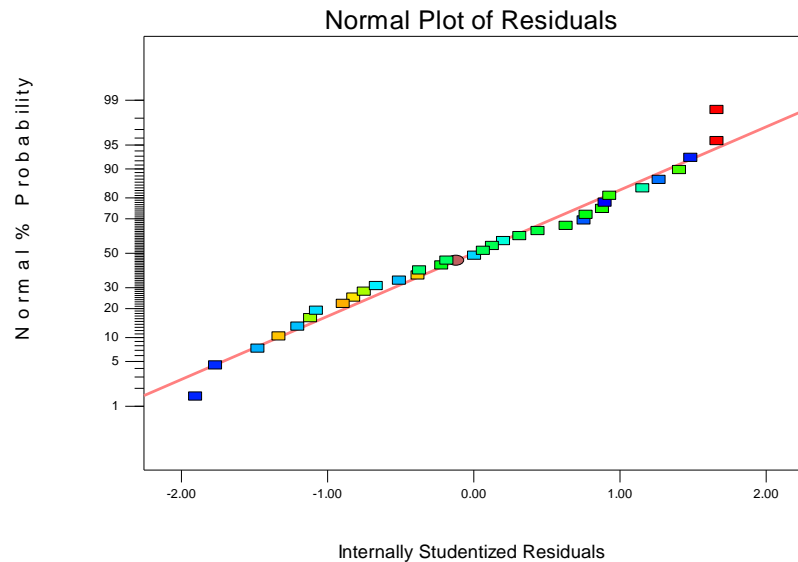
Figure 4.150 Normal probability plots of Residuals obtained from HADC

The Perturbation graph is shown in Fig 4.151 and 152. It shows the deviation from the reference point in terms of coded terms. The reference point of a deviation is the mean. For PVDC, the reference point is at a mointure content of 69% db while for HADC, the reference point is at moisture content of 63%db. From the figures, it is also seen that time has the greatest deviation from the reference point with value of 52%db to 97%db for PVDC and 41%db to 108%db for HADC from 1.00 to -1.00.
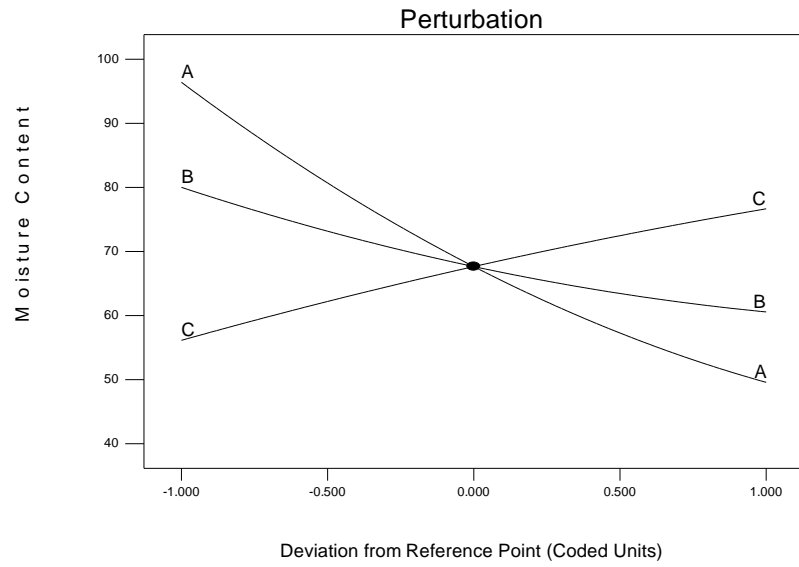
Perturbation

Fig 4.151   Perturbation plot showing deviation from the Reference point for PVDC
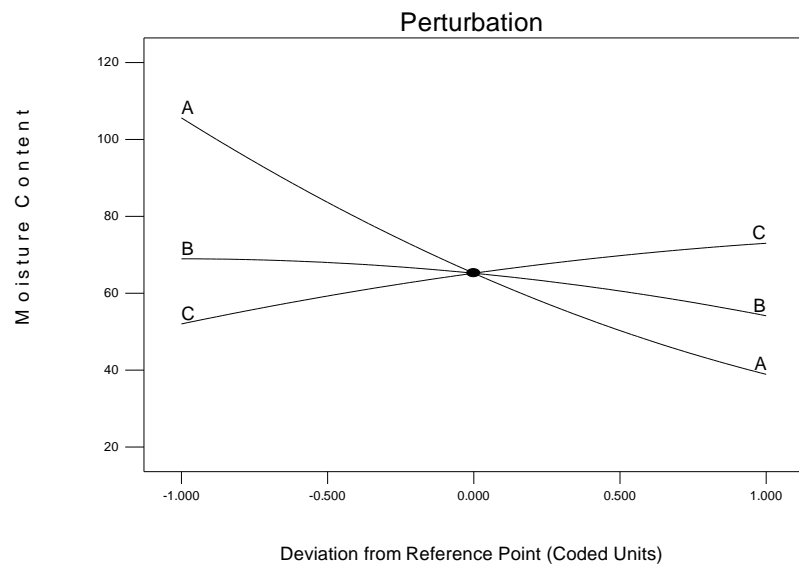
Perturbation

Fig 4.152   Perturbation plot showing deviation from the Reference point for HADC

4.21.3 The Three Dimensional (3-D) response surface plots for PVDC and HADC

The 3-D response surface plots for PVDC and HADC are presented in Figures 4.153 to 4.158. The 3-D response surface plots are graphical representation of the interactive effects of any two variablesthe factors.

Response surface estimation for minimum moisture content plots as a function of two factors at a time maintaining all other factors at fixed levels. These are more helpful in understanding both the main and the interaction effects of these two factors. These plots can be easily obtained by calculating from the model, the values taken by one factor where the second varies with constraint of a given Y value. The response surface curves were plotted to understand the interaction of the variables and to determine the optimum level of each variable for maximum response.

The nature of the response surface curves shows the interaction between the variables. The elliptical shape of the curve indicates good interaction of the two variables and circular shape indicates no interaction between the variables. From figures, it was observed that the elliptical nature of the contour in graphs the mutual depicted interactions of all the variables. There was a relative significant interaction between every two variables, and there was a maximum predicted yield as indicated by the surface confined in the smallest ellipse in the contour diagrams.
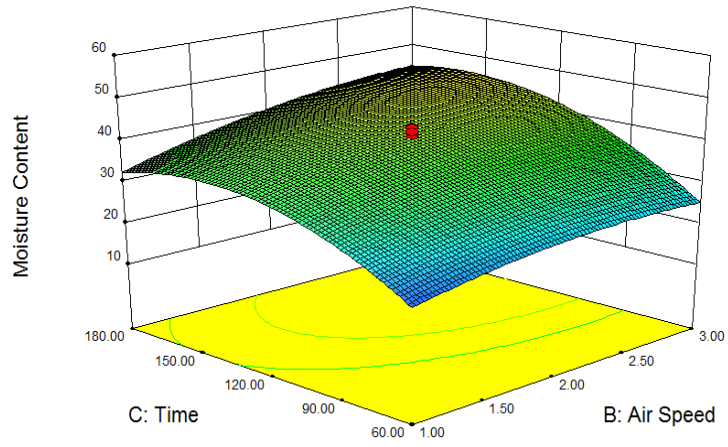
Fig 4.153   3D surface plot showing the combined effects of Time and Air Speed for
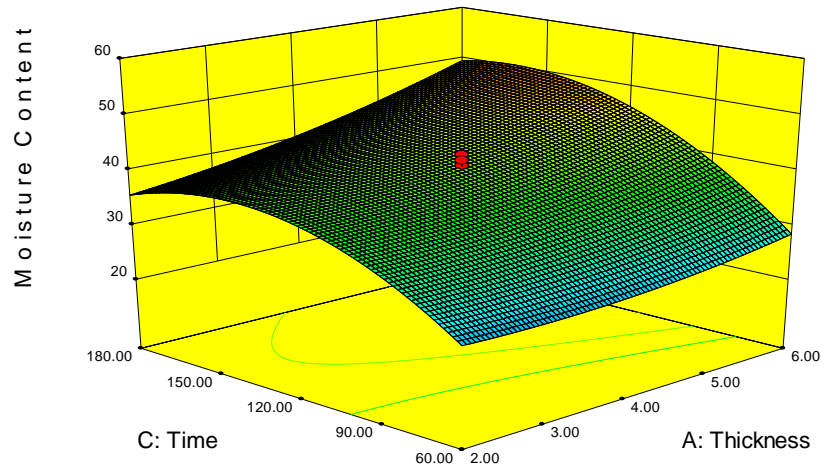
PVDC

Fig 4.154 3D surface plot showing the combined effects of Time and Slice Thickness for PVDC
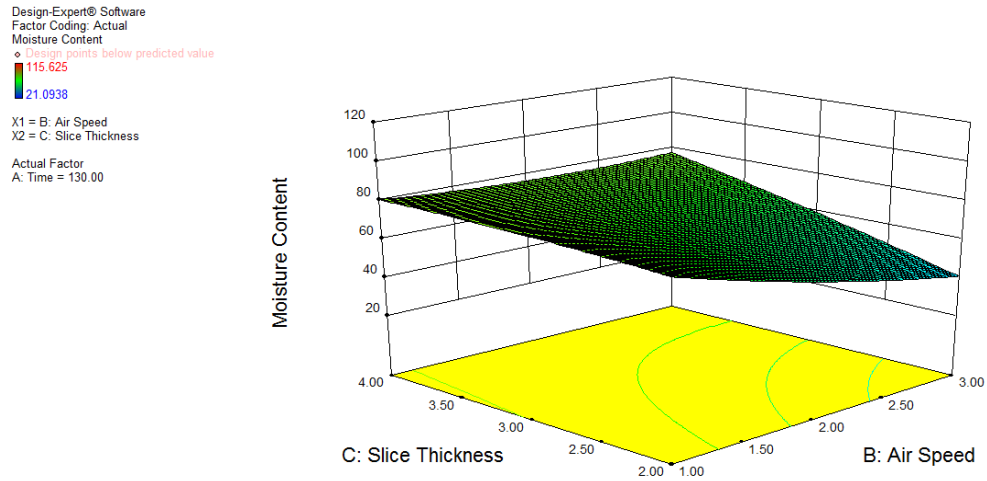

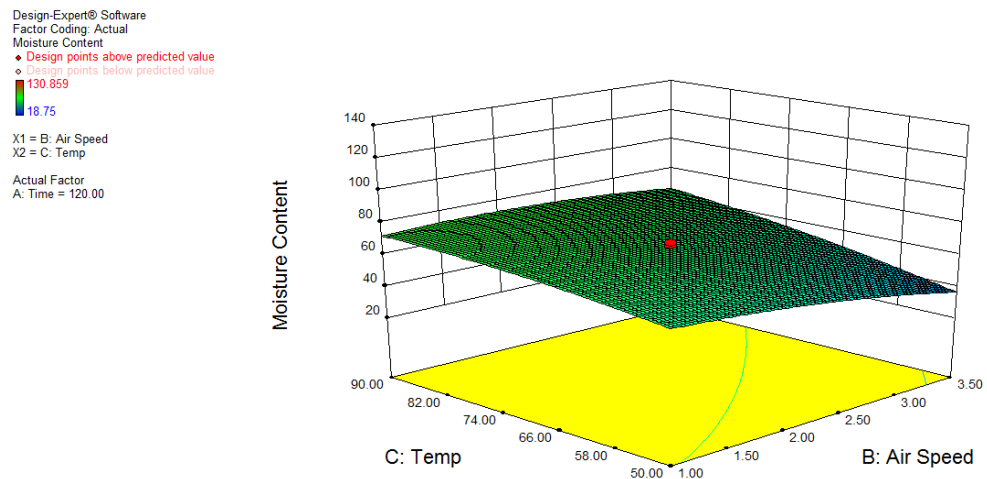Fig 4.155 3D surface plot showing the combined effects of Slice Thickness and Air Speed for PVDC

Fig 4.156 3D surface plot showing the combined effects of Temperature and Air Speed for HADC
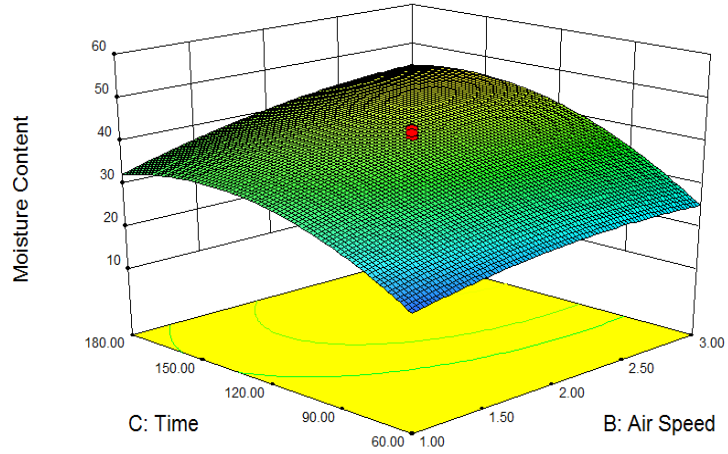
Fig 4.157 3D surface plot showing the combined effects of Time and Air Speed for HADC
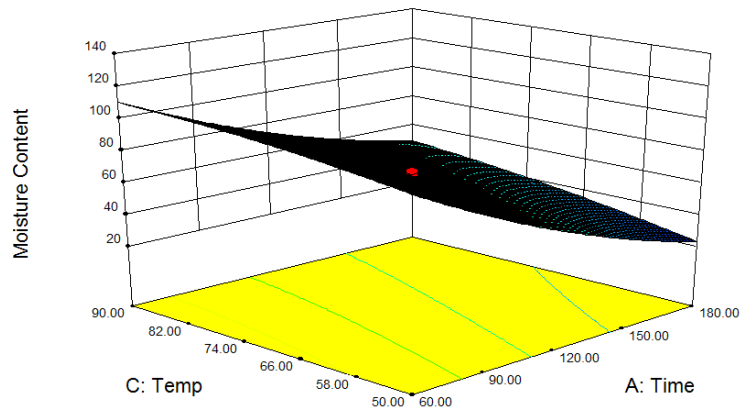
Fig 4.158 3D surface plot showing the combined effects of Time and Temperature for HADC

The 3D surface plots show that the minimum moisture content of 21.09 %db was obtained at a time of 180 minutes, an air speed of 3.0 m/s and slice thickness of 2.0 mm which is in accordance with the model. It is seen that the effect of the air speed decreasing from 3 m/s to 1 m/s is that the moisture content reduced from 80%db to 64%db. As the slice thickness decreased from 4 mm to 2 mm, the moisture content linearly decreased from 80 %db to 56%db. This is because as the slice thickness decreases, the moisture dissipation inside the product and finally its departure from the product would face less resistance (Mohammad et al, 2013). The thicker the slice, the slower the approach to equilibrium moisture content and the slower the drying rate (Etoamaihe and Ibeawuchi, 2010).

Wankhade et al (2012) and Saeed et al (2008) reported that air temperature had a significant effect on the moisture content of samples.
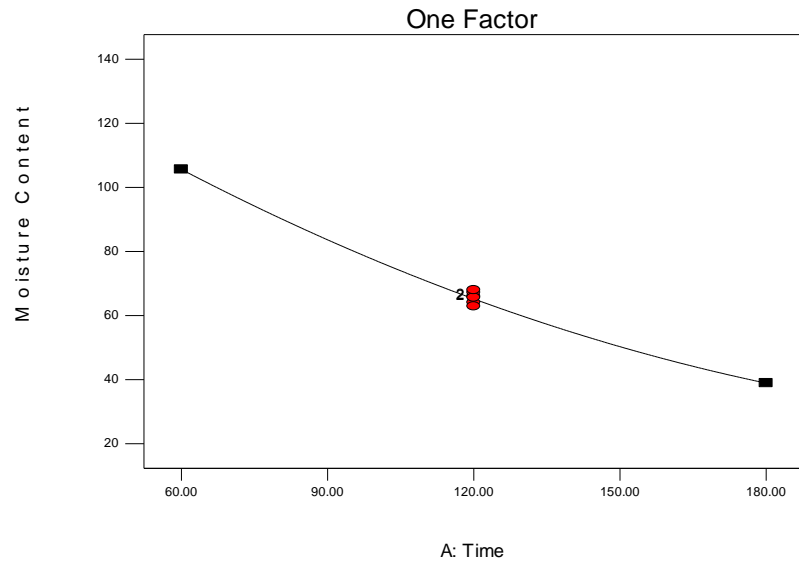
Fig 4. 159   Plots for a one factor at a time of Moisture content and time for PVDC
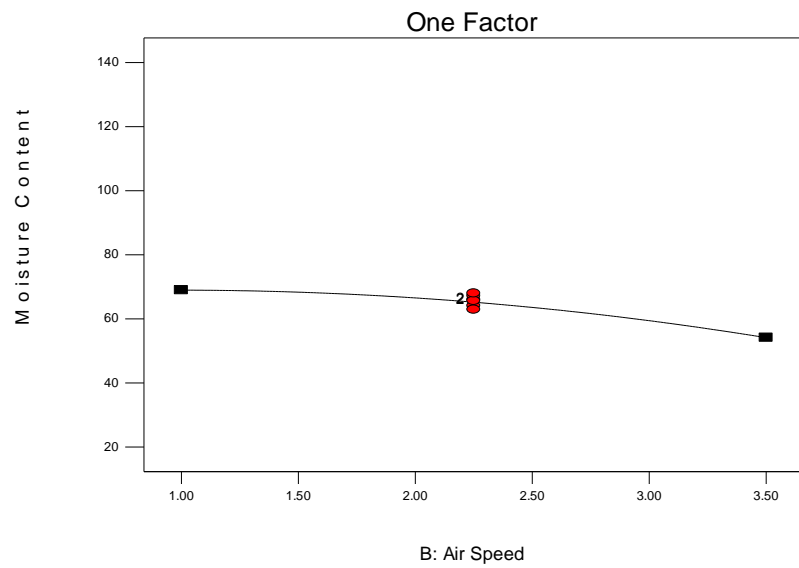
Fig 4. 160   Plots for a one factor at a time of Moisture content and air speed for PVDC
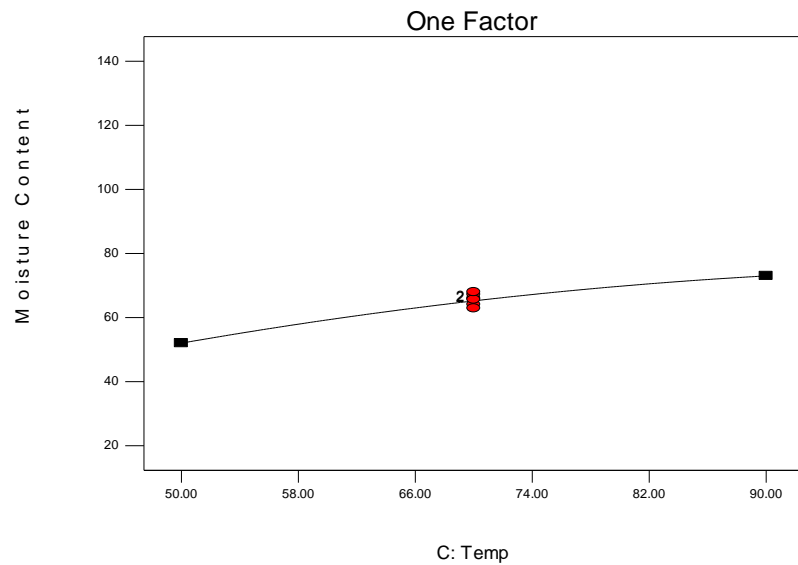
Fig 4. 161   Plots for a one factor at a time of Moisture content and temperature for PVDC

4.21.4 Validation of Optimization Result for PVDC and HADC.

Investigation of the optimum process parameters for maximizing the removal efficiency of moisture is one of the primary objectives of the present study. From Table 4.57, it can be seen that, time of 180 mins, air speed of 3.0 m/s and slice thickness of 2.0 are the optimum conditions required for maximum drying of PVDC while for the maximum drying of HADC, a temperature of 90°C, air speed of 3.5 m/s and time of 180 minutes is required. Under these conditions, the predicted moisture content of PVDC was 20.11%db and 37.03%db for HADC. These are in good agreement with the experimental value of 21.09%db and 36.72%db for HADC and HADC respectively, performed at the same optimum values of the process variables. The optimization was performed using the numerical method of the Design Expert version 9.0 by State Ease U.S.A.

Table 4.57a: The Predicted Optimum Conditions and Experimental Validation Result for PVDC

Material	Optimum Conditions Predicted			Predicted Moisture content (%db)	Experimental Validation Result (%db)
	Time (mins)	Air Speed (m/s)	Slice Thickness (mm)		
PVDC	180	3.0	2.0	20.11	21.09

Table 4.57b: The Predicted Optimum Conditions and Experimental Validation Result for HADC

Material	Optimum Conditions Predicted			Predicted Moisture content (%db)	Experimental Validation Result (%db)
	Time (mins)	Air Speed (m/s)	Temperature (^{o}C)		
HADC	180	3.5	90	37.03	36.72

4.22 The Artificial Neural Network Function Analysis for PVDC and HADC

In fitting problem for the drying of PVDC and HADC, the neural network was required to map between a data set of numeric inputs of the various process parameters (such as time, slice thickness, air speed and temperature) influencing the drying process and a set of numeric targets. Artificial neural networks (ANN's) are inspired by biological neural systems. In this approach weighted sum of inputs arriving at each neuron is passed through an activation function (generally nonlinear) to generate an output signal (Manpreet*et al.,* 2011; Haykyn, 2003). Neural network function fitting is used to select

data, create and train a network, and evaluate its performance using mean square error and regression analysis. Interest in using artificial neural networks (ANNs) for predicting has led to a tremendous surge in research activities in the past two decades (Omid*et al.,* 2009; Aghbashlo*et al.,* 2011).

A two-layer feed-forward network with sigmoid hidden neurons and liner output neurons, was used to fit the multi-dimensional mapping problems arbitrarily well, given consistent data and enough neurons in its hidden layer. The network was trained with Levenberg-Marquardt (LM) back propagation algorithm which is one of the Multi-Layer Perceptron (MLP) networks that is used for error minimization. If there was not enough memory, the case scaled conjugate gradient back propagation was used. MLPs are normally trained with error back-propagation (BP) algorithm. It is a general method for iteratively solving for weights and biases (Nourbakhsh*et al.,* 2014).

The network architecture was given as shown in the Figure 4.162 and 163
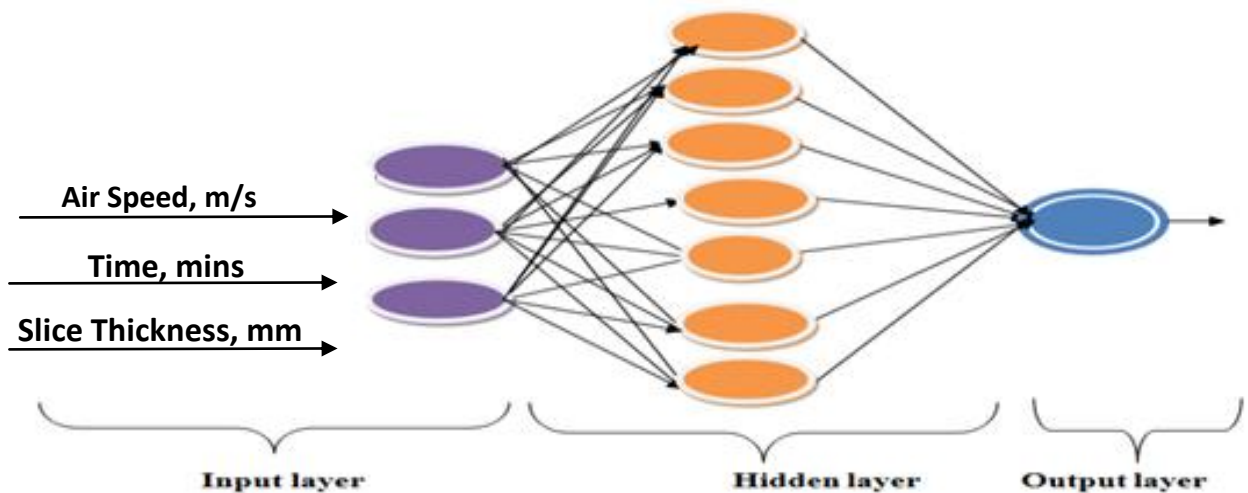
Figure 4.162: The Neural Network Architecture of PVDC
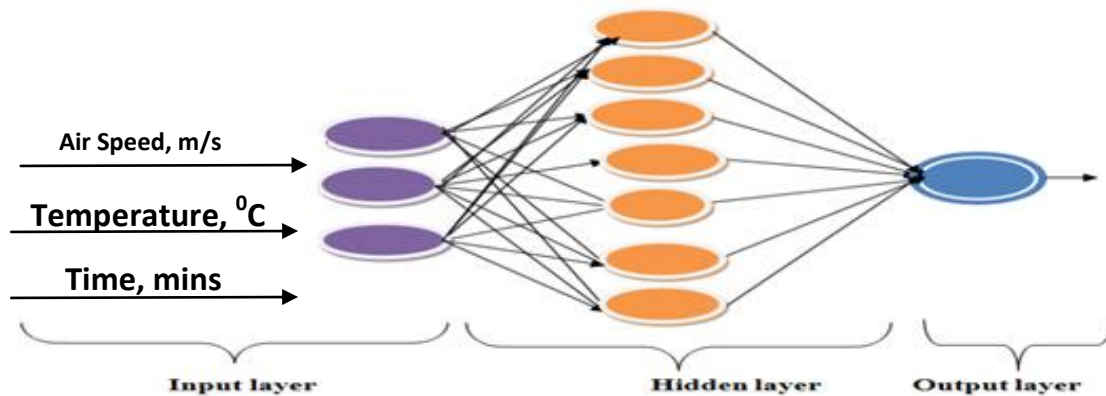
Figure 4.163: The Neural Network Architecture of HADC

4.22.1 Artificial Neural Network Training, Validation and Testing.

For the drying of both PVDC and HADC, a total of 24 samples were set aside for training, 5 samples for testing and 5 samples for validation representing 70% training, 15% testing and 15% validation. For the training, the network was trained and adjusted according to its error. In the validation, the network generalization was measured by network validation and halted when generalization stops improving to stop over fitting. The testing have no effect on training and so provide an independent measure of network performance during and after training.

The ANN model was evaluated for the network performance with different hidden neurons of 10, 20 and 30 to define a fitting neural network model architecture.

271

Mean Square Error (MSE) is the average squared difference between outputs and targets. Lower values are better. Zero means no error. Regression R values (RRV) measures the correlation between outputs and inputs. An R-value of 1 means a close relationship, 0 a random relationship. A close observation of the values revealed that the best performance was given by the network architecture of 10 hidden neurons for both PVDC and HADC.

After the selection of the hidden number of neurons, a number of trainings runs were performed to look out for the best possible weights in error back propagation framework and the final selected network architecture was trained for 10 iterations. The mean square error of the trained networks were 0.2256 and 12.4857 for PVDC and HADC respectively while the regression coefficients were 0.9998 and 0.9912 for PVDC and HADC respectively.

4.22.2 Post-Training Analysis (Network Validation)

After the training, the network was analyzed to check the network performance and to determine if any changes needed to be made to the training process, the network architecture or the data sets. Figure 4.164 and 165 shows the plot of the training errors, validation errors, and testing errors.
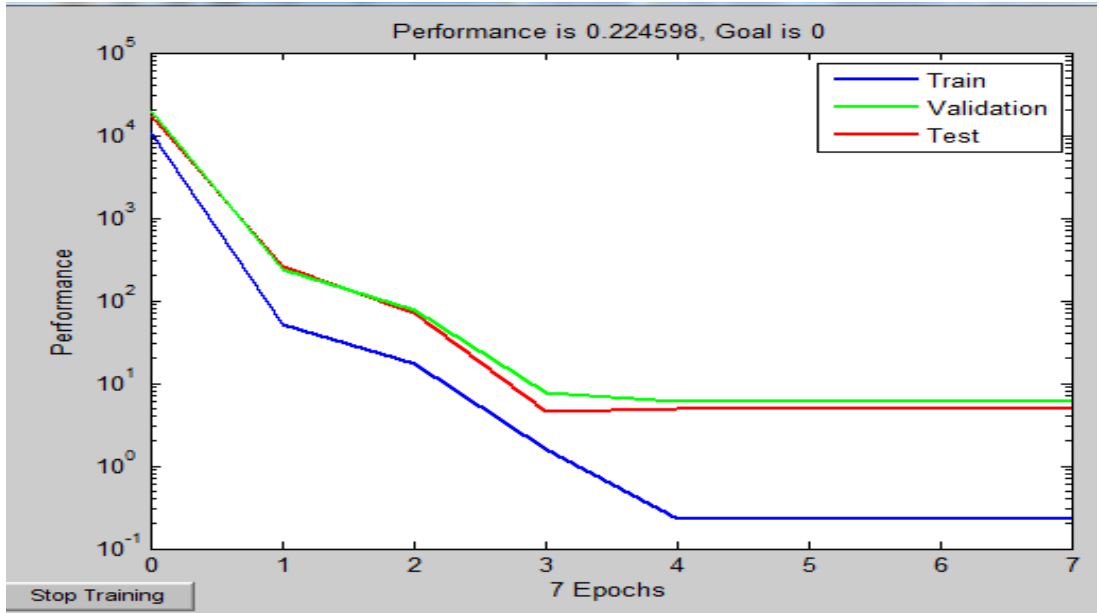
Figure 4.164: Plot of the network validation performance for PVDC
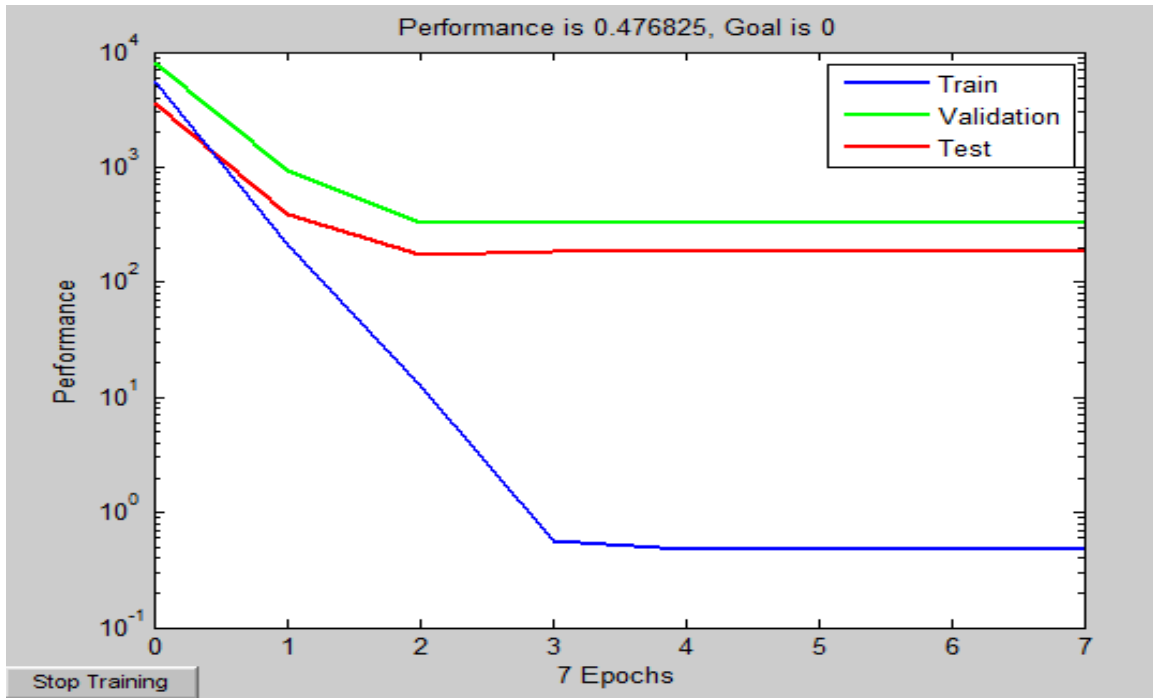
Figure 4.165: Plot of the network validation performance for HADC

The best training performance shows a training error of 0.2246 at Epoch 4 when the validation and testing error are at 3 for PVDC. For HADC, the best training performance was at 0.4768 at epoch 3. The validation and the test curves are similar.

 The result is valid because of the following:

a) The final mean-square error is small.

b) The test set error and the validation set error have similar characteristics.

c) No significant overfitting has occurred by epoch 7 (where the validation performance occurs).

The figure does not indicate any major problems with the training. If the test curve had increased significantly before the validation curve increased, then it could be possible that some over fitting might have occurred.
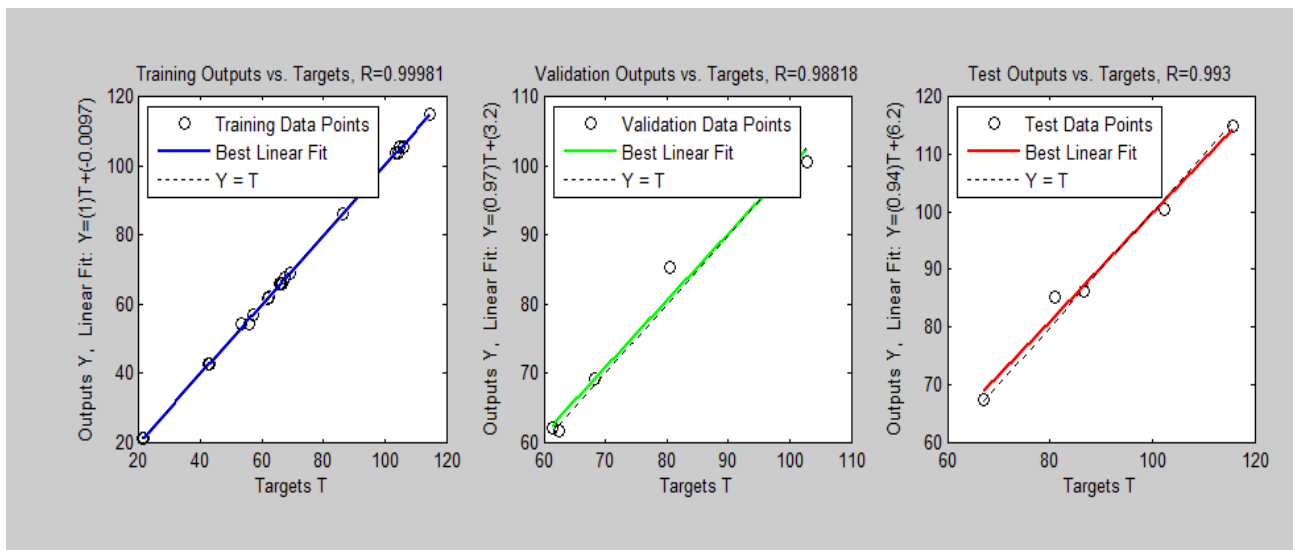
Figure 4.166   Regression plots showing outputs vs targets for training, validation and test of PVDC
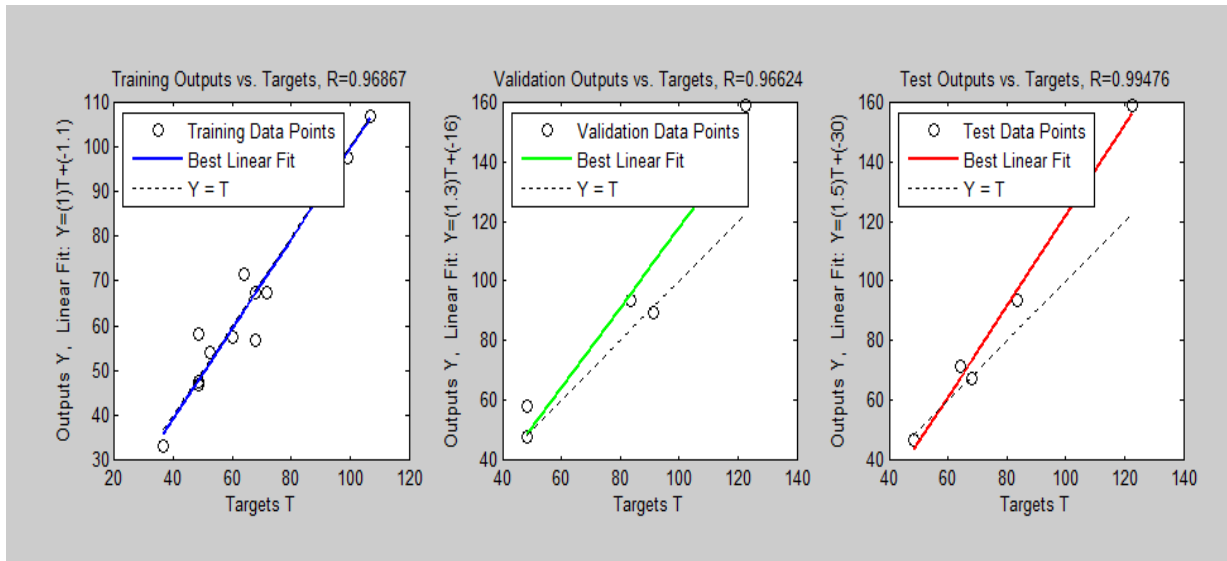
Figure 4.167 Regression plots showing outputs vs targets for training, validation and test of HADC

The regression plots in figure 4.166 and 4.167 displays the network outputs with respect to targets for training, validation, and test sets. The data fall reasonably along a 45 degree line, where the network outputs are equal to the targets. For this process, the fit is reasonably good for all data sets, with R values in each case very close to unity.

4.22.3 Comparison of RSM and ANN for the drying of cocoyam

In order to establish the superiority of either of the models generated by the CCD and ANN, a couple of techniques are applied. These include;

1) Absolute Average Deviation (AAD) observed for both models;
2) Coefficient of determination for both models.

The AAD observed for both models give an indication of how accurate the model predictions can be. (Josh *et al.,* 2014).

$$\text{AAD } (\%) = \left(\frac{1}{n}\sum_{i=1}^{n}\left\{\frac{(R_{art.pred} - R_{art.exp})}{R_{art.exp}}\right\}\right) x \ 100 \qquad (4.22)$$

where n is the number of sample points, $R_{art,pred}$ is the predicted moisture content and $R_{art,exp}$is the experimentally determined moisture content. (Josh *et al.,* 2014).
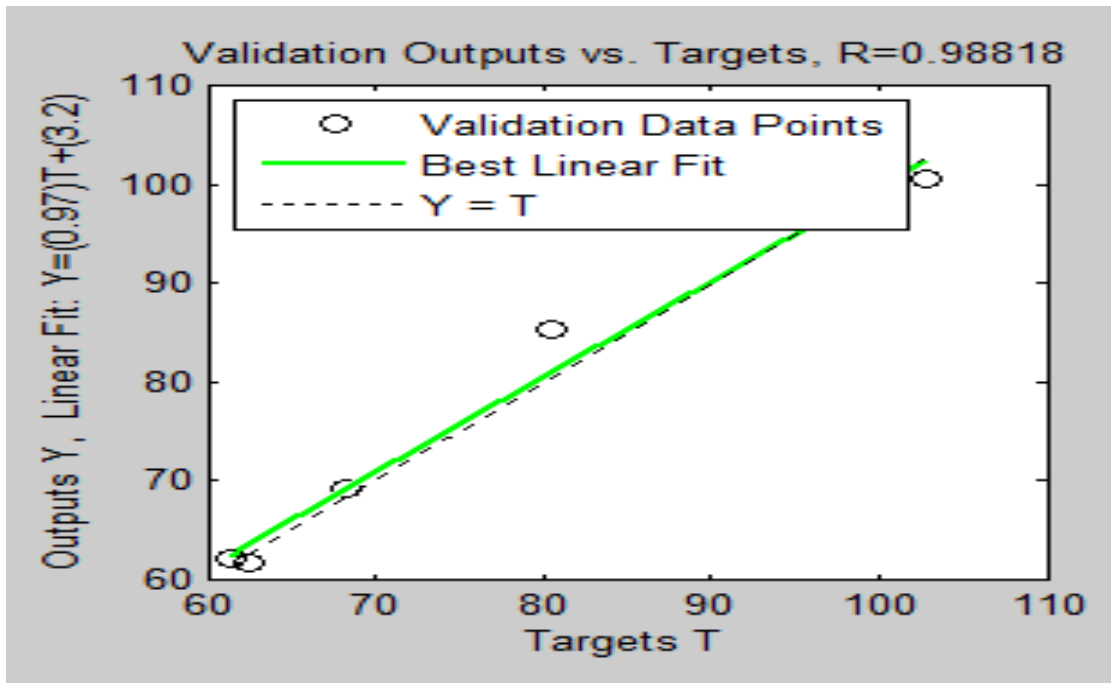
Figure 4.168   Plot of Validation output vs. Actual output for PVDC
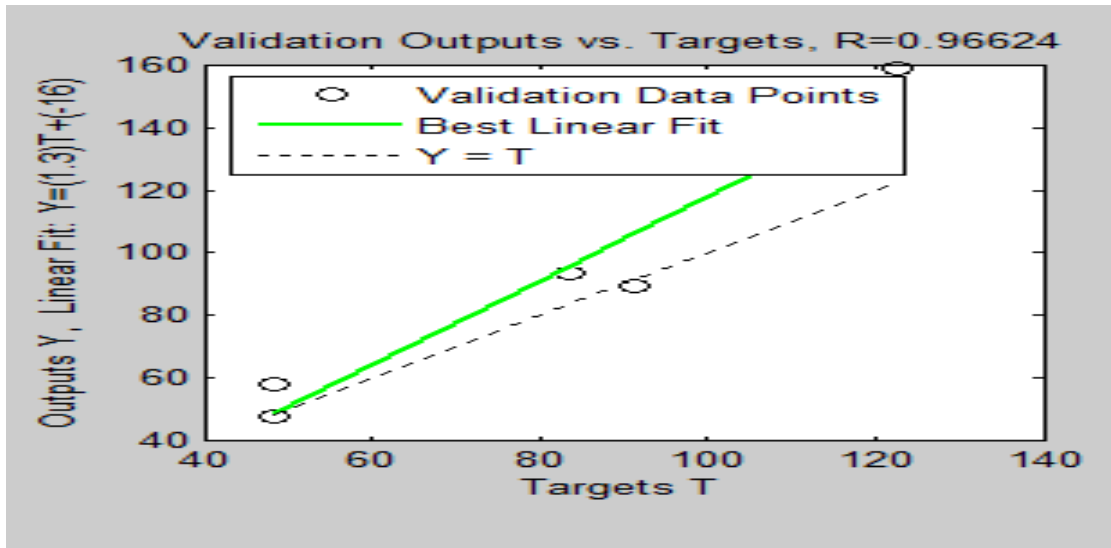
Figure 4.169 Plot of Validation output vs. Actual output for HADC

The linear fit model generated by validation outputs vs target plots in Fig. 4.168 and

4.169 are:

For PVDC, $Y = (0.97)T + (3.2)$ (4.23)

For HADC, $Y = 1.3T + (-16)$ (4.24)

    Where Y = the ANN model value,

        T (Target) = the experimental value used to generate the corresponding

    ANN value.

These are used to predict the ANN model values.

These values are tabulated on Table 4.58 and compared with the values generated by the

CCD. The graph of the correlation between the experimental values and the predicted

values by CCD and ANN are shown on Fig. 4.170 and 4.171.

Table 4.58 Table of Comparison of model prediction for PVDC and HADC

PVDC			HADC		
Experimental Value	CCD	ANN	**Experimental Value**	CCD	ANN
104.69	107.27	104.7493	122.656	122.79	143.4528
105.86	107.27	105.8842	122.656	122.79	143.4528
57.03	56.73	58.5191	64.0625	64.53	67.28125
57.03	56.73	58.5191	64.0625	64.53	67.28125
69.14	72.40	70.2658	99.2188	98.6	112.9844
68.36	72.40	69.5092	99.2188	98.6	112.9844
21.09	20.11	23.6573	48.4375	50.11	46.96875
21.48	20.11	24.0356	48.4375	50.11	46.96875
104.30	106.90	104.371	91.4063	90.18	102.8282
103.52	106.90	103.6144	91.4063	90.18	102.8282
67.58	65.54	68.7526	48.4375	49.5	46.96875
67.19	65.54	68.3743	48.4375	49.5	46.96875
102.34	104.65	102.4698	67.9688	67.94	72.35944
102.73	104.65	102.8481	67.9688	67.94	72.35944
61.33	61.53	62.6901	36.7187	37.03	31.73431
62.11	61.53	63.4467	36.7187	37.03	31.73431
114.84	107.73	114.5948	107.031	108.52	123.1403
115.63	107.73	115.3611	107.031	108.52	123.1403
42.58	464.10	44.5026	52.3438	49.84	52.0469

					4
42.97	46.10	44.8809	52.3438	49.84	52.04694
86.71	85.02	87.3087	83.5938	83.43	92.67194
86.33	85.02	86.9401	83.5938	83.43	92.67194
62.50	59.54	63.825	60.1563	59.3	62.20319
61.72	59.43	63.0684	60.1563	59.3	62.20319
53.13	51.98	54.7361	79.6875	78.59	87.59375
55.86	51.98	57.3842	79.6875	78.59	87.59375
80.86	78.99	81.6342	48.4375	48.52	46.96875
80.47	78.99	81.2559	48.4375	48.52	46.96875
66.01	67.65	67.2297	71.875	69.7	77.4375
66.41	67.65	67.6177	67.9688	69.7	72.35944
65.63	67.65	66.8611	67.9688	69.7	72.35944
65.63	67.65	66.8611	67.9688	69.7	72.35944
65.63	67.65	66.8611	71.875	69.7	77.4375
66.02	67.65	67.2394	67.9688	69.7	72.35944
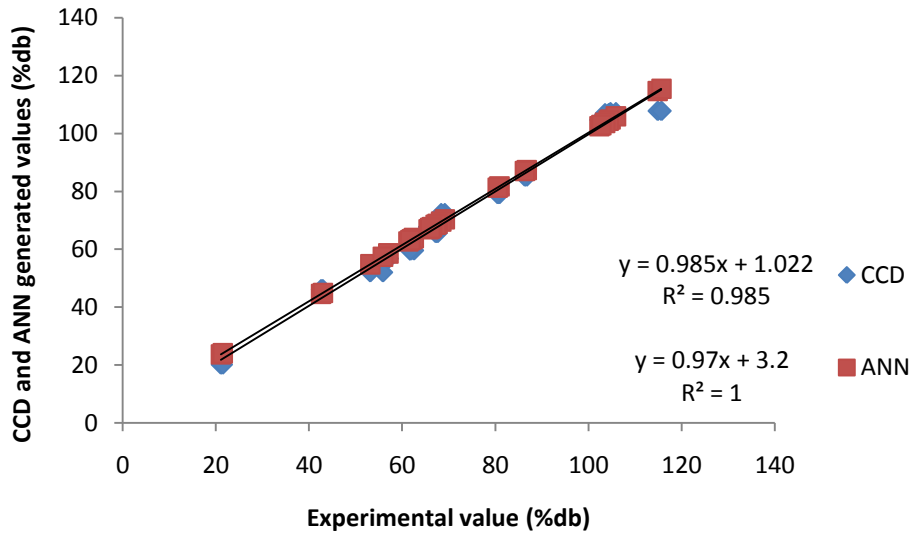
Figure 4.170 Interactive plot for RSM and ANN model appraisal of PVDC
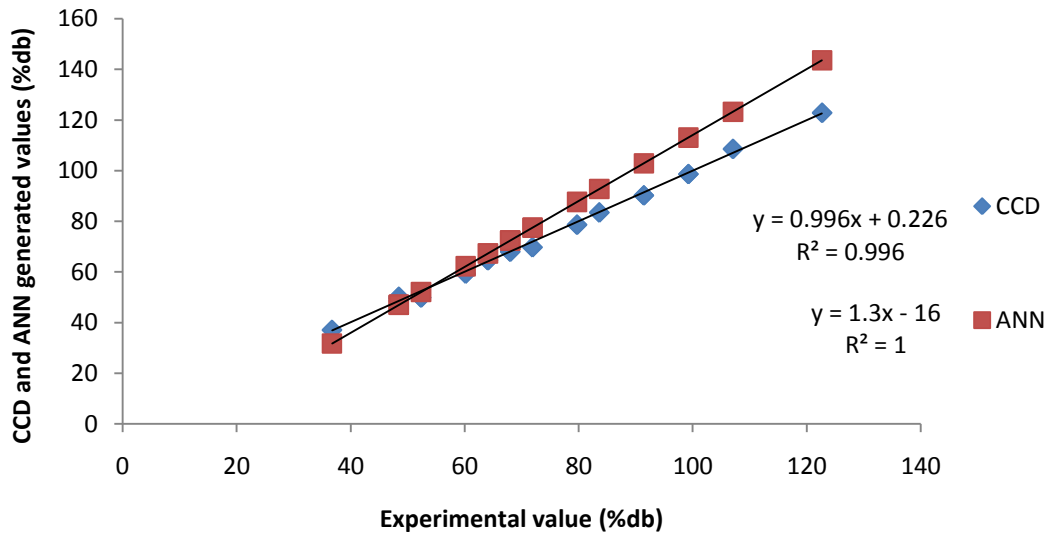
Figure 4.171 Interactive plot for RSM and ANN model appraisal of HADC.

From the graphs on figure 4.170 and 4.171, it is observed that the correlation coefficient for the ANN model is close to unity, while that for the CCD is 0.985 (for PVDC) and 0.996 (for HADC). These values are a measure of how close the predicted value is the response is to the actual experimental values.

The AAD analysis revealed that the CCD and ANN deviated slightly from the experimental value

From these analyses it is evident that both ANN and CCD are sufficient and appropriate for the drying process and therefore the models should be adopted for the optimization of the drying process.

4.23 Sensory evaluation

The result of the sensory attributes of the flour produced from cocoyam and potato is as shown in Figures 4.172 to 4.176. The rating was summarized in overall like and dislike disposition. To enable the ratings of the like and dislike to be made in a continuous manner, it was constructed as a bipolar scale with neutral in the centre. This makes the positive and negative descriptors to be statistically symmetrical around the neutral hence, agreeing in general with other affective scales (Guest et al, 2007; Schutz and Cardello, 2001). Of the 50 panelists used, 64% were females while 72% were between the age bracket of 25 and 35 years. As shown in Figure 4.172, the overall best score in all the tested categories was the cocoyam flour prepared from PDC followed by ODC,

SDC and SDP. This showed that PDC has the most overall acceptability index to the panelists. The deviations observed in the numerical ratings among the panelists are due to individual differences (Juyun et al, 2009). Generally, the cocoyam flour received a greater acceptability than the potato flour for all the drying methods. The drying method used was not very significant except for the flour produced from the hot-air conventional dried products which received the lowest rating for both the cocoyam flour and potato flour. This may be due to the kind of combined speed and temperature that was employed which resulted in the lowest drying time and the distorted colour of the products.

92% of the panelists considered the colour of the cocoyam flour obtained from PDC as acceptable. 60% liked the flour obtained from PDP. The most dislike was observed in the general appearance and aroma of the flour of ODC and ODP respectively.
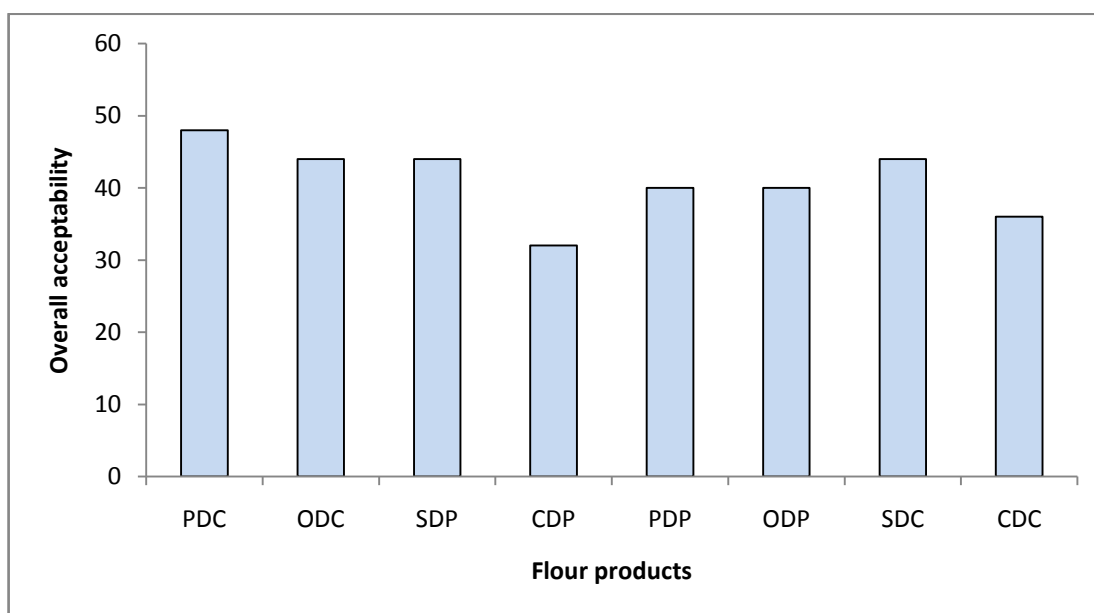

Fig 4.172 Evaluation of sensory analysis based on overall acceptance
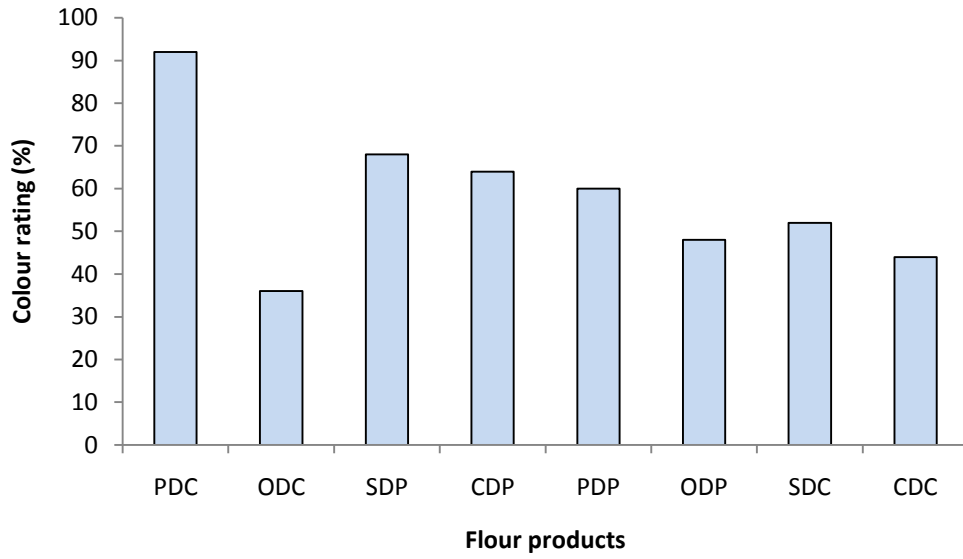
Fig 4.173 Evaluation of sensory analysis based on colour acceptance
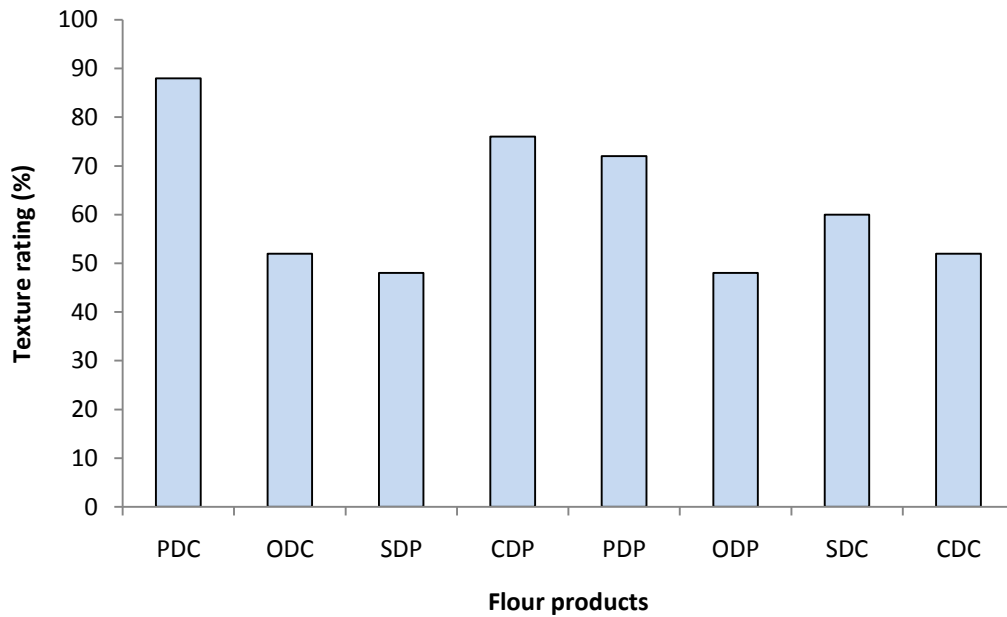
Fig 4.174 Evaluation of sensory analysis based on texture acceptance
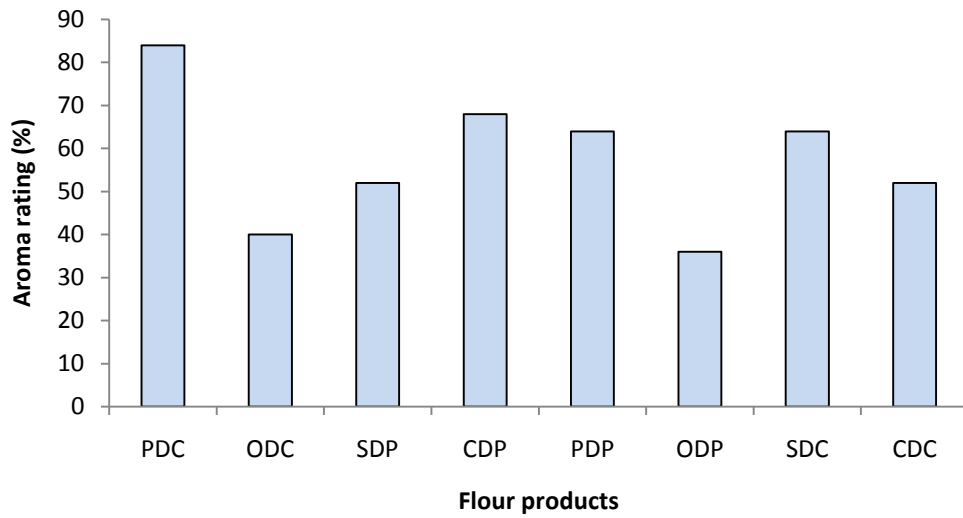
Fig 4.175 Evaluation of sensory analysis based on aroma acceptance
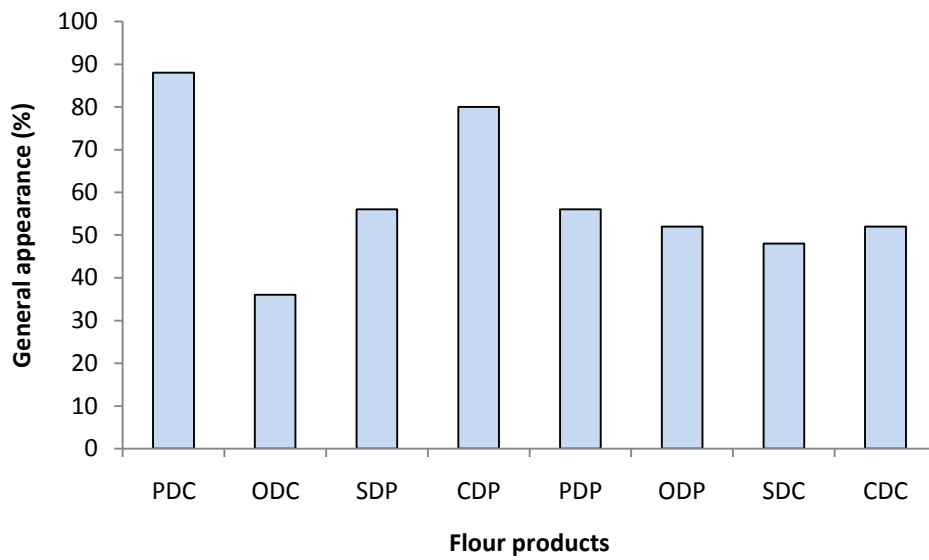
Fig 4.176 Evaluation of sensory analysis based on general appearance

CHAPTER FIVE

CONCLUSION AND RECOMMENDATION

5.1 Conclusion

The study revealed that the drying of cocoyam and potato slices can be achieved using the open sun drying, the Solar cabinet dryer (solar dryer), the oven dryer and the conventional dryer though their drying characteristics differed. From the study, the following conclusions are drawn:

➤ The drying of cocoyam and potato occur mainly in the falling rate period. The drying time decreased with air-speed and temperature but increased with slice thickness for the samples used

➤ The true density, the bulk density and the tapped density decreased with respect to the dried potato and cocoyam while the thermal diffusivity of the food products increased for the dried products.

➤ The effective moisture diffusivity increased with slice thickness, air speed and temperature.

➤ The activation energy of cocoyam was higher than the activation energy of potato.

➤ The total energy consumption increased with increase in the slice thickness and the values obtained in this work is consistent with the values reported by other authors.

➤ The convective heat transfer coefficient was maximum at 4 mm slice thickness for both cocoyam and potato but increases with mass.

➤ The system efficiency decreased with drying time with the least slice thickness decreasing fastest while the thermal efficiency of the dryers is highest in the Solar cabinet dryer and least in the oven dryer.

➢ The water activity depends on the moisture content and its value affects the estimated mold-free shelf life.

➢ The kinetic models that best described the drying process were the Logarithmic model, the Modified page 1 model, the Approximation of diffusion model and the Two term models.

➢ Response Surface Methodology and Artificial Neural Network were successfully applied in the optimization of the drying process.

5.2 Recommendations for further research

➢ As our country continues to strive to attain self-sufficiency in importation of food item such as flour, it is recommended that more research should be carried out on the suitability and qualities of the flours that can be milled from these dried products. This will help to reduce the dependency on wheat flour which is imported into the country.

➢ Other types of dryers should be compared with the Solar cabinet dryer in other to determine the best economically drying system that will also give good quality of the dried products.

5.3 Contribution to knowledge

➢ Four kinetic models (Logarithmic model, the Modified page 1 model, the Approximation of diffusion model and the Two term models) were successfully used to describe the drying mechanism of potato and cocoyam.

➢ Response surface methodology and the Artificial neural network have been successfully applied to optimize the drying of potato and cocoyam.

- The engineering properties were determined and will be useful in designing industrial dryers and as a useful addition to the storage bank of research institutes and the government.

REFERENCES

Abbaszadeh, A., Motevali, A., Ghobadian, B., Khoshtaghaza, M. H. & Minaei, S. (2012) Effect of air velocity and temperature on energy and effective moisture diffusivity for Russian olive (Elaeugnusan gastifolial) in thin-layer drying. Iran journal of chemistry and chemical engineering. 31, (1) : 75-79.

Ademiliyu, T., Abowei, M.F, Chinewhu, S.C. & Fubara, T.E. (2006). Effect of variety on the drying and engineering properties of fermented ground cassava. Journal of new views in engineering analysis and modelling. 1, (1): 80-96.

Adu, E. A., Bodunde, A. A., Awagu, E. F. & Olayemi F. F. (2012) Design, Construction and Performance Evaluation of a solar Agricultural Drying Tent. International journal of engineering research and technology. 1, (10) : 1 – 12.

Afolabi, T. J. & Tunde-Akintunde, T. Y. (2014) Effect of drying conditions on energy utilization during cocoyam drying. Agricultural Engineering International: CIGR Journal 16 (4) 135 – 145.

Agarry, S. E. & Aworanti, O. A. (2012) Modelling the drying characteristics of osmosised coconut strips at constant air temperature. Journal of Food Processing and Technology 3, (4) : 1 – 6.

Aghbashlo, M., Kianmehr, M. H. & Samimi-Akhijahani, H. (2008) : Influence of drying conditions on the effective moisture diffusivity, energy of activation and energy consumption during the thin-layer drying of beriberi fruit (Beriberidaceae). Energy Conversion and Management, 49 (10) : 2865-2871.

Aghbashlo, M., Kianmehr, M. H., Nazghelichi, T. & Rafiee, S. (2011). Optimization of an artificial neural network topology for predicting drying kinetics of carrot cubes using combined response surface and genetic algorithm. Drying technology. 29, 770–779.

Ajao, K. R. & Adedeji, A. A. (2008) Assessing the Drying rates of some crops in solar Dryer. Case study: Vegetables, tuber and grain crop. Journal of research information in civil engineerung. 5 (1).

Akinneye, J.O., Amoo, I.A. & Arannilewa, S. T. (2007) Effect of drying methods on the nutritional composition of three species of fish (Bonga sp. Sardinella sp. and Heterotis niloticus).Journal of fisheries International. 2, (1) : 99-103.

Akinola, O.A., Akinyemi, A. A. & Bolaji, B. O. (2006) Evaluation of Traditional and solar fish drying systems toward, Enhancing fish storage. Journal of fisheries international (2-4) 44-49

Akintunde, M. A. (2007). Effect of scattering Extinction coefficient on drying Rate. Journal of engineering and applied sciences. 2, (1):116-120.

Akpinar, E., Midilli, A. & Bicer, Y (2003) Single layer drying behaviour of potato slices in a convective cyclone dryer and mathematical modeling. Energy Conversion Management. 44: 1689–1705.

Alam, Z., Muyibi, S. A. & Kamsldin, N. (2008) Production of activated carbon from oil palm empty fruit bunches for removal of zinc. Proceedings of Twelfth International Water Technology Conference, Aixeandria Egypt, 373-382.

Amin, T. G., Shahin, R. & Alireza , K. (2011). Study on effective moisture diffusivity,

activation energy and mathematical modeling of thin layer kinetics of bell pepper, Australian journal of crop science. 5, (2) : 128-131.

Amira, T., Saber, C. & Fethizayrouba, K. (2014) Moisture diffusivity and shrinkage of fruit and cladode of ountice ficus-indica during infrared drying. Journal of food processing, 1, 1-9.

Amiri C. R., Amiri P. J. & Esna-Ashari, M. (2011) Modeling of moisture diffusivity, activation energy and specific energy consumption of high moisture corn in a fixed and fluidized bed convective dryer. Spanish journal of agricultural research. 9, (1): 28 – 40.

Amiri C. R. (2012) Modeling Some Drying Characteristics of High Moisture Potato Slices in Fixed, Semi Fluidized and Fluidized Bed Conditions. Journal of Agricultural Science and Technology. 14: 1229-1241

Anil, K. & Tiwari, G.N. (2006) Effect of mass on convective heat transfer coefficient during onion flakes drying. American Journal of food technology. 1, (1) : 1-18.

Anna, H., Iva, K., Rithy, C., Petra, C. & Jan, B. (2014) Development of solar drying model for selected Cambodian Fish species. The scientific word journal, 4, 1-10.

Anwar, S.I & Tiwari, G.N. (2001) Evaluation of convective heat transfer coefficient in crop drying under open sun drying. Energy conversion and management. 42 :627-637.

AOAC (1990) Association of Analytical Chemistry. Methods for Proximate Analysis. 2217 - 2280.

AOAC (2000). In: Official Methods of Analysis of the Association of Official Analytical Chemists (17th ed.) (ed.W. Horwitz). AOAC International, Maryland, USA

Aremu, A. K., Adedokun, A. J. & Abdulganiy, O. R. (2013) Effects of slice thickness and temperature on the drying kinetics of mango. International journal of research and reviews in applied sciences. 15, (1) :41-50.

Assidjo E., Yao B., K. Kisselmina & D. Amané (2008). Modeling of an industrial drying process by artificial neural networks. Brazilian Journal of Chemical Engineering. 25 (3), 515 – 522

Atul, H. P., Shah, S.A. & Hitesh, B. (2013) Review on Solar Dryer for Grains, Vegetables and Fruits. Drying characteristics of okra slices using different drying Methods by Comparative Evaluation. International Journal of Engineering Research and Technology. 2, (1) :1 – 7

Baballs, J. & Belessiotis V.G. (2014) Influence of the drying conditions on the drying contents and moisture diffusivity during the thin layer drying of figs. Journal of food engineering. 65, 449-458.

Bao-meng, Z., Xue-sen, W. & Guo-dong, W. (2013) Hot-air Drying of Rehmannia Root: Its Kinetic Parameter, Shrinkage and Mathematical Modelling. International journal of engineering research and technology. 2, (11) : 1172 – 1178

Boubekri, A., Benoussa, H. & Mennouche, D. (2007) Solar Drying of date palm fruits simulated as multi-step Temperature drying. Journal of engineering and applied science. 2, (12) :1700-1706.

Charidrakumar, B. P. & Jiwanlal, L. B. (2013). Development and performance evaluation of mixed mode solar dryer with forced convection. International journal of energy and environmental engineering. 4, (23) : 1-8.

Chen, G., Chen, J., Srinivasakannan, C. & Peng, J. (2011). Application of response surface methodology for optimization of the synthesis of synthetic rutile from titania slag. Applied surface science, 258(7), 3068–3073

Chenchaiah, M. & Muthukumarappan, K. (2014) Processing Aids for Improving Heat Transfer during drying of granular food materials. Journal of Food Processing and Technology. 4(8) 1 – 4.

Coulson, J.M. & Richardson, J. F. (2004) Chemical Engineering vol 1: flow flow, heat transfer and mass transfer. Butterwork-Heinemann Elsevier publishers.

Dagde, K. K. & Nmegbu, C. G. (2014) Mathematical modeling of a tray dryer for the drying of potato chips using hot air medium.   International Journal of Advancements in Research & Technology, 3 (7) 104 –107.

Devarly, P., Kartika Y., Indraswati N. & Ismadji, S. (2008) Activated carbon from jackfruit peel waste by H_3PO_4 chemical activation: pore structure and surface chemistry characteristization". Chemical Engineering Journal 140: 32-40

Dhanorc, R. T. & Jibhakate, Y. M. (2014) A solar Tunnel Dryer for Drying Red Chilly as an Agricultural Product. International Journal of Engineering Research and Technology. 3(7) 310 – 314

Dianmante, L.M. & Munro. P. A. (1993). Mathematical modeling of the thin layer solar drying of sweet potato slices. Solar Energy 51:271-276.

Divine, N. B., Charles, F. A., Dzudie, T., Cesar, I., Clerge, T. & Zephirin, M. (2013). Indirect solar drying kinetics of sheanut (vitellaria paradoxa Gaetn) Kernels. Journal of Engineering and Applied science. 8(6) 183-191.

Domenec, J. & Natalie, S. (2014) Enhanced Biosolids drying with a solar thermal application. Journal of fundamental of Renewable Energy and Applications. 4,(2) :1-5

Doymaz, I, (2006). Drying kinetics of black grapes treated with different solutions. Journal of food engineering. 76: 212–217.

Doymaz, I. (2011) Thin-layer drying characteristics of sweet potato slices and mathematical modeling. Heat and mass transfer 47 (3) 277-285.

Egbuonu, A. C., Nzewi, D. C. & Egbuonu, O. N. C. (2014) Effect of soaking prior to oven-drying on some nutrient and anti-nutrient properties of biffer yam (Dioscorea dumetorum) Journal of Nutrition and food sciences 4(3) 1-4

Eke, A. B. (2013). Identification of suitable materials for solar thermal collector in rural areas of Zaria Nigeria. International journal of Engineering and Technology. 3 (8) 834-841.

Etoamaihe, U. J. & Ibeawuchi, K. O. (2010) Prediction of the drying rates of cassava slices during oven drying. Journal of Eng and Applies sciences 5(4) 308-311.

Fortes, M & Okos, M. R. (1981) A non-equilibrium thermodynamics approach to Transport phenomena in capillary porous media. Trans. ASAE, 24(3) 756-760

Goldfarb, D. & Ramachandrumi, H. (2003) Measurement of bulk and tapped density on pharmaceutical powders. American Physical Society, Division of fluid dynamics, 56th Annual Meeting, 20030 NYC/New Jersey. USA.

Guadalupe, L. & Diane, M. B. (2006). Influence of pre-drying treatments on quality and safety of sun –dried tomatoes. Journal of food science. 71, (1) : 32-37.

Guest, S., Essick, G., Patel, A., Prajapati, R. & McGlone, F. (2007) Labeled magnitude scales for oral sensations of sweetness, dryness, pleasantness and unpleasantness. Food Quality Pref. 18:342 – 352.

Haykyn, S. (2003) Neural Networks, a comprehensive foundation. Prentice Hall, India.

Hadush, H., Walelign, W. & Abuhay, T. (2014) Effect of Drying off Period and Harvest Age on Quality and Yield of Ratoon Cane (Saccharium officinarium L.). Advances in Crop Science and Technology. 2(3) 1 – 5

Hamed, Mirhosseini & Bahareh Tabatabaee Amid (2013) Effect of different drying techniques of flow ability characteristics and chemical properties of natural carbohydrate-protein gum from durian fruit seed. Chemistry central Journal. 7 (1) 1-14.

Ian, T. & Arun, M. (1997) Mathematical modeling and Numerical techniques in drying technology. Marcel Dekker Inc, USA.

Ici Turk, T. G. (2005) Convective heat transfer coefficient of some fruits under open sun drying conditions. Journal of food technology 3(1) :10-14.

Igbeka, J.C. (2013) Agricultural proceedings and Storage Engineering. First edition. Ibadan University press Nigeria.

Ingh, P., Amar, S., Singh, J., Singh, S., Arya, A. & Singh, B.R. (2014) Effect of drying characteristics of Garlic-A Review. Journal of Food Process Technology 5(4)1 – 6

Prem, K., Ramanathan, J. M. & Ranganathan. T. V. (2014) Ohmic Heating Technology in Food Processing – A Review. International Journal of Engineering Research and Technology. 3(2) 1236 – 1241.

Jain, R.K. & Bal, S., (1997). Physical properties of Pearl millet. Journal of Agricultural Engineering Resources. 66: 85- 91.

Jayaraman, K.S. & Gupta. D.K.D. (2006). Drying of fruits and vegetables. In Handbook of industrial drying, ed. by Arun S. Mujumdar, 606-631 CRC Press, New York.

John, S. R., David, R. K. & Olga, P. Z. (2008) Drying kinetics of grape seeds. Journal of food Engineering .89 (2008) 460- 465.

Josh, L. P., Chris, P. & Rachel, L. G. (2014). Comparison of response surface methodology (RSM) and artificial neural networks (ANN) towards efficient extraction of artemisinin from artemisiaannua. Industrial crops and products, 58, 15–24.

Junling, S., Zhongli, P., Tara, H. M., Delilah ,W., Edward, H. & Don, O. (2008) Elsevier – Food Science and Technology. 41, 1962 – 1972.

Juyun Lim, Alison Wood & Barry G. Green (2009) Derivation and Evaluation of a Labeled Hedonic Scale. Oxford University Press on Chemical Senses 34: 739–751.

Juyun Lim (2011) Hedonic scaling: A review of methods and theory. Elsevier on Food Quality and Preference 22 : 733–747.

Kajuna, S. T. A. R, Silayo, V.C.K, Mkenda, A & Makungu, P.J .J. (2001). Thin –layer drying of sliced cassava roots. African Journal of science and Technology 2, (2) : 94-100.

Kaptso, K. G., Njintang, Y. N., Nguemtechouin, M. M. G., Scher, J., Hounhouinyan, J. & Mbofuny C. M. (2013) Drying kinetics of two varieties of Bambara groundnuts (vigna subterranca) seeds. Journal of food Technology. 11,(2): 30-37.

Karthanos, V. T., Villabos, G. & Saravacos, G. D. (1990). Comparism of two methods of estimation of the effective moisture diffusivity from drying data. Journal of food science 55, (1), 218-231.

Khaled, M. Y. & Sayed, M. M. (2014) Effect of drying methods on the antioxidant capacity, colour and phytochemicals of Portulaca Oleraceal leaves. Journal of Nutrition and Food Science. 4(6) 1 – 6

Kingsly, R. P., Goyal, R. K., Manikantan, M.R., & Ilyas, S.M. (2007). Effects of pretreatments and drying air temperature on drying behaviour of peach slice. International Journal of Food Science and Technology, 4: 65–69.

Kulsum, Jan, Riarcis & Saxena E.C. (2014) Mathematical modeling, of thin layer drying kinetics of biodegrable pellets JFPT, 5(9) 1-5

Krumar, A., Prasad, B. & Mishra, I. M. (2007) Process parametric study of ethane carboxylic acid removal onto power activated carbon using Box-Behnken design. Chem. Eng. Technol. 30(7), 932-937.

Krumar, A., Prasad, B. & Mishra, I. M. (2008) Adsorption removal of acrylonitrile using powered activated carbon. Journal of Environmental protection Science, 2, 54-62.

Kumar, S. A., Panner, S. R. & Sivakum, A. R T. (2010) Isolation, characteristion and formulation properties of a new plant gum obtained from mangifera indica. Int J. of pharm Biomedic Res. 1: 35-41.

Ladunni, E., Aworh, O. C., Oyeyinka, S. A. & Oyeyinka, A. T. (2013). Effects of Drying Method on Selected Properties of Ogi (Gruel) Prepared from Sorghum (Sorghum vulgare), Millet (Pennisetum glaucum) and Maize (Zea mays). Journal of Food Processing and Technology. 4, (7) : 1 – 4.

Leandro, S. O. & Kamyar, H. (1997) Finite element modeling of grain drying. Mathematical modeling and numerical techniques in drying technology. 309 – 338.

Lee, S., Tran, T., Park, Y., Kim, S., & Kim, M., (2006). Study on the kinetics of iron oxide leaching by oxalic acid. Int. Journal Mineral Process. 80, 144–152

Luikov, A. V. (1966) Heat and Mass Transfer in Capillary-Porous Bodies, Pergammon Press, Oxford, USA.

Luther, R. W., Dwayne, A. S. & Gerald, H. B. (2003). Food and Process Engineering Technology. ASAE Publication, USA.

Madamba P.S, Driscoll R.H., & Buckle K.A., (1996). The thin layer drying characteristics of garlic slices. J. Food Eng 29,81-88.

Man C. D. & Jones A. A. (2000) Shelf life evaluation of foods. 2nd Ed. Springer

Majid Rasouli, Sadegh Seiiedlou, Hamid R. Ghasemzadeh & Habibeh Nalbandi (2011) Influence of drying conditions on the effective moisture diffusivity and energy of activation during the hot air drying of garlic. Australian Journal of Agricultural Engineering. 2 (4) : 96 – 101.

Mahdi, M., Ali, M. & Mohammad, A. G. (2013) Mathematical modeling, moisture diffusion and Energy efficiency of thin-layer drying of potato. International Journal of Agriculture and crop science 5 (15) 1663-1669.

Manpreet, S. Bhatti, DhritiKapoor, Rajeev K. Kalia, Akepati S. Reddy, Ashwani K.

Thukral (2011). RSM and ANN modeling for electrocoagulation of copper from simulated wastewater: multi objective optimization using genetic algorithm approach. Desalination 274, 74–80.

McCabe, W.L., Smith, J. C. & Harriott. P. (1986). Unit Operations of Chemical Engineering. McGraw-Hill Press, New York.

Midilli, A., Kucuk, H. & Yapar. Z. (2002). A New model for single-layer drying. Drying Technology. 20, (7):1503-1513.

Minaei, S., Motevali, A., Ahmadi, E. & Azizi, M.H. (2012) Mathematical models of drying pomegranate arils I n vacuum and microwave dryers. Journal of Agricultural science and Technology. 13: 655-664.

Mirzaee, E., Rafiee, S., Keyhani, A. & Emam-Djomeh, Z. (2009) Determination of moisture diffusivity and activation and activation energy in drying of apricots. Res. Agr. Eng. 55(3) : 114 – 120.

Mohammad, Z., Seyed, H. S. & Barat, G. (2013) Kinetic drying and mathematical modeling of apple slices in dehydration process. Journal of food process and technology. 4, (7) : 1-4.

Mohsenin N.N., (1978). Physical Properties of Plant and Animal Materials. Gordon and Breach Sci. Publ., New York.

Mojtaba Tohidi, Morteza Sadeghi, Seyed Rasoul Mousavi, & Seyed Ahmad Mireei (2012). Artificial neural network modeling of process and product indices in deep bed drying of rough rice. Turk J Agric. 36 : 738-748

Moshen, B. (2016) Energy efficiency and moisture diffusivity of apple slices during

convective drying. Food science and technology. 36, (1) :145-150.

Motevali, A., Abbaszadeh, A, Minaei S, Khoshtaghaza M, & Ghobadian, B (2012) Effective moisture diffusivity, activation energy and energy consumption in thin-layer drying of jujube. Journal of Agricultural science and Technology. 14: 523-532.

Mousavi, M. & Javan, S. (2009) Modeling and Simulation of Apple Drying, Using Artificial Neural Network and Neuro -Taguchi's Method. J. Agr. Sci. Tech. (2009) Vol. 11: 559-571.

Navale, S.R., Harpale V.M. & Mohite K.C. (2015) Comparative study of open sun and cabinet solar drying for fenugreek leaves. International Journal of Renewable Energy Technology Research 4 (2)1-9.

Ndukwu, M. C. (2009) Effect of Drying Temperature and Drying Air velocity on the Drying rate and Drying constant of cocoabean. Agricultural Engineering international: the CIGR Ejournal. Manuscript 1091. 11, 1 – 7.

Ngankham Joykumar Singh & Ram Krishna Pandey (2011). Neural network approaches for prediction of drying kinetics during drying of sweet potato. Agricultural Engineering International: CIGR Journal. Manuscript No.1734. Vol. 13, No.1, 2011.

Nicholas, A. M. (2012) Drying characteristics of cocoa beans using an Artificial Dryer. Journal of Engineering and Applied science 7 (2) 194-197

Nwabanne, J. T. (2008) Drying characteristics and Engineering properties of fermented ground cassava. African Journal of Biotechnology. 8, (5) 873 – 876.

Nwajinka, C.O, Nwuba E.I.U & Udoye B.O. (2014) Moisture diffusivity and activation energy of drying of melon seeds. International Journal of Applied science and Engineering 2 (2) 37-43.

Nwajinka, C.O., Okpala C.D. & Benjamin U. (2014) Thin layer drying characteristics of cocoyam corn slices. International Journal of Agriculture and Biosciences 3 (5) 241-244.

Okos, M.R., Narsimhan, G., Singh, R.K., & Wetnauer, A.C., (1992). Food Dehydration. In: +Heldman, D.R., Lund, D.B. (Eds.), Handbook of Food Engineering. Marcel Dekker Inc., New York, p. 462.

Obot, M. S., Okokon, F. B. & Ogunlowo, A. S. (2013) The Effects Of Temperature, Thickness And Air Velocity On The Air Drying Characteristics Of Taro (Colocassia Esculenta). International Journal of Engineering Research and Technology. 2(3) 1- 10

Okoye, O.S., Washeed M.A & Lucas E.B (2014) Experimental studies of effects of geometry on drying rate and properties of ginger (Zingiber officinale Rose.) with solar-hybrid dryer. Journal of biology, agriculture and health care. 4, (24) : 45-56.

Omid, M., Baharlooei, A., & Ahmadi, H.,(2009). Modeling drying kinetics of pistachio nuts with multi-layer feed-forward neural network. Drying technologies 27, 1069–1077.

Onyinge, G. O., Oduor, A. O. & Othieno, H. E. (2014) Investigating the thin layer drying characteristics of vegetable kales in a Natural convection solar cabinet dryer, under the climatic conditions of Maseno, Kenya. International Journal of Engineering Research and Technology. 3, (8):335 – 337

Oyoh, K. B & Menkiti, M. C. (2008) Optimum safe drying temperature for seed grains.Agricultural Journal. 3, (3):190-192

Patomsok, W. (2014) Cassava slices drying by using a combined hot air single-plane microwave dryer. Journal of Agricultural chemistry and Environment. 3, 1-4.

Paulo, C. C., Osvaldo, R., & Deise, M. R. (2009) Drying Characteristics and Kinetics of Coffee Berry. Revista Brasileira de Produtos Agroindustriais, Campina Grande, 8, (1) : 1-10

Peleg, M. & Bagley, E. B. (1983) Physical properties of food. AVI Publishers Co. Westport CN.

Peryam, D. R. & Girardot, N. F. (1952). Advanced taste test method. Food Engineering, 24, 58-61.

Rajeev B., AbdKarim A. & Gopinadhan P. (2012) Factors affecting the growth of microorganisms in Food. Progress in Food Preservation. John Wiley & sons Ltd.

Ravinder, K. S. (2014) Open sun and green house drying of agricultural food products: a review. International Journal of Engineering Research and Technology 3, (3):1053-1065.

Ravinder, K. S., Sandeep, K. & Mahesh, K. (2013) An Experimental Study on Open Sun Drying of Corn Kernels. International Journal of Engineering Research and Technology. 2, (7) :1112 – 1119

Rayaguru, K. & Routray, W. (2012) Mathematical modeling of thin layer drying kinetic of store apple slices. International food Research Journal. 19, (4) : 1503-1510.

Reyes, A., Mahn A., Huenulaf P. & Gonzalez T. (2004) Tomato dehydration in a hybrid solar Dryer. Journal of Chemical Engineering and Process Technology. 5, (4) 1 – 8

Reza, A. C., Kamran, S., Qasem, A. & Ali, A. S. (2013). Modeling moisture diffusivity, activation and specific energy consumption of squash seeds in a semi fluidized and fluidized bed drying. Journal of food science and Technology 50, (4) : 667-667.

Rockland, L. B. & Beuchat, R. L. (1987) Water Activity: Theory and Application to food (2nd Ed.) Marcel Dekker. New York

Sacilik, K. (2007). Effect of drying methods on thin-layer drying characteristics of hull less seed pumpkin (*Cucurbita pepo* L.). J. Food Eng. 79: 23-30.

Saeed, I.E., Sopian, K & Zainol, A. Z. (2008) Thin-layer drying of Roselle Mathematical modeling and drying experiments. Agricultural engineering international : CIGR Journal S 1-22.

Sajith, K. G. & Muraleedharan, C. (2004) Economic Analysis of a Hybrid Photovoltaic/Thermal Solar Dryer for drying Amla. International Journal of Engineering Research and Technology. 3,(8) :907 – 911.

Samapundo, S., Devlieghere, F., Meulenaer, B. D., Atukwase, A., Lamboni, Y., & Debevere, J. M. (2007). Sorption isotherms and isosteric heats of sorption of whole yellow dent corn. Journal of Food Engineering, 79(1), 168-175.

Samira, N., Nasrin, E., Arefe, P. N. & Majid, G. F. (2015) Mathematical modeling of drying of potato slices in a forced convective dryer based on important parameters. Food science and nutrition. 110 – 118

Schutz, H. G. & Cardello, A. V. (2001) A labeled affective magnitude (LAM) scale for assessing food liking/disliking. Journal of sensory studies. 16:117 – 159.

Senudeera, W. & Klaugalage, I. S. (2004) Performance evaluation of an affordable solar dryer for drying crops. In proceedings biennial conference of the society of Engineering in Agriculture 2004, Dubbo, Australia.

Shahi, N. C., Anupama, Singh. & Kate A.E. (2014) Activation energy kinetics in thin layer drying of basil leaves. International Journal of science Research 3, (7): 1836-1840.

Shahzad, F., Ruhi, T. & Vishal, K. (2013) Performance Evaluation and Process Optimization of Potato Drying using Hot Air Oven. Journal of Food Processing and Technology. 4,(10) :1 – 9

Shekhar, F. L. & Bawane N. G. (2012) Drying rate analysis of different size paddy processed under various condition in L. S. U. Dryer. International Journal of Engineering Research and Technology. 1(7) 1 – 4

Shrivastava, A., Sandagar, P., Baja, I. & Singhal, R. (2008) Media optimization for the production of U-linolenic acid by cunninghamella echinulata varielegans MTCC 522 using response surface methodology. International Journal of food Engineering, 4(2), 1-32.

Singh, V., Singh S. K. & Maurga, S. (2010) Microwave poly (acrylic acid) modification of cassia javanica seed gum for efficient Hg (II) removal from solution. Chemical Engineering Journal. 160: 129-137.
.
Stuart, Barbara. (2004) Infrared spectroscopy: Fundamentals and applications. John Wiley and Sons Ltd. Inc USA.

Sturm, H., Schartel, B., Weib, A. & Braum, U. (2012) SEM/EDX: Advanced investigation of structured fire residues and residue formation. Elsevier on polymer texting. 31: 606-619 of opalinus clay (mont Terri, Switzerland). Insights from representative 2D BIB-SEM investigations on mm to mm scale. Elsevier on Applied clay science. 71:82-97.

Sukanya, W. & Michael, O'M. (2014) The 9-point hedonic scale and hedonic ranking in food science: some reappraisals and alternatives. Journal of the Science of Food and Agriculture. 1-13

Sushrut, S. H., Prajmal, S., Naveen, H., Karthik H. & Siddharth, Gokhale. (2015) Experimental Analysis of solar air Dryer for Agricultural products. International Research Journal of Engineering and Technology. 2(3): 1517-1523.

Taran, M. & Aghaie, E. (2015).Designing and optimization of separation process of iron impurities from kaolin by oxalic acid in bench-scale stirred-tank reactor. Applied clay science. 107, 109-116.

Tinuade J. A., Toyosi, Y. T. & Oluseyun, J. O. (2014) Influence of drying conditions on the effective moisture diffusivity and energy requirements of ginger slices. Journal of food research 3, (5): 103-112.

Togrul, I. T. & Pehlivan, D. (2002). Mathematical modeling of solar drying of apricots in thin layers. Journal of food engineering, 55: 209–216.

Tribeni, D. & Tiwari, G.N. (2008) Heat and mass transfer of green house fish drying under forced convection mode. International Journal of Agricultural research, 3:69-76.

Tunde –Akin, T.Y & Afon, A. A. (2009) Modelling of Hot-Air Drying of Pretreated cassava chips. Agricultural Engineering international. 1493:1-11.

Ugonna C.U, Jolaoso M. O. & Onwualu A. P. (2013) A technical appraisal of potato value chain in Nigeria. International Research Journal of Agricultural Science and Soil Science. 3 (8) : 291-301.

UN Report (2013) Department of Economic and Social Affairs. http://sustainabledevelopment.un.org/topics

Vasiliki, P. O., Magdalini, K. K. & Vaios, T. K. (2011). The influence of freeze drying conditions on microstructural changes of food products. Elsevier. Procedia food science 1, 647-654.

Vyazoykin, S.(2012) Thermogravimetric analysis. Characterization of materials. Seconded. John Wiley and Sons Inc. USA, pp:1-12.

Wang Y, Zhang M, Mujumdar AS, Mothibe K.J & Azam SMR (2012). Effect of blanching on microwave freeze drying of stem lettuce cubes in a circular conduit drying chamber. *Journal of Food Engineering*, 113: 177-185.

Wang, S., F. Chen, J. Wu, Z. Wang, X. Liao & X. Hu, (2007). Optimization of pectinextraction assisted by microwave from apple performance using response surface methodology. Journal of food engineering, 78, 693-700.

Wang, Z., Sun, J., Liao, X., Chen, F., Zhao, G., Wu, J. & X. Hu, (2007a). Mathematical Modeling on hot air drying of thin layer apple pomace. Food research international 40:39-46.

Wankhade, P. K., Sapkal, R. S. & Sapkal, V. S. (2012) Drying Characteristics of Okra Slices using Different Drying Methods by Comparative Evaluation. Proceedings of the World Congress on Engineering and Computer Science San Francisco, US October 24-26, 2012.

Whitaker, S. (1977) Simultaneous heat, mass and moisture transfer in porous media: a theory of drying. Advances in heat transfer, 13, 119-203.

www.foodsafetysite.com/foreducatorscompetencies/generalbacteriaexplanation/

   wateractivity. Retrieved 22 May, 2016.

APPENDIX A

Table A.1: Density Analysis

Material	TRUE DENSITY	BULK DENSITY	TAPPED DENSITY	COMPRESSIBLITY INDEX	POROSITY
UDP	1.15	0.601	1.128	46.71986	0.477391
UDC	1.33	0.823	1.286	36.00311	0.381203
SDP	0.777	0.508	0.684	25.73099	0.346203
CDP	0.832	0.476	0.664	28.31325	0.427885
PDP	0.89	0.516	0.724	28.72928	0.420225
ODP	0.925	0.528	0.731	27.77018	0.429189
SDC	0.851	0.524	0.708	25.9887	0.384254
CDC	1.053	0.48	0.692	30.63584	0.54416
PDC	1.108	0.544	0.717	24.12831	0.509025
ODC	0.95	0.531	0.725	26.75862	0.441053

Table A.2: Thermal Properties

Material	WC	AC	PC	CF	FC	CC	K	Cp	α
UDP	0.684	0.0495	0.0187	0.051	0.0405	0.1518	0.450731	3.249021	0.000121
UDC	0.728	0.0545	0.0109	0.071	0.021	0.1146	0.463297	3.328971	0.000105
SDP	0.2465	0.1285	0.021	0.054	0.055	0.495	0.296123	2.054839	0.000185
CDP	0.258	0.097	0.028	0.053	0.052	0.462	0.290895	2.029446	0.000172
PDP	0.2445	0.0745	0.0365	0.052	0.059	0.462	0.282465	1.980633	0.00016
ODP	0.252	0.1325	0.0205	0.0565	0.0485	0.49	0.297485	2.060332	0.000156
SDC	0.2655	0.1385	0.0135	0.1075	0.0305	0.4445	0.290785	2.005123	0.00017
CDC	0.2735	0.1235	0.0175	0.1045	0.0285	0.4525	0.2957	2.040305	0.000138
PDC	0.267	0.1195	0.0195	0.104	0.0315	0.4585	0.29368	2.027994	0.000131

ODC	0.2715	0.1475	0.013	0.1115	0.026	0.4305	0.291183	2.007181	0.000153

WC = Water content; AC = Ash content; PC = Protein content

CF = Crude Fibre; FC = Fats content; CC = Carbohydrate Content

K = Thermal conductivity; Cp = Specific heat capacity

α = Thermal diffusivity

Table A.3: Average Daily variation of Temperature and Relative Humidity for November, 2015

Time (mins)	Ambient Temp (^{o}C)	Drying Chamber Temp (^{o}C)	Exit Temp (^{o}C)
0	38.1	69.5	46.2
15	38.3	70.3	47.3
30	39.7	73.2	47.7
45	41.8	76.1	48.3
60	43	76.6	48.5
75	42.2	76.7	48.4
90	41.5	76.9	45.8
105	40.6	72.9	46.4
120	40.1	70.8	43.7
135	40.6	66.5	41.6
150	37.3	59.1	42.3
165	38.2	61.8	43.5
180	37.1	61.9	46.2
195	35.6	58.5	44.5
210	34.2	54.7	42.4

Table A.4: Average Daily variation of Temperature and Relative Humidity for December, 2015

Time (mins)	Ambient Temp (^{o}C)	Drying Chamber Temp (^{o}C)	Exit Temp (^{o}C)
0	42.3	76.5	47.2
15	43.6	78.2	47.7
30	43.3	77.1	44.9
45	43.9	78.1	45.6
60	42.6	78.4	45.8
75	43.9	78.8	47.8
90	44.3	79.2	47.6
105	44.5	78.7	47.5
120	43.9	76.7	46.3
135	44.2	76.8	46.3
150	45.1	76.9	46.5
165	44.5	76.3	45.6
180	44.2	75.8	43.4
195	43.1	75.3	42.6
210	40.5	73.5	41.6
240	37.8	69	40.4
270	36.3	66.3	38.8

Table A.5: Average Daily variation of Temperature and Relative Humidity for January, 2016

Time (mins)	Ambient Temp (^{o}C)	Drying Chamber Temp (^{o}C)	Exit Temp (^{o}C)
0	36.7	72.3	46.5
15	37.8	73.5	45.6
30	39.2	76.7	43.4
45	41.5	76.9	46.2
60	41.8	75.8	47.3
75	41	78.8	47.7
90	40.7	76.9	48.3
105	41.2	75.3	46.8
120	38.8	75.6	47.4
135	41	73.4	46.5
150	36.9	75.6	45.8
165	38.7	73.4	46.4
180	39.9	71.1	43.7
195	40.5	69	41.6
210	38.7	67.5	42.3
240	36.3	66.5	40.7
270	35.6	65.8	38.5

Table A.6: Average Daily variation of Temperature and Relative Humidity for February, 2016

Time (mins)	Ambient Temp (^{o}C)	Drying Chamber Temp (^{o}C)	Exit Temp (^{o}C)
0	42.3	71.8	46.4
15	43.5	70.3	43.7
30	42.8	71.5	45.6
45	44.5	68.7	46.2
60	43.4	69.5	46.8
75	44.2	70.2	45.7
90	44.7	73.2	47.2
105	45.2	72.4	46
120	44.7	74.3	45.3
135	43.4	74.3	46.1
150	42.8	71.8	45.7
165	41.4	73.5	45.2
180	42.2	72.7	44.8
195	39.8	71.4	42.5
210	37.4	68.6	41.3

Table A. 7 Water Activity and Mold-free shelf life

Material	Mf	M	a_W	MFSL
UDP	54.7	1.207506	0.937595	2.067685
UDC	70.4	2.378378	0.982848	0.889058
SDP	13.93	0.161845	0.590663	1335.466
PDP	15.17	0.178828	0.611288	909.001
ODP	11.76	0.133273	0.550917	2802.675
CDP	13.31	0.153536	0.579814	1634.948
SDC	16.8	0.201923	0.636474	568.2776
PDC	16.41	0.196315	0.630631	633.7021
ODC	14.84	0.17426	0.605931	1004.517
CDC	14.06	0.163603	0.59289	1281.12

Table A. 8 Effect of Water activity (a_w) on Spoilage of Foods

a_w	Spoilage microorganism
0.90 – 1.00	Bacteria
0.85 – 0.9	Bacteria, molds, yeasts
0.80 – 0.85	Yeasts
0.75 – 0.80	Xerophilic molds, molds and yeasts
0.70 – 0.75	Yeasts
0.65 – 0.70	Osmophilic yeasts
0.60 – 0.65	Xerophilic molds, osmophilic yeasts

(www.foodsafetysite.com)

APPENDIX B
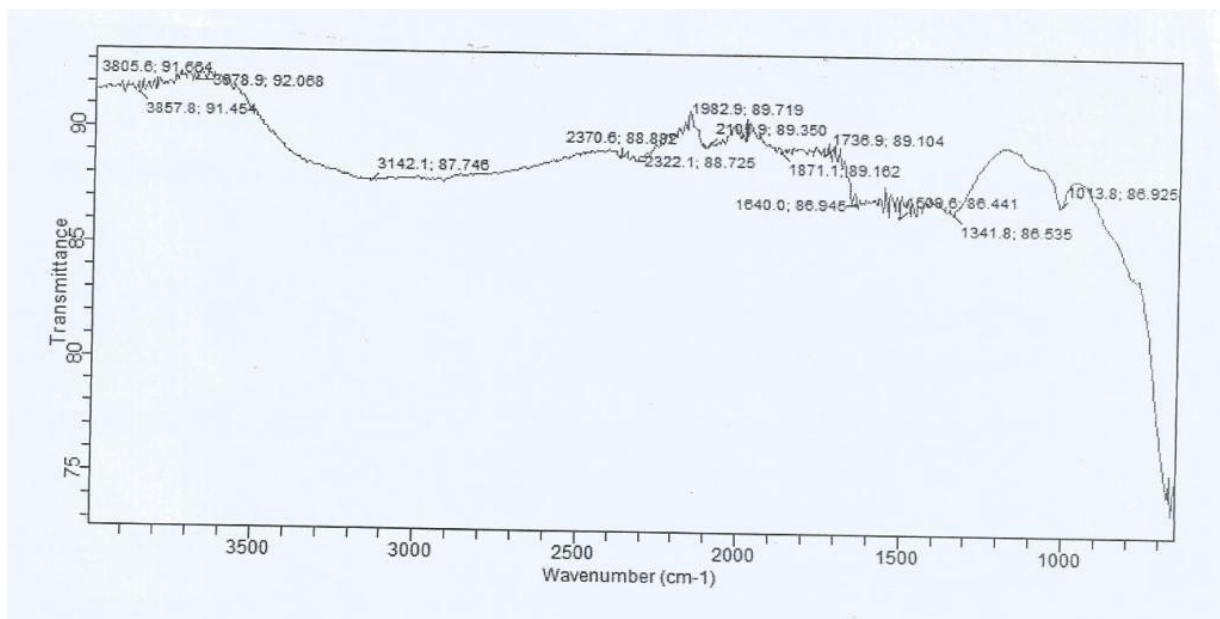
FTIR and SEM results
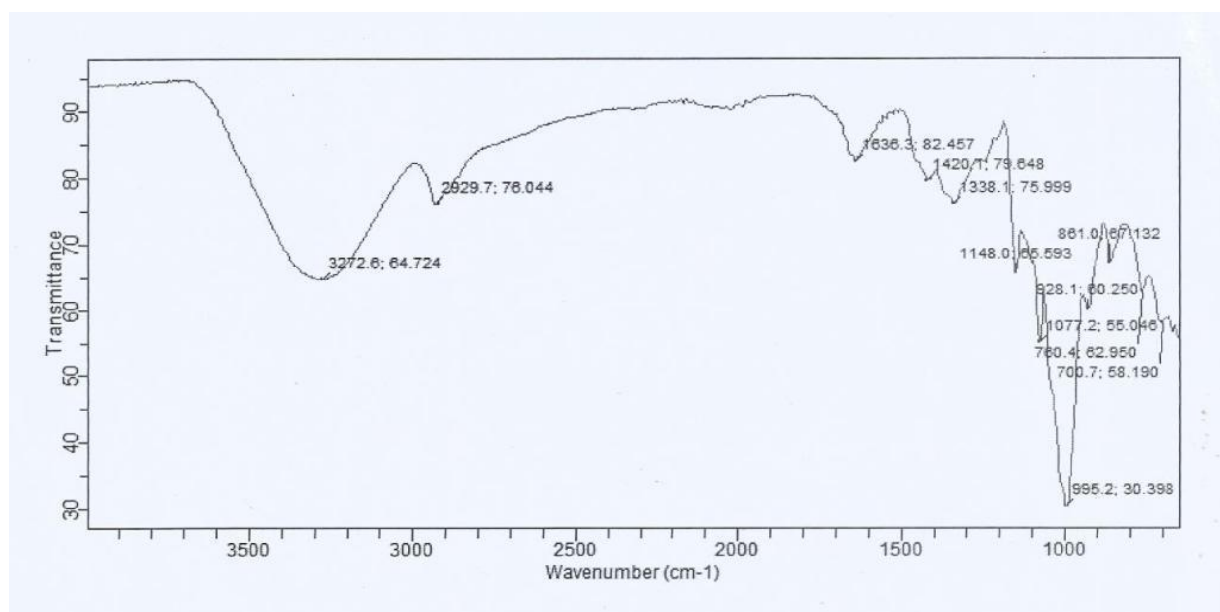

Figure B.1: FTIR Spectrum for UDP
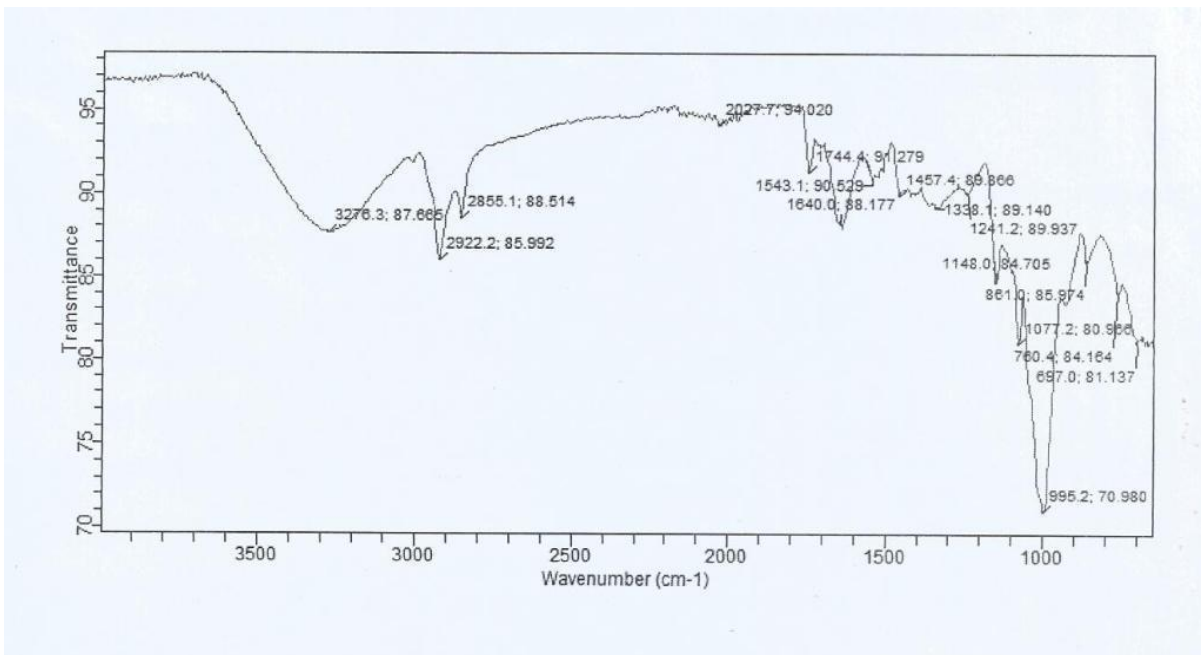

Figure B.2: FTIR Spectrum for UDC
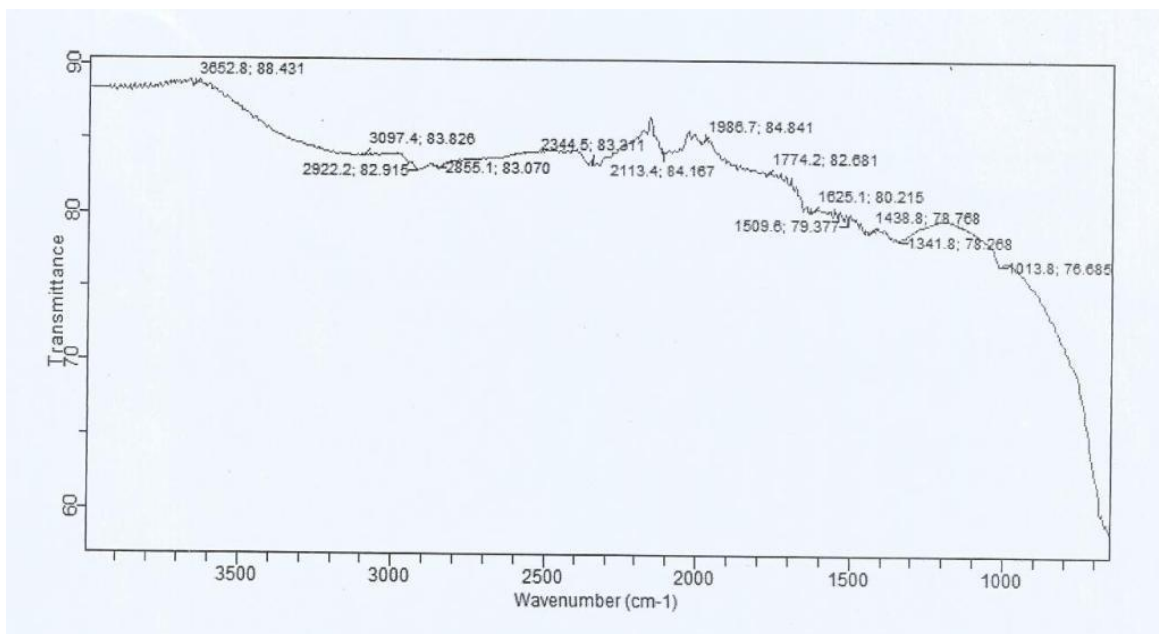
Figure B.3: FTIR Spectrum for SDP

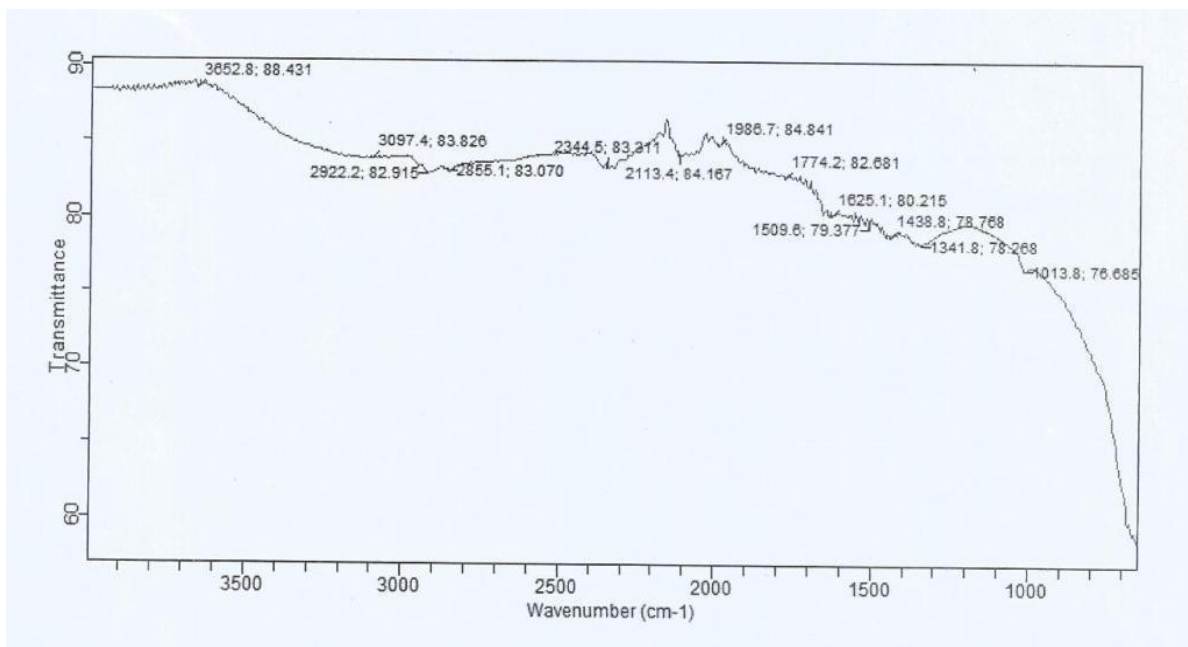Figure B.4: FTIR Spectrum for CDP

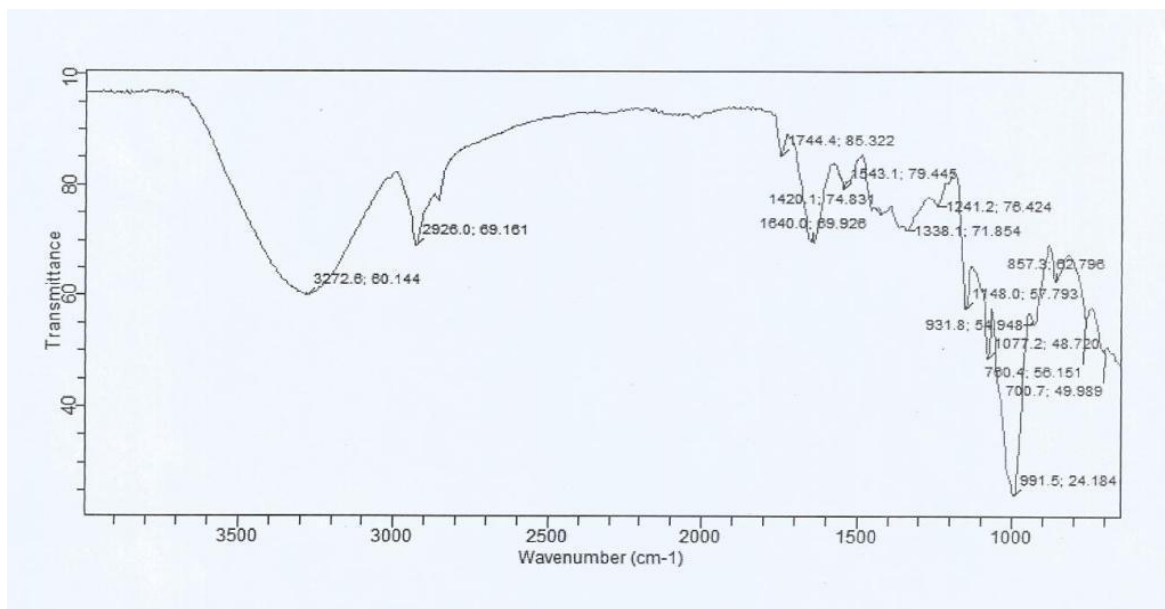Figure B.5: FTIR Spectrum for PDP

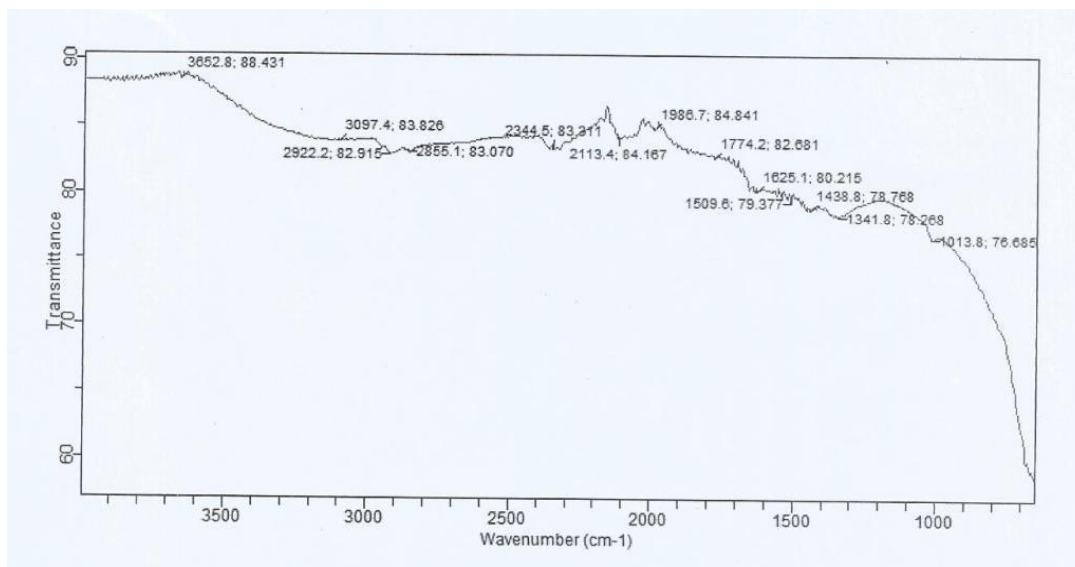Figure B.6: FTIR Spectrum for ODP

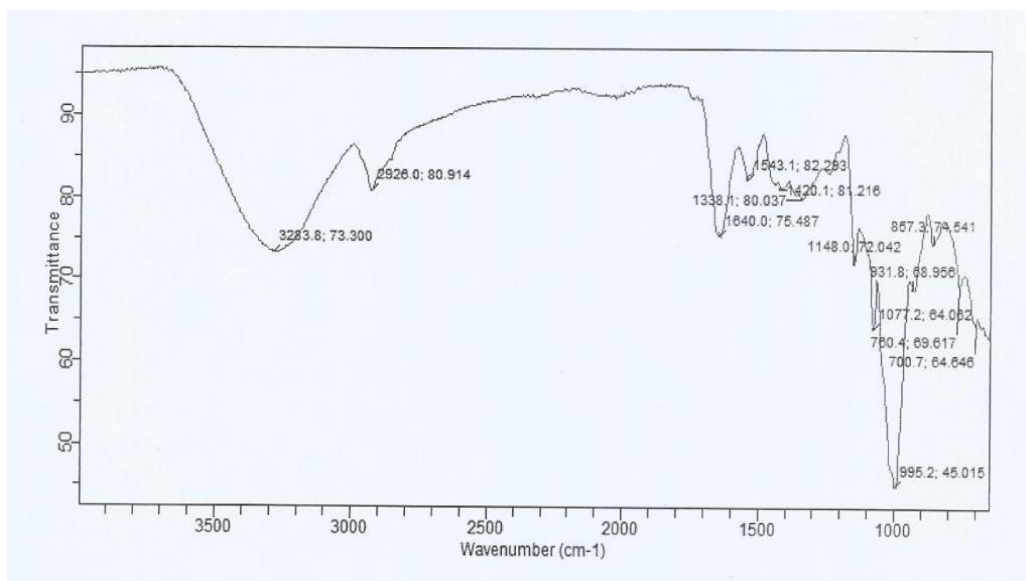Figure B.7: FTIR Spectrum for PDC
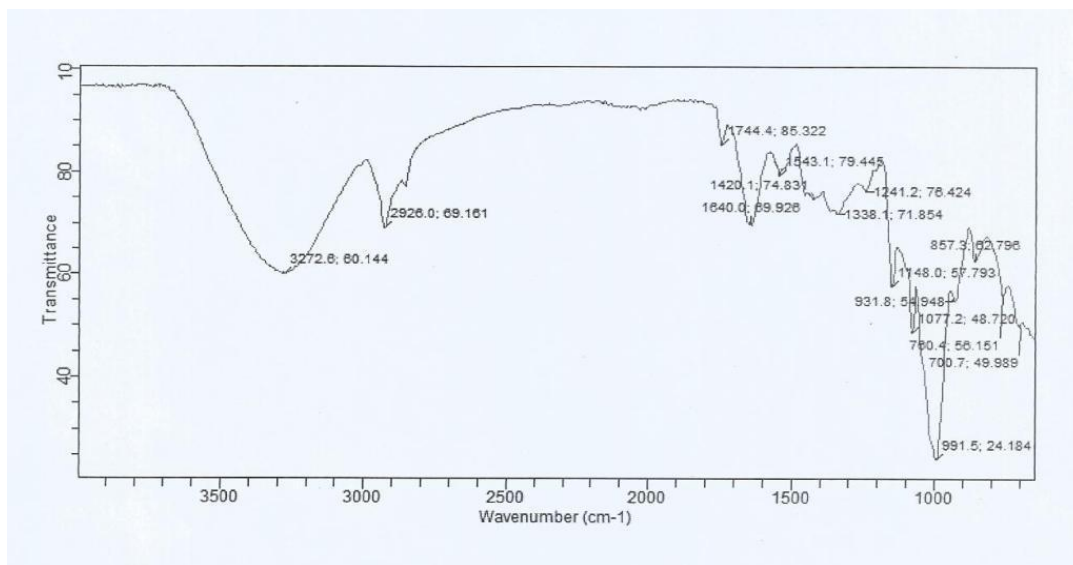

Figure B.8: FTIR Spectrum for PDC

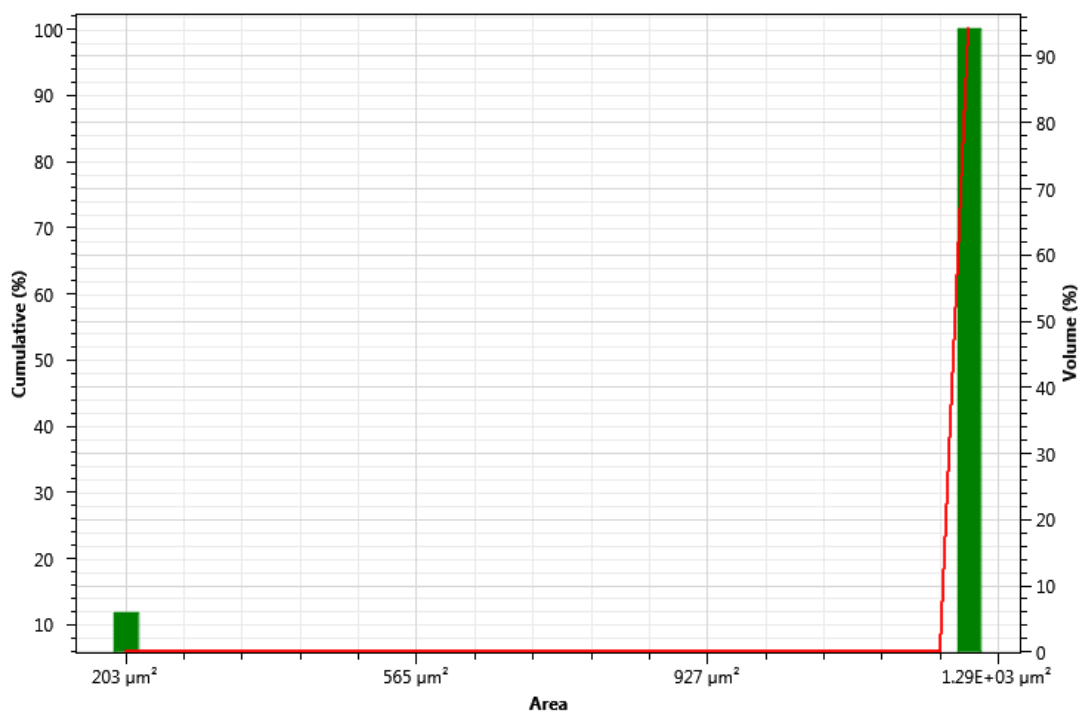Figure B.9: FTIR Spectrum for ODC

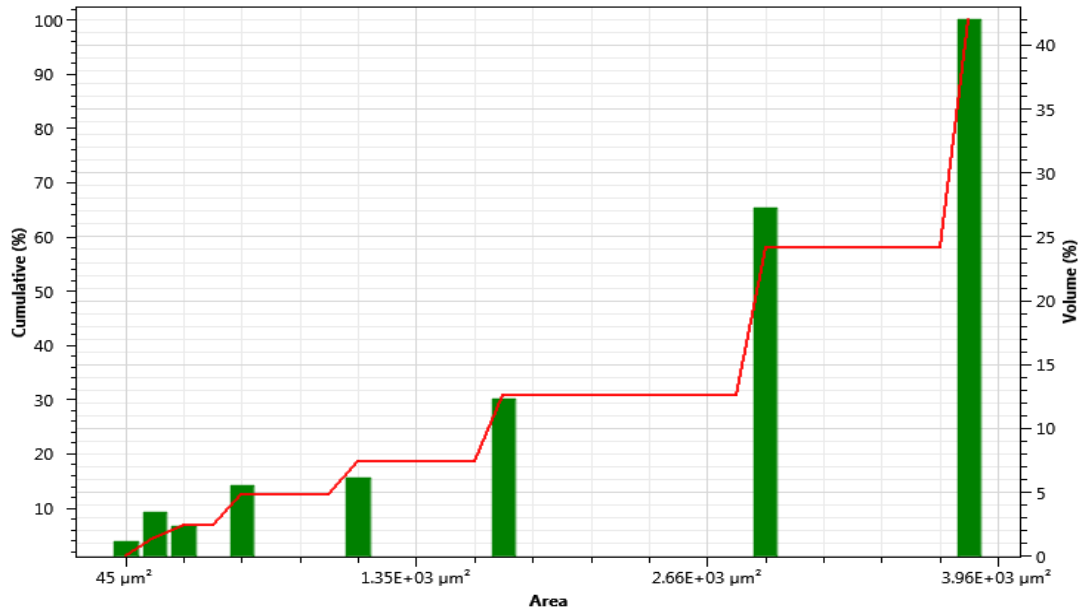Figure B.10 SEM cumulative graph for UDP

317

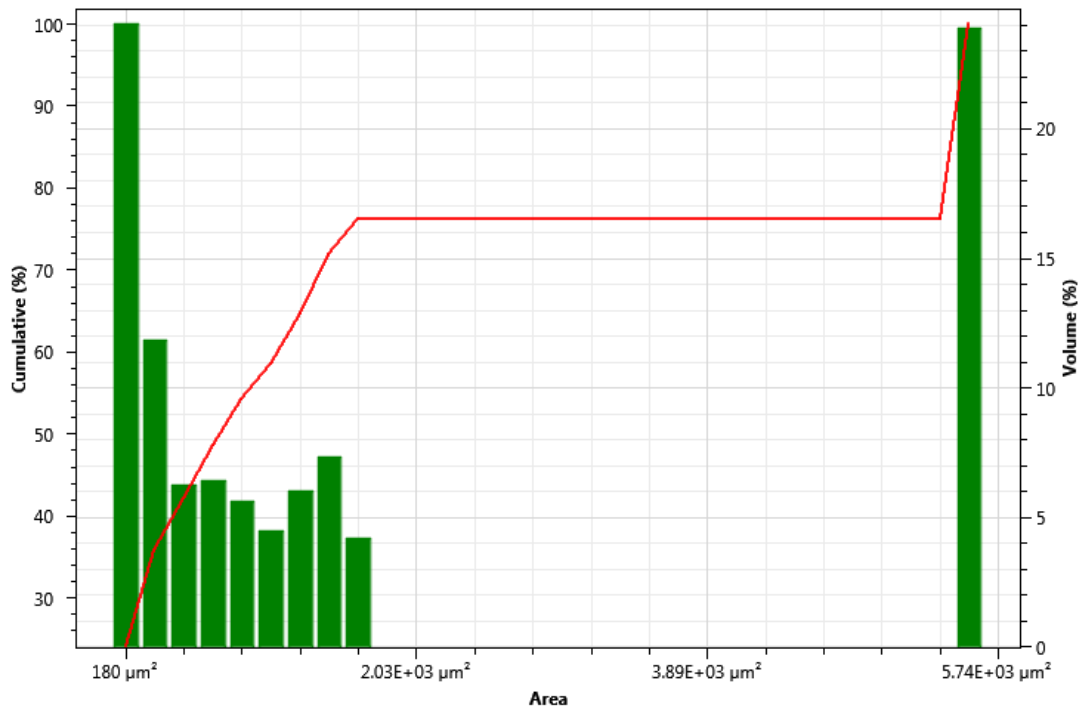Figure B.11 SEM cumulative graph for UDC

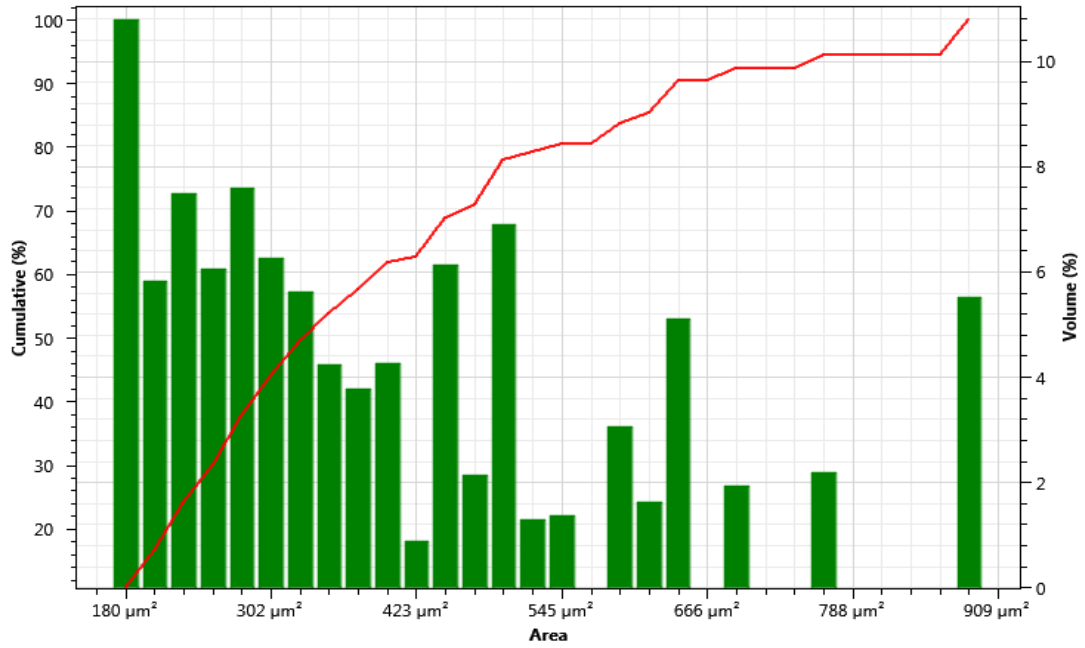Figure B.12 SEM cumulative graph for SDP

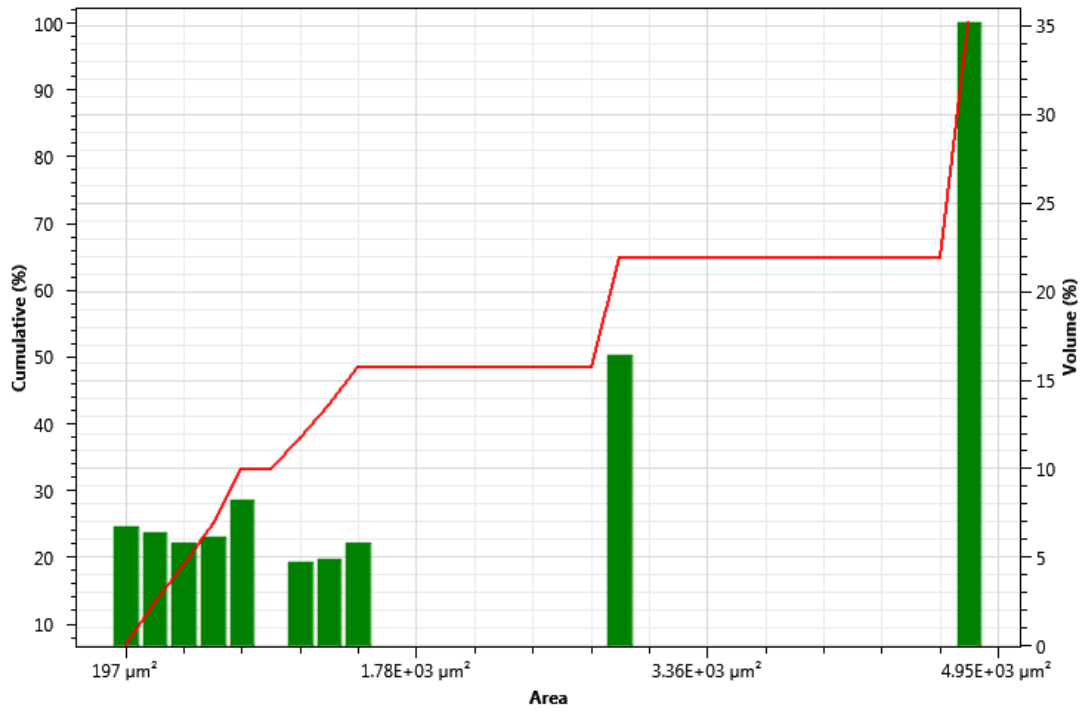Figure B.13 SEM cumulative graph for ODP

Figure B.14 SEM cumulative graph for PDC

APPENDIX C

CALCULATION OF EFFICIENCY

Table C.1: Calculation of system efficiency for 2mm slice potato

Time, h	Time Interval	Me (kg)	L	I_c	Sun A	Solar A	T	Sun Eff	Solar Eff
1	1	0.0303	2264.76	250	0.4	0.45	0.7	0.6862223	0.871393
2	1	0.0187	2264.76	250	0.4	0.45	0.7	0.4235101	0.537791
3	1	0.0088	2264.76	250	0.4	0.45	0.7	0.1992989	0.253078
4	1	0.0042	2264.76	250	0.4	0.45	0.7	0.0951199	0.120787
5	1	0.0017	2264.76	250	0.4	0.45	0.7	0.0385009	0.04889
6	1	0.0007	2264.76	250	0.4	0.45	0.7	0.0158533	0.020131

Table C.2: Calculation of system efficiency for 4mm slice potato

Time	Time	Me (kg)	L	I_c	Sun A	Solar A	τ	Sun Eff	Solar Eff
1	1	0.0233	2264.76	250	0.4	0.45	0.7	0.5276891	0.670081
2	1	0.0128	2264.76	250	0.4	0.45	0.7	0.2898893	0.368113
3	1	0.0097	2264.76	250	0.4	0.45	0.7	0.2196817	0.278961
4	1	0.0061	2264.76	250	0.4	0.45	0.7	0.1381504	0.175429
5	1	0.0052	2264.76	250	0.4	0.45	0.7	0.1177675	0.149546
6	1	0.0047	2264.76	250	0.4	0.45	0.7	0.1064437	0.135167

Table C.3: Calculation of system efficiency for 6mm slice potato

Time	Time	Me (kg)	L	I_c	Sun A	Solar A	τ	Sun Eff	Solar Eff
1	1	0.0156	2264.76	250	0.4	0.45	0.7	0.3533026	0.448638
2	1	0.0083	2264.76	250	0.4	0.45	0.7	0.1879751	0.238699
3	1	0.0083	2264.76	250	0.4	0.45	0.7	0.1879751	0.238699
4	1	0.0093	2264.76	250	0.4	0.45	0.7	0.2106227	0.267457
5	1	0.0069	2264.76	250	0.4	0.45	0.7	0.1562684	0.198436
6	1	0.0063	2264.76	250	0.4	0.45	0.7	0.1426799	0.181181

Table C.4: Calculation of system efficiency for 2mm slice cocoyam

Time	Time	Me (kg)	L	I_c	Sun A	Solar A	τ	Sun Eff	Solar Eff
1	1	0.0345	2264.76	250	0.4	0.45	0.7	0.7813422	0.992181
2	1	0.0139	2264.76	250	0.4	0.45	0.7	0.3148016	0.399748
3	1	0.0109	2264.76	250	0.4	0.45	0.7	0.2468588	0.313472
4	1	0.0071	2264.76	250	0.4	0.45	0.7	0.160798	0.204188
5	1	0.0031	2264.76	250	0.4	0.45	0.7	0.0702076	0.089152
6	1	0.0018	2264.76	250	0.4	0.45	0.7	0.0407657	0.051766

Table C.5: Calculation of system efficiency for 4mm slice cocoyam

Time, h	Time, h	Me (kg)	L	I_c (W/m^2)	Sun A (cm^2)	Solar A (cm^2)	τ	Sun Eff	Solar Eff
1	1	0.019	2264.76	250	0.4	0.45	0.7	0.4303044	0.546418
2	1	0.0141	2264.76	250	0.4	0.45	0.7	0.3193312	0.4055
3	1	0.0098	2264.76	250	0.4	0.45	0.7	0.2219465	0.281837
4	1	0.0087	2264.76	250	0.4	0.45	0.7	0.1970341	0.250202
5	1	0.0078	2264.76	250	0.4	0.45	0.7	0.1766513	0.224319
6	1	0.005	2264.76	250	0.4	0.45	0.7	0.113238	0.143794

Table C.6: Calculation of system efficiency for 6mm slice cocoyam

Time, h	Time, h	Me (kg)	L	I_c (W/m^2)	Sun A (cm^2)	Solar A (cm^2)	τ	Sun Eff	Solar Eff
1	1	0.0171	2264.76	250	0.4	0.45	0.7	0.387274	0.491776
2	1	0.0123	2264.76	250	0.4	0.45	0.7	0.2785655	0.353734
3	1	0.0078	2264.76	250	0.4	0.45	0.7	0.1766513	0.224319
4	1	0.0059	2264.76	250	0.4	0.45	0.7	0.1336208	0.169677
5	1	0.0062	2264.76	250	0.4	0.45	0.7	0.1404151	0.178305
6	1	0.0062	2264.76	250	0.4	0.45	0.7	0.1404151	0.178305

CALCULATION OF ENERGY USED IN THE DRYER

Table C.7: Calculation of total energy and SEC in photovoltaic drying of potato

Velocity, m/s	Time, h	Me (kg)	L	I_c (W/m^2)	Sun A (cm^2)	Solar A (cm^2)	τ	Sun Eff	Solar Eff
1	3.75	36	59	23	1.0634	1.006091	18.45537	0.064	288.3652
1.5	3.5	36	62	26	1.053877	1.006317	28.95258	0.064	452.3841
2	3.25	36	64	28	1.047622	1.006472	38.38027	0.064	599.6916
3	3	36	67	31	1.038379	1.006712	58.33043	0.064	911.4129
3.5	2.75	36	68.8	32.8	1.03291	1.006859	65.66532	0.064	1026.021

Table C.8: Calculation of total energy and SEC in photovoltaic drying of cocoyam

Velocity, m/s	Time, h	Me (kg)	L	I_c (W/m^2)	Sun A (cm^2)	Solar A (cm^2)	τ	Sun Eff	Solar Eff
1	3.5	35.5	59.6	24.1	1.061482	1.006135	18.01706	0.07	257.3866
1.5	3.5	36	63	27	1.05074	1.006394	29.97896	0.07	428.2709
2	3.25	35.5	65.3	29.8	1.043597	1.006575	40.69476	0.07	581.3537
3	3	35.5	67	31.5	1.038379	1.006712	59.27124	0.07	846.732
3.5	2.75	36	69.7	33.7	1.030198	1.006934	67.29493	0.07	961.3562

Table C.9: Calculation of total energy and SEC in oven drying of potato

Temp	Velocity (m/s)	Time h	Ambient Temp	Drying Temp	ΔT (K)	Density (g/m³)	heat capacity	T Energy (KWh)		SEC (Kwh/kg
60	1.5	5.5	33	60	27	1.060207	1.006165	16.63319	0.064	259.893
70	1.5	4	34	70	36	1.029297	1.006959	15.67128	0.064	244.863
80	1.5	3.1	34	80	46	1.000138	1.007841	15.09249	0.064	235.820
90	1.5	2.5	33.5	90	56.5	0.972586	1.008807	14.55171	0.064	227.370

Table C.10: Calculation of total energy and SEC in oven drying of cocoyam

Temp	Velocity (m/s)	Time h	Ambient Temp	Drying Temp	ΔT (K)	Density (g/m³)	heat capacity	T Energy (KWh)		SEC (Kwh/kg
60	1.5	5.8	33	60	27	1.060207	1.006165	17.54045	0.07	250.5779
70	1.5	4.3	34.5	70	35.5	1.029297	1.006959	16.61264	0.07	237.3234
80	1.5	3.3	34	80	46	1.000138	1.007841	16.0662	0.07	229.5171
90	1.5	2.7	34.5	90	55.5	0.972586	1.008807	15.43769	0.07	220.5384

Table C.11: Effect of slice thickness on the drying of potato

Temp	Velocity (m/s)	Time h	Ambient Temp	Drying Temp	ΔT (K)	Density (g/m³)	heat capacity	T Energy (KWh)		SEC (Kwh/kg)
2mm	1.8	4.67	33.5	50	16.5	1.09303	1.005461	10.67011	0.064	166.7204
4mm	1.8	6	34.3	50	15.7	1.09303	1.005461	13.04424	0.064	203.8163
6mm	1.8	7.17	35	50	15	1.09303	1.005461	14.89287	0.064	232.701

Table C.12: Effect of slice thickness on the drying of cocoyam

Temp	Velocity (m/s)	Time h	Ambient Temp	Drying Temp	ΔT (K)	Density (g/m³)	heat capacity	T Energy (KWh)		SEC (Kwh/kg)
2mm	1.8	4.83	33	50	17	1.09303	1.005461	11.37009	0.07	162.4299
4mm	1.8	7	34.5	50	15.5	1.09303	1.005461	15.02442	0.07	214.6345
6mm	1.8	8	34	50	16	1.09303	1.005461	17.72466	0.07	253.2094

APPENDIX D

CONVECTIVE HEAT TRANSFER COEFFICIENT

Table D.1 Convective heat transfer coefficient for 2 mm slice thick potato

Time h	T_i	M_e	R.H %	K_v	C_p	μ_v	ρ_v	n	C	h_c
1	36.35	0.0303	0.313	0.026862	1004.555	1.89E-05	1.141971	0.032	0.712	4.698392
2	37.15	0.0187	0.285	0.026916	1004.676	1.89E-05	1.139027	0.032	0.712	4.695566
3	38.25	0.0088	0.268	0.026991	1004.842	1.89E-05	1.135003	0.032	0.712	4.722881
4	40.75	0.0042	0.253	0.02716	1005.222	1.91E-05	1.125964	0.032	0.712	4.748262
5	38.5	0.0017	0.243	0.027008	1004.88	1.9E-05	1.134093	0.032	0.712	4.694322
6	38	0.0007	0.258	0.026974	1004.804	1.89E-05	1.135915	0.032	0.712	4.689277

Table D.2 Convective heat transfer coefficient for 4 mm slice thick potato

Time h	T_i	M_e	R.H %	K_v	C_p	μ_v	ρ_v	n	C	h_c
1	36.65	0.0233	0.323	0.026882	1004.6	1.89E-05	1.140865	0.111	1.763	11.52393
2	37.7	0.0128	0.282	0.026953	1004.759	1.89E-05	1.137011	0.111	1.763	11.04725
3	38.65	0.0097	0.266	0.027018	1004.903	1.9E-05	1.133547	0.111	1.763	11.51944
4	40.05	0.0061	0.258	0.027113	1005.115	1.9E-05	1.12848	0.111	1.763	11.14927
5	38.9	0.0052	0.253	0.027035	1004.941	1.9E-05	1.132639	0.111	1.763	10.96616
6	39.45	0.0047	0.247	0.027072	1005.024	1.9E-05	1.130646	0.111	1.763	11.09514
7	37	0.0031	0.255	0.026906	1004.653	1.89E-05	1.139578	0.111	1.763	11.0838

Table D.3 Convective heat transfer coefficient for 6 mm slice thick potato

Time h	Ti	Me	R.H %	Kv	Cp	μv	ρv	n	C	hc
1	36.4	0.0156	0.317	0.026865	1004.562	1.89E-05	1.141786	0.083	1.19	7.730516
2	38.2	0.0083	0.275	0.026987	1004.835	1.89E-05	1.135185	0.083	1.19	7.600654
3	38.55	0.0083	0.267	0.027011	1004.888	1.9E-05	1.133911	0.083	1.19	7.747013
4	40.3	0.0093	0.253	0.02713	1005.153	1.9E-05	1.12758	0.083	1.19	7.520822
5	39.9	0.0069	0.248	0.027102	1005.093	1.9E-05	1.129021	0.083	1.19	7.753516
6	39.9	0.0063	0.239	0.027102	1005.093	1.9E-05	1.129021	0.083	1.19	7.596268
7	38.35	0.005	0.245	0.026997	1004.858	1.9E-05	1.134639	0.083	1.19	7.565049
8	36.95	0.0021	0.279	0.026903	1004.646	1.89E-05	1.139761	0.083	1.19	7.495166

Table D.4 Convective heat transfer coefficient for 2 mm slice thick cocoyam

Time h	Ti	Me	R.H %	Kv	Cp	μv	ρv	n	C	hc
1	36.35	0.0345	0.313	0.026862	1004.555	1.89E-05	1.141971	0.04	0.753	4.947229
2	37.15	0.0139	0.285	0.026916	1004.676	1.89E-05	1.139027	0.04	0.753	4.941019
3	38.25	0.0109	0.268	0.026991	1004.842	1.89E-05	1.135003	0.04	0.753	4.973537
4	40.75	0.0071	0.253	0.02716	1005.222	1.91E-05	1.125964	0.04	0.753	4.999146
5	38.5	0.0031	0.243	0.027008	1004.88	1.9E-05	1.134093	0.04	0.753	4.935198
6	38	0.0018	0.258	0.026974	1004.804	1.89E-05	1.135915	0.04	0.753	4.930115

Table D.5 Convective heat transfer coefficient for 4 mm slice thick cocoyam

Time h	Ti	Me	R.H %	Kv	Cp	μv	ρv	n	C	hc
1	36.65	0.019	0.323	0.026882	1004.6	1.89E-05	1.140865	0.106	1.719	11.25039
2	37.7	0.0141	0.282	0.026953	1004.759	1.89E-05	1.137011	0.106	1.719	10.80685
3	38.65	0.0098	0.266	0.027018	1004.903	1.9E-05	1.133547	0.106	1.719	11.24874
4	40.05	0.0087	0.258	0.027113	1005.115	1.9E-05	1.12848	0.106	1.719	10.90503
5	38.9	0.0078	0.253	0.027035	1004.941	1.9E-05	1.132639	0.106	1.719	10.73253
6	39.45	0.005	0.247	0.027072	1005.024	1.9E-05	1.130646	0.106	1.719	10.85372
7	37	0.0033	0.255	0.026906	1004.653	1.89E-05	1.139578	0.106	1.719	10.84013

Table D.6 Convective heat transfer coefficient for 6 mm slice thick cocoyam

Time h	Ti	Me	R.H %	Kv	Cp	μv	ρv	n	C	hc
1	36.4	0.0171	0.317	0.026865	1004.562	1.89E-05	1.141786	0.094	1.27	8.213861
2	38.2	0.0123	0.275	0.026987	1004.835	1.89E-05	1.135185	0.094	1.27	8.052934
3	38.55	0.0078	0.267	0.027011	1004.888	1.9E-05	1.133911	0.094	1.27	8.227819
4	40.3	0.0059	0.253	0.02713	1005.153	1.9E-05	1.12758	0.094	1.27	7.951668
5	39.9	0.0062	0.248	0.027102	1005.093	1.9E-05	1.129021	0.094	1.27	8.231953
6	39.9	0.0062	0.239	0.027102	1005.093	1.9E-05	1.129021	0.094	1.27	8.043131
7	38.35	0.0058	0.245	0.026997	1004.858	1.9E-05	1.134639	0.094	1.27	8.009825
8	36.95	0.0049	0.279	0.026903	1004.646	1.89E-05	1.139761	0.094	1.27	7.929775

Table D.7 Convective heat transfer coefficient for 50g mass cocoyam

Time h	Ti	Me	R.H %	Kv	Cp	μv	ρv	n	C	hc
1	34.95	0.0198	0.305	0.026767	1004.343	1.88E-05	1.14716	0.069	0.86	5.50523
2	35.9	0.0093	0.287	0.026832	1004.487	1.88E-05	1.143634	0.069	0.86	5.458483
3	36.65	0.0046	0.262	0.026882	1004.6	1.89E-05	1.140865	0.069	0.86	5.456961
4	36.15	0.0021	0.238	0.026848	1004.525	1.89E-05	1.142709	0.069	0.86	5.585356

Table D.8 Convective heat transfer coefficient for 100g mass cocoyam

Time h	Ti	Me	R.H %	Kv	Cp	μv	ρv	n	C	hc
1	35.35	0.0345	0.317	0.026794	1004.404	1.88E-05	1.145673	0.09	1.377	8.604343
2	36.4	0.0136	0.298	0.026865	1004.562	1.89E-05	1.141786	0.09	1.377	8.564627
3	36.45	0.0112	0.301	0.026869	1004.57	1.89E-05	1.141602	0.09	1.377	8.508334
4	37.2	0.0071	0.275	0.02692	1004.683	1.89E-05	1.138843	0.09	1.377	8.710559
5	36.25	0.0031	0.252	0.026855	1004.54	1.89E-05	1.14234	0.09	1.377	8.544142
6	35.6	0.0016	0.259	0.026811	1004.442	1.88E-05	1.144745	0.09	1.377	8.749996

Table D.9 Convective heat transfer coefficient for 200g mass cocoyam

Time h	Ti	Me	R.H %	Kv	Cp	μv	ρv	n	C	hc
1	35.1	0.0647	0.302	0.026777	1004.366	1.88E-05	1.146602	0.293	2.14	10.53179
2	36.2	0.037	0.284	0.026852	1004.532	1.89E-05	1.142525	0.293	2.14	9.262595
3	37.05	0.0149	0.253	0.026909	1004.661	1.89E-05	1.139394	0.293	2.14	8.273863
4	38.2	0.0086	0.245	0.026987	1004.835	1.89E-05	1.135185	0.293	2.14	9.925246
5	37.6	0.0075	0.235	0.026947	1004.744	1.89E-05	1.137377	0.293	2.14	10.51115
6	36.6	0.0059	0.238	0.026879	1004.593	1.89E-05	1.141049	0.293	2.14	10.86784
7	35.2	0.0021	0.253	0.026784	1004.381	1.88E-05	1.14623	0.293	2.14	11.04455

Table D.10 Convective heat transfer coefficient for 300g mass cocoyam

Time h	Ti	Me	R.H %	Kv	Cp	μv	ρv	n	C	hc
1	35.85	0.132	0.314	0.026828	1004.479	1.88E-05	1.143819	0.262	2.396	13.67989
2	36.8	0.0487	0.298	0.026892	1004.623	1.89E-05	1.140313	0.262	2.396	12.70231
3	37.6	0.017	0.283	0.026947	1004.744	1.89E-05	1.137377	0.262	2.396	10.85694
4	37.9	0.0084	0.265	0.026967	1004.789	1.89E-05	1.13628	0.262	2.396	10.58782
5	36.95	0.005	0.245	0.026903	1004.646	1.89E-05	1.139761	0.262	2.396	9.461675
6	36.5	0.0024	0.238	0.026872	1004.577	1.89E-05	1.141418	0.262	2.396	11.57058
7	35.75	0.0013	0.247	0.026821	1004.464	1.88E-05	1.144189	0.262	2.396	11.68126
8	35.1	0.0009	0.258	0.026777	1004.366	1.88E-05	1.146602	0.262	2.396	11.57764

Table D.11 Convective heat transfer coefficient for 50g mass Potato

Time h	Ti	Me	R.H %	Kv	Cp	μv	ρv	n	C	hc
1	35.2	0.0172	0.307	0.026784	1004.381	1.88E-05	1.14623	-0.055	0.4	2.828921
2	36.15	0.0061	0.283	0.026848	1004.525	1.89E-05	1.142709	-0.055	0.4	2.824929
3	36.8	0.0039	0.262	0.026892	1004.623	1.89E-05	1.140313	-0.055	0.4	2.826763
4	36.9	0.0021	0.238	0.026899	1004.638	1.89E-05	1.139945	-0.055	0.4	2.805997

Table D.12 Convective heat transfer coefficient for 100g mass Potato

Time h	Ti	Me	R.H %	Kv	Cp	μv	ρv	n	C	hc
1	35.6	0.0291	0.313	0.026811	1004.442	1.88E-05	1.144745	0.061	0.636	4.036923
2	36.55	0.0187	0.298	0.026876	1004.585	1.89E-05	1.141233	0.061	0.636	4.037723
3	36.95	0.0088	0.301	0.026903	1004.646	1.89E-05	1.139761	0.061	0.636	4.014098
4	37.7	0.0042	0.275	0.026953	1004.759	1.89E-05	1.137011	0.061	0.636	4.052483
5	36.05	0.0017	0.252	0.026842	1004.509	1.88E-05	1.143079	0.061	0.636	4.069391
6	35.75	0.0011	0.259	0.026821	1004.464	1.88E-05	1.144189	0.061	0.636	4.098323

Table D.13 Convective heat transfer coefficient for 200g mass Potato

Time h	Ti	Me	R.H %	Kv	Cp	μv	ρv	n	C	hc
1	34.7	0.055	0.302	0.02675	1004.306	1.88E-05	1.148092	0.441	0.636	2.611375
2	36.5	0.0372	0.284	0.026872	1004.577	1.89E-05	1.141418	0.441	0.636	1.9151
3	37.2	0.0226	0.253	0.02692	1004.683	1.89E-05	1.138843	0.441	0.636	1.684026
4	38.4	0.0069	0.245	0.027001	1004.865	1.9E-05	1.134457	0.441	0.636	2.279451
5	37.55	0.0021	0.235	0.026943	1004.736	1.89E-05	1.13756	0.441	0.636	2.69769
6	36.7	0.0014	0.238	0.026886	1004.608	1.89E-05	1.140681	0.441	0.636	2.737102
7	35.4	0.0001	0.253	0.026798	1004.411	1.88E-05	1.145487	0.441	0.636	2.745858

Table D.14 Convective heat transfer coefficient for 400g mass Potato

Time h	Ti	Me	R.H %	Kv	Cp	μv	ρv	n	C	hc
1	36.65	0.1325	0.317	0.026882	1004.6	1.89E-05	1.140865	0.249	1.759	9.607727
2	37.3	0.0591	0.295	0.026926	1004.698	1.89E-05	1.138476	0.249	1.759	8.782319
3	37.7	0.0302	0.283	0.026953	1004.759	1.89E-05	1.137011	0.249	1.759	7.938032
4	37.8	0.0158	0.265	0.02696	1004.774	1.89E-05	1.136646	0.249	1.759	8.128441
5	37.05	0.0056	0.245	0.026909	1004.661	1.89E-05	1.139394	0.249	1.759	6.841383
6	36.85	0.0051	0.238	0.026896	1004.63	1.89E-05	1.140129	0.249	1.759	8.037013
7	35.9	0.003	0.247	0.026832	1004.487	1.88E-05	1.143634	0.249	1.759	8.478308
8	35.1	0.0019	0.258	0.026777	1004.366	1.88E-05	1.146602	0.249	1.759	8.638211

APPENDIX E

Table E1: Summary of P-values for PVDP

Source	Sequential p-value	Lack of Fit p-value	Adjusted R-Squared	Predicted R-Squared	
Linear	< 0.0001	< 0.0001	0.9287	0.9145	
2FI	0.0003	< 0.0001	0.9596	0.9506	
Quadratic	< 0.0001	< 0.0001	**0.9860**	**0.9780**	**Suggested**
Cubic	< 0.0002	< 0.0001	0.9977	0.9952	Aliased

Table E2: Lack of Fit Test for PVDP

Source	Sum of Squares	df	Mean Square	F-Value	p-value Prob> F	
Linear	661.78	11	60.16	862.09	< 0.0001	
2FI	336.99	8	42.12	603.61	< 0.0001	
Quadratic	**102.54**	**5**	**20.51**	**293.86**	< 0.0001	**Suggested**
Cubic	13.05	1	13.05	186.95	< 0.0001	Aliased
Pure Error	1.33	19	0.36			

Table E3: Sequential Model Sum of Squares for PVDP

Source	Sum of Squares	df	Mean Square	F Value	p-value Prob> F	
Mean vs Total	64492.08	1	64492.08			
Linear vs Mean	9571.20	3	3190.40	144.34	< 0.0001	
2FI vs Linear	324.79	3	108.26	8.64	0.0003	

Quadratic vs 2FI	234.45	3	78.15	18.06	< 0.0001	Suggested
Cubic vs Quadratic	89.49	4	22.37	31.13	< 0.0002	Aliased
Residual	14.37	20	0.72			
Total	74726.38	34	2197.83			

Table E4: Summary of P-values for HADP

Source	Sequential p-value	Lack of Fit p-value	Adjusted R-Squared	Predicted R-Squared	
Linear	< 0.0001	< 0.0001	0.9260	0.9112	
2FI	0.0021	< 0.0001	0.9517	0.9484	
Quadratic	< 0.0001	0.0003	**0.9915**	**0.9879**	**Suggested**
Cubic	0.0001	0.3156	0.9966	0.9962	Aliased

Table E5: Sequential Model Sum of Squares for HADP

Source	Sum of Squares	df	Mean Square	F Value	p-value Prob> F	
Mean vs Total	82448.01	1	82448.01			
Linear vs Mean	10454.16	3	3484.72	138.57	< 0.0001	
2FI vs Linear	311.80	3	103.93	6.34	0.0021	
Quadratic vs 2FI	**373.36**	**3**	**124.45**	**43.13**	**<0.0001**	**Suggested**

Cubic vs Quadratic	45.87	4	11.47	9.81	0.0001	Aliased
Residual	23.38	20	1.17			
Total	93656.58	34	2754.61			

Table E6: Lack of Fit Test for HADP

Source	Sum of Squares	df	Mean Square	F-Value	p-value Prob> F	
Linear	732.27	11	66.57	57.12	< 0.0001	
2FI	420.47	8	52.56	45.10	< 0.0001	
Quadratic	**47.11**	**5**	**9.42**	**8.08**	0.0003	**Suggested**
Cubic	1.24	1	1.24	1.06	0.3156	Aliased
Pure Error	22.14	19	1.17			

Table E7: Model Summary Statistics for PVDP

Source	Std. Dev.	R-Squared	Adjusted R-Squared	Predicted R-Squared	PRESS	
Linear	4.70	0.9352	0.9287	0.9145	874.94	
2FI	3.54	0.9669	0.9596	0.9506	505.92	
Quadratic	2.08	0.9899	0.9860	0.9780	225.44	Suggested
Cubic	0.85	0.9986	0.9977	0.9952	48.89	Aliased

Table E8: Model Summary Statistics for HADP

Source	Std. Dev.	R-Squared	Adjusted R-Squared	Predicted R-Squared	PRESS	
Linear	5.01	0.9327	0.9260	0.9112	995.63	
2FI	4.05	0.9605	0.9517	0.9484	578.64	
Quadratic	1.70	0.9938	0.9915	0.9879	135.96	Suggested
Cubic	1.08	0.9979	0.9966	0.9962	42.89	Aliased

Table E9: Summary of P-values for PVDC

Source	Sequential p-value	Lack of Fit p-value	Adjusted R-Squared	Predicted R-Squared	
Linear	< 0.0001	< 0.0001	0.8908	0.8674	
2FI	< 0.0001	< 0.0001	0.9526	0.9489	
Quadratic	**< 0.0001**	**< 0.0001**	**0.9806**	**0.9714**	**Suggested**
Cubic	< 0.0002	< 0.0001	0.99212	0.9858	Aliased

Table E10: Lack of Fit Test for PVDC

Source	Sum of Squares	df	Mean Square	F-Value	p-value Prob> F	
Linear	1883.11	11	171.19	470.22	< 0.0001	
2FI	731.87	8	91.48	251.28	< 0.0001	
Quadratic	**261.86**	**5**	**52.37**	**143.85**	< 0.0001	**Suggested**
Cubic	84.24	1	84.24	231.38	< 0.0001	Aliased

Pure Error	6.92	19	0.36			

Table E11: Sequential Model Sum of Squares for PVDC

Source	Sum of Squares	df	Mean Square	F Value	p-value Prob> F	
Mean vs Total	1.772E+05	1	1.772E+05			
Linear vs Mean	17149.24	3	5716.47	90.94	< 0.0001	
2FI vs Linear	1151.24	3	383.75	14.02	< 0.0001	
Quadratic vs 2FI	**470.01**	**3**	**156.67**	**13.99**	**< 0.0001**	**Suggested**
Cubic vs Quadratic	177.62	4	44.40	9.74	< 0.0002	Aliased
Residual	91.16	20	4.56			
Total	1.963E+005	34	5772.35			

Table E12: Summary of P-values for HADC

Source	Sequential p-value	Lack of Fit p-value	Adjusted R-Squared	Predicted R-Squared	
Linear	< 0.0001	< 0.0001	0.9371	0.9250	
2FI	0.0022	< 0.0001	0.9590	0.9574	
Quadratic	< 0.0001	0.0012	**0.9957**	**0.9943**	**Suggested**
Cubic	0.0029	0.0436	0.9976	0.9976	Aliased

Table 413: Sequential Model Sum of Squares for HADC

Source	Sum of Squares	df	Mean Square	F Value	p-value Prob> F	
Mean vs Total	1.745E+05	1	1.745E+05			
Linear vs Mean	16312.87	3	5437.62	164.98	< 0.0001	
2FI vs Linear	408.17	3	136.06	6.33	0.0022	
Quadratic vs 2FI	**525.99**	**3**	**175.33**	**77.0**	< 0.0001	**Suggested**
Cubic vs Quadratic	29.30	4	7.32	7.78	0.0029	Aliased
Residual	25.35	20	1.27			
Total	1.918E+05	34	5641.91			

Table E14: Lack of Fit Test for HADC

Source	Sum of Squares	df	Mean Square	F-Value	p-value Prob> F	
Linear	968.46	11	88.04	82.22	< 0.0001	
2FI	560.29	8	70.04	65.41	< 0.0001	
Quadratic	**34.30**	**5**	**6.86**	**6.41**	0.0012	**Suggested**
Cubic	5.00	1	5.00	4.67	0.0436	Aliased
Pure Error	20.35	19	1.07			

Apart from the F-value and the lack of fit, the R-squared values for the quadratic and cubic models show a high value of 0.9859 and 0.9952 respectively for PVDC and 0.9665 and 0.9975 respectively for HADC when compared to the other models (2FI and linear) as shown on Table 4.68 and 4.69. The measure of how efficient the variability in the actual response values can be explained by the experimental variables and their interactions is given by the R-Squared value.

Table 4.68: Model Summary Statistics for PVDC

Source	Std. Dev.	R-Squared	Adjusted R-Squared	Predicted R-Squared	PRESS	
Linear	7.94	0.9007	0.8908	0.8674	2524.76	
2FI	5.23	0.9612	0.9526	0.9489	972.96	
Quadratic	**3.35**	**0.9859**	**0.9806**	**0.9714**	**544.70**	**Suggested**
Cubic	2.13	0.9952	0.9858	0.9858	270.00	Aliased

Table E15: Model Summary Statistics for HADC

Source	Std. Dev.	R-Squared	Adjusted R-Squared	Predicted R-Squared	PRESS	
Linear	5.74	0.9428	0.9371	0.9250	1296.86	
2FI	4.64	0.9664	0.9590	0.9574	736.46	
Quadratic	**1.51**	**0.9968**	**0.9957**	**0.9943**	**99.02**	**Suggested**
Cubic	1.13	0.9985	0.9976	0.9976	41.55	Aliased

Table E16:   Performance ANN model table for 5 Hidden Neurons

Material	Effects	Sample	MSE	RV
PVDP	Training	26	21.299	0.9624
	g	5	26.929	0.9821
	Validation	3	126.488	0.9189
	Testing			
HADP	Training	26	16.919	0.9793
	g	5	0.7190	0.9959
	Validation	3	0.9152	0.9999
	Testing			

Table E17:   Performance ANN model table for 10 Hidden Neurons

Material	Effects	Sample	MSE	R
PVDP	Training	26	88.6347	0.8821
	g	5	12.457	0.9798
	Validation	3	125.7912	0.7814
	Testing			
HADP	Training	26	33.7869	0.9684
	g	5	1.1845	0.9986

	Validation	3		14.6700	0.9958
	Testing				

Table E18:   Performance ANN model table for 15 Hidden Neurons

Material	Effects	Sample	MSE	R
PVDP	Training	26	3.141	0.9994
		5	5.020	0.9998
	Validation	3	15.469	0.9999
	Testing			
HADP	Training	26	39.9800	0.9467
		5	163.34	0.8952
	Validation	3	13.23	0.9943
	Testing			

Table E19:   Performance ANN model table for 20 Hidden Neurons

Material	Effects	Sample	MSE	R
PVDP	Training	26	0.00118	0.9998
		5	0.2352	0.9965
	Validation	3	0.0601	0.9995
	Testing			
HADP	Training	26	16.917	0.9755
		5	1.0364	0.9997

		3	0.6467	0.9975
	Validation			
	Testing			

Table E20:   Performance ANN model table for 10 Hidden Neurons

Material	Effects	Sample	MSE	R
PVDC	Training	24	0.2256	0.9998
		5	6.0563	0.9882
	Validation	5	4.8435	0.9930
	Testing			
HADC	Training	24	12.4857	0.9912
		5	328.7205	0.9162
	Validation	5	173.9346	0.8094
	Testing			

Table E21:   Performance ANN model table for 20 Hidden Neurons

Material		Sample	MSE	R
PVDC	Training	24	0.7257	0.9997
		5	3.6062	0.9974
	Validation	5	35.2643	0.6746
	Testing			

		Sample	MSE	R
HA DC	Trainin g	24 5	26.9286 302.573	0.9867 0.9662
	Validat ion	5	293.8092	0.9948
	Testing			

Table E22:   Performance ANN model table for 30 Hidden Neurons

Mat erial		**Sample**	**MSE**	**R**
PVD C	Trainin g	24 5	0.08386 305.917	0.9799 0.8782
	Validat ion	5	292.33	0.7975
	Testing			
HA DC	Trainin g	24 5	9.7950 102.825	0.9911 0.5376
	Validat ion	5	101.001	0.9376
	Testing			

APPENDIX F
LETTER OF INTRODUCTION

Department of Chemical Engineering,

Nnamdi Azikiwe University,

Awka.

18th September, 2016.

Dear Respondent,

I am a postgraduate student of the above named institution and department. I am carrying out a research on the general acceptability of flour produced from cocoyam and potato.

You are kindly requested to supply answers to the questions contained in this questionnaire as it reflects your opinions. The information is strictly for academic purposes. I promise to handle all the information supplied confidentially.

Thanks for your anticipated co – operation.

Yours sincerely,

Onu Chijioke Elijah

(Researcher)

QUESTIONNAIRE ON THE 9-POINT HEDONIC SCALE RANKING OF FLOUR

PRODUCED FROM COCOYAM AND POTATO

INSTRUCTION:

This questionnaire is divided into two parts: part I and part II.

Part I deals on demographic data of the respondents, while part II is deals on the hedonic scale.

PART I: DEMOGRAPHIC DATA

Please, you are required to tick (√) as it applied to you

(A) Gender: Male (   )   Female (   )

(B) Age Bracket

    Below 25 years (   )   Between 25 and 35 years (   )

    Between 35 and 45 years (   )   Above 45 years (   )

PART II: HEDONICS SCALE RANKING

You are requested to indicate by ticking (√) in the sections below your opinion on each of the items using 9 – point scale of:

Dislike extremely	=	DE
Dislike very much	=	DVM
Dislike moderately	=	DM
Dislike slightly	=	DS
Neither like nor dislike	=	NLS
Like Slightly	=	LS
Like Moderately	=	LM
Like Very Much	=	LVM
Like Extremely	=	LE

S/N	ITEM A (PDC)	I E	D VM	I M	S	N LS	S	M	L VM	E
1	General appearance									
2	Aroma									
3	Colour									
4	Texture									
	ITEM B (ODC)									
1	General appearance									
2	Aroma									
3	Colour									
4	Texture									
	ITEM C (SDP)									
1	General appearance									
2	Aroma									
3	Colour									
4	Texture									
	ITEM D (CDP)									
1	General appearance									
2	Aroma									
3	Colour									
4	Texture									
	ITEM E (PDP)									
1	General appearance									
2	Aroma									
3	Colour									

4	Texture									
	ITEM F (ODP)									
1	General appearance									
2	Aroma									
3	Colour									
4	Texture									
	ITEM G (SDC)									
1	General appearance									
2	Aroma									
3	Colour									
4	Texture									
	ITEM H (CDC)									
1	General appearance									
2	Aroma									
3	Colour									
4	Texture									

RESULT OF ANALYSIS

Socio-demographic characteristics of Respondents   **N=50**

Variables		Frequency	Percent
Gender	Male	18	36
	Female	32	64
Age	<25years	6	12
	25-35years	36	72
	36-45years	8	16

The table above shows that 36.0%(18) are males while 64%(32) are females.

The table further shows that 12.0%(6) of the respondents are below 25years of age, 72.0%(36) are between 25 and 35 years old while 16.0%(8) are between 36 and 45 years old.

Crosstabulation of Gender, age and Item A (PDC)

Variable	PDC		
Gender	**Dislike**	**Like**	**Total**
	n(%)	**n(%)**	**n(%)**
Male	10(20.0)	8(16.0)	18(36.0)
Female	16(32.0)	16(32.0)	32(64.0)
Total	26(52.0)	24(48.0)	50(100.0)
Age			
<25years	4(8.0)	2(4.0)	6(12.0)
25-35years	18(36.0)	18(36.0)	36(72.0)
36-45years	4(8.0)	4(8.0)	8(16.0)
Total	20(52.0)	24(48.0)	50(100.0)

The table above shows that 20.0%(10) of the males disliked PDC while 16.0%(8) liked it. Also, 32.0%(16) of the females disliked PDC while 32.0%(32.0) liked it. In total, 52.0%(26) of the respondents disliked PDC while 48.0%(24) liked PDC.

The table further shows that 8.0%(4) of the respondents that are below age 25 disliked PDC while 4.0%(2) of them liked PDC. About 36.0%(18) of the respondents that are between ages 25 and 35 disliked PDC while another 36.0%(18) liked PDC, 8.0%(4) of the respondents that are between the ages of 36 and 45 disliked PDC while another 8.0%(4) liked PDC.

Crosstabulation of Gender, age and Item B (ODC)

Variable	ODC		
Gender	**Dislike**	**Like**	**Total**
	n(%)	**n(%)**	**n(%)**
Male	10(20.0)	8(16.0)	18(36.0)
Female	18(36.0)	14(28.0)	32(64.0)
Total	28(56.0)	22(44.0)	50(100.0)
Age			
<25years	2(4.0)	4(8.0)	6(12.0)
25-35years	20(40.0)	16(32.0)	36(72.0)
36-45years	6(12.0)	2(4.0)	8(16.0)
Total	28(56.0)	22(44.0)	50(100.0)

The table above shows that 20.0%(10) of the males disliked ODC while 16.0%(8) liked it. Also, 36.0%(18) of the females disliked ODC while 28.0%(14.0) liked it. In total, 56.0%(28) of the respondents disliked ODC while 44.0%(22) liked ODC.

The table further shows that 4.0%(2) of the respondents that are below age 25 disliked ODC while 8.0%(4) of them liked ODC. About 40.0%(20) of the respondents that are between ages 25 and 35 disliked ODC while 32.0%(16) liked ODC, 12.0%(6) of the respondents that are between the ages of 36 and 45 disliked PDC while 4.0%(2) liked ODC.

Crosstabulation of Gender, age and Item C (SDP)

Variable	SDP		
Gender	**Dislike**	**Like**	**Total**
	n(%)	**n(%)**	**n(%)**
Male	10(20.0)	8(14.0)	18(36.0)

Female	18(36.0)	14(28.0)	32(64.0)
Total	28(56.0)	22(44.0)	50(100.0)
Age			
<25years	4(8.0)	2(4.0)	6(12.0)
25-35years	20(40.0)	16(32.0)	36(72.0)
36-45years	4(8.0)	4(8.0)	8(16.0)
Total	28(56.0)	22(44.0)	50(100.0)

The table above shows that 20.0%(10) of the males disliked SDP while 14.0%(8) liked it. Also, 36.0%(18) of the females disliked SDP while 28.0%(14.0) liked it. In total, 56.0%(28) of the respondents disliked SDP while 44.0%(22) liked SDP.

The table further shows that 8.0%(4) of the respondents that are below age 25 disliked SDP while 4.0%(2) of them liked it. About 40.0%(20) of the respondents that are between ages 25 and 35 disliked SDP while 32.0%(16) liked it, 8.0%(4) of the respondents that are between the ages of 36 and 45 disliked SDP while 8.0%(4) liked it.

Crosstabulation of Gender, age and Item D (CDP)

Variable	CDP		
Gender	**Dislike**	**Like**	**Total**
	n(%)	**n(%)**	**n(%)**
Male	12(24.0)	6(12.0)	18(36.0)
Female	22(44.0)	10(20.0)	32(64.0)
Total	34(64.0)	16(32.0)	50(100.0)
Age			
<25years	2(4.0)	4(8.0)	6(12.0)
25-35years	26(52.0)	10(20.0)	36(72.0)
36-45years	6(12.0)	2(4.0)	8(16.0)
Total	34(60.0)	16(32.0)	50(100.)

The table above shows that 24.0%(12) of the males disliked CDP while 12.0%(6) liked it. Also, 44.0%(22) of the females disliked CDP while 20.0%(10.0) liked it. In total, 64.0%(34) of the respondents disliked CDP while 32.0%(16) liked CDP.

The table further shows that 4.0%(2) of the respondents that are below age 25 disliked CDP while 8.0%(4) of them liked CDP. About 52.0%(26) of the respondents that are between ages 25 and 35 disliked CDP while 20.0%(1O) liked CDP, 12.0%(6) of the respondents that are between the ages of 36 and 45 disliked CDP while 4.0%(2) liked CDP.

Crosstabulation of Gender, age and Item E (PDP)

Variable	PDP		
Gender	**Dislike** n(%)	**Like** n(%)	**Total** n(%)
Male	12(24.0)	6(12.0)	18(36.0)
Female	18(36.0)	14(28.0)	32(64.0)
Total	30(60.0)	20(40.0)	50(100.0)
Age			
<25years	0(0.0)	6(12.0)	6(12.0)
25-35years	24(48.0)	12(24)	56(72.0)
36-45years	6(12.0)	2(4.0)	3(6.0)
Total	30(60)	20(40.0)	50(100.0)

The table above shows that 24.0%(12) of the males disliked PDP while 12.0%(6) liked it. Also, 36.0%(18) of the females disliked PDP while 28.0%(14.0) liked it. In total, 60.0%(30) of the respondents disliked PDP while 44.0%(20) liked PDP.

The table further shows that 0.0%(0) of the respondents that are below age 25 disliked PDP while 12.0%(6) of them liked PDP. About 48.0%(24) of the respondents that are between ages 25 and 35 disliked PDP while 24.0%(12) liked PDP, 12.0%(6) of the respondents that are between the ages of 36 and 45 disliked PDC while 4.0%(2) liked PDP.

Crosstabulation of Gender, age and Item F (ODP)

Variable	ODP		
Gender	**Dislike**	**Like**	**Total**
	n(%)	**n(%)**	**n(%)**
Male	10(20.0)	8(16.0)	18(36.0)
Female	20(40.0)	12(24)	32(64.0)
Total	30(60.0)	20(40.0)	50(100.0)
Age			
<25years	0(0.0)	6(12.0)	6(12.0)
25-35years	24(48.0)	12(24.0)	36(72.0)
36-45years	6(12.0)	2(4.0)	8(16.0)
Total	30(60.0)	20(40.0)	50(100.0)

The table above shows that 20.0%(10) of the males disliked ODP while 16.0%(8) liked it. Also, 40.0%(20) of the females disliked ODP while 24.0%(12.0) liked it. In total, 60.0%(30) of the respondents disliked ODP while 40.0%(20) liked ODP.

The table further shows that 0.0%(0) of the respondents that are below age 25 disliked ODP while 12.0%(6) of them liked ODP. About 48.0%(24) of the respondents that are between ages 25 and 35 disliked ODP while 24.0%(12) liked ODP, 12.0%(6) of the respondents that are between the ages of 36 and 45 disliked ODP while 4.0%(2) liked it.

Crosstabulation of Gender, age and Item G (SDC)

Variable	SDC		
Gender	**Dislike**	**Like**	**Total**
	n(%)	**n(%)**	**n(%)**
Male	12(24.0)	6(12.0)	18(36.0)
Female	16(32.0)	16(32.0)	32(64.0)
Total	28(56.0)	22(44.0)	50(100.0)

Age

<25years	2(4.0)	4(8.0)	6(12.0)
25-35years	22(44.0)	14(28.0)	36(72.0)
36-45years	4(8.0)	4(8.0)	8(16.0)
Total	28(56.0)	22(44.0)	50(100.0)

The table above shows that 24.0%(12) of the males disliked SDC while 12.0%(6) liked it. Also,32.0%(16) of the females disliked SDC while 16.0%(32.0) liked it. In total, 56.0%(28) of the respondents disliked SDC while 44.0%(22) liked SDC.

The table further shows that 4.0%(2) of the respondents that are below age 25 disliked SDC while 8.0%(4) of them liked SDC. About 44.0%(22) of the respondents that are between ages 25 and 35 disliked SDC while 28.0%(14) liked SDC, 8.0%(4) of the respondents that are between the ages of 36 and 45 disliked SDC while 8.0%(4) liked SDC.

Crosstabulation of Gender, age and Item H (CDC)

Variable	CDC		
Gender	Dislike n(%)	Like n(%)	Total n(%)
Male	10(20.0)	8(16.0)	18(36.0)
Female	22(44.0)	10(20.0)	32(64.0)
Total	32(64.0)	18(36.0)	50(100.0)
Age			
<25years	0(0.0)	6(12.0)	6(12.0)
25-35years	24(48.0)	12(24.0)	36(72.0)
36-45years	8(16.0)	0(0.0)	8(16.0)
Total	32(64.0)	18(36.0)	50(100.0)

The table above shows that 20.0%(10) of the males disliked CDC while 16.0%(8) liked it. Also,44.0%(22) of the females disliked CDC while 20.0%(10) liked it. In total, 64.0%(32) of the respondents disliked CDC while 36.0%(18) liked CDC.

The table further shows that 0.0%(0) of the respondents that are below age 25 disliked CDC while 12.0%(6) of them liked CDC. About 48.0%(24) of the respondents that are between ages 25 and 35 disliked CDC while 24.0%(12) liked CDC, 16.0%(8) of the respondents that are between the ages of 36 and 45 disliked CDC while 0.0%(0) liked CDC.

Crosstabulation of gender and PDC (general appearance)

Variable	Dislike n(%)	Neither n(%)	Like n(%)	Total n(%)
Male	0(0.0)	2(4.0)	16(32.0)	18(36)
Female	2(4.0)	2(4.0)	28(56.0)	32(64.0)
Total	2(4.0)	4(8.0)	44(88.0)	50(100.0)

Crosstabulation of gender and PDC (aroma)

Variable	Dislike n(%)	Neither n(%)	Like n(%)	Total n(%)
Male	0(0.0)	0(0.0)	18(36.0)	18(36)
Female	2(4.0)	6(12.0)	24(48.0)	32(64.0)
Total	2(4.0)	6(12.0)	42(84.0)	50(100.0)

Crosstabulation of gender and PDC (colour)

Variable	Dislike n(%)	Neither n(%)	Like n(%)	Total n(%)
Male	2(4.0)	0(0.0)	16(32.0)	18(36)
Female	0(0.0)	2(4.0)	30(60.0)	32(64.0)
Total	2(4.0)	2(4.0)	46(92.0)	50(100.0)

Crosstabulation of gender and PDC (texture)

Variable	Dislike n(%)	Neither n(%)	Like n(%)	Total n(%)
Male	0(0.0	4(8.0)	14(28.0)	18(36.0)
Female	0(0.0)	2(4.0)	30(60.0)	32(64.0)
Total	0(0.0)	6(12.0)	44(88.0)	50(100.0)

Crosstabulation of gender and ODC (general appearance)

Variable	Dislike n(%)	Neither n(%)	Like n(%)	Total n(%)
Male	4(8.0)	6(12.0)	8(16.0)	18(36)
Female	6(12.0)	16(32.0)	10(20)	32(64.0)
Total	10(20)	22(44.0)	18(36.0)	50(100.0)

Crosstabulation of gender and ODC (colour)

Variable	Dislike n(%)	Neither n(%)	Like n(%)	Total n(%)
Male	2(4.0)	2(4.0)	14(26.0)	18(36)
Female	8(16.0)	10(20.0)	14(28.0)	32(64.0)
Total	10(20)	22(44.0)	28(56.0)	50(100.0)

Crosstabulation of gender and ODC (aroma)

Variable	Dislike n(%)	Neither n(%)	Like n(%)	Total n(%)
Male	8(16.0)	4(8.0)	6(12.0)	18(36)
Female	16(32.0)	2(4.0)	14(28.0)	32(64.0)
Total	24(48.0)	6(12.0)	20(40.0)	50(100.0)

Crosstabulation of gender and ODC (texture)

Variable	Dislike n(%)	Neither n(%)	Like n(%)	Total n(%)
Male	2(4.0)	6(12.0)	10(20.0)	18(36)
Female	2(4.0)	14(28.0)	16(32.0)	32(64.0)
Total	4(8.0)	20(40.0)	26(52.0)	50(100.0)

Crosstabulation of gender and SDP (general appearance)

Variable	Dislike n(%)	Neither n(%)	Like n(%)	Total n(%)
Male	0(0.0)	6(12.0)	12(24.0)	18(36)
Female	2(4.0)	14(28.0)	16(32.0)	32(64.0)
Total	2(4.0)	20(40.0)	28(56.0)	50(100.0)

Crosstabulation of gender and SDP (aroma)

Variable	Dislike n(%)	Neither n(%)	Like n(%)	Total n(%)
Male	6(12.0)	4(8.0)	8(16.0)	18(36)
Female	4(8.0)	8(16.0)	20(40.0)	32(64.0)
Total	10(20.0)	12(24.0)	28(56.0)	50(100.0)

Crosstabulation of gender and SDP (colour)

Variable	Dislike n(%)	Neither n(%)	Like n(%)	Total n(%)
Male	0(0.0)	4(8.0)	14(28.00	18(36)
Female	2(4.0)	10(20.0)	20(40.0)	32(64.0)
Total	2(4.0)	14(28.0)	34(68.0)	50(100.0)

Crosstabulation of gender and SDP (texture)

Variable	Dislike n(%)	Neither n(%)	Like n(%)	Total n(%)
Male	0(0.0)	4(8.0)	14(28.0)	18(36)
Female	2(4.0)	10(20.0)	20(40.0)	32(64.0)
Total	2(4.0)	14(28.0)	24(48.0)	50(100.0)

Crosstabulation of gender and CDP (general appearance)

Variable	Dislike n(%)	Neither n(%)	Like n(%)	Total n(%)
Male	0(0.0)	2(4.0)	16(32.)	18(36)
Female	6(12.0)	2(4.0)	24(48.0)	32(64.0)
Total	6(12.0)	4(8.0)	40(80.0)	50(100.0)

Crosstabulation of gender and CDP (aroma)

Variable	Dislike n(%)	Neither n(%)	Like n(%)	Total n(%)
Male	2(4.0)	8(16.0)	8(16.00	18(36)
Female	0(0.0)	6(12.0)	26(52.0)	32(64.0)
Total	2(4.0)	14(28.0)	34(68.0)	50(100.0)

Crosstabulation of gender and CDP (colour)

Variable	Neither n(%)	Like n(%)	Total n(%)
Male	8(16.0)	10(20.0)	18(36.0)
Female	10(20.0)	22(44.0)	32(64.0)
Total	18(36.0)	32(64.0)	50(100.0)

Crosstabulation of gender and CDP (texture)

Variable	Dislike n(%)	Neither n(%)	Like n(%)	Total n(%)
Male	2(4.0)	2(4.0)	14(28.0)	18(36)
Female	0(0.0)	8(16.0)	24(48.0)	32(64.0)
Total	2(4.0)	10(20.0)	38(76.0)	50(100.0)

Crosstabulation of gender and PDP (general appearance)

Variable	Dislike n(%)	Neither n(%)	Like n(%)	Total n(%)
Male	0(0.0)	8(10.0)	10(20.0)	18(36)
Female	0(0.0)	14(36.0)	18(36.0)	32(64.0)
Total	0(0.0)	22(44.0)	28(56.0)	50(100.0)

Crosstabulation of gender and PDP (aroma)

Variable	Dislike n(%)	Neither n(%)	Like n(%)	Total n(%)
Male	4(8.0)	4(8.0)	10(20.0)	18(36)
Female	6(12.0)	4(8.0)	22(44.0)	32(64.0)
Total	10(20.0)	8(16.0)	32(64.0)	50(100.0)

Crosstabulation of gender and PDP (colour)

Variable	Dislike n(%)	Neither n(%)	Like n(%)	Total n(%)
Male	2(4.0)	6(12.0)	10(20.0)	18(36)
Female	0(0.0)	12(24.0)	20(40.0)	32(64.0)
Total	2(4.0)	18(36.0)	30(60.0)	50(100.0)

Crosstabulation of gender and PDP (texture)

Variable	Dislike n(%)	Neither n(%)	Like n(%)	Total n(%)
Male	0(0.0)	4(8)	14(28.0)	18(36)
Female	0(0.0)	10(20.0)	22(44.0)	32(64.0)
Total	0(0.0)	14(28.0)	36(72.0)	50(100.0)

Crosstabulation of gender and ODP (general appearance)

Variable	Dislike n(%)	Neither n(%)	Like n(%)	Total n(%)
Male	8(16.0)	0(0.0)	10(20.0)	18(36)
Female	8(16.0)	8(16.0)	16(32.0)	32(64.0)
Total	16(32.0)	8(16.0)	26(52.0)	50(100.0)

Crosstabulation of gender and ODP (aroma)

Variable	Dislike n(%)	Neither n(%)	Like n(%)	Total n(%)
Male	8(16.0)	4(8.0)	6(12.0)	18(36)
Female	4(8.0)	16(32.0)	12(24.0)	32(64.0)
Total	12(24.0)	20(40.0)	18(36.0)	50(100.0)

Crosstabulation of gender and ODP (colour)

Variable	Dislike n(%)	Neither n(%)	Like n(%)	Total n(%)
Male	8(16.0)	2(4.0)	8(16.0)	18(36)
Female	14(28.0)	10(20.0)	8(16.0)	32(64.0)
Total	22(44.0)	12(24.0)	24(48.0)	50(100.0)

Crosstabulation of gender and ODP (texture)

Variable	Dislike n(%)	Neither n(%)	Like n(%)	Total n(%)
Male	4(8)	6(12)	8(16)	18(36)
Female	10(20.0)	6(12.0)	16(32.0)	32(64.0)
Total	14(28.0)	12(24.0)	24(48.0)	50(100.0)

Crosstabulation of gender and SDC (general appearance)

Variable	Dislike n(%)	Neither n(%)	Like n(%)	Total n(%)
Male	0(0.0)	8(16.0)	10(20.0)	18(36)
Female	0(0.0)	18(36.0)	14(28.0)	32(64.0)
Total	0(0.0)	26(52.0)	24(48.0)	50(100.0)

Crosstabulation of gender and SDC (aroma)

Variable	Dislike n(%)	Neither n(%)	Like n(%)	Total n(%)
Male	4(8.)	4(8.0)	10(20.0)	18(36)
Female	6(12.0)	4(8.0)	22(44.0)	32(64.0)
Total	10(20.0)	8(16.0)	32(64.0)	50(100.0)

Crosstabulation of gender and SDC (Colour)

Variable	Dislike n(%)	Neither n(%)	Like n(%)	Total n(%)
Male	4(8.0)	6(12.0)	8(16.0)	18(36)
Female	2(4.0)	12(24.0)	18(36.0)	32(64.0)
Total	6(12.0)	18(36.0)	26(52.0)	50(100.0)

Crosstabulation of gender and SDC (texture)

Variable	Dislike n(%)	Neither n(%)	Like n(%)	Total n(%)
Male	0(0.0)	8(16.0)	10(20.0)	18(36)
Female	0(0.0)	12(24.0)	20(40.0)	32(64.0)
Total	0(0.0)	20(40.0)	30(60.0)	50(100.0)

Crosstabulation of gender and SCDC (general appearance)

Variable	Dislike n(%)	Neither n(%)	Like n(%)	Total n(%)
Male	2(4.0)	4(8.0)	12(24.0)	18(36)
Female	4(8.0)	14(28.0)	14(28.0)	32(64.0)
Total	6(12.0)	18(36.0)	26(52.0)	50(100.0)

Crosstabulation of gender and CDC (aroma)

Variable	Dislike n(%)	Neither n(%)	Like n(%)	Total n(%)
Male	0(0.0)	10(20.0)	8(16.0)	18(36)
Female	0(0.0)	14(28.0)	18(36.0)	32(64.0)
Total	0(0.0)	24(48.0)	26(52.0)	50(100.0)

Crosstabulation of gender and CDC (colour)

Variable	Dislike n(%)	Neither n(%)	Like n(%)	Total n(%)
Male	2(4.0)	10(20.0)	6(12.0)	18(36)
Female	0(0.0)	16(32.0)	16(32.0)	32(64.0)
Total	2(4.0)	26(52.0)	22(44.0)	50(100.0)

Crosstabulation of gender and CDC (texture)

Variable	Dislike n(%)	Neither n(%)	Like n(%)	Total n(%)
Male	6(12.0)	2(4.0)	10(20.0)	18(36)
Female	6(12.0)	10(20.0)	16(32.0)	32(64.0)
Total	12(24.0)	12(24.0)	26(52.0)	50(100.0)